Wearable Sensing and Feedback with Applications in Health and Lifestyle

Majid Janidarmian

Department of Electrical and Computer Engineering
McGill University, Montréal, Québec

A Thesis submitted to McGill University in partial fulfillment of the requirements for the degree of Doctor of Philosophy in Electrical Engineering

April 2017

Acknowledgement

First and foremost, I would like to express my immense gratitude towards my advisors, Prof. Zeljko Zilic and Prof. Katarzyna Radecka for their outstanding supervision throughout my graduate career. Thanks for giving me the opportunity to be part of the research and guiding me with the great thoughts.

I take this moment to extend my thankfulness to my committee members, Prof. Michael Rabbat and Prof. Muthucumaru Maheswaran for their insightful comments and suggestions during my dissertation proposal and seminar. My special thanks must go to Atena Roshan Fekr who provided great help during the entire process with the data, experiments, and the great ideas. I would also like to thank my brilliant friends and lab-mates, especially, Omid Sarbishei, Benjamin Nahil, Ashraf Suyyagh, Steve Ding, Jason Tong, Dimitrios Stamoulis, Ari Ramdial, Jonathan Bohbot and Amir Shahshahani for all the discussions, encouragement, and good memories. The Integrated Microsystems Laboratory (IML) has been a source of friendships as well as good advice and collaboration. I am also grateful to Mr. Louis Ross, CEO of Motion Engine Company, for the advice and supports he provided during our collaborative project. I would like to acknowledge Jonathan Bohbot for his French translation of the abstract.

Finally, I deeply thank my family for their continuous love, care, support, and encouragement during my whole life. Moreover, most of all for my beloved wife who has been my best friend and great companion, and helped me get through difficult times in the most positive way. Thank you.

Abstract

The maturity of wearable sensing, wireless technology, and data processing techniques enables the remote monitoring of physical activity and vital signs to promote health and well-being of individuals. Recently, much of research has focused on machine learning approaches to sensor data for delivering more intelligence into different health and fitness applications. However, there are different challenges associated with these approaches that limit us to reach an acceptable accuracy level. In this thesis, a comprehensive analysis of wearable accelerometer sensors in human activity recognition problem is conducted to address the classification issues while dealing with inter-person differences and data diversities. In addition, novel feature extraction and classification techniques are proposed to improve the accuracy as well as the worst-case sensitivity in the multi-class classification. The introduced techniques are experimentally validated by considering two state-of-the-art case studies. This work presents significant evidence that we can build accurate predictive models for sensor-based recognition and diagnostic problem under more realistic conditions. Furthermore, to reduce the computational costs of the decision-making process, an innovative algorithm is presented to analyze the variations in the periodic signals. It reduces the learning efforts by detecting any significant changes in the signals. There is also an increasing potential for integration of wearable sensors and haptic systems to improve human motion learning in a wide range of applications. Therefore, we investigate how real-time corrective feedback improves the user's performance in a health application. Finally, a 2D vibrotactile display is developed to transmit tactile stimuli onto the lower back of the users who can personalize the vibration variables. The customization capability of this system reduces the cognitive loadings for the users. This system can be beneficial and efficient not only for delivering complex feedback, but also for people with hearing and visual impairments.

Abrégé

La maturité des senseurs portables, de la technologie sans fil, et des techniques de traitement des données permet de surveiller à distance l'activité physique et les signes vitaux pour promouvoir la sante et le bien-être des individus. Récemment, la plus grande partie de la recherche était concentrée sur les démarches de l'apprentissage par machine pour traiter les données des senseurs dans le domaine de la santé et l'application de conditionnement physique. Toutefois, il y a plusieurs défis qui sont associés avec ces approches et qui nous limitent à atteindre un niveau de précision acceptable. Dans cette thèse, une analyse compréhensive d'un accéléromètre portable dans le but de reconnaître l'activité humaine est faite pour adresser les problèmes de classification tout en considérant les différences d'interpersonnelles et la diversité des données. En plus, l'extraction originale des caractéristiques et les techniques de classification est proposée pour améliorer la précision et la sensibilité dans le pire des cas dans une classification multi-classe. Les techniques présentées sont validées expérimentalement en considérant deux études de cas dernier cri. Ceci est preuve du fait que nous pouvons construire des modèles prédictifs précis pour des problèmes reliés à la reconnaissance par les capteurs et le diagnostic de ceux-ci dans les conditions plus réalistes. De plus, pour réduire les coûts de calcul du processus de prise de décision, un algorithme innovant est présenté pour analyser les variations des signaux périodiques. L'algorithme réduit les efforts liés à l'apprentissage en détectant tout changement significatif des signaux. Il y a aussi un potentiel croissant pour l'intégration des senseurs portables et les systèmes haptiques pour améliorer l'apprentissage du mouvement humain dans un large éventail d'applications. Donc, nous enquêtons sur une rétroaction corrective en temps réel pour savoir comment celle-ci améliore la performance de l'utilisateur dans une application de sante. Enfin, un affichage 2D vibrotactile est développé pour transmettre des stimuli tactiles dans les lombes des utilisateurs qui peuvent personnaliser les variables de

vibration. La capacité de personnalisation de ce système réduit les chargements cognitifs des utilisateurs. Ce système peut être bénéfique et efficace non seulement pour délivrer un retour d'information complexe, mais aussi pour les gens souffrant de troubles de vue et d'audition.

Contents

List of Figures

List of Tables

List of Acronyms

BLE:	Bluetooth Low Energy
BSN:	Body Sensor Network
BUp:	Bottom-UP
CHF:	Chronic Heart Failure
COPD:	Chronic Obstructive Pulmonary Disease
DA:	Discriminant Analysis
DT:	Decision Tree
DTB:	Decision Tree Bagging
ECG:	Electroencephalogram
FDA:	Food and Drug Administration
EDGE:	Enhanced Data GSM Environment
EEG:	Electrocardiogram
FCC:	Federal Communications Commission
FFT:	Fast Fourier Transform
FNSQ:	Fixed-size Non-overlapping Sliding Window
FOSW:	Fixed-size Overlapping Sliding Window
GPRS:	General Packet Radio Service
GSR:	Galvanic Skin Response
HAR:	Human Activity Recognition
HIPAA:	Health Insurance Portability and Accountability Act
HR:	Heart Rate
HS:	Healthcare System
HSPA:	High Speed Packet Access
IP:	Impedance Pneumography
KNN:	K-Nearest Neighbors
LOSO:	Leave-One-Subject-Out
LTE:	Long-Term Evolution
MEMS:	Micro-Electro-Mechanical System
MICS:	Medical Implant Communication Service
ML:	Machine Learning
NB:	Naive Bayes
NDEP:	National Diabetes Education Program
NFC:	Near Field Communications
NN:	Neural Network

OSA:	Obstructive Sleep Apnea
PA:	Physical Activity
PCA:	Principal Components Analysis
PGS:	Polysomnography
RR:	Respiration Rate
SoC:	System-on-Chip
SVM:	Support Vector Machine
SWAB:	Sliding Window and Bottom-up
TDM:	Time Division Multiplexing
ToD:	Top-Down
TV_{var}:	Tidal Volume variability
UWB:	Ultra-Wide Band
VSW:	Variable-size Sliding Window
WHO:	World Health Organization

Chapter 1

Introduction

This chapter includes an overview of the thesis, along with a description of the challenges. A summary is also given on contributions that are brought forth into this thesis.

1.1 Research Problem and Scope

The wearable sensors, coupled with the advanced data processing and communication technologies have opened the window to a new era of cost-effective remote healthcare services. Wireless stand-alone sensors are now available in small size, and we expect the smaller format in the near future such that they become hardly noticeable for their users. Today, the miniature sensors can be unobtrusively attached to the body or can be part of clothing items to promote health and well-being of individuals

[1]. They enable the remote monitoring of physical activity, vital signals, the early diagnosis of serious conditions, and the remote control of medical treatments. Sensor-based recognition system integrates the wearable sensors with novel machine learning techniques to make sense of low-level sensor data and provide rich contextual information in a real-life application.

The process of discerning valuable information from wearable sensors is a non-trivial task and is an on-going research area. Many research areas have focused on machine learning-based approaches to sensor data for better understanding and meeting people's needs. However, there are different challenges associated with these approaches that limit us to reach an acceptable accuracy level. The performance of recognition models depends on many considerations such as the dataset quality, segmentation, feature extraction, and learning algorithms. Each step needs to be thoroughly investigated to find the optimal solution that is highly dependent on the application. Furthermore, different factors including the type of sensory node (commercial mass-marketed or research-only devices), acquisition protocol (under naturalistic circumstances or laboratory environments), participants' characteristics, sensors placements, and sampling rates mainly influence the choice of techniques and parameter settings. Considering the mentioned challenges makes it difficult to obtain a robust Machine Learning (ML) model that is invariant to biases and performs well on unseen datasets. Therefore, we need to work on novel feature extraction and classifiers that outperform classical methods considering inter-person differences and data diversities. Finding an effective combination of multiple classifiers can be a promising direction for the development of highly reliable prediction systems. The runtime complexity of the machine learning models and the number of functions calls are other important challenges as the whole recognition procedure should quickly handle the online data processing requirements. In this dissertation, we address these concerns and focus on building highly accurate and efficient predictive models.

There is an increasing potential for integration of wearable sensors and haptic systems to improve human motion learning in a wide range of applications including motor rehabilitation, sports training, and breathing exercises. The miniature soft actuators could ensure light haptic devices that do not hinder the normal motions of the human body. The deviation from the desired movement perceived tactually can provide training guidance sufficient to improve the quality of prescribed exercises. However, the inherent complexity of the subject-to-subject differences raises serious challenges in developing highly effective haptic systems. It is worth noting that even the subject's level of familiarity with the system and the mental overload influence the effectiveness of the feedback system. These issues necessitate the development of a haptic system based on each subject's characteristics individually rather than a fixed training model. In addition, delivering complex feedback and rich information through multiple vibration motors presents more cognitive challenges leading to exhaustion and frustration over time. Thus, another challenge is to find an effective and personalizable solution to deliver complex meanings and expressions without adding significant user's perceptual and memory loadings.

1.2 Motivation behind this Research

In the fitness and health fields, wearable sensors generate large-scale big data. The machine learning techniques use the data to assess individuals' health in real time and identify trends that may lead to better diagnoses and treatment. Applying efficient algorithms to learn from data can aid physicians to evaluate the state of human actions and diagnose the illnesses. Therefore, in this thesis, we first focus on improving the algorithms and parameters in two sensor-based applications that can offer valuable information on health, wellbeing, and fitness of monitored persons. Then, we design a system to benefit from integration of a wearable sensor and haptic feedback. We show that even a single-point vibration feedback can be immensely useful in the performance of movement exercises prescribed to keep a satisfactory functional level. Furthermore, the haptic system is extended to deliver complex meanings and to make the world more accessible to those with some level of sensory impairment. In the following sections, we will explain the importance of each topic addressed in this thesis.

1.2.1 Human Activity Analysis

The motion tracking sensors are becoming pervasive, and consequently, we face an impressive growth in physical activity data. Therefore, there is a big opportunity to develop intervention strategies and derive rich contextual information from accurate measurement of physical activity (PA). Indeed, PA is commonly known to be one of the key elements of a healthy life regardless of the age, from school-aged children [2] to older adults [3]. Adequate physical activity can decrease the occurrence and severity of many adverse diseases such as obesity, cancer, depression, cardiovascular and pulmonary diseases [4]. According to World Health Organization (WHO), more than 1.9 billion adults aged 18 years and older were overweight in 2014, with prevalence increasing at staggering rates in many countries [5]. The common health consequences of overweight and obesity are diabetes, cardiovascular diseases, musculoskeletal disorders (particularly osteoarthritis – a highly disabling degenerative disease of the joints) and some cancers (including ovarian, endometrial, breast, prostate, gallbladder, liver, kidney, and colon) [5]. The easiest solution for this issue is limiting the energy intake from fat and sugars and engaging in the regular physical activity. National Diabetes Education Program (NDEP) [6] reported that total healthcare and related costs for the treatment of diabetes run about $174 billion annually and physical activity can be as powerful as glucose-lowering medication.

Health monitoring, based on wearable and non-invasive sensors, modern communication and information technologies offers an efficient and cost-effective solution that encourages people to increase their physical activity. In addition to providing objective information about activity intensity and duration, automated monitoring helps us to analyze the relationship between physical activity and health outcomes [7]. Moreover, according to a study presented in [8], on-body sensing also proves to be the most common monitoring technology for the fall detection of elderly and gait assessment. Population aging due to rising life expectancy enforces more demands in healthcare services [9]. A recent global study released that the number of people aged 60 years or over in the world will reach two billion by 2050 and the elderly are more prone to health problems compared to other age groups [10]. For example, a simple fall can have devastating consequences for older persons and is an important reason for nursing home admission. The increasing health care and nursing costs place a tremendous stress on the society and the government. Therefore, promoting independent living amongst elderly and individuals with cognitive impairment is another major motivating factor for the sensor-based system. With effective monitoring of daily activities, the adverse effects of unpredictable incidents such as sudden illnesses, falls, and so on can be bettered to some extent.

Another important aspect of body motion monitoring is how the sequences of time series data are processed for prediction, diagnosis, and guidance to lead a healthy lifestyle. Thus, it is an utmost necessity to develop and apply novel algorithms to provide better health care services at an affordable price. Human Activity Recognition (HAR) is introduced to automatically detect which specific activity a user is performing at each particular moment. HAR is used to assess human movements and provide contextual information to not only ambient-assisted living [11] and health management [12], but also sports training [13], security and entertainment [14] applications.

For human activity recognition, the available technologies can be divided into three categories: vision-based recognition, radio-based recognition, and sensor-based recognition [15]. The vision-based approaches that cause a privacy concern for the users require a camera and right lighting conditions to monitor human activity. Their performance is significantly reduced in outdoor environments due to the influence of variable lighting and different disturbances [16]. Vision-based systems are expensive and limited by other factors such as install locations. Radio-based HAR does not work in areas, where a base station is unavailable to communicate with the tags attached on the users' body [17]. Alternatively, due to the rapid development of MEMS sensors, activity recognition based on wearable sensors has become popular. Among the wearable sensors, accelerometers have been given the most attention in HAR to achieve continuous monitoring beyond carefully restricted environments. With efficient signal processing and learning algorithms, the accelerometers are capable of taking the lead role in not only activity recognition, but also early diagnosis and treatment of diseases such as breathing disorders.

1.2.2 Respiratory Analysis

The human Respiration Rate (RR) is a vital physiological parameter that can reveal health status. Abnormal breathing rate can be the first symptom of different physiological, mechanical, or psychological dysfunctions. A disordered breathing pattern denotes inefficient oxygen inhalation and carbon dioxide expulsion from the body's tissues. The abnormal respiration is indicative of many diseases such as anemia, asthma, sleep apnea, sudden death syndrome, Chronic Heart Failure (CHF) and Chronic Obstructive Pulmonary Disease (COPD) [18]. About 4% of Canadians, aged 35 to 79 were diagnosed with COPD [19]. This type of breathing problem is expected to become one of the major health challenges of the next few decades [20]. In addition, more than 2.4 million Canadians aged 12 years and over were living with Asthma in 2009 [21]. One of many complications in Asthma managements is that many patients with Asthma are misdiagnosed as other respiratory problems such as common cold or acute bronchitis [22]. Moreover, a survey by the Public Health Agency of Canada reported that 22% of Canadian adults were diagnosed with Obstructive Sleep Apnea (3%) or at high risk for OSA (19%) [23]. Obstructive sleep apnea stops the patients from having a restful sleep they need to stay healthy. Sleep apnea can cause daytime sleepiness and reduce cognitive function. People with untreated OSA have an increased risk of cardiovascular disease, hypertension, and early death.

Polysomnography (PGS) is the gold standard method to record the vital signs and physiological variables such as respiratory effort, airflow, and oxygen saturation. Because PGS is costly, invasive, and inconvenient, various approaches for long-term respiratory monitoring have been introduced. The approaches can be generally categorized as either directly detecting airflow during the breathing process or indirectly responding to chest and abdomen expansion and contraction during breathing [24]. In the direct monitoring, a sensor is placed near the nose or mouth to extract the breath flow by analysis of the carbon dioxide concentration, humidity, or air temperature as respiration occurs [25]. The main issue with this method is the placement of the sensor that is very inconvenient to the user.

On the other hand, the indirect method measures physical parameters such as detecting the changes in lung volume related to respiration. Different approaches have achieved measurements of lung movement during inhalation and exhalation without reducing user comfort. Integrating coated piezoresistive sensors into garments [26] and strain sensors [27] are two examples of monitoring RR by tracking the movements of predominant breathing compartment and are capable of detecting a pause in breathing to be used in sleep apnea research. Impedance Pneumography (IP) is another indirect method, which measures the respiration effort from changes in transthoracic impedance.

There are different studies, e.g. [28], that show the feasibility of IP-based techniques in the determination of respiratory frequency, periods of apnea, and an estimate of volume; however, artifacts may invalidate the signal quality. Another indirect method is the use of wearable motion sensors to detect the small movements of the chest wall that occur during expansion and contraction of the lungs. It has been shown that with proper signal processing, this approach can produce results that closely match the measurements of nasal cannula pressure [29]. For example, the designed system in [30] used accelerometer sensors for diagnosis and treatment of patients with disordered breathing. This method shows a great potential to integrate the use of inertial sensors with machine learning techniques to model a broad range of human respiratory patterns for the goal of cloud-based recognition of different respiratory problems. In addition, accelerometer-derived respiration signal has been proven itself particularly effective in providing an affordable platform for yogic breathing practices.

1.2.3 Haptic Feedback and Sensory Substitution

Human skin has long been accepted as a receptor for communicating information through various sensations such as stretch, pressure, and vibration [31]. Haptic feedback has been used to train human movement when the kinematics are measured in real time and compared with ideal kinematics (predefined or expert's movement pattern). The feedback amplitude or frequency can be often modulated proportionally to error signals to warn users of desired changes. One approach is the expert-trainee paradigm in which the expert performs movements, and the trainee tries to mimic when their performance is tracked by a motion capture system [32]. The performance of the expert and trainee is compared to generate vibrotactile feedback for the trainee. The joints moving in a wrong way will get vibrations proportional to the amount of error. In another approach, the trainee is asked to perform the exercise under expert's supervision to record desired movements by sensors or other tracking systems [33], [34]. Then, the trainee receives the feedback based on the errors between the predefined and testing kinematics. Tactile feedback can be also initiated in periodic pulses instead of continuously in training repetitive movements such as swimming or gait [35], [36]. In these systems, the haptic feedback automatically guides new movement patterns through cutaneous cuing information, where no sensory impairment is involved [37]. Wearable sensors and haptic feedback could also enable a significant impact in correcting behavioral deficits such as retraining gait patterns to decrease knee loading for individuals with knee osteoarthritis [38].

In case of *partial sensory impairment*, sensory signals are degraded due to old age or the partial sensory loss from disease or injury. As the world's population ages, the problems of vision loss, stroke, or audition loss will likely rise, given the susceptibility to sensory impairments in older populations. Haptic wearables have the potential to address sensory impairments such as vestibular deficits, where the vibrotactor arrays could reduce anterior-posterior trunk tilt during quiet standing in elderly people [39]. Individuals who have suffered a motor function disability need to practice appropriate rehabilitation treatments. As presented in [32], a significant accuracy improvement in rehabilitation practices can be obtained by placing vibrotactile actuators near body joints. Such a system also has the potential to reduce injuries during therapy, which may be caused by improper patient's joint movement. Therefore, in these applications, the haptic can be used as a means of *sensory augmentation* facilitating motor control and rehabilitation [40].

Sensory substitution is defined as a means to use input from one sensory modality to obtain information for another sensory modality, such as acquiring visual information through audio or tactile stimuli. This approach can be used for people with some level of sensory impairment or total disability. The opportunity of helping these people to step out of their normal routine appears to be one of the major motivating factors of haptic biofeedback design. For example, a sound-to-touch sensory substitution device was recently presented to deliver processed auditory information to the skin of the deaf people using vibratory motors [41]. This solution has been proven successful as the participants evidently showed the ability to identify spoken word audio mapped to tactile stimulation. In another project, McDaniel *et al.* [42] designed a tactile belt of seven equidistantly spaced tactors around the waist to hint a blind user of another person's existence.

The applications described above motivate us to examine haptic feedback in a health application called "Breathing Therapy" to retrain breathing maneuvers by applying periodic tactile cues to instruct desired corrective breathing patterns. We further design a customizable system to be used as a means of sensory substitution bringing more benefits through haptic displays.

1.3 Thesis Contributions

The major contributions of this thesis are summarized as follows:

- An extensive analysis on feature representations and classification techniques (the most comprehensive comparison yet with 293 classifiers) for activity recognition problem is conducted. In total, accelerometer data from 228 subjects with various sources of heterogeneities are used to evaluate different factors in recognition accuracy. The trade-off between window size and recognition performance is also explored for different sensor positions. It is for the first time (up to our best knowledge) that such a wide set of techniques was directly compared and made accessible for future work. This investigation will help the developers in selecting the methods and parameter settings to best balance between the accuracy requirements and prediction time constraints.

- An innovative algorithm is proposed to fuse specific windowed raw data for extracting information-rich features from the wearable sensors signals. The classification models can take great advantage of these features to classify different patterns based on comparing the sensor samples in each window with a predefined template. We make use of Dynamic Time Warping technique to create the template from a selected set of feature vectors. The results show the feasibility of the proposed method to better classify the motion patterns in health and fitness applications.
- A new multi-classification technique is introduced for delivering more intelligence into real applications and better discerning knowledge from wearable sensors. It improves two main conflicting objectives of classification problems i.e. classification accuracy and the worst-case sensitivity using Pareto-based multi-objective optimization methodology. The proposed technique is experimentally validated by considering two state-of-the-art case studies. This work presents significant evidence that we can build accurate predictive models for sensor-based recognition and diagnostic problem under more realistic conditions.
- To reduce the computational costs of the feature extraction and classification, a novel algorithm is proposed to analyze the variations in the periodic signals. It reduces the learning efforts by detecting any significant changes in the signal. We used the idea of pheromone trail employed in ant colony optimization algorithm to keep track of the signal updates. This finding enables the design of a highly effective real-time predictive model for wearable applications.
- A new haptic-based feedback system is presented to support self-guided exercise and provide subject-specific training and treatment. We investigate artificial tactile stimuli for providing real-time feedback on the performance of breathing exercises captured by an accelerometer. This system significantly improves the subjects’

performance and increases adherence to breathing instructions with minimal intrusion and cost.

- A 2D vibrotactile display is developed to transmit tactile stimuli onto the lower back of the users who can personalize the vibration variables including spatial location, vibratory rhythm, burst duration, and intensity. The customization capability of the system alleviates the perceptional and memory loadings of the users. This system can be beneficial and effective not only for delivering complex feedback, but also for people with hearing and visual impairments.

In this thesis, ethical approvals were received from McGill University Ethics Committee for all experiments involving human subjects. All participants were informed about the experimental procedures before starting the trial sessions. The rest of this thesis is organized as follows. Chapter 2 begins with a review of wearable connected health system and outlines the challenges associated with the sensor-based classification. In Chapter 3, we comprehensively analyze wearable acceleration sensors in human activity recognition. A novel feature extraction and a tree-based hierarchical ensemble method are described in Chapter 4 to improve the performance of the recognition. This chapter ends with an efficient approach to speed up the conventional recognition methods by reducing the number of calls of feature extraction and classification functions. Chapter 5 addresses our proposed vibrotactile system, acting as a real-time feedback and sensory substitution. Finally, Chapter 6 summarizes the results of this thesis and offers remarks on possible future work.

1.4 List of Publications

- **M. Janidarmian,** A. Roshan Fekr, K. Radecka, Z. Zilic, "*A Comprehensive Analysis on Wearable Acceleration Sensors in Human Activity Recognition*," Sensors Journal 2017, 17, 529.

- **M. Janidarmian,** A. Roshan Fekr, K. Radecka, Z. Zilic, "*Multi-Objective Hierarchical Classification Using Wearable Sensors in a Health Application*," in IEEE Sensors Journal, vol. 17, no. 5, pp. 1421-1433, 2016.
- **M. Janidarman**, A. Roshan Fekr, K. Radecka, Z. Zilic, "*Sensory Substitution with Personalized Tactile Patterns*," IEEE-EMBS International Conference on Biomedical and Health Informatics (BHI), Orlando, Florida, NV, 2017.
- **M. Janidarman**, A. Roshan Fekr, K. Radecka, Z. Zilic, "*Haptic feedback and human performance in a wearable sensor system*," IEEE-EMBS International Conference on Biomedical and Health Informatics (BHI), Las Vegas, NV, 2016.
- **M. Janidarman**, A. Roshan Fekr, K. Radecka, Z. Zilic, "*Analysis of Motion Patterns for Recognition of Human Activities*," ACM-EAI International Conference on Wireless Mobile Communication and Healthcare, Great Britain, London, 2015.
- **M. Janidarmian**, A. Roshan Fekr, K. Radecka, Z. Zilic, "*Automated Diagnosis of Knee Pathology Using Sensory Data*," IEEE-EAI International Conference on Wireless Mobile Communication and Healthcare - "Transforming healthcare through innovations in mobile and wireless technologies", Athens, Greece, 2014.
- **M. Janidarmian**, A. Roshan Fekr, K. Radecka, Z. Zilic, "*Affordable eRehabilitation Monitoring Platform*," IEEE International Humanitarian Technology Conference, Montreal, Canada, 2014.
- **M. Janidarmian**, A. Roshan Fekr, K. Radecka, Z. Zilic, "*Cloud-based Mobile Rehabilitation Platform*," ACM International Conference on Wireless Health, Baltimore, USA, 2013.
- **M. Janidarmian**, Z. Zilic, K. Radecka, "*Issues in Multi-valued Multi-modal Sensor Fusion*", IEEE International Symposium on Multiple-Valued Logic, Victoria, Canada, 2012.

- **M. Janidarmian**, A. Roshan Fekr, K. Radecka, Z. Zilic, "*Test and Calibration on the STLM75 Temperature Sensor of the iNEMO Microsystem Using the Temptronic TP4500 Environmental Thermal Chamber*," Application Note, McGill University, in co-operation with CMC Microsystems, Montreal, Canada, 2012.
- A. Roshan Fekr, **M. Janidarmian**, K. Radecka, Z. Zilic, "*Respiration Disorders Classification with Informative Features for m-Health Applications*," in IEEE Journal of Biomedical and Health Informatics, vol. 20, no. 3, pp. 733-747, 2016.
- A. Roshan Fekr, **M. Janidarmian**, K. Radecka, Z. Zilic, "*Movement analysis of the chest compartments and a real-time quality feedback during breathing therapy*," Journal of Network Modeling Analysis in Health Informatics and Bioinformatics, vol. 45, no. 1, 2015.
- A. Roshan Fekr, **M. Janidarmian**, K. Radecka, Z. Zilic, "*A Medical Cloud-based Platform for Respiration Rate*," Sensors journal 2014, 14, 11204-11224.
- A. Roshan Fekr, **M. Janidarmian**, K. Radecka, Z. Zilic, "*Development of a Cloud-Based Monitoring System for Respiration Rate Measurement and Breath Analysis*," International Conference on IoT Technologies for HealthCare, Springer press, Roma, Italy, 2014.
- A. Roshan Fekr, **M. Janidarmian**, K. Radecka, Z. Zilic, "*Multi-Sensor Blind Recalibration in mHealth Applications*," IEEE International Humanitarian Technology Conference, Montreal, Canada, 2014.
- O. Sarbishei, **M. Janidarmian**, K. Radecka, Z. Zilic, "*Multi-sensory System Integration Dependability*," Chapter 18 in Book Technologies for Smart Sensors and Sensor Fusion, CRC press, edited by K. Yallup and K. Iniewski, pp. 319-335, 2013.

- A. Roshan Fekr, **M. Janidarmian**, K. Radecka, Z. Zilic, "*Remote Blind Calibration of Multi-Sensory Systems in Medical Applications*," ACM International Conference on Wireless Health, Baltimore, USA, 2013.
- A. Roshan Fekr, **M. Janidarmian**, O. Sarbishei, B. Nahill, K. Radecka, Z. Zilic, "*MSE minimization and fault-tolerant data fusion for multi-sensor systems*," IEEE International Conference on Computer Design, Montreal, Canada, 2012.
- O. Sarbishei, A. Roshan Fekr, **M. Janidarmian**, B. Nahill, K. Radecka, "*A Minimum MSE Sensor Fusion Algorithm with Tolerance to Multiple Faults*," IEEE European Test Symposium, Avignon, France, 2013.
- O. Sarbishei, B. Nahill, A. Roshan Fekr, **M. Janidarmian**, K. Radecka, Z. Zilic, "*An Efficient Fault-Tolerant Sensor Fusion Algorithm for Accelerometers*," IEEE International Conference on Body Sensor Networks, Cambridge, USA, 2013.

Chapter 2

Background on Wearable Systems for Health Monitoring

It is predicted that the U.S. healthcare spending will reach $5.4 trillion by 2024, but the Healthcare System (HS) quality is far from optimal [43]. Recent advances in wearable sensor technology, telecommunication, and data analysis have permitted continuous capturing of physiological signals for subjects' status monitoring [44]. More than 120 million wearable sensors are projected to be sold by 2018 [45]. This number confirms that the wearable sensors opened up new possibilities to achieve a range of health outcomes. Accordingly, we need to take advantage of the collected signals and integrate them into computer-based clinical decision support systems. In addition to the sensors, haptic actuators have been widely integrated into the portable electronic devices. They provide different types of feedback in compliance with particular inputs. Due to various types and functions of portable devices, the scope of utilizing haptic actuators is enlarged day by day, and the number of haptic actuators employed in a single electronic device is gradually increasing. Considering the trend of sensors and haptic actuators, the outlook is that the wearable devices will evolve into the direction of developing new applications by using sensors for detecting biosignals and haptic actuators for providing biofeedback [46].

In this dissertation, we demonstrate the feasibility of wearable systems backed by robust machine learning models for extracting knowledge in real-life applications, ranging from activity recognition to breathing disorders diagnosis and treatment. We use mobile and wearable technologies to collect data from human's activities and respiration patterns. The raw data gathered by the sensors is valuable only when it is appropriately transformed and harnessed to reveal insights into human behavior and activities. However, we have recognized interoperability challenges related to the collection and processing of data from wearable devices.

This chapter provides an overview of the key development factors in the wearable collection systems to transform the sensory data to information and then to knowledge. We briefly discuss the challenges and potentials in sensing, transmission, storage, and processing. Each challenge depends on the application, for example, the data collection step should be specifically tailored for each case study. The sensor type and placement need to be properly selected for detecting a given movement or physiological phenomenon. Even a small sensor displacement may influence the outcomes of the previous models. This problem is often addressed by calibration or fusion of multiple sensors. This chapter continues with providing background materials necessary for the classification of the real-time data that will be thoroughly discussed in later chapters.

Each step in data stream assessments introduces some critical issues, which are considered in this thesis on a case-by-case basis.

2.1 Architecture of Wearable Collection Systems

As more wearable computing devices are brought to market, there is ample opportunity for improving the quality of life and reducing healthcare cost. The overview of the remote health monitoring system, where the data collected from body sensors is sent to a remote backend system for analysis and assessment, is presented in Figure 2.1. The main design criteria of the e-health systems [44] are also shown in this figure.

The goal of the wearable physiological measurement systems is to build decision-making paradigms to enhance the quality of life for chronic disease patients and the elderly, as well as healthy individuals. Such a system can affordably transmit patient's data even from locations, where medical support is not within reach, and receive specialist's real-time feedback on patient's progress. The wearable collection system is defined in three main layers to act as viable diagnostic tools to the healthcare personnel for monitoring vital signs and activities of the patients [47]. In the first layer, wireless body-worn sensors are used to collect motion signals and vital signs from users automatically. The sensors are commonly connected through a Body Sensor Network (BSN) while the central BSN node transfers the collected data to a mobile gateway via preferably a low-power and short-range wireless medium, for example, Bluetooth, ZigBee, ANT and Near Field Communications (NFC) [48], [49]. The wearable products can also send biometric data directly to the cloud via a Wi-Fi access point, but they require frequent battery charging. In the second layer, a mobile gateway such as a tablet or smartphone is responsible for delivering data to a cloud. The gateway performs limited processing before transmitting the data to the advanced processing platform and acts as a data entry interface and users' data dashboard for the healthcare provider or the user.

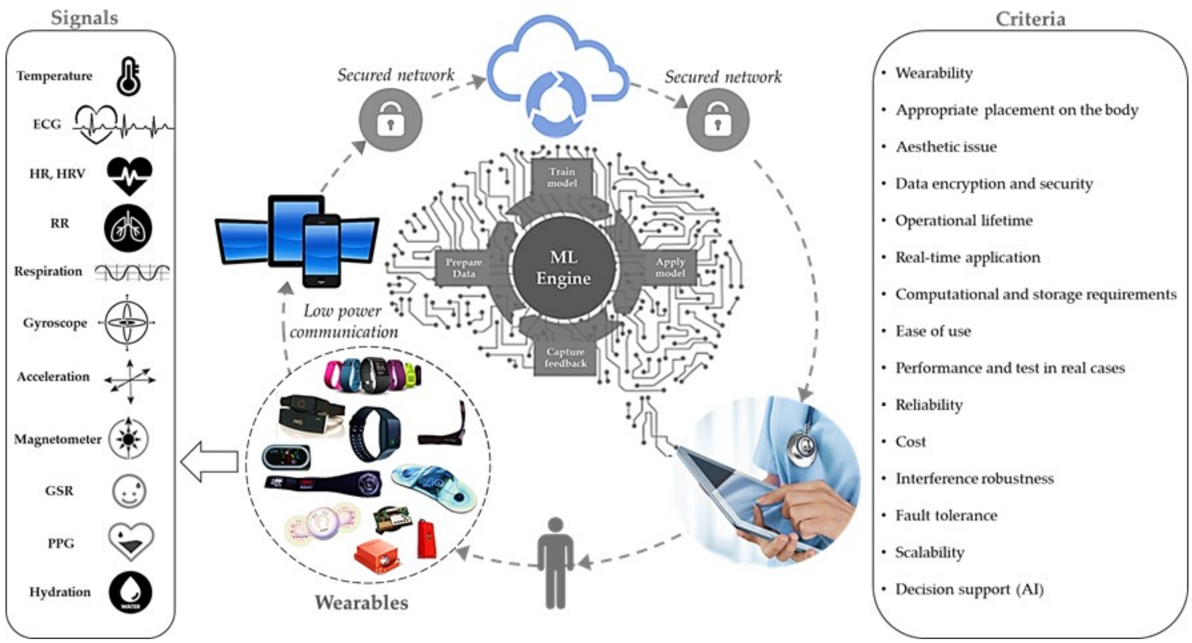

Figure 2.1: General overview of the remote health monitoring system and its criteria

The measurements are stored in the cloud, where the decision-making engine flags up any changes in a patient's condition, thus leading to a better understanding of people' status. The signal processing and decision algorithms can be also run on the gateway node e.g. smartphone. However, the gateway nodes with limited processing capabilities may fail to afford the necessary computing power to deploy machine learning techniques across growing datasets. The scalable cloud computing framework in the third layer provides on-demand computing capabilities and efficient storage on commodity hardware, thereby achieving flexible deployment environments for the analysis of large datasets [50]. Cloud computing is a great potential for tremendous innovations in healthcare using machine learning to deliver real-time personalized, predictive analytics. As described, the wearable collection system can employ the advances in sensing and computing with the ultimate goal to provide better healthcare at low cost.

2.2 Wearable Sensors

Nowadays, the wearable devices and smartphones equipped with a set of embedded sensors become the ubiquitous sensing and computing platform in people's daily life.

With the support of the mobile and wearable sensing devices, ubiquitous computing makes it possible to construct a patient-centered model to effortlessly deliver personalized healthcare in our everyday lives, regardless of space and time [51].

State-of-the-art wearable sensors have been broadly used during the recent years in research for capturing diverse physiological signals including electroencephalogram (ECG), Heart Rate (HR), Respiration Rate (RR), electrocardiogram (EEG), Galvanic Skin Response (GSR), arterial oxygen saturation (SpO2), Blood Glucose. In addition, Micro-Electro-Mechanical System (MEMS) based small sensors such as accelerometers, gyroscopes, and magnetic field sensors are widely used for measuring motion data in applications such as fall detection, gait pattern and sleep assessment [44], [52]. They progressively become more comfortable and less obtrusive for monitoring an individual's health or wellness without disturbing their daily activities.

A variety of application-specific wearable sensors, physiological, and activity monitoring systems were proposed in the literature as listed in Table 2.1. Apart from that, various wearable commercial products are now available on the market. The *fitbit* [72], for activity assessments, the *Zeo Sleep Monitor* [73], for sleep disorders analysis, and the *Zephyr Bioharness* [74], for reporting biometrics from medical-grade ECG, HR, and RR to motion, are some examples of commercial health monitoring devices. The *Visi Mobile* [75] is a wearable device worn around the wrist, which allows clinicians to check for the patients' vital signs such as ECG, HR, BP, RR, and body temperature at any given moment. The *Zio Patch* by iRhythm [76] is an FDA-cleared device for detection of infrequent or asymptomatic arrhythmias. *Equivital LifeMonitor* [77] provides the acceleration data along with other metrics such as GSR, SpO2, or geopositioning. Table 2.2 provides the details on these commercial devices that help people maintain their energy balance and stay physically fit and healthy.

Table 2.1: Some examples of physiological and activity monitoring systems proposed in the literature

Ref.	Monitored Signals	Type of Sensor	Connectivity	Sampling Rate	Description
[53]	**ECG + Heart Rate**	Dry foam electrode that detects the electrical changes on the skin	Bluetooth v2.0, and GSM	512Hz	99.51% correlation with pre-recorded reference ECG data, QRS detection accuracy about 98.14%.
[54]		Dry textile electrodes _ Snap buttons	Bluetooth Low Energy	512Hz	Sensorized T-shirt and textile belt tested both in the laboratory and with elderly people.
[55]		Active capacitive electrodes_ Adhesive tape with no gel	NA	2KHz	Common Electrode-Free ECG monitoring System has been evaluated, and the feasibility of it has been proved.
[30]	**Respiration Signal + Respiration Rate**	Accelerometer on the chest wall	Bluetooth Low Energy	50Hz	Error in respiration rate calculation is obtained 0.53% considering SPR-BTA spirometer as the reference. The respiration waveform has more than 80% correlation versus the reference.
[56]		Piezoelectric respiration transducer in a belt around chest	WiFi or GSM/GPRS	10Hz	The wireless breathing system described in this paper is composed of a wireless breathing module attached to the patient, a monitoring device for displaying the signals and processing data, telemonitoring server and terminal monitors.
[57]		Accelerometer on the suprasternal notch	Wired	2KHz	Respiration rate estimated by error 1.55% with correlation coefficient 0.88 ± 0.09 versus spirometer.
[57]		Strain Gauge	Wired	2KHz	Respiration rate estimated by error 4.9% with correlation coefficient 0.68 ± 0.21.
[58]		Microphone	Wired	NA	The respiratory waveform was obtained by using a piezoelectric respiration transducer vs. pneumotach on trachea at the level of the thyroid cartilage. The tidal volume was estimated in different positions with an error of 13.2% ± 8%.
[59]	**Temperature (body and skin)**	Digital temperature sensor DS18B20	Bluetooth	in 750ms	This study showed the feasibility of obtaining body temperature from a dual channel body temperature measurements placed within the left and right ear canals.

[60]		TI LM35	ZigBee and WLAN	NA	Skin temperature has been measured from the hand with an error of 0.37%.
[61]		EM4325	Wireless	780-950 MHz band	A prototype of the stretched epidermal RFID temperature sensor over poli ε-caprolacton membrane was proposed.
[62]	**Galvanic Skin Response (GSR)**	Conductive fabric with Ag/AgCl electrodes	Radio Transceiver 2.4 GHz	32Hz	Small wristband for continuous EDA measurements during everyday activities was proposed with overall correlation 93%-99%.
[63]		Conductive polymer foam	Bluetooth	NA	Wearable and reliable GSR sensor are worn on the back and compared to a finger reference GSR with an average correlation of 76.8%.
[64]		Ag/AgCl electrodes in Shimmer System	Bluetooth	30Hz	Wearable sensors to measure the autonomic function and stress level in the ambulatory setting from the palm of the non-dominant hand.
[65]	**SpO2**	Reflectance oximetry	ZigBee	240Hz	A small, low-cost pulse oximeter design appropriate for wearable and surface-based applications was proposed. The design's "filter-free" embodiment distinguishes it from conventional pulse oximeters that incorporate filters for signal extraction and noise reduction.
[66]		Reflectance oximetry	CC2500 RF TRX	NA	This paper proposed a wristband pulse oximeter that offers an effective means of home monitoring oxygen saturation.
[67]		Reflectance oximetry	Wi-Fi	NA	The Sensor Module was placed on the forehead using an elastic headband. The preliminary bench testing showed that the SpO2 and HR readings are within an acceptable clinical range.
[68]		Reflectance oximetry	Both wired and wireless	125Hz	This paper proposed an electronic patch with an optical biomedical sensor attached on the third digit of the left hand.
[69]		accelerometer (Shimmer)	Bluetooth	52Hz	The sensor is attached to the chest of the subjects. The activity types include: walking, walking and talking, standing, standing up, talking while standing, going up/down stairs, etc.

[70]	**Motion signal + Activity**	accelerometer gyroscope (MotionNode)	Wired	100Hz	There were five trials for each activity, and each subject performed the experiments on different days at indoor and outdoor places.
[71]		accelerometer gyroscope magnetometer (Xsens MTx unit)	Bluetooth	50Hz	The dataset includes a broad range of physical activities (warm up, cool down and fitness exercises). The sensors are placed on the right and left calves, right and left thighs, back, right and left lower arms and right, left upper arms.

Table 2.2: Some examples of commercial health monitoring devices

Devices / **Information**					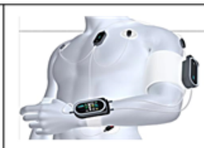			
Device names	Fitbit Alta HR, charge 2	Zoe Sleep Monitor	Zephyr Bioharness 3	Zephyr BioPatch	Visi Mobile from Sotera Wireless, Inc.	ZIO XT patch form iRhythm technologies Inc.	Equivital	E4 wristband from Empatica Co.
Monitored signals	3-axis Acceleration, PPG	EEG	3-axis Acceleration, single channel ECG, Pressure sensor for respiration rate	3-axis Acceleration, single channel ECG, impedance based respiration signal	3-5 channels ECG, impedance based respiration signal, Temperature, SpO2 waveform,	single channel ECG	2-leads ECG, Respiration, 3-axis accelerometer, GPS, Temperature, SpO2	3-axis Acceleration, Infrared Thermopile, GSR Sensor, PPG,
Placement	Wrist	Adjustable headband	Over the torso	Left side of upper chest	Wrist + chest	Chest	Chest	Wrist
Cost	~$200	~$40	~$700	~$500	NA	~$200	NA	$1,690.00
FDA	No	No	No	Yes	Yes	Yes	Yes	Yes
Functions	Heart rate, steps taken, distance traveled, floors climbed, active minutes, exercise, calories burned, and how long and how well the user sleeps.	Smart alarm clock with sleep monitor	Real time monitoring of heart rate, breathing rate, position/posture, Activity (Stationary, walk, run)	ECG Heart Rate Respiration Posture and Activity Monitor	Heart Rate, Pulse Rate, Respiration Rate, Continuous Non-Invasive Blood Pressure, and Skin Temperature	Small, adhesive, water-resistant sensor that can be worn for 24-hour monitoring over 2 weeks. It is used for arrhythmia diagnosis	Heart rate; R-R interval, Respiratory rate; -Skin temperature; Body position; Motion status; Fall alert	Real time monitoring of physiological data

In this thesis, we make use of accelerometer sensors, which are among cheap, small, and low-power nodes and can deliver rich information, especially in movement analysis applications.

2.2.1 Accelerometer Sensor

For motion capture, the previous systems can be mainly categorized as acoustic tracking, mechanical, magnetic and optical systems. The acoustic tracking system uses ultrasonic pulses. The position is determined through time-of-flight of the pulse and accuracy is vulnerable to the reflection of sound [78]. Mechanical systems are expensive, and uncomfortable to wear and can potentially impede the motion. The magnetic fields can be easily disturbed by magnetic materials nearby and rapidly reduce in power while using the magnetic system for capturing the motions. In optical motion capture system, reflective markers, or light-emitting diodes are placed in the subject's body, and the exact 3D marker locations are computed from the images recorded by the surrounding cameras [79]. However, cost and portability are the main concerns of this approach. Resistive sensors such as flex sensors and pressure sensors can be also utilized for specific motion applications. They have different resistance outputs when deformed or pressed with some forces.

In the recent years, MEMS inertial sensors, especially accelerometers, have been attached to the body or embedded in most fitness trackers to monitor the wearer's body movements. An accelerometer measures both dynamic and static accelerations, where dynamic acceleration is due to any force applied to a rigid body and the static acceleration is due to the gravitational force. The output of an accelerometer can be an analog voltage or digital signal whose duty cycles are proportional to the acceleration [80]. Different specifications such as the number of axes, output range (±g), bandwidth (Hz), noise floor, sensitivity, drift, linearity, dynamic range, and power consumption define different accelerometers for a variety of practical purposes. Table 2.3 listed some of the common accelerometer sensors in wearable devices.

Table 2.3: Some examples of accelerometer sensors with their specifications

Accelerometer	Manufacturer	Acceleration Range	Sensitivity	Output Type	Output Data Rates (ODR) (Normal Mode)	Resolution	Zero-g Level Offset Accuracy	Output Noise
MMA8452Q	Freescale Semiconductor	±2g, 4g, 8g	1024 count/g, 512 count/g, 256 count/g (12 bit representation)	I²C	1.56 Hz to 800 Hz	12-bit/8-bit	±17 mg	126 μg/√Hz (99 μg/√Hz in Low Noise Mode) (ODR = 400 Hz)
MMA8451Q	Freescale Semiconductor	±2g, 4g, 8g	4096 count/g, 2048 count/g, 1024 count/g (14 bit representation)	I²C	1.56 Hz to 800 Hz	14-bit/8-bit	±17 mg	126 μg/√Hz (99 μg/√Hz in Low Noise Mode) (ODR = 400 Hz)
LSM303DLH	STMicroelectronics	±2g, 4g, 8g	1024 count/g, 512 count/g, 256 count/g (12 bit representation)	I²C	50/100/ 400/1000 Hz	16-bit	±20 mg	218 μg/√Hz
KXTJ9	Kionix	±2g, 4g, 8g	1024 count/g, 512 count/g, 256 count/g (12 bit representation)	I²C	0.781 Hz to 1600 Hz	14-bit/12-bit/8-bit	±25 mg	275 μg / √Hz
LIS3DH	STMicroelectronics	±2g, 4g, 8g, 16g	1 mg/digit, 2 mg/digit, 4 mg/digit, 12 mg/digit	I²C, SPI	1/10/25/50/100 200/400/1025 Hz	16-bit	±40 mg	220 μg / √Hz (ODR = 100 Hz)
LIS331DLH	STMicroelectronics	±2g, 4g, 8g	1 mg/digit, 2 mg/digit, 3.9 mg/digit	I²C, SPI	50/100/ 400/1000 Hz	16-bit	±20 mg	218 μg / √Hz (ODR = 100 Hz)

2.2.2 Sensor Placement

The number and locations of wearable sensors on the body drastically influence the learning algorithm performance. More sensors worn on the body and optimal positions improve the classification accuracy and knowledge quality. However, the usability, wearability, and intrusiveness concerns should be also considered while still ensuring a sufficiently high performance.

In real-world applications, having fewer sensors attached to the body is preferable since wearing multiple ones can become burdensome. In addition, fewer sensors can be affordably deployed and require lower computational requirements. In case of wearing the sensors for a long time, their placements should be comfortable and socially accepted. For minimal usability burden, integration of the sensors into smartphones, existing clothing, or devices already worn such as watches and shoes is preferable. The optimal sensor placement for increasing the quality of algorithms is still a subject of much debate. For example, the impact of sensor placement has been evaluated in [8], and the results show that trunk/torso and head are the most efficient and effective placement sites for fall detection and posture analysis. They found that the wrist is not an efficient position to distinguish between falls and daily activity accurately, because it produces many high acceleration movements and consequently measured signals widely vary [81].

As in this thesis we concentrate on accelerometer sensor, we also need to keep in mind that the sensors should be firmly attached to the body; otherwise, potential errors could be expected under the event of sensor displacements. Loose-fitting garments or accessories are subject to placement drifts during their use (e.g., a bracelet moves from the wrist to the elbow) [82].

2.2.3 Sensor Fusion

The current sensing system specifications require high accuracies, as well as tolerance to external noise and potential faults [83]. Numerous research studies have aimed to improve such parameters in sensing systems [84], [85]. Multi-sensor data fusion [86], [87] is also a common approach, which combines data from multiple sensors to obtain more accurate readouts compared to the case, where a single sensor is used [88]-[90]. Sensor fusion can be used to detect faulty sensors [90] as well as to deliver fault-tolerant measurements. Considering the reliability issue is crucial since the technology trends show that sensing has by far the highest fault rates [92], [93]. Furthermore, high-risk applications such as medical and control necessitate delivering fault tolerant sensor readouts in real time.

We can define three levels of fusion for classification problem [94]. In the low-level fusion, the raw data from multiple sources is combined to produce new data that is expected to be more informative than the inputs. The fusion at this level generally includes the actual combination of sensory information into one representational format. For example, the proposed approach [95] used convex optimization to find the coefficients to the data fusion process with accelerometers data. The intermediate-level fusion is called feature fusion, where various features are combined meaning the synergistic use of sensor data for the completion of a classification task. The feature fusion is the most common fusion level in sensor-based classification, where the heterogeneous sensors can be also integrated to provide complementary information to improve the recognition performance [96]. In case of using multiple learning algorithms, the last level that is called decision fusion combines decisions from several classifiers using voting, fuzzy-logic, or statistical methods. Some heterogeneous sensors cannot be fused at the feature level due to the compatibility issues arising from different time shift, window length configurations, and different sampling frequencies.

It is worth mentioning that, the fusion of heterogeneous raw data can provide new useful information, for instance, the joint angle can be accurately calculated by fusion of accelerometer and gyroscope sensors. It is crucial to efficiently track of rotational and translational body movements in many applications such as rehabilitation exercises [99]. Accelerometer or gyroscope alone cannot provide an absolute measurement of

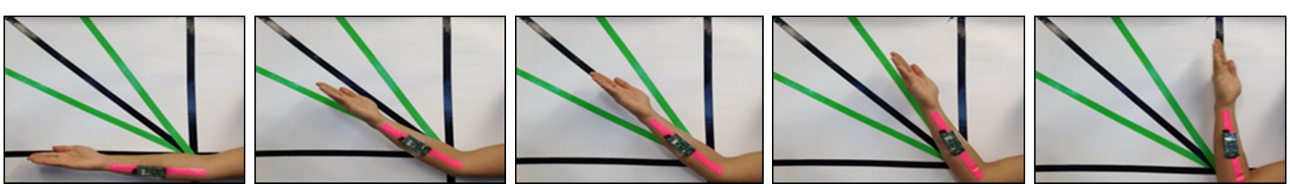

Figure 2.2: Elbow motions

orientation [97]. For a non-moving object, the pitch and roll angles can be obtained with 3-axis accelerometer. However, the orientation is not valid if the sensory node moves due to the consequence of a force and so the calculated orientation is not accurate anymore. A gyroscope that gives angular rate around the three axes cannot be used alone as it suffers from drifting values and the integration of its measurement errors will lead to an accumulating error in the calculated orientation.

An optimal fusion of measurements data is presented in [97] based on a Newton optimization using an analytic formulation of the gradient that is derived from a quaternion representation of motion. This method can precisely simulate a goniometer functionality in different applications such as rehabilitation therapy and diagnosis of knee abnormalities [98]. As presented in [99], the goniometer functionality is accurately achieved by using sensor-based orientation technique and is useful for people who suffer a motor function disability and need to practice appropriate rehabilitation treatments. Figure 2.2 shows a sample of rehabilitation practice, where the subject's elbow flexes from 0° to 30°, 45°, 60° and 90°. The fusion of KXTJ9 tri-axis accelerometer and IMU-3000 tri-axis gyroscope are employed in estimating the orientation of the SensorTag [100] device worn on the forearm.

2.2.4 Communication Technologies

In most wearable systems, there is a short-range communication to transfer the measured data to a gateway node such as a smartphone, tablet, or a customized processing board over a wireless medium. The gateway is responsible for some data processing, display and transmitting the processed data to a remote server. In case of using multiple sensors on the body, a central Body Sensor Network (BSN) node commonly collects data from the sensors using wired, wireless medium or conductive fabric yarns integrated into clothing [101].

To transmit data to a gateway, there are various communication protocols available for use in wearables, including Bluetooth Classic and Wi-Fi. These standards have not been designed with low power to satisfy the primary design consideration in wearable systems. Bluetooth Low Energy (BLE) as an ultralow-power version of Bluetooth technology was introduced to achieve the lower power for short-range communication. BLE that operates in the 2.4 GHz band supports only 40 channels in comparison to Bluetooth's 79 channels [102]. It is the most used technology for portable and wearable devices with limited battery capacity [103]. The standard range for BLE is about 10 meters and up to 100 meters at maximum power with a clear path. It offers low power wireless connectivity (<10mW for range up to 10m) and, thereby is a convincing candidate for short-range communication. The peer-to-peer communicating mode is the most common; however, Bluetooth is also capable of communicating with seven slave devices, called piconets. In addition, the portable devices have long been equipped with a dual transceiver supporting both standard Bluetooth and BLE.

As an alternative to Bluetooth, ANT, and ANT+ are proprietary ultra-low-power wireless sensor network, technologies that primarily used in the healthcare, telemedicine, sport, and fitness sectors. ANT is already integrated into modern smartphones and tablets, such as the Sony Xperia or Samsung's S4 and Galaxy. The technology divides the 2.4 GHz industrial, scientific, and medical band into 1-MHz channels. A Time Division Multiplexing (TDM) scheme accommodates multiple sensors. ANT+ supports multiple network topologies such as star, tree, mesh, and peer-to-peer topologies. ZigBee is an open wireless standard that uses the Physical and MAC layer specifications of IEEE 802.15.4 and its own network, security and application layers [102]. It provides a complete protocol stack designed to implement multiple types of radio networks that include P2P, star, tree and mesh network topologies. ZigBee can reach maximum 250 kbps for the 2.4 GHz band that is lower compared to the data rate of Bluetooth technology [104]. Some other technologies such as Medical Implant Communication Service (MICS) and Ultra-Wide Band (UWB) are impractical for wearable systems due to their range of transmission and limited availability in the commercial systems [52].

Wi-Fi is a common way to connect mobile devices or even sensors to the cloud. In case of no available accessible Wi-Fi router, cellular networks can offer seamless access to the internet through 3G, High Speed Packet Access (HSPA), General Packet Radio Service (GPRS), Enhanced Data GSM Environment (EDGE) and Long-Term Evolution (LTE) services [105], [106]. In our experiments, we used SensorTag from Texas Instruments [100] and cB-OLP425 from u-blox [107] to capture accelerometer data. Both systems are equipped with The CC254X that is a power-optimized system-on-chip (SoC) solution for Bluetooth Low Energy (BLE).

2.2.5 Cloud Storage and Computing

A wearable sensor collects an enormous amount of raw data about physical behavior and the physical states of users. However, it is very difficult to manage, store, and process raw data in real time or near-real time. Due to limited storage, computational, and energy resources, the mobile gateways have to exploit cutting-edge cloud services in order to complete the tasks at an optimal level. Data aggregated by the gateway needs to be transferred to the cloud for long-term storage and further complex processing. Logging the data on the cloud makes it possible for the physicians to track their patients wherever they are with devices such as an iPhone, iPad or the web regardless of their proximity to the patients. Therefore, offloading data storage to the cloud offers significant advantages over traditional methods, including increased scalability and accessibility on demand, by both patients and clinical institutions.

The rich datasets of sensors data represent a great opportunity for data analytics to extract hidden tendencies and conditions. The machine learning techniques are now commonly available as toolboxes in several software packages [108]-[110]. In addition, we can easily integrate the power of machine learning into our applications with computing services provided by cloud providers. Many companies such as IBM, Amazon, Microsoft, and Google, now offer machine learning as a service on top of their existing cloud services. Thus, the trained model is immediately available for use and can support thousands of users and TBs of data.

The two main concerns using cloud computing in healthcare are safety/security of data as a threat to privacy, and reliability and transparency of data handling by third parties [111]. Privacy is of very importance while storing individual's health data on the cloud. According to the terms defined by Health Insurance Portability and Accountability Act (HIPAA), the cloud providers' healthcare products should protect patients' data and meet FDA Code of Federal Regulations compliance requirements [112]. Appropriate privacy preserving measures need to be taken to avoid unauthorized parties from retrieving the information when the medical records and sensors data are outsourced to the secure cloud for storage and processing.

2.2.6 Machine Learning Engine

Recent improvements in signal processing and machine learning tools have taken wearable data to the next level from the simple reasoning of sensor readings (e.g. the number of steps per day or sleep hours) to the higher level of data processing. The classification, where a decision-making process is made to categorize the data into different groups is one of the main types of data mining tasks to have deeper knowledge representation. In this thesis, we mainly focus on sensor-based classification and data-driven approaches to provide a more stable and robust decision-making techniques. Figure 2.3 shows the main steps of sensor data classification. We employ the effective approach of dividing the sensor data into segments, converting each segment into a feature vector, and considering each feature vector as a training instance for a supervised

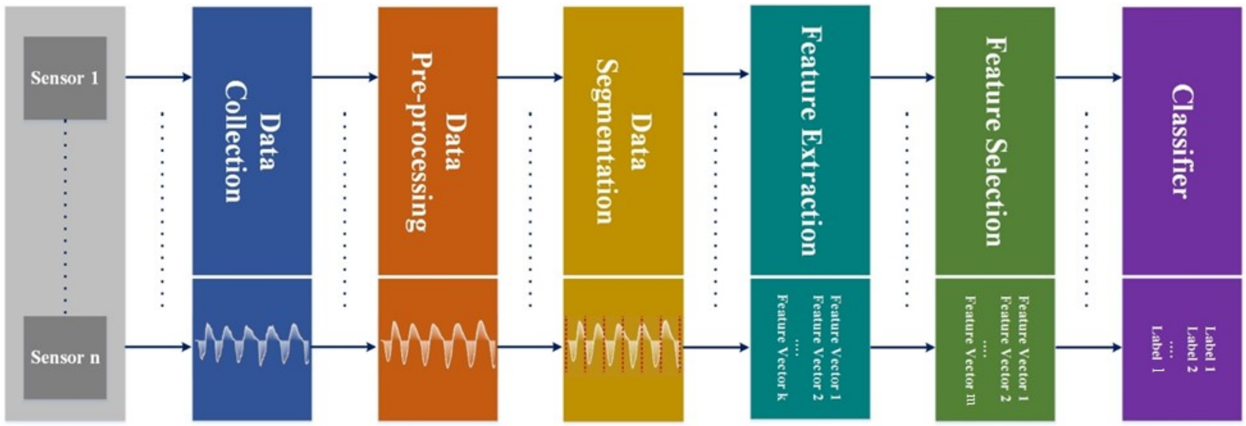

Figure 2.3: Main steps of sensors data analysis and classification

learning algorithm. In the following sections, we outline the most common approaches used with wearable sensor data to deliver valuable information. Each step varies based on the problem. We will bring all details of each step later when we describe our experiments.

2.2.6.1 Data Collection

The acquisition process comprises the measurement of the physical phenomena, conversion to electrical signals and encoding into machine-readable digital data to be processed by computers [113]. Sensor data is sampled at different frequencies, which is a trade-off between power consumption and acquiring enough signal data [8]. Unnecessary noise and anomalies are captured if the sampling rate is selected more than sufficient for the given application. On the other side, the samples should not be recorded at a very low frequency to lose the necessary data [114]. Bouten *et al.* [115] stated that the frequency of human behavior by voluntary muscular work is under 20Hz; therefore, the sampling rate of around 50Hz is adequate for tilt or human motion sensing.

Most studies have been conducted in lab conditions and provided very promising results. However, the applicability of these results to out-of-lab monitoring is unclear. A realistic assessment of movements and disorders can be derived from the continuous out-of-lab settings. In the free-living environment, there is no continuous supervision from experts or researchers. Therefore, sensor-based features are susceptible to variation from different sources such as mounting uncertainty and physiological variation, which are challenging to control or estimate [116]. For example, the factors such as mood, types of shoe, terrain, and energy levels significantly affect the gait speed analysis [117]. As we work with accelerometer sensors in this thesis, they are sensitive to orientation changes, and mounting location shifts can cause significant variations in the sensor data. Therefore, various naturalistic circumstances should be considered to account for sources of variation in wearable data, thus alleviating the adverse effect of sensors displacements, biases, and motion artifacts.

2.2.6.2 Data Preprocessing

The main data preprocessing stages are signal filtering, sensor calibration and handling missing data points. The use of various filters reduces the measurements corruption introduced by instrumentation noise, random noise, electric and magnetic noise, or artifact [8]. The most common used filters for de-noising wearable sensors data are Savitzky–Golay smoothing, median, Butterworth low-pass and Kalman filters [118]. The preprocessing step plays an increasingly important role especially when we analyze the signal itself such as breathing patterns. Different studies [82] show that the raw sensor readings can be utilized for the activity recognition or diagnosis systems, as the filtering does not significantly effect on the features extracted from each window of data. Capturing data directly through the sensors allows us to focus on the potential impact of the new feature extraction effects.

The accelerometer sensors are subject to degradation and damage due to inherent deficiency or aging problems. Calibration, which is defined as the process of mapping raw sensor readings into corrected values, can be used to compensate the systematic offset and gain [119]. Calibration of sensors requires experience and special accurate tools; however, a straightforward method to calibrate accelerometer is performed at six stationary positions [120]. The misalignment of the sensor in these stationary positions will influence the calibration procedure. Therefore, in our experiments to collect the breathing signals in chapters 4 and 5, we use two boxes and a goniometer to help fix the module in different positions to obtain stable acceleration measures. In our setting, the boxes are put on a flat surface, the module is placed between two boxes, where it faces of one box, and the other box is used to stop the module from gliding. The two boxes keep the module in a stationary position determined by the goniometer for at least 10 seconds. Then the least square method is applied to obtain the 12 calibration parameters. The calibration procedure is simple, and needs to be executed once and can be briefly explained as:

$$[A_{x\prime}, A_{y\prime} A_{z\prime}] = [A_x \; A_y A_z \; 1]. \begin{bmatrix} ACC_{11} \; ACC_{21} ACC_{31} \\ ACC_{12} \; ACC_{22} ACC_{32} \\ ACC_{13} \; ACC_{23} ACC_{33} \\ ACC_{10} \; ACC_{20} ACC_{30} \end{bmatrix} \tag{2-1}$$

$$Y = w.X \tag{2-2}$$

Where:

- Matrix X is the 12 calibration parameters that are determined as below:

$$X = [w^T.w]^{-1}.w^T.Y \tag{2-3}$$

- Matrix w is accelerator sensor raw data collected at six stationary positions
- Matrix Y is the known normalized Earth gravity vector.

We used this calibration method in different studies [30], [99]. In case of multiple sensors, a blind calibration method can be also applied to find the optimum reference [121]. The multi-sensor self-calibration is critical especially in applications that deal with high risks such as patients’ health.

Regarding the accelerometer sensor, the calibration process can be continued by comparing the calibrated sensor readouts with reference values obtained from a high-speed camera [95]. For example, as shown in Figure 2.4, we designed a system of five MMA8451Q 3-axis accelerometers on FRDM-KL25Z development boards [122] that are placed and fixed with identical positions on the train model. Accelerometers are networked together and synchronized by the STM32F4 board [123]. The accelerometers sample 14-bit readings at 800Hz. They deliver 32-sample packets using a Serial Peripheral Interface to the STM32F4 board, which buffers them in its SRAM for later delivery to a PC over USB interface. Ball bearings are used as wheels to ensure smooth travel on the track. The filtered acceleration measurements were compared with the values measured by CASIO EX-F1 camera reading 1200 frames per second. After performing the linear least-square curve fitting approach to match calibrated sensor readouts and reference accelerations, the post-calibration parameters that are important in multi-sensor fusion can be also computed.

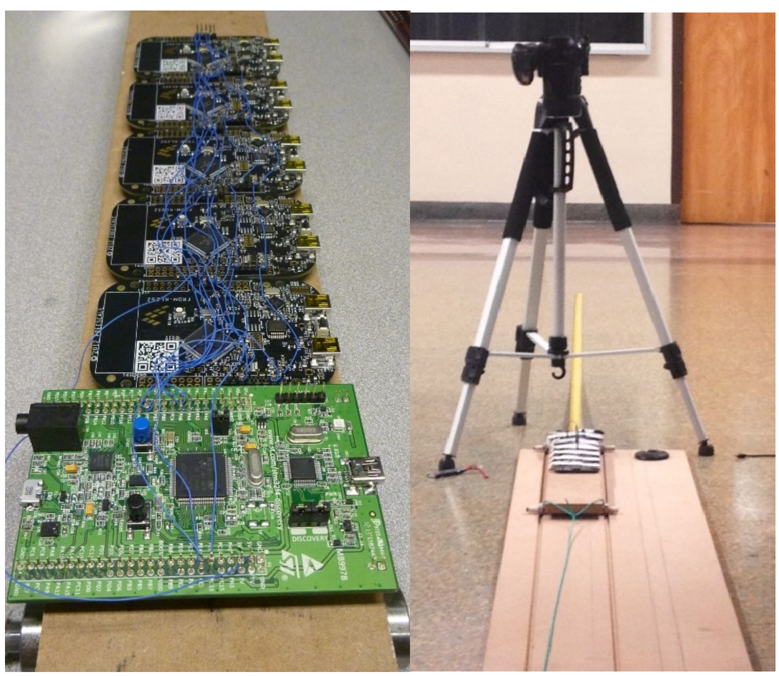

Figure 2.4: System configuration with accelerometers: (a) STM32F4 board and sensor network on the test platform (train) (b) The test platform being monitored by CASIO EX-F1 high-speed camera

2.2.6.3 Data Segmentation

In this thesis, we deal with stream sensors data, and hence data segmentation is a requirement for feature extraction. There are diverse segmentation techniques including Fixed-size Non-overlapping Sliding Window (FNSW), Fixed-size Overlapping Sliding Window (FOSW), Bottom-UP (BUp), Top-Down (ToD), Sliding Window and Bottom-up (SWAB), and Variable-size Sliding Window (VSW) [124]. The most employed segmentation technique is FNSW that partitions a time series into windows of consecutive samples [8]. The window size is a major factor in data analysis and classification performance and should be large enough to contain a span of the target event. From activity recognition point of view, a wide range of window sizes has been used in previous studies from 0.5s to more than 15s [125]. In addition, the use of overlap between successive sliding windows helps the classifiers to be trained by more feature vectors that improve the recognition performance [126].

2.2.6.4 Feature Extraction

Feature extraction is to obtain the essential characteristics of a data and represent them into a set of features [127]. Machine learning techniques need informative feature representation of the data to yield accurate predictions and comprehensive insights. The select of features with high information content for classification purpose is a key phase and a highly problem-dependent task. The features are extracted from each separate window of data and then used as the inputs to the classifiers. For example, the features extracted from 3-axis accelerometer sensor are normally combined into a single feature vector. Signal characteristics such as time-domain and frequency-domain features are widely used in the feature calculation. Time-domain features include mean, median, variance, standard deviation, minimum, maximum, skewness, kurtosis, range, etc. Peak frequency, FFT peak, spectral entropy, and spectral power on different frequency bands

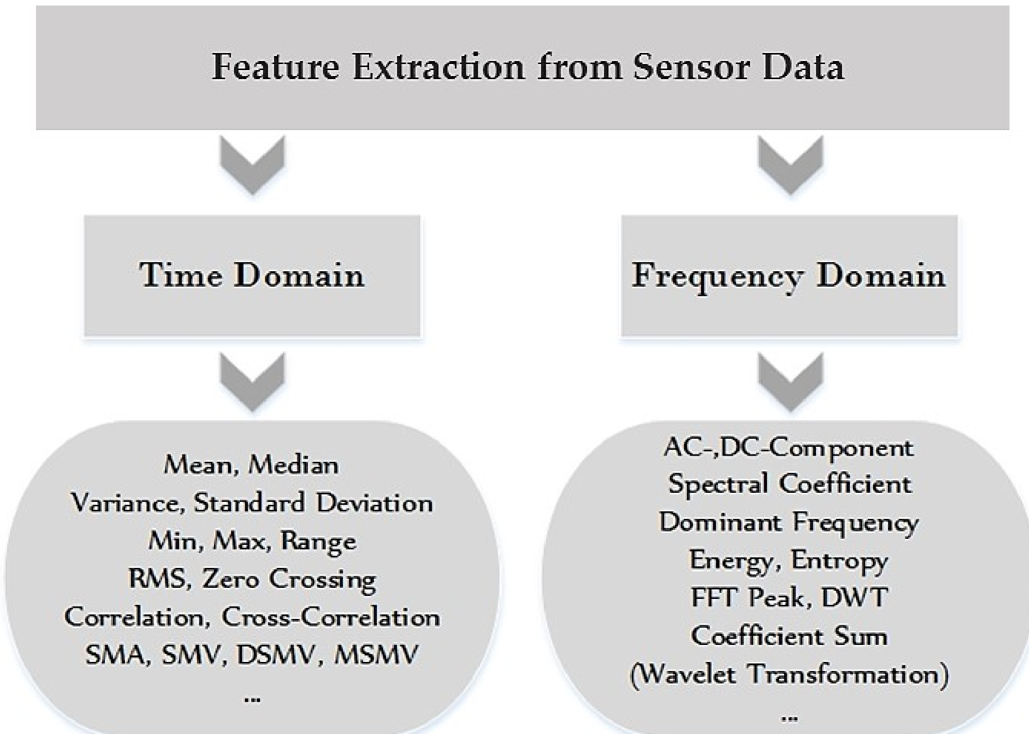

Figure 2.5: Feature extraction methods

are generally included in the frequency-domain features. Figure 2.5 shows the most common time, and frequency domain features to be extracted from wearable sensors data [128].

It is worth to noting that, when the range of feature values widely varies, some classifiers such as k-nearest neighbor, which is based the distance between two points, cannot provide accurate predictions. To overcome this issue, rescaling the range of features is used. If f is an original value, the normalized value f' (in range [0, 1]) is:

$$f' = \frac{f - \min(f)}{\max(f) - \min(f)} \tag{2-4}$$

2.2.6.5 Feature Selection

The problem of decreasing the dimension of the features list to improve performance and most likely accuracy is called feature selection. The classifier performance will be reduced by using the irrelevant features. Apparently, the feature space with higher

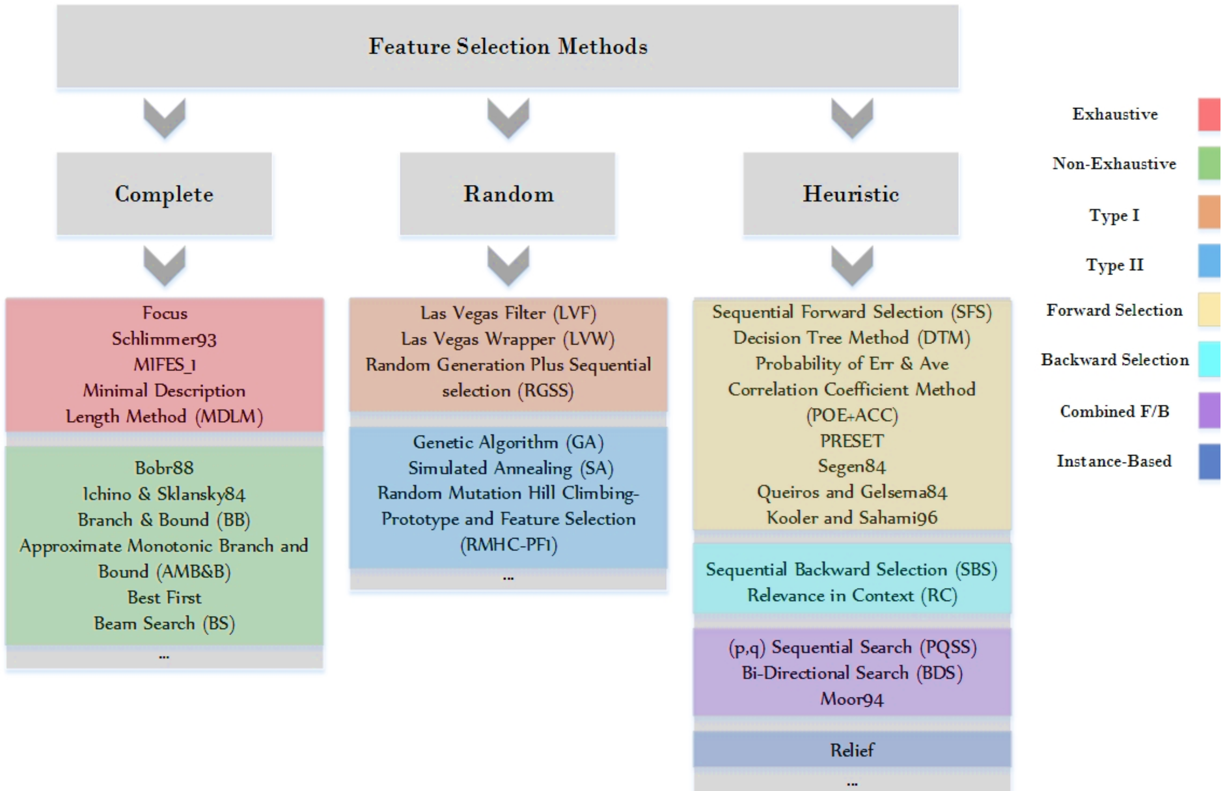

Figure 2.6: Feature Selection Methods

dimension needs more computation for reasoning process. In [129], the feature selection algorithms are categorized into three ways i.e. complete, heuristic, and random. The complete or exhaustive category includes algorithms, which examine all combination of feature subset. The order of search space is $O(2^P)$, where P is the number of features. However, as discussed in [130], a complete search can be non- exhaustive without jeopardizing the chances of finding the optimal subset such as Branch & Bound algorithm. In the heuristic techniques, the selection is directed under certain guideline and optimal subset may not be achieved. However, the search space is smaller and faster than complete methods and generation of subsets is incremental. In random category, there is no predefined way to select feature candidate, and features are picked at random e.g. based on a probabilistic approach. In each random generation procedure, some input parameters should be carefully assigned for achieving good results [130].

Figure 2.6 listed the most well-known feature selection techniques. Moreover, feature transformation methods such as Principal Component Analysis can be also utilized to transform a set of features into a projection of the feature space that has lower dimensionality. PCA linearly transforms predictors to remove less descriptive features and generates a new set of variables called principal components. This method is very common in sensor-based classification to reduce the size of the original feature space without losing redundant information [131].

2.2.6.6 Classification

In this dissertation, the learning models are trained and tested with the instances labeled by human and hence they fall into the category of supervised learning. The primary goal of a supervised ML is to mathematically map feature vectors into their corresponding labels, and store the predictor model for future predictions. The trained ML model identifies a new observation, or instance belongs to which class. Various machine learning approaches are used in this study to build predictive models from labeled sensors data. For example, Naive Bayes (NB) uses the Bayes theorem to predict the class with the highest probability given a label-feature probabilistic relationship [132]. Support Vector Machine (SVM) relies on finding optimal separating decision hyperplanes between classes with the maximum margin between patterns of each class. The key advantage of this classifier is the ability to minimize both structural and empirical risks [133]. These properties make SVM to be a strong generalization for new data classification even in case of limited training dataset [30].

Neural Network (NN), inspired from simulation of the biological nervous system in the human brain, is based on propagating activation signals and encoding knowledge in the network links. A multilayer perceptron uses back propagations to train a neural network structure that minimizes an objective cost function and predicts the label of new data instances through forward propagation. The data is propagated through successive layers, and the result is available at the output layer [134]. An ensemble method describes rules for a meta-learner to build a predictive model by integrating multiple models [135]. It is well known that ensemble methods can be used for improving prediction performance. For instance, AdaBoost is the most widely used boosting algorithm, which trains learners sequentially and requires the weak learner to output an array of confidences associated with each possible labeling of an example. This process is based on increasing the weight of previously misclassified data instances [136]. A large number of classification techniques will be described and compared in later chapters.

2.2.7 Feedback through Wearable Haptic

Recently, the wearable haptic (touch) feedback devices have been shown to be particularly effective for notifying humans to move in new ways. In many applications such as physical therapy [137], there is a need to guide and correct the user's movements until the ideal practice is achieved. By integration of real-time motion sensing and haptic feedback, humans can be trained to move in correct ways that, increase athletic performance, prevent injury, treat musculoskeletal or neurological disease. The resulting system is expected to adapt to each user's needs by determining how the user should move when practicing a predefined movement. Therefore, in the training process on motor skills, if the user performs the movement very well, he/she can receive a weak vibration. In turn, if the user performs the movement in an incorrect way, the system can generate some force so that the user identifies resistance to that movement.

Different studies show that vibrotactile devices are an appropriate means of delivering instant feedback for motor learning [138]. For instance, Ma *et al.* [139] demonstrated the potential of applying wearable sensors and biofeedback to enhance static and dynamic balance performance in elderly and patients. Many studies have shown that real-time feedback can be used to train relatively faster movements such as gait [36], [141], [142]. Another research study presented a wearable automatic feedback device for assisting people during daily physical activities and for supporting instructors and students during sports training [143]. These systems are supposed to detect harmful and incorrect posture and movements using body-worn sensors and to provide tactile feedback for corrections with actuators placed at key positions across the body.

No attempt has been made to investigate the use of haptic feedback and motion sensor data in yogic breathing practices, where the small movements of the chest wall are sensed with a wearable accelerometer. This kind of system involves data collection from an accelerometer sensor, real-time analysis of collected data and triggering a response at the corresponding user interface. There are some mobile applications currently available, which are implemented to guide the breath to support mindfulness meditation and paced breathing practices. They mainly focused on audio/visual cues, rather than haptic cues [144]. Therefore, in chapter 5, we will discuss the value of vibrotactile feedback to support the learning of a correct way of breathing.

Chapter 3

Comprehensive Analysis of Human Activity Recognition

Advances in miniaturization permit accelerometer sensor, which can offer us acceleration and velocity information, to be easily embedded into personal carry-on devices and apparels. Sensor-based motion recognition integrates the emerging area of wearable sensors with novel machine learning techniques to make sense of low-level sensor data and provide rich contextual information in a real-life application, ranging from pervasive computing and security to ambient-assisted living systems, medical diagnosis, and treatment. Although Human Activity Recognition (HAR) problem has been drawing the attention of researchers, it is still a subject of much debate due to the diverse nature of human activities and their tracking methods. Finding the best predictive model for this problem can be very difficult to analyze theoretically, which stresses the need of an experimental study. Therefore, in this chapter, we first create the most complete dataset, focusing on accelerometer sensors, with various sources of heterogeneities. In total, accelerometer data from 228 subjects as they performed activities such as walking, jogging, running, cycling, sitting, standing, lying down, ascending, and descending stairs has been exploited. We then conduct an extensive analysis on feature representations and classification techniques (the most comprehensive comparison yet with 293 classifiers) for activity recognition. Principal component analysis is applied to reduce the feature vector dimension while keeping most of the data information. Our work presents significant evidence that we can build accurate predictive models for HAR problem under more realistic conditions. This study will help the developers in selecting the methods and parameter settings to best balance between the accuracy requirements and prediction time constraints. To the best of our knowledge, the presented results are obtained from the most realistic and transparent dataset for HAR problem. Therefore, our study can be used as a baseline of future experimental works.

3.1 Motivation

The maturity of pervasive sensing, wireless technology, and data processing techniques enables us to provide an effective solution for continuous monitoring and promote individual’s health. Today, small sensors can be unobtrusively attached to the body or can be part of clothing items to observe people’s lifestyle and behavior changes [1]. According to a study presented in [8], on-body sensing proves to be the most prevalent monitoring technology for the gait assessment, fall detection, and activity recognition/classification. As such, extensive research has been undertaken to select or develop reasoning algorithms to infer activities from the wearable sensor data. Human activity recognition that targets the automatic detection of people activities is one of the most promising research topics in different areas such as ubiquitous computing and ambient assistive living [145]. The low-cost, yet highly reliable accelerometer is the most broadly used wearable sensor for the sake of activity recognition and could provide high classification accuracy of 92.25% [146], 96% [147], and 99.4% [148]. 3-D accelerations can be represented as:

$$\vec{A} = \frac{d\vec{v}}{dt} = \left(\vec{g} + \vec{l}\right), \begin{pmatrix} A_x \\ A_y \\ A_z \end{pmatrix} = \begin{pmatrix} g_x + l_x \\ g_y + l_y \\ g_z + l_z \end{pmatrix} \tag{3-1}$$

Where $\vec{A}$ (acceleration), $\vec{g}$ (acceleration due to gravity) and $\vec{l}$ (applied linear acceleration) are measured in $\frac{m}{s^2}$. There is a large amount of work on the use of sensing for activity monitoring and behavior profiling. For example, there are surveys [14], [149], [150] that provide an outline of relevant research and applicable techniques. In the real-life scenarios, the performance of a recognition system is often significantly lower than in reported research results. This is because there exist variations in training and testing device hardware, sensor models, data heterogeneity, and their operating system characteristics among others [151].

The performance of recognition models mainly depends on the activity set, training data quality, extracted features, and learning algorithms. Since each machine learning model in the literature was trained with a specific dataset and activity set, there is no significant evidence to claim that any predictive model is more precise than the others. In other words, the classification model is built based on the collected samples under specific conditions involving sensor type, position, and orientation of sensors on the human body, sampling rate, and activity performance style. Therefore, the trained model may not be directly applied to other related datasets, if there is any change in the sensor characteristics, data acquisition scenarios or the users (concerning e.g. age, weight, or physical fitness). For instance, different accelerometer sensors often suffer from various biases and thus differ in precision and resolution. This issue, combined with sampling rate instability of each device introduce major challenges for the HAR system design [152]. The difference in the styles of performance of an activity also poses some challenges for application developers and researchers. Stisen *et al.* [151] showed that even OS type and CPU load also have severe adverse effects on recognition accuracy. Therefore, we aim to evaluate the machine learning algorithms comprehensively to extend the applicability of the trained model dealing with diverse accelerometer measurements.

In this work, we have aggregated 14 well-known benchmark datasets that are publicly available to the research community. In each dataset, data has been collected with different devices (commercial mass-marketed or research-only devices), acquisition protocols (under naturalistic circumstances or laboratory environments), participants, sensors placements, models and biases, motion artifacts and sampling rate heterogeneities to have a big realistic dataset. Considering these challenges makes it difficult to obtain a robust activity recognizer that is invariant to biases and performs well on unseen datasets. This is the first time to the best of our knowledge that such rigorous activity recognition evaluation at a large-scale on ML techniques is investigated. This study will explain the pros and cons of a variety of learning methods and will speed up implementation of robust recognition algorithms using wearable accelerometer sensors.

We report the effects of heterogeneities on various classifiers considering two cross-validation techniques. K-fold ($k = 10$) is the most widely accepted methodology to compute the accuracy of a developed model in HAR problem [153]. In this technique, the model is trained using $k - 1$ of the folds as training data and the obtained model is validated on the remaining part of the data to compute the accuracy or other performance metrics. However, to explore the limitations of finding a personalization approach caused by large variance in per-user accuracy, a subject-independent cross-validation technique, Leave-One-Subject-Out (LOSO), is also considered.

This chapter in organized as follows: In Section 3.2, background in the field of human activity recognition and the adopted methodologies including feature extraction/selection and classification techniques with the parameters of prediction functions are addressed. The used datasets in this study will be discussed and listed in Section 3.3. Section 3.4 presents the experimental results obtained with different cross-validation techniques. Finally, a conclusion and some research perspectives are given in Section 3.5.

3.2 Methodologies

Human activity recognition starts with collecting data from the motion sensors. The data is partitioned into windows to apply feature extraction thereby filtering relevant information in the raw signals. Afterward, extracted features are used as inputs of each classifier that ultimately yields the HAR model. To evaluate the effect of sensing heterogeneity on classifiers, we do not perform any preprocessing steps. This problem is formulated as follows:

Definition: With p extracted features from the motion sensors, given a set $W = \{w_1, w_2, \dots, w_n\}$ of labeled and equal-sized time windows, and a set $A = \{a_1, a_2, \dots, a_l\}$ of activity labels, the goal is to find the best classifier model C, such that for any $w_k$which contains a feature set $F_k = \{f_{k,1}, f_{k,2}, \dots, f_{k,p}\}$, the predicted label $\hat{a}_k = C(F_k)$ is as identical as possible to the actual activity performed during w_k. p is the number of features in vector F_k extracted from w_k. Figure 3.1 depicts the whole system flow of sensor-based activity recognition for nine activities.

3.2.1 Data Segmentation, Feature Extraction, and Selection

As described in Chapter 2, a stream of sensory data needs to be divided into subsequent segments. Fixed-size Sliding Window (FSW) is the most common method in

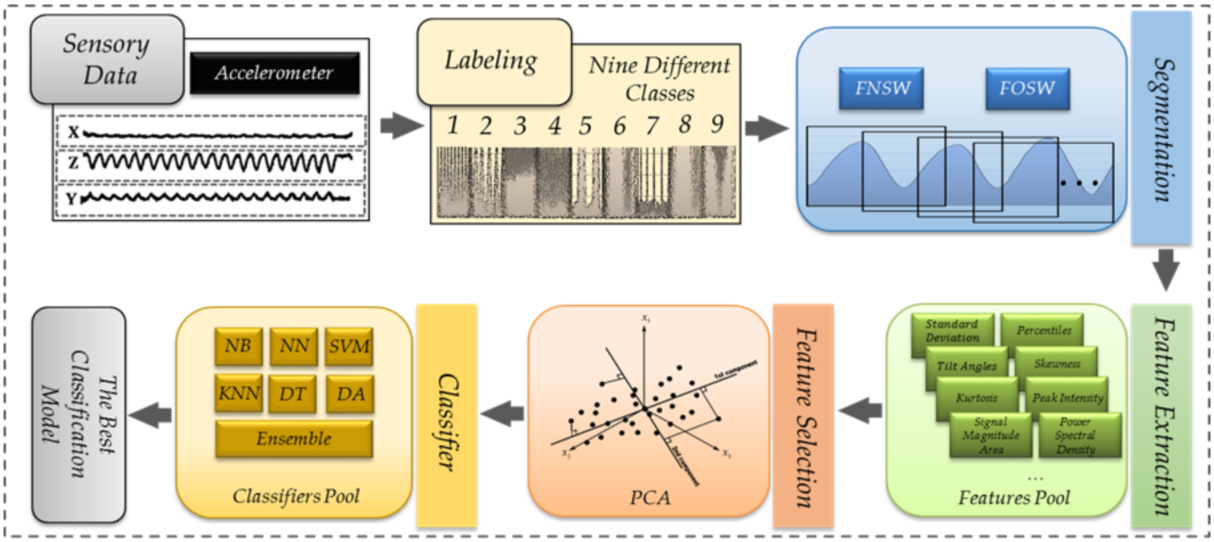

Figure 3.1: Sensor-based activity recognition procedure

segmentation step, where the data stream is allotted into fixed-length windows with no inter-window gaps. If there is no degree of overlap between adjacent windows, it is called Fixed-size Non-overlapping Sliding Window (FNSW). The second method is Fixed-size Overlapping Sliding Window (FOSW), which is similar to FNSW except that the windows overlap during segmentation [149], [150]. The use of overlap between adjacent windows has been shown to be effective in classification problem using wearable sensors data [98], [154].

Finding the optimal window size is an application-dependent task. The window size should be properly determined in such a way that each window is guaranteed to contain enough samples (at least one cycle of an activity) to differentiate similar movements. In addition, increasing the window size does not necessarily enhance the accuracy but may add computational complexity (causing higher latency). To better address the challenge, we analyze the influence of window sizes (ranging from 1 sec to 15 sec) on the classification performance. On each window, a feature vector is used as an instance for learning. Feature extraction is to obtain the important characteristics of a data and represent them into a feature vector used as input of a classier [127].

Table 3.1: The features list

Feature	Description	Feature	Description
Mean	$\mu_s = \frac{1}{n}\sum_{i=1}^{n} s_i$	***Skewness***	$\frac{1}{n{\sigma_s}^3}\sum_{i=1}^{n}(s_i-\mu_s)^3$
Minimum	$min(s_1, s_2, \dots s_n)$	***Kurtosis***	$\frac{1}{n{\sigma_s}^4}\sum_{i=1}^{n}(s_i-\mu_s)^4$
Maximum	$max(s_1, s_2, \dots s_n)$	***Signal Power***	$\sum_{i=1}^{n} s_i^2$
Median	$median(s_1, s_2, \dots s_n)$	***Root Mean Square***	$\sqrt{\frac{1}{n}\sum_{i=1}^{n} {s_i}^2}$
Standard Deviation	$\sigma_s = \sqrt{\frac{1}{n}\sum_{i=1}^{n}(s_i-\mu_s)^2}$	***Peak Intensity***	*The number of signal peaks within a certain period of time*
Coefficients of Variation	$\frac{\sigma_s}{\mu_s}$	***Pearson's Correlation Coefficient***	$\frac{cov(a,b)}{\sigma_a\sigma_b}$
Peak-to-peak Amplitude	$max\ (s) - \ min(s)$	***Inter-axis Cross-Correlation***	$\frac{\sum_{i=1}^{n}(a_i-\mu_a)(b_i-\mu_b)}{\sqrt{\sum_{i=1}^{n}(a_i-\mu_a)^2\sum_{i=1}^{n}(b_i-\mu_b)^2}}$
Percentiles	$percentile(s, p_i) = (1-f)s_k + fs_{k+1}$ $t = \frac{np_i}{100} + 0.5,$ p_i *= 10, 25, 50, 75, 90* *k = integer part of t; f = fractional part of t*	***Autocorrelation***	$R(k) = \frac{1}{(n-k){\sigma_s}^2}\sum_{i=1}^{n-k}(s_i-\mu)(s_{i+k}-\mu)$ $\forall\ k < n$*; the height of the first and second peaks and the position of the second peak of* $R(k)$
Interquartile Range	$percentile(s, 75) - percentile(s, 25)$	***Trapezoidal Numerical Integration***	$\int_1^n s(x)dx$ *using Multiple Segment Trapezoidal Rule*
Pitch Angle	$arctan(\frac{x_i}{\sqrt{y^2+{z_i}^2}})$	***Signal Magnitude Area***	$\frac{1}{n}\sum_{i=1}^{n}(\lvert x_i\rvert + \lvert y_i\rvert + \lvert z_i\rvert)$
Roll Angle	$arctan(\frac{y_i}{\sqrt{x^2+{z_i}^2}})$	***Signal Vector Magnitude***	$\frac{1}{n}\sum_{i=1}^{n}\sqrt{{x_i}^2+y^2+{z_i}^2}$
Median Crossings	t = s - $median(s)$ $MC = \sum_{i=1}^{n} sgn(t_i \, . \, t_{i+1})$ *sgn(a,b) = {1 if (a.b) < 0; 0 if (a.b) > 0}*	***Power Spectral Density***	$\frac{1}{n}\sum_{i=1}^{n-1}(s_i\cos\frac{2\pi fi}{n})^2 + (s_i\sin\frac{2\pi fi}{n})^2$ *f denotes the fth Fourier coefficient in the frequency domain; the positions and power levels of highest 6 peaks of PSD computed over the sliding window; total power in 5 adjacent and pre-defined frequency bands.*

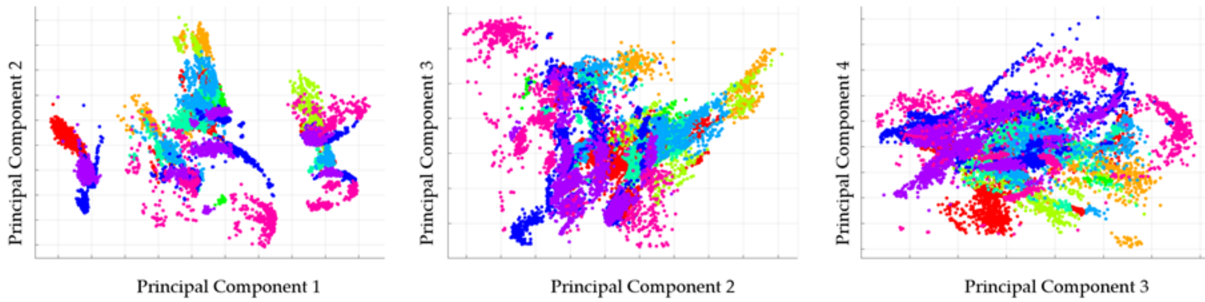

Figure 3.2: The pairwise scatter plots of the first four components (the colors indicate the class labels)

Table 3.1 gives details about the most effective time/frequency-domain and heuristic features in the literature in the context of activity recognition. Due to the low computational cost and the high discriminatory ability of time-domain features, they are the most frequently employed features for real-time applications. We compute all the features listed in Table 3.1 using each reading of accelerometer sensor consists of 3-D accelerations (x, y, z). However, to minimize the effects of sensor orientation, we add another dimension to the sensor readouts which is called the magnitude of the accelerometer vector, i.e. $\sqrt{x^2 + y^2 + z^2}$, because it is less sensitive to the orientation changes [155].

It is worth noting that the correlation features are calculated between each pair of axes and the tilt angles are estimated by a combination of all three axes as shown in Table 3.1. Each classifier is fed with the feature vectors obtained by fusing data at the feature level. Because of the above feature extraction process, 176 features are obtained for each segment and then scaled into the interval [0, 1] using min-max normalization to be used for classification.

As not all features are equally useful in discriminating between activities, Principal Component Analysis (PCA) is applied to map the original features $F_k = \{f_{k,1}, f_{k,2}, \dots, f_{k,p}\}$ into a lower dimensional subspace (i.e. new mutually uncorrelated features) $F'_k = \{f'_{k,1}, f'_{k,2}, \dots, f'_{k,m}\}$, where m≤p [156]. It also significantly reduces the computational effort of the classification process. The PCA components can be counted by X = YP, where X and Y are centering and input matrix, respectively and P is a matrix of eigenvector of the covariance vector matrix Cx = PΛPT. Λ is a diagonal matrix whose diagonal elements are the eigenvalues corresponding to each eigenvector [157]. The new feature vectors are so-called principal components and arranged according to their variance (from largest to lowest). To keep the essential information in acceleration data that describes human activity, we take the first principal components that explain 95% of the total variance. The pairwise scatter plots of the first four components (transformed features) of one of test cases are given in Figure 3.2. As expected, the first components (the first component against the second component) for different classes are better clustered and more distinct.

3.2.2 Machine Learning Techniques

In this study, we are dealing with the supervised machine learning methods, where the class labels are used to train the feature vectors extracted from each separate segment of data. Each window has a class label chosen from l labels, a_1 to a_l. Then, the problem is to build a classifier C to predict the labels for all new windows (w_{n+1} to w_∞) while windows w_1 to w_n are used for training the classifier based on the labeled windows. We attempt the most complete analysis on performance of classifiers to discriminate among different types of activity.

Wide range of machine learning methods have been applied for recognition of human activities such as decision tree (DT) [158]-[162], Support Vector Machines (SVM) [146], [147], [158], [160], [162]-[165], K-Nearest Neighbors (KNN) [158], [71], [160], [162], [164], Naïve Bayes (NB) [158], [160], [162], [166], artificial Neural Network (NN) [160], [161], [163], [167] and ensemble of classifiers [148], [158], [162], [163]. We explore 293 different classifiers including Decision Tree, Discriminant Analysis, Support Vector Machines, K-Nearest Neighbors, Ensemble Methods, Naïve Bayes, and Neural Network with their different parameters. The methods and their parameters setting are described and given in section 3.6. The main objective of implementing different classification techniques is to review, compare, and evaluate their performance considering the most well-known heterogeneous datasets publicly open to the research community. We are going to intertwine different issues and suggest solutions if we expect reasonable results in the practical applications.

3.3 Datasets

To design a robust learning model working in a realistic condition, we combined 14 datasets, focusing on accelerometer sensors that contain several sources of heterogeneities such as measurement units, sampling rates and acquisition protocols that are present in most real-world HAR problems. Table 3.2 listed the datasets and brought the details of the collected data in each project. In total, the aggregated dataset has about 35 million acceleration samples from 228 subjects (with age ranging from 19 to 83) of more than 70 different activities. This is the most complete, realistic, and transparent dataset in this context. The samples were collected at different sampling rates that range from 8 Hz to 100 Hz. We considered 10 major positions on the body i.e. Waist (W), Right Lower Arm (RLA), Left Lower Arm (LLA), Right Upper Arm (RUA), Left Upper Arm (LUA), Right Lower Leg (RLL), Left Lower Leg (LLL), Right Upper Leg (RUL), Left Upper Leg (LUL), and Chest (C). All sensors positions described in each dataset have been mapped into the major positions. For example, if a subject puts the cell phone in the left front pants pocket, we consider it as Left Upper Leg (LUL) position, or wrist, which is a great place for many commercial wearables, is considered as RLA/LLA in this work. Moreover, in dataset 7, the back position is counted as the chest position. In this field, numerous studies [168], [169] have shown that the performance of HAR systems strongly depends on sensor placement because the number and the placement of inertial sensors have direct effects on the measurement of human motions. Each placement turns out to be more suitable regarding performance for particular activities. Besides, having fewer sensors attached to

Table 3.2: The datasets used in this chapter

Dataset	Number of Subjects	Sensor Type	Frequency	Sensor Placement	Activity Type	Description
(1) [147]	30 (19-48 yr)	accelerometer gyroscope (Samsung Galaxy S II smartphone)	50Hz	waist (1)	walking, ascending stairs, descending stairs, sitting, standing, laying (6)	In the first trial, each subject placed the smartphone in a predetermined position i.e. the left side of the belt. However, in the second attempt, they could fix the phone in a desired position on the waist.
(2) [148]	4 (28-75 yr) (45±21.49)	ADXL335 accelerometer (connected to an ATmega328V microcontroller)	~ 8Hz	waist, left thigh, right ankle, right arm (4)	walking, sitting, sitting down, standing, standing up (5)	The data has been collected during 8 hours of five different activities for all subjects.
(3) [164]	8 (20-30 yr)	accelerometer gyroscope magnetometer (Xsens MTx unit)	25 Hz	chest, right and left wrists, right side of the right knee, left side of the left knee (5)	walking in a parking lot, sitting, standing, lying, ascending/descending stairs, walking on a treadmill with a speed of 4 km/h (in flat and 15° inclined positions), etc. (19)	The subjects performed nineteen activities by their own style. They were not controlled during data collection sessions.
(4) [170]	16 (19-83 yr)	accelerometer (6-bit resolution)	32 Hz	right wrist (1)	walking, climbing stairs, descending stairs, laying down on bed, sitting down on chair, brushing teeth, eating meat, etc. (14)	There are postural transitions, reiterated and complex activities in the dataset.
(5) [69]	22 (25-35 yr)	accelerometer (Google Nexus One)	30 Hz	jacket pocket on the chest (1)	walking (1)	The walking data of several subjects was collected in indoor and outdoor under real-life circumstances.

Dataset	Number of Subjects	Sensor Type	Freq.	Sensor Placement	Activity Type	Description
(6) [69]	15 (27-35 yr)	accelerometer (Shimmer)	52 Hz	chest (1)	walking, walking and talking, standing, standing up, talking while standing, going up/down stairs, etc. (7)	They used a low power; low-cost BeagleBoard with a Linux embedded operating system to transmit data over Bluetooth.
(7) [71]	17 (22-37 yr)	accelerometer gyroscope magnetometer (Xsens MTx unit)	50 Hz	right and left calves, right and left thighs, back, right and left lower arms and right, left upper arms (9)	walking, jogging, running, jump up, rowing, cycling, etc. (33)	The dataset includes a wide range of physical activities (warm up, cool down and fitness exercises).
(9) [70]	14 (21-49 yr) (30.1±7.2)	accelerometer gyroscope (MotionNode)	100 Hz	front right hip (1)	walking forward, left and right, sitting and fidgeting, standing, going upstairs and downstairs, running forward, jumping up and down, etc. (12)	There were 5 trials for each activity and each subject performed the experiments on different days at indoor and outdoor places.
(10) [171]	20 (19-75 yr)	accelerometer 2-axis gyroscope (attached to Tmote Sky)	30 Hz	waist, right and left wrists, right and left ankle (5)	walking forward, right-circle and left-circle, sitting, lying down, standing, going upstairs and downstairs, jogging, jumping, turning right and left etc. (13)	The design of the wearable sensor network was based on platform named DexterNet that implemented a 3-level architecture for controlling heterogeneous body sensors.
(11) [160]	4 (25-30 yr)	accelerometer gyroscope (Samsung Galaxy S II)	50 Hz	belt, right arm, right wrist and right jeans pocket (4)	walking, sitting, standing, walking upstairs and downstairs, running (6)	Every participant performed each activity between 3– and 5 minutes. The smartphone was horizontally kept for belt and vertically for the arm, wrist, and pocket.

Dataset	Number of Subjects	Sensor Type	Freq.	Sensor Placement	Activity Type	Description
(12) [161]	36	accelerometer (Android-based smartphone)	20 Hz	front pants leg pocket (1)	walking, sitting, standing, upstairs, downstairs, jogging (6)	The android app, through a simple graphical user interface, permits to record the user's name, start and stop the data collection, and label the activity being performed.
(13) [172]	19 (23-52 yr)	accelerometer gyroscope magnetometer (Xsens MTx unit)	100 Hz	belt either on the right or the left part of the body, at the subject's choice (1)	walking, sitting, standing, lying, running, falling, jumping (9)	Data was logged in indoor and outdoor settings under semi-naturalistic conditions.
(14) [69]	10 (25-30 yr)	accelerometer gyroscope magnetometer (Samsung Galaxy S II)	50 Hz	right and left jeans pocket, belt position towards the right leg, right upper arm, right wrist (5)	walking, sitting, standing, walking upstairs and downstairs, jogging, biking (8)	All test protocols were carried inside a building, except biking.

the body is preferable since wearing multiple ones is not well accepted. Therefore, we limited our modeling and analysis for single-accelerometer data while we still expect a sufficiently high recognition rate for the picked activities. According to the datasets, the most examined activities (top activities) are walking, running, jogging, cycling, standing, sitting, lying down, ascending and descending stairs which also represent the majority of everyday living activities. Another observation we find is that in eight major positions we have data for all top activities.

Therefore, we choose them as target activities for eight separate positions (W, RLA, LLA, RUL, LUL, RLL, LLL, and C). We created a rectangular tree map that presents dense volumes of data in a space-filling layout allowing for the visual comparison of datasets contributions in each target position (see Figure 3.3).

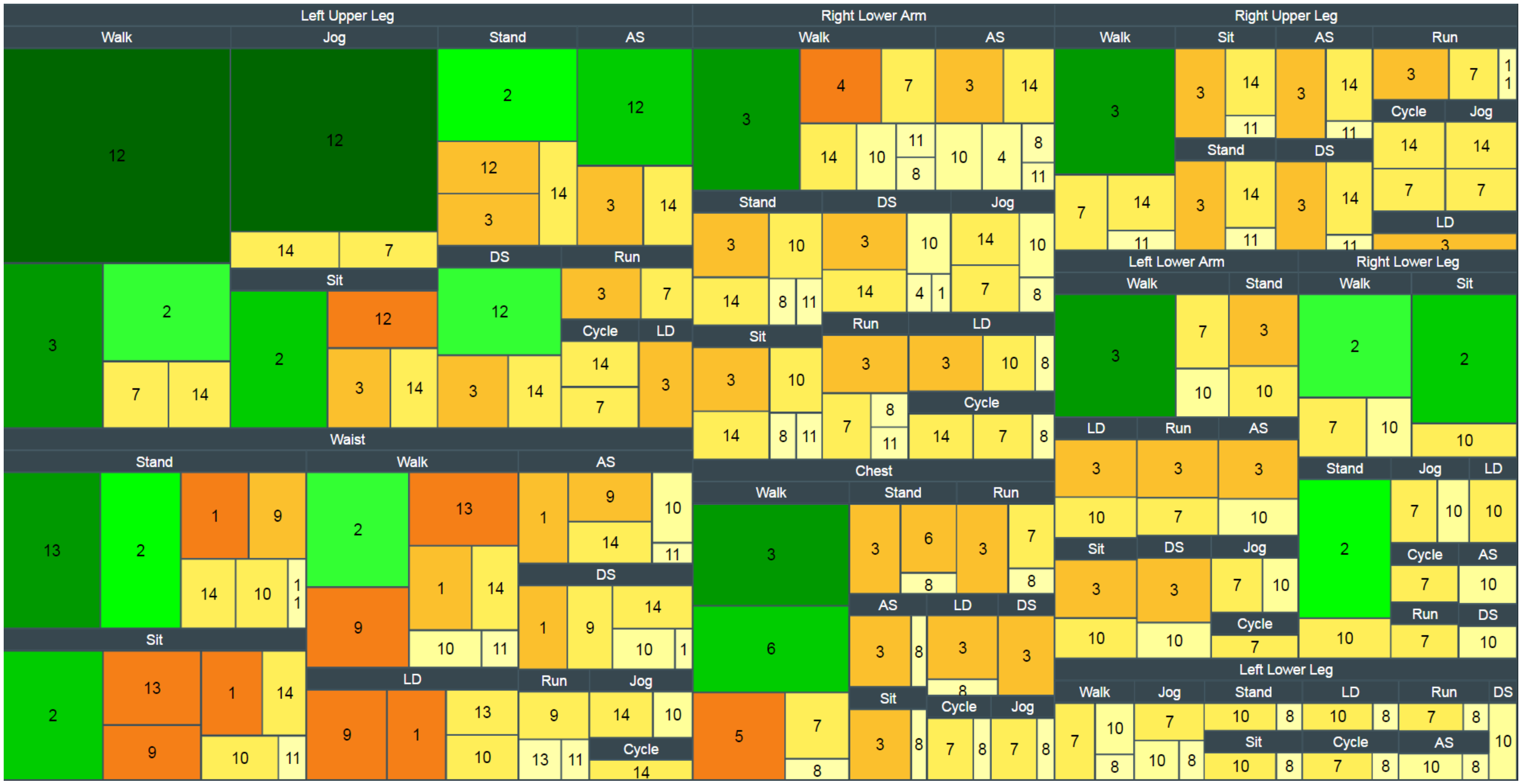

Figure 3.3: The rectangular tree map that presents dense volumes of data in a space-filling layout to see datasets contributions in each target position. Laying Down (LD), Ascending Stairs (AS), Descending Stairs (DS). The number inside each rectangle indicates the dataset number (see the first column of Table 3.2)

For example, as depicted in Figure 3.3, datasets 3, 5, 6, 7 and 8 contribute data for constructing the chest dataset with nine activities.

3.4 Experimental Results and Discussions

In this section, we report the effects of the heterogeneities, from sensors characteristics, data collection scenarios, and subjects, on various feature representation techniques and 293 classifiers considering two cross-validation techniques. First, the 10-fold cross-validation strategy is applied as one of the most accurate approaches for model selection. Figure 3.4 shows the minimum and maximum obtained accuracy of each classifier over different window sizes with the waist accelerometer data. The algorithms are sorted according to their obtained accuracy. Considering the best accuracy for each classification category in this position, the ensemble methods KNN (Subspace) and Tree (Bagging) achieved the highest activity recognition rate whereas DT performed the worst. Furthermore, DA, DA (Subspace), Tree (AdaBoost), Tree (RUSBoost) and NB performed almost equal but worse than SVM, NN, and KNN. As seen, some classification learning algorithms are more sensitive to parameters settings and window size and may thus be more likely to exhibit significant differences. To have a better and deeper investigation, we extract the classifiers with top 5% accuracies and call them "*topClassifiers*" for each position. Figure 3.5 depicts the range of *topClassifiers* accuracies for each position. The red dashed line annotation shows the 95th percentile of obtained accuracies.

As demonstrated in this figure, most of the recognition methods remain consistent in their relative performance across different accelerometer data obtained from various positions. As explained in Section 3.2, finding the optimal length of window size is an application-dependent task. The window size should be properly determined in such a way that each window is guaranteed to contain enough samples to differentiate similar activities or movements. Thus, we consider different window sizes ranging from 1 sec to

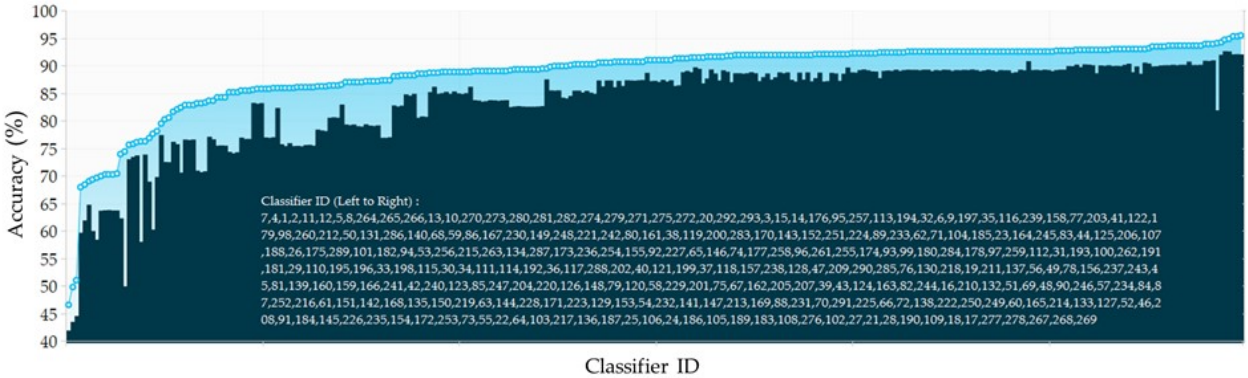

Figure 3.4: The minimum and maximum accuracy of each classifier over different window sizes, ranging from 1 sec to 15 sec, with the waist accelerometer data

15 sec in steps of 1 sec to ensure the statistical significance of the calculated features. It comprises most of the values used in the previous activity recognition systems [149]. Each window of n samples ($n = freq \times t$) is used to calculate the feature set for a particular activity, where $freq$ is the sampling frequency of the acceleration data and t is the window size in seconds.

Figure 3.6 describes the ranking of different window sizes in providing the best accuracy (among all classifiers) in each position. For example, the window of length 7 sec provides the best classification accuracy when the sensor is attached on RLA. The second best accuracy value for RLA is achieved with window size 8 sec. The first line in this figure shows the window sizes of the best accuracies for each position. In contrast to LLL, where the top four accuracy values have been observed in small window sizes ranging from 2 to 5 sec, chest provides the top-rank accuracy values in large window sizes from 10 sec to 15 sec. This observation is more highlighted in orange line (w = 1 sec), where all positions obtain the worst-case accuracy values except for the LLL. However, in some cases, we can change the window size (increase/decrease) at the expense of a subtle performance drop. For example, in chest position, the window size can be reduced from 15 to 7 sec by only tolerating 0.16% in recognition performance.

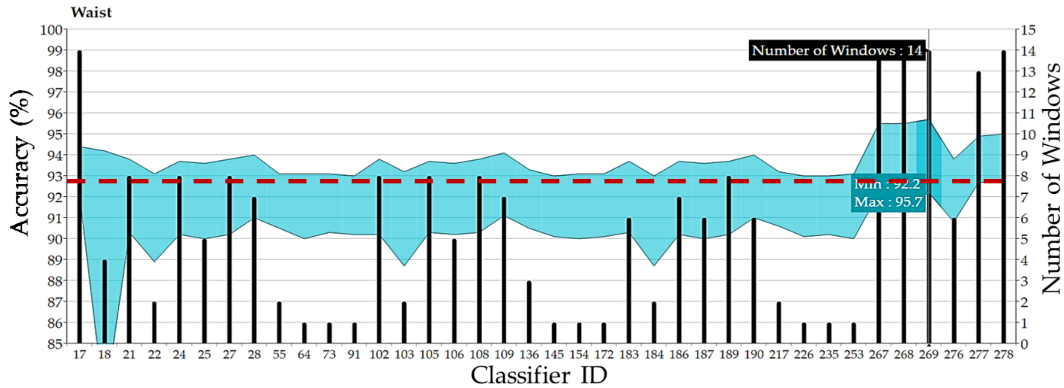
Waist
Number of Windows : 14
Max : 95.7
Accuracy (%)
Number of Windows
Classifier ID

(a)

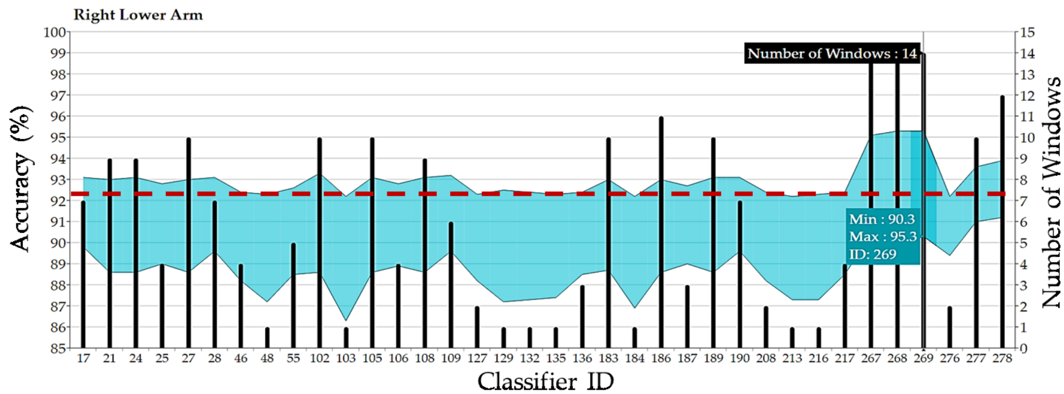
Right Lower Arm
Number of Windows : 14
Min : 90.3
Max : 95.3
ID: 269
Accuracy (%)
Number of Windows
Classifier ID

(b)

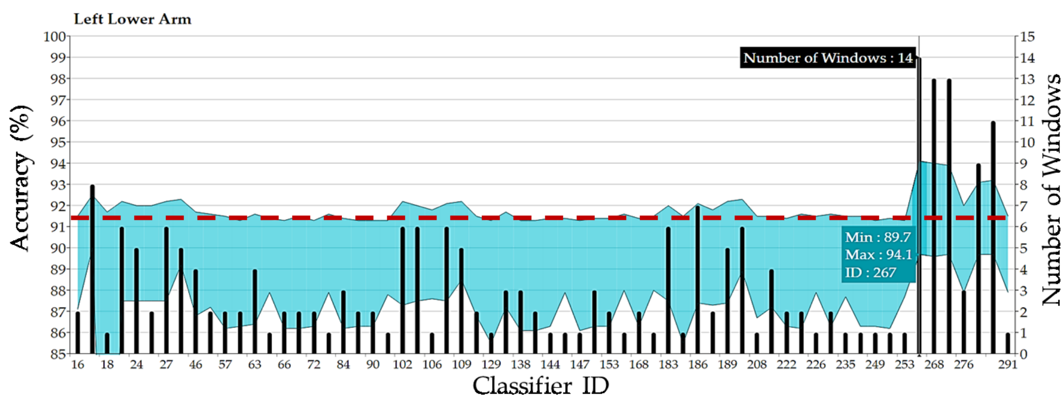
Left Lower Arm
Number of Windows : 14
Min : 89.7
Max : 94.1
ID : 267
Accuracy (%)
Number of Windows
Classifier ID

(c)

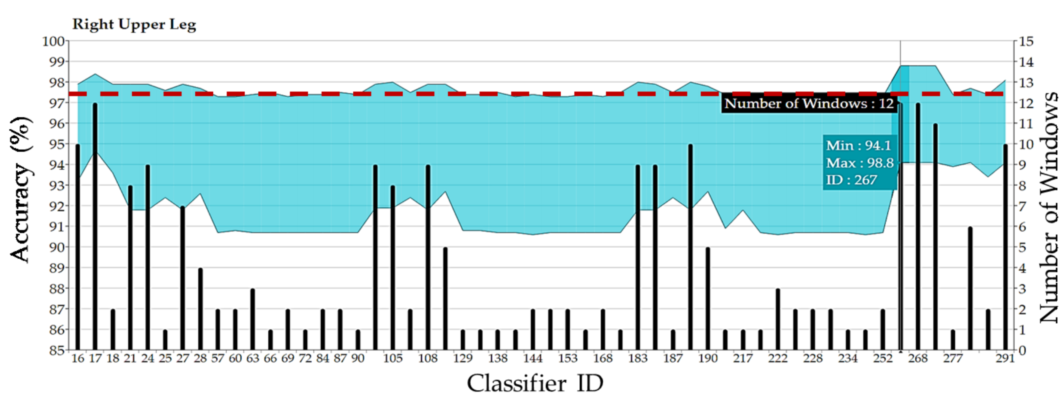
Right Upper Leg
Number of Windows : 12
Min : 94.1
Max : 98.8
ID : 267
Accuracy (%)
Number of Windows
Classifier ID

(d)

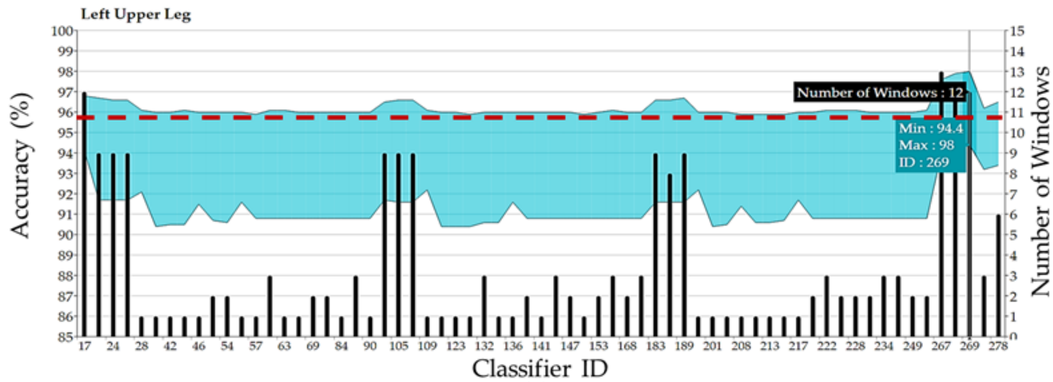

(e)

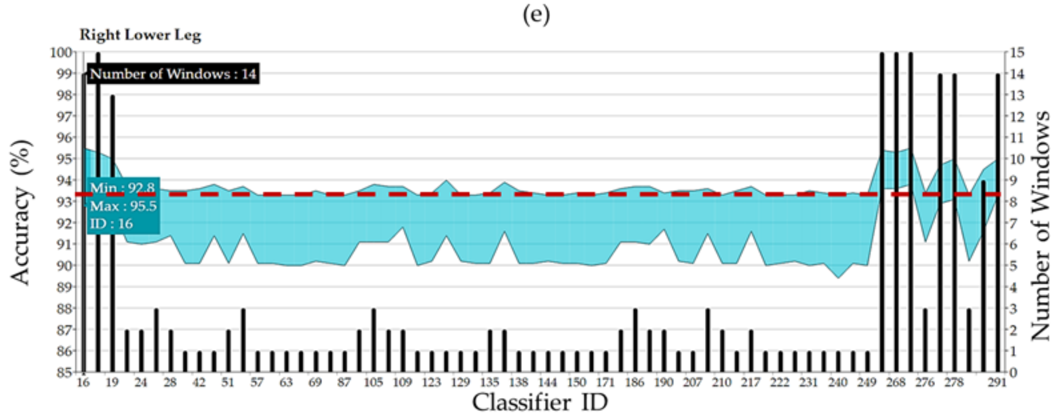

(f)

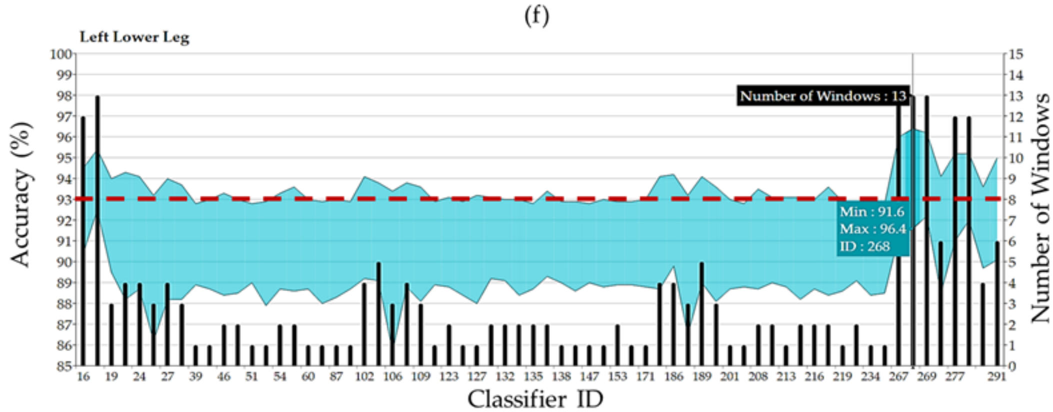

(g)

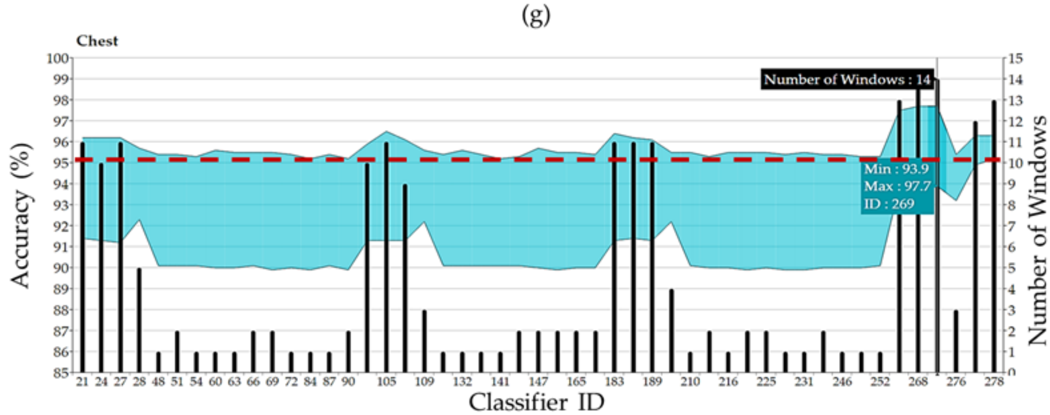

(h)

Figure 3.5: The range of *topClassifiers* accuracies for (a) Waist, (b) RLA, (c) LLA, (d) RUL, (e) LUL, (f) RLL, (g) LLL, and (h) Chest

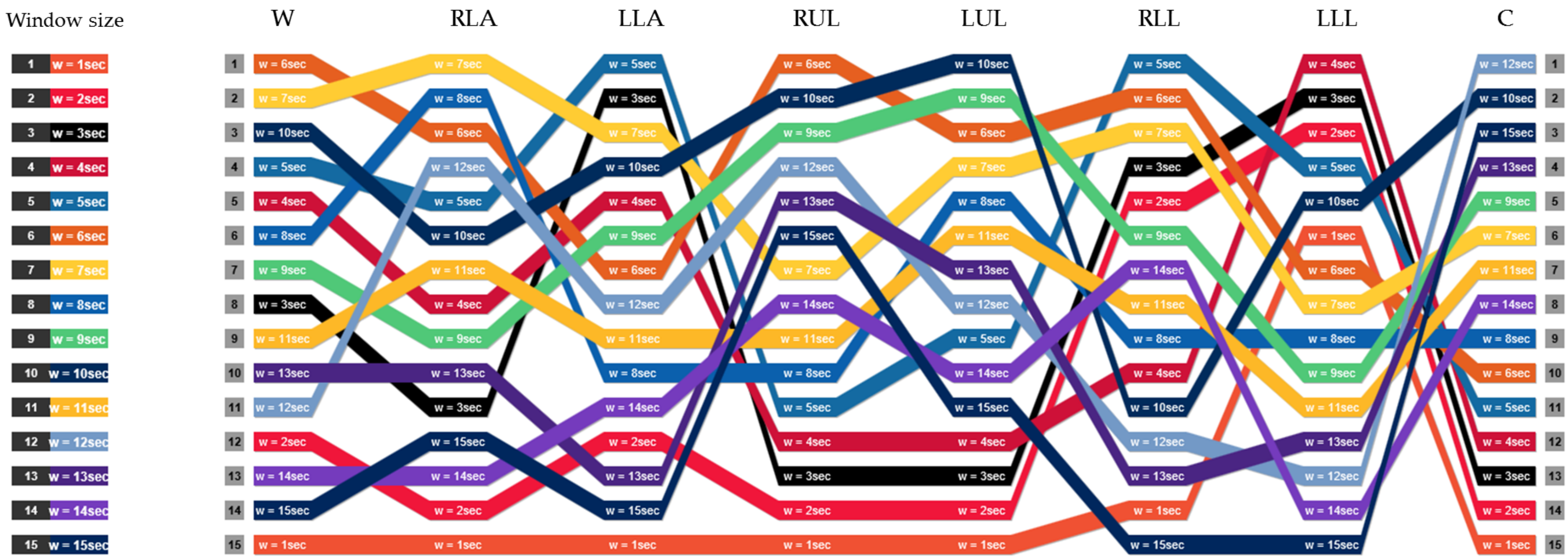

Figure 3.6: The rank of window sizes in providing the best accuracy in each position

The bar charts in Figure 3.6 indicate the number of window sizes (1 sec to 15 sec) in which the *topClassifiers* provided good results (top 5%). An interesting observation from the bars is that some classifiers such as KNN (Subspace), Tree (Bagging), and SVM work well with most window sizes. In other words, these methods could mitigate the effect of window size to gain meaningful information for the activity classification process. To have a better understanding of window size effect on accuracy, Figure 3.7 shows the *topClassifiers* across all window sizes in each position.

As can be observed, the interval 3–10 sec proves to provide the best accuracies in most cases considering the target activities. This range can be reduced if fusion of multiple sensors is used for feature extraction. Another point worth mentioning that is large window sizes do not necessarily translate into a better recognition performance for the underlying periodic activities. Although accuracy is necessary for all recognition algorithms, it is not the only parameter to consider in designing a recognition model. The runtime complexity (classification step) is another important challenge, as the model should be working fast and responsive regardless of where it is deployed. Thus, we make use of the concept of Pareto optimality to extract superior solutions from *topClassifiers* to trade off classifier accuracy and runtime. We consider two objective functions i.e. misclassification and runtime, to be minimized. A feasible solution x dominates a feasible solution y when:

$$\forall\, i, f_i(x) \leq \; f_i(y) \tag{3-2}$$

Where f_i is the i^{th} objective function. In many problems, usually no single solution is superior to all others, so the non-dominated solutions compose the Pareto front. For example, in Figure 3.8, we populate the runtime-accuracy plane with some *topCalssifiers* for waist position and depict the Pareto front. The shaded area represents the region in $f_1 \times f_2$ space that is dominated by the point x which is non-dominated and hence belong

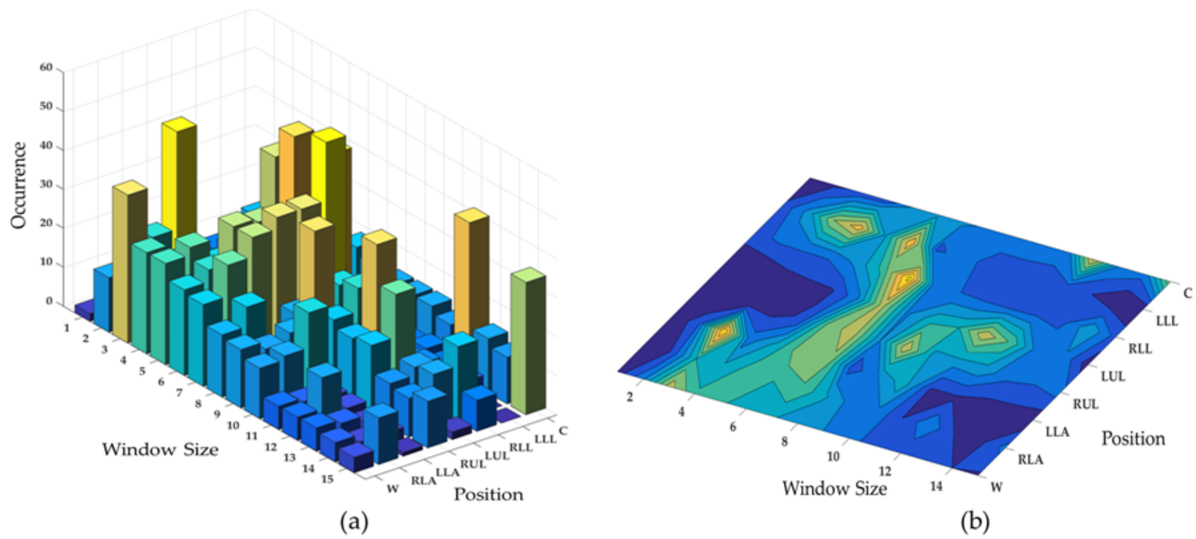

Figure 3.7: Effect of window size to gain meaningful information for the activity classification in (a) 3D and (b) 2D representations

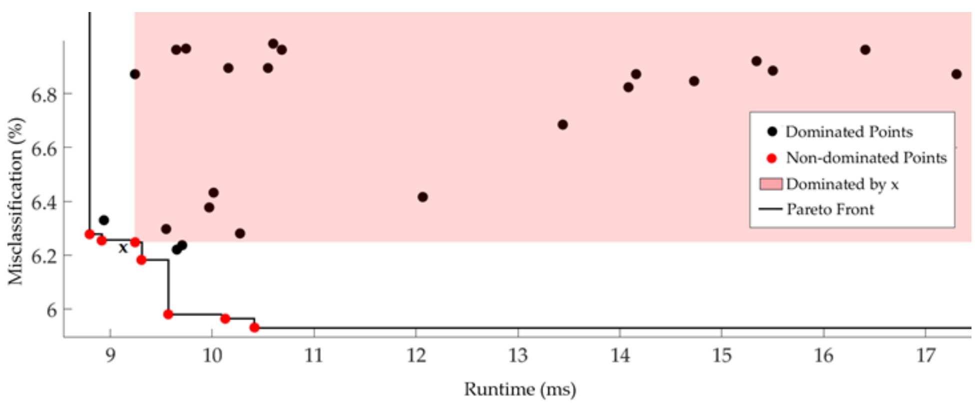

Figure 3.8: Illustration of some Pareto fronts when minimizing two objectives (misclassification and classification runtime) according to the obtained results in waist

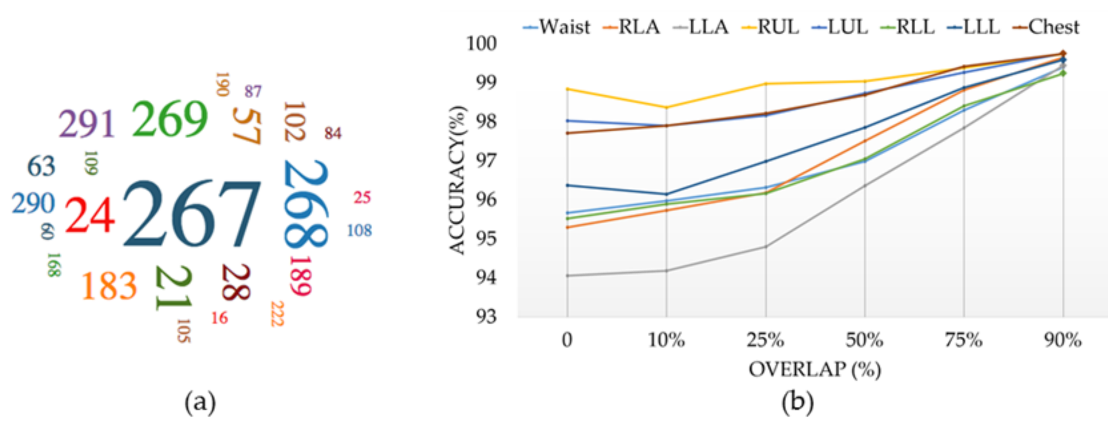

Figure 3.9: (a) Overall view of the non-dominated classifiers (classifier ID) and their power in providing high recognition accuracy (b) recognition system capabilities for diverse overlap values

to the Pareto front [173]. All points in this region are inferior to x in both objectives. In addition, if we want to minimize an objective to a constraint, e.g. $f_1(x) < c$, the Pareto front provides the solution for all possible values of the cap c [173]. Therefore, the Pareto front contains significantly richer information than one obtains from single-objective formulations. Table 3.3 summarizes the non-dominated classifiers in each position. The results show a clear trade-off between classifiers runtime and accuracy. There is no strong relation between the sensor position and classification performance.

In overall, the highest classification accuracy was achieved by KNN (Subspace), and KNN stayed in the second place, which is followed by SVM and NN. Figure 3.9 (a) depicts the overall view of the non-dominated classifiers and their power in providing high recognition accuracy. The size of each classifier ID in this figure represents the number of times that the corresponding classifier has been reported in Table 3.3. The KNN has the best classification runtime (7 ± 1.78 ms) fed with a feature vector among all of them. While for classification accuracy, it is always after its ensemble method KNN (Subspace). In all cases, KNN (Subspace) with average accuracy (96.42% ± 1.63 %) provided better results than all other non-dominated classifiers, with the exception of data from the RLL, where the SVM (95.52%) provided superior accuracy. However, SVM's prominence is negligible while considering its runtime (113.05 ms) and no significant accuracy improvement (0.1%). Given the accuracy results stated in Table 3.3, although NN classifiers provide promising results in most cases, they are dominated by other techniques and could be only among the selected methods in three positions RUL, RLL, and LLL. With a closer look at the classifications results in Figure 3.6 and tabulated results, we find out ensemble method Tree (Bagging) is a very strong method and is among *topClassifiers* in all cases, but is always outperformed by other methods in terms of both accuracy and runtime. According to the selected KNN classifiers, the distance

Table 3.3: The accuracy and runtime of non-dominated classifiers

Classifier ID	Accuracy (%)	Misclassification (%)	Runtime (ms)
Waist			
21	93.82	6.18	9.31
28	94.02	5.98	9.57
108	93.75	6.25	9.24
109	94.07	5.93	10.41
183	93.75	6.25	8.92
189	93.72	6.28	**8.80**
190	94.04	5.96	10.13
267	95.48	4.52	45.95
268	95.51	4.49	121.58
269	**95.67**	**4.33**	196.10
Right Lower Arm			
24	93.11	6.89	**7.61**
102	93.29	6.71	8.01
267	95.14	4.86	33.90
268	95.29	4.71	87.80
269	**95.30**	**4.70**	149.78
Left Lower Arm			
28	92.29	7.71	7.59
57	91.50	8.50	**7.31**
63	91.61	8.39	7.35
102	92.24	7.76	7.50
267	**94.06**	**5.94**	32.50
Right Upper Leg			
24	97.93	2.07	7.04
57	97.33	2.67	**6.94**
63	97.43	2.57	**6.94**
183	98.05	1.95	7.49
189	97.97	2.03	7.21
267	**98.85**	**1.15**	32.12
291	98.14	1.86	8.08

Classifier ID	Accuracy (%)	Misclassification (%)	Runtime (ms)
Left Upper Leg			
21	96.69	3.31	3.52
24	96.62	3.38	3.39
57	95.93	4.07	**2.92**
60	96.11	3.89	3.11
222	96.15	3.85	3.16
267	97.63	2.37	34.73
268	97.86	2.14	102.90
269	**98.03**	**1.97**	151.83
Right Lower Leg			
16	**95.52**	**4.48**	113.05
24	93.82	6.18	8.03
28	93.45	6.55	**8.02**
267	95.36	4.64	30.73
290	94.52	5.48	8.25
291	94.97	5.03	9.14
Left Lower Leg			
21	94.26	5.74	7.91
25	93.16	6.84	**7.79**
267	95.99	4.01	32.36
268	**96.38**	**3.62**	83.45
290	93.64	6.36	7.89
291	95.02	4.98	8.85
Chest			
21	96.17	3.83	6.97
84	95.25	4.75	**6.58**
87	95.43	4.57	6.95
105	96.48	3.52	7.63
168	95.39	4.61	6.91
183	96.37	3.63	7.02
267	97.52	2.48	29.64
268	97.67	2.33	76.49
269	**97.72**	**2.28**	125.10

method affects most in the performance. City block and Euclidean have been the best choices, and too large value for k does not improve the performance as it destroys locality.

We also can draw another conclusion that there was no significant difference in KNN (Subspace) performance with a different number of learners (i.e. 10, 20, and 40).

Therefore, applying fewer learners is preferentially utilized due to its much lower runtime. Regarding the position analysis, the best performance (98.85% and 98.03%) is achieved with the aggregated data on RUL and LUL. The chest is the next best performing placement (97.72%) compared to the RLL (95.52%), LLL (96.38%), RLA (95.30%), LLA (94.06%), and Waist (95.67%). Different studies [98], [126], [163] show that the use of overlap between successive sliding windows help the classifiers to be trained with more feature vectors and consequently improve the recognition performance. However, it might lead to a situation called overfitting in addition to adding more computational work needed to process the overlapped data multiple times. To evaluate the effectiveness of the degree of overlap, the overlaps of 10%, 25%, 50%, 75% and 90% are used, where the percentage is the amount the window slides over the previous window. For instance, a sliding window with 25% overlap will start the next window while the previous window is 75% complete. The value can range from 0% to 99% since a 100% sliding window is erroneous. Figure 3.10 (b) illustrates the recognition system capabilities for diverse overlap values while keeping the best window size in each position (see Figure 3.6).

The results demonstrate that the performance tendency is increased in most cases by overlapping more data segmentations. An average increase of 3.28% in the best accuracy was found between the 0 and 90% overlap scenarios and all obtained with an ensemble of KNN. Figure 3.10 also illustrates the number of classifiers that provide good results (90%-99%) by considering different overlap sizes. The larger the overlap, the more improvement is expected in performance. As described, more features can be trained and consequently the predictive model almost certainly works better in testing phase; however, it suffers from more training time. In activity recognition problem, K-fold cross-validation is an accurate approach for model selection; however, Leave-One-Subject-Out

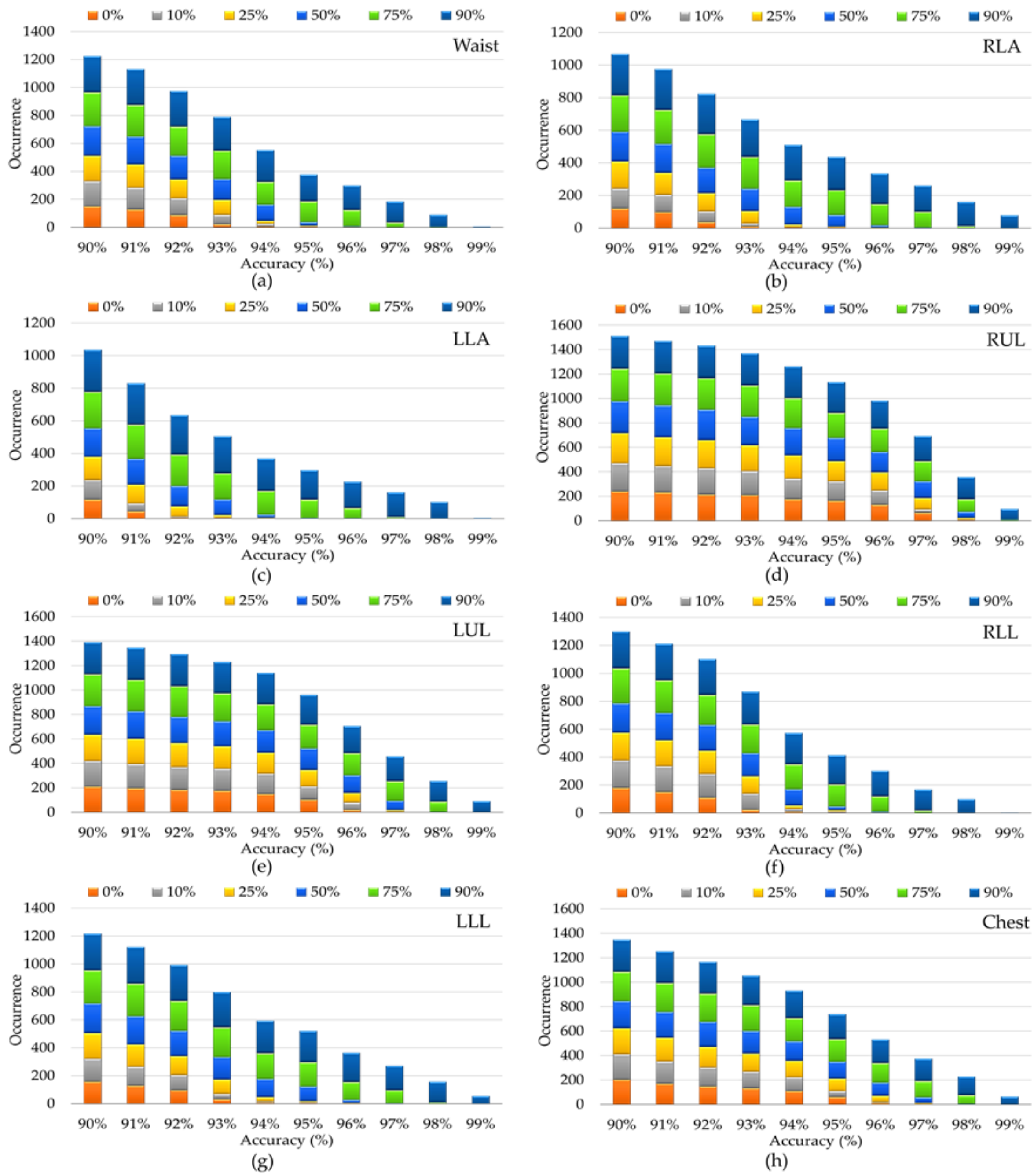

Figure 3.10: Analysis of number of classifiers, which provide good results (90%-99%) by taking different overlap sizes into account for different positions.

(LOSO), which is also called subject-independent cross-validation, is one of the best data approaches in estimating realistic performance. LOSO reflects inter-subject variability and tests on yet-unseen data. According to combined datasets in each position (see Figure

3.3), we conducted LOSO evaluation, where the KNN (Subspace) is trained on activity data for all subjects except one. Then, the classifier is tested on the data for only the subject left out of the training dataset. The procedure is then repeated for all subjects in each position, and the mean accuracy is reported. For each position, the window size and overlap are set based on the best results from 10-fold evaluation. Based on the aggregated for each position, the models trained in LUL (92.35%) and LLL (90.03%) positions were not affected much by interpersonal differences in the body movement of subjects. These positions could obtain relatively good results of accuracy. They are followed by Chest (86.31%) and RLL (83.51%) which are better performing placements compared to the lower arm positions.

The RLA (64.62%) was influenced the most, and LLA (77.12%) accounted for a substantial decrease in accuracy, as well. The result of Waist (72.53%) was very similar to one reached by RUL (72.91%), but both suffer performance degradation by more than 25%. As expected the accuracy of recognition in all positions was reduced since the trained model deals with a set of data that might have new measurement characteristics. As the best classifier of each position in average goes down 17.13% in accuracy, there is a need for further studies investigating new relevant features and novel machine learning model to be sufficiently flexible in dealing with inter-person differences.

3.5 Conclusion

In this chapter, different machine learning techniques were deeply explored when heterogeneity of devices and their usage scenarios are intrinsic. In addition, each position was analyzed based on the aggregated tri-axial accelerometer data from different datasets. Hence, the quantitative comparison of the classifiers was hindered by the fact that each position is explored with a different aggregated dataset. In each position investigation, in addition to various sources of heterogeneities in data, there are also different factors such as body shape, clothing, straps, belt and accidental displacements/disorientations (in the form of rotations or translations) that make the analysis harder to have a solid model. The averaged results showed 96.44% ± 1.62 % activity recognition accuracy when using K-fold and 79.92% ± 9.68 % accuracy when using a subject-independent cross-validation. According to the obtained results, it is clear that new data with different sources of heterogeneities could significantly reduce the accuracy with more than 32% (e.g. in RLA) based on LOSO evaluation.

An overall look at the results, KNN, and its ensemble methods showed stable results over different positions and window sizes, indicating its ability in designing a robust and responsive machine learning model in the wearables, and they are followed by NN and SVM. However, as we showed in this work, the choice of parameter values in each classifier can have a significant impact on recognition accuracy (see Appendix). Considering the promising results of this pilot study, we intend to work on novel features extraction methods and classifiers that outperform classical classification methods while better dealing with inter-person differences and data diversities. Another point that deserves to be further assessed is optimizing the runtime performance since it has a great role in the efficiency of the cloud-based machine learning deployments.

3.6 Appendix

In this section, the utilized approaches for the activity classification problem are summarized while considering different parameters settings.

3.6.1 Decision Tree

In this method, the discriminatory ability of the features is examined one at a time to create a set of rules. Decision Tree (DT) has been used in many studies [98], [126] and the results show that it performs well with time and frequency domain features. In the top-down tree structure, each leaf represents a classification label, and each branch denotes

Table 3.4: The common techniques for splitting nodes in DT

Split criterion	Description	Split criterion	Description	Split criterion	Description
Gini's Diversity Index (GDI)	$\sum_i p(i)(1-p(i)) = 1-\sum_i p^2(i)$ *p(i) is the probability that an arbitrary sample belongs to class li.*	***Deviance***	$-\sum_i p(i) log\, p(i)$ *based the concept of entropy from information theory*	***Towing rule***	$p(L)p(R)\left(\sum_i \lvert L(i)-R(i)\rvert\right)^2$ *Let L(i)/R(i) denote the fraction of members of class i in the left/right child node after a split and p(L)/p(R) are the fractions of observations that split to the left/right*

conjunctions of attributes that lead to the leaves. In other words, decision trees classify instances by starting at the root of the tree and moving through it (with the decision being made at each node) until a leaf node. The utilized growing and pruning algorithms in decision tree induction are greedy and follow a recursive manner. The construction of a tree involves determining split criterion, stopping criterion and class assignment rule [174]. The most common techniques to measure the node impurity (for splitting nodes) are explained in Table 3.4 [175]. They define the node splits, where each split maximizes the decrease in impurity. In this study, we split branch nodes layer by layer until there are 4, 20, or 100 branch nodes. Therefore, we define nine different decision trees considering the mentioned split and stopping criteria. When a node is determined to be a leaf, it has to be given a class label. A commonly used class assignment function is the majority rule meaning that class k is assigned to node t as follows [176]:

$$l_k = \max_i p(i|t), \quad t \in \tilde{T} \tag{3-3}$$

The set of terminal nodes (leafs) denoted by $\widetilde{T}$.

3.6.2 Discriminant Analysis

Discriminant Analysis (DA) is widely used in classification problems [177], [178]. In this algorithm, there are three main elements: prior probability, posterior probability, and cost [179]. A prior probability *P(k)* is the probability that an observation will fall into class

k before you collect the data. There are two main choices i.e. uniform and empirical. If the prior probability of class k is 1 over the total number of classes, it is called uniform. Besides, the number of training feature vectors of class k divided by all training features set defines the empirical prior probability.

A posterior probability is the probability of assigning observations to classes given the data. The product of the prior probability and the multivariate normal density explains the posterior probability that a point x belongs to label k. With mean μ_k and covariance Σ_k at a point x, the density function of the multivariate normal can be described as below [179]:

$$(x|k) = \frac{1}{(2\pi|\Sigma_k|)^{1/2}} exp\left(-\frac{1}{2}(x-\mu_k)^T \sum\nolimits_k^{-1} (x-\mu_k)\right) \quad (3\text{-}4)$$

The observed data x (the feature vector of one analysis segment) is classified to label k with the largest posterior probability. The posterior probability that an observation x belongs to label k is:

$$\hat{P}(k|x) = \frac{P(x|k)P(k)}{P(x)} \quad (3\text{-}5)$$

Where *P(x)* indicates the probability of the feature vector x and is the sum over k of *P(x|k)P(k)*. Therefore, the predicted classification $\hat{y}$ with m classes is:

$$\hat{y} = arg \min_{y=1\dots k} \sum_{k=1}^{m} \hat{P}(k|x)\, C(y|k) \quad (3\text{-}6)$$

$C(y|k)$ is the cost of classifying an observation y when its correct label is k [179]. In this work, we consider five types of discriminant analysis classifiers: linear; and diagonal and pseudo variants of linear and quadratic types.

3.6.3 Support Vector Machine

A Support Vector Machine (SVM) is defined based on one or a set of separating hyperplanes in a high dimensional space and was first proposed for binary classification problems. SVM generates linear functions by considering a set of labels obtained from the training dataset. The linear separator is created considering the maximum margin from the hyperplane to the support vectors [180]. By n training samples, (x_i, y_i); $i = 1, 2, \dots, n$ we have:

$$\{x_i, y_i\}, i = 1, \dots n, y_i \in \{-1, +1\}, x_i \in R^d$$

y_i shows the binary nature of the classifier with either 1 or −1, representing the class of x_i. The R^d is a d-dimensional vector space over the real numbers. The decision boundary of a linear SVM classifier is as follows:

$$w^T x + b = 0 \tag{3-7}$$

Where w and b indicate a weight vector and bias, respectively. There are different linear separators; though SVM targets the one with maximum-margin hyperplane from any data point. The linear classifier is as follows:

$$f(x) = sign(w^T x + b) \tag{3-8}$$

The main goal is to find the best *w* and *b,* which can maximize the geometric margin $(\frac{2}{||w||})$, with linear constrains $y_i(w^T x_i + b) \geq 1$ for all (x_i, y_i). This optimization problem can be defined as a minimization problem as follows:

$$\begin{gathered} \min_{w,b}(\frac{1}{2}||w||^2) \\ s.t.\, y_i(w^T x_i + b) \geq 1, i = 1, \dots n \end{gathered} \tag{3-9}$$

To solve this problem, the optimization function is transformed into the Lagrangian dual with the Karush–Kuhn–Tucker (KKT) conditions so that the Lagrange multiplier vector α_i is linked with each inequality of the constraints as:

$$\max_{\alpha\geq 0} \min_{w,b} \{\frac{1}{2}||w||^2 - \sum_{i=1}^{n} \alpha_i [\, y_i(w^T x_i \, + \, b) - 1]\},$$

$$\max_{\alpha\geq 0} \left\{ \sum_{i=1}^{n} \alpha_i - \frac{1}{2} \sum_{i=1}^{n} \sum_{j=1}^{n} \alpha_i \, \alpha_j y_i y_j x_i^T x_j \right\}, \qquad s.t. \sum_{i=1}^{n} \alpha_i \, y_i = 0 \tag{3-10}$$

Thus, the optimal linear classification function is obtained as below, where n_{sv} denotes the number of support vectors. Different studies show that SVM could provide an efficient non-linear classification and provide very promising results [181], [182]. $K(x_i, x_j) = \phi(x_i)^T \phi(x_j)$ is the kernel function which provides the inner product value of x_i and x_j in the feature space.

$$f(x) = \; sign(w^T x \; + \; b) = sign(\sum_{i,j=1}^{n_{sv}} \alpha_i \, y_i x_i^T x_j + b) \tag{3-11}$$

$$f(x) = \; sign\left(\sum_{i,j=1}^{n_{sv}} \alpha_i \, y_i K(x_i, x_j) + b \right) \tag{3-12}$$

The most often used kernels in SVM are as described in Table 3.5. The type of the kernel function that transforms data from input space to a higher dimensional feature space has a direct impact on the performance of the SVM classifier. Although there exist no well-defined rules for selecting the kernel type [180], here three well-known kernel functions are applied in SVM with Error-Correcting Output Codes (ECOC) with One-Versus-One (OVO) technique to evaluate our multi-classification problem. ECOC breaks

Table 3.5: The applied kernels in SVM

Kernel	Formula	Kernel	Formula	Kernel	Formula
Linear	${x_i}^T x_j$	***Polynomial***	$({x_i}^T x_j + 1)^d$	***Radial basis function (RBF)***	$exp(-\frac{\left\|x_i - x_j\right\|^2}{2\sigma^2})$

the multiclass task into a number of binary classification tasks, which are then combined to output the result [183]. The OVO coding design exhausts all combinations of class pair assignments. Therefore, if we have K distinct classes, the number of learners is $\frac{k(k-1)}{2}$. For each binary learner, one class is positive, another is negative, and the rest are ignored.

3.6.4 K-Nearest Neighbors

K-Nearest Neighbor (KNN) is based on a neighborhood majority voting scheme and assigns the new instance to the most common class amongst its K nearest. Simplicity and runtime are the main advantages of this method, which used in several research works [98], [163], [184]. There are different metrics to determine the distance $d(x_s, y_t)$ between two vectors x_s and y_t. Table 3.6 describes the methods used in this study. The three applied distance weights are equal (no weighting), inverse (1/d) and squared inverse ($1/d^2$). If multiple classes have the same smallest cost, the smallest index, the class with the nearest neighbor or a random tiebreaker among tied groups is used. Regarding

Table 3.6: The distance metrics in KNN

Distance Metric	Description	Distance Metric	Description	Distance Metric	Description
Euclidean	$\sqrt{\sum_{i=1}^{n}(x_{si}-y_{ti})^2}$	*Standardized Euclidean*	$\sqrt{\sum_{i=1}^{n}\frac{(x_{si}-y_{ti})^2}{s_i^2}}$ s_i *is the standard deviation of the* x_{si} *and* y_{ti} *over the sample set*	*Correlation*	$-\frac{1}{\frac{(x_s-\overline{x_s})(y_t-\overline{y_t})'}{\sqrt{(x_s-\overline{x_s})(x_s-\overline{x_s})'}\sqrt{(x_s-\overline{x_s})(y_t-\overline{x_s})'}}}$ $\overline{x_s}=\frac{1}{n}\sum_i x_{si}$ *and* $\overline{y_s}=\frac{1}{n}\sum_i y_{ti}$
City Block	$\sum_{i=1}^{n}\lvert x_{si}-y_{ti}\rvert$	*Minkowski*	$\sqrt[p]{\sum_{i=1}^{n}\lvert x_{si}-y_{ti}\rvert^p}$ *In this work, p = 3*	*Mahalanobis*	$\sqrt{(x_{si}-y_{ti})\,C^{-1}(x_{si}-y_{ti})'}$ *C is the covariance matrix*
Chebychev	$\max_i\{\lvert x_{si}-y_{ti}\rvert\}$	*Cosine*	$-\frac{1}{\frac{x_s y_t'}{\sqrt{(x_s x_s')(y_t y_t')}}}$	*Spearman*	$1-\frac{(r_s-\overline{r_s})(r_t-\overline{r_t})'}{\sqrt{(r_s-\overline{r_s})(r_s-\overline{r_s})'}\sqrt{(r_s-\overline{r_s})(r_t-\overline{r_s})'}}$ r_{si} *is the rank of* x_{si} *over* x_s*. If any* x_s *values are tied, their average rank is computed*

selection of k, larger value may improve performance and reduce the effect of noise on the classification, but makes boundaries between classes are less distinct [185]. In addition, setting k to a too large value may destroy locality, and as a result, KNN looks at samples that are not neighbors. They are different techniques to select and find a good k [186], [187]. Here, we consider three values 1, 10, and 100 for k; therefore, in total we run 243 KNNs with different settings.

3.6.5 Ensemble Methods

Ensemble classifier refers to a combination of different classifiers that are cooperatively trained on the dataset. The ensembling learning method classifies new data by taking a weighted vote of their predictions to obtain better predictive performance. Indeed, within the sensor-based recognition domain, different studies [98], [148], [158], [162], [163] report where an ensemble method outperformed a range of other classification models. Bagging, as named from the phrase "bootstrap aggregating" is used to improve results of classification algorithms and help to avoid overfitting [188]. This ensemble method constructs bootstrap samples by repetitively resampling training instances with replacement. A sequence of classifiers $c_{1:b}$ (b = 10, 30, 50) in respect to variation of the training set is created by the bagging method. The prediction of a compound classifier, derived from the combinations of $c_{1:b}$ is given as:

$$c(d_i) = sign\left(\sum_{m=1}^{b} \alpha_m c_m(d_i)\right) \tag{3-13}$$

The above formula can be interpreted as to classify an example d_i to the class with majority voting, and α should be chosen so that more accurate classifiers have stronger impact on the final prediction than less accurate classifiers [189]. More details about the theory of classifier voting can be found in [190].

Another approach is boosting which attempts to turn a weak learner into a strong learner by gradually adapting how models are made. Each new model added to the ensemble is biased to take more notice to training instances that earlier models misclassified [179]. AdaBoost.M2 is a very prevalent boosting algorithm for multi-class classification. The algorithm trains learners sequentially and requires the weak learner to output an array of confidences associated with each possible labeling of an example. For every learner with index t, AdaBoost.M2 computes the weighted pseudo-loss for N observations and k classes as below [179]:

$$\varepsilon_t = \frac{1}{2}\sum_{n=1}^{N}\sum_{k\neq y_n} d_{n,k}^{(t)}\big(1 - h_t(x_n, y_n) + h_t(x_n, k)\big) \tag{3-14}$$

Where $h_t(x_n, k)$ and $d_{n,k}^{(t)}$ are the confidence of prediction by learner and observation weights at step t for class k, respectively. The second sum is over all classes other than y_n that is the true class. For more details, the reader is referred to [191].

RUSBoost is designed to improve the performance of models trained on skewed data. It combines data sampling and boosting, providing an effective method for classifying imbalanced data. It applies Random Under Sampling (RUS), a method that randomly takes out examples from the majority class for each weak learner in the ensemble until a preferred class distribution is found. If the smallest class has N training instances, classes with more instances are under sampled by taking only N observations. For reweighting and constructing the ensemble, it follows the procedure in AdaBoost.M2 [192].

Random subspace ensembles (Subspace) are similar to bagging except that the features are randomly sampled. Thus, subspace ensembles have the advantage of less memory and computations than ensembles with all features resulting in considerably shorter model training times. To train a weak learner, this technique selects a random set of m predictors (in this study, m =12) from the d possible values without replacement. It repeats this procedure until there are 10, 30, 50 weak learners. Finally, it takes an average of the score prediction of the weak learners and classifies the observation with the maximum mean score [193].

In this chapter, the boosting and bagging algorithms are based on tree learners, and the subspace has been applied to the discriminant analysis and k-nearest neighbor learners.

3.6.6 Naïve Bayes

Naïve Bayes (NB) is a powerful probabilistic classifier employing a simplified version of Bayes formula to decide on a class of a new instance [132]. In activity recognition, NB proved to perform well in the previous studies [158], [194]. The following equation shows the Naïve Bayes under the assumption of feature independence, though the assumption is usually violated in practice.

$$P(l|f_1 \dots f_n) = \frac{p(l)\prod_{i=1}^{n} p(f_i|l)}{p(f_1 \dots f_n)} \tag{3-15}$$

Where l represents labels/classes (l = $1, 2 \dots L$) and f_i is a feature vector. The denominator of the right side of the equation is a constant, and $p(l)$ is a prior. The posterior probability $P(l|f_1 \dots f_n)$ is determined by the likelihood $\prod_{i=1}^{n} p(f_i|l)$ and $p(f_1 \dots f_n)$ is the joint density of the predictors, so, $p(f_1 \dots f_n) = \sum_{l=1}^{L} p(l)\prod_{i=1}^{n} p(f_i|l)$. The Naïve Bayes classifier combines the independent feature mode with a decision rule. The common rule is known as the maximum a posteriori or MAP decision rule.

$$arg\,\max_{l} P(l|f_1 \dots f_n) = arg\,\max_{l} \prod_{i=1}^{n} p(f_i|l) \tag{3-16}$$

A typical assumption when dealing with the data stream is that continuous values associated with each class are distributed according to a Normal (Gaussian) distribution. However, to alleviate this assumption, NB classifier computes a separate kernel density estimate for each class according to its training data [179]. There exists a large range of kernels that can be exploited for the kernel density estimate. Table 3.7 shows the kernel smoother types we applied in this chapter.

Table 3.7: The applied kernel smoother types in NB

Kernel type	Formula	Kernel type	Formula
Uniform	$0.5\ I\{\lvert x\rvert \leq 1\}$	***Epanechnikov***	$0.75\ (1-x^2)\ I\{\lvert x\rvert \leq 1\}$
Normal (Gaussian)	$\frac{1}{\sqrt{2\pi}} e^{-0.5\,x^2}$	***Triangular***	$(1-\lvert x\rvert)\ I\{\lvert x\rvert \leq 1\}$

3.6.7 Neural Network

Artificial Neural Network (NN) is generally presented as a system of interconnected neurons that are capable of machine learning. The basic processing unit of an NN is called perceptron and is a decision-making unit with several inputs and a single output. The input neuron p_i is weighted with an appropriate w_i. The perceptron sums the dot product of weights and inputs vectors, and adds a bias b. The obtained total signal will be transformed by a function which not only can be linear, but is most often a nonlinear transformation (e.g. log-sigmoid and tan-sigmoid) [195]. This process is summarized as:

$$a = f\left(b + \sum_{j=1}^{i} w_j p_j\right) \tag{3-17}$$

Feedforward neural networks are one of the most broadly used models in many real-world scientific problems. The network is divided into layers; therefore, it can learn nonlinear relationships between input and output vectors with nonlinear transfer functions. In the input layer, the nodes pass the values to the neurons or hidden units placed in the subsequent layer, which is called hidden layer. In this work, we considered 10, 20, and 40 hidden neurons. The final layer is the output layer that depends upon the number of class labels in the classification problem [196]. In training the network, its parameters are adjusted incrementally until the difference between the output units and the target values is minimized. Resilient backpropagation [197], scaled conjugate gradient [198] and Levenberg–Marquardt backpropagation are the most well-known network training algorithms. For example, Levenberg–Marquardt optimization uses the Hessian matrix approximation, $J^T J$, in the following Newton-like update [179]:

$$w_i(t+1) = w_i(t) - [J^T J + \mu I]^{-1} J^T e \tag{3-18}$$

Where Jacobian matrix J holds the first derivatives of the network errors in respect of the weights and biases. μ stands for an adjustment factor, e for a vector of network errors and I for the identity matrix [195], [199]. Resilient backpropagation network training algorithm updates weight and bias values according to the algorithm explained in [197]. In this method, the magnitude of the derivative has no influence on the weight update, and only the sign of the derivative can define the direction of the weight update. Therefore, in total, there are 293 different classifiers with the various settings as listed in Figure 3.11.

1	DT_SC(gdi)MS(4)	75	KNN_BT(SM)D(MI)EX(3)DW(EQ)N(1)	149	KNN_BT(NE)D(MA)DW(EQ)N(100)	223	KNN_BT(RA)D(EU)DW(IN)N(10)
2	DT_SC(gdi)MS(20)	76	KNN_BT(SM)D(MI)EX(3)DW(EQ)N(10)	150	KNN_BT(NE)D(MA)DW(IN)N(1)	224	KNN_BT(RA)D(EU)DW(IN)N(100)
3	DT_SC(gdi)MS(100)	77	KNN_BT(SM)D(MI)EX(3)DW(EQ)N(100)	151	KNN_BT(NE)D(MA)DW(IN)N(10)	225	KNN_BT(RA)D(EU)DW(SI)N(1)
4	DT_SC(towing)MS(4)	78	KNN_BT(SM)D(MI)EX(3)DW(IN)N(1)	152	KNN_BT(NE)D(MA)DW(IN)N(100)	226	KNN_BT(RA)D(EU)DW(SI)N(10)
5	DT_SC(towing)MS(20)	79	KNN_BT(SM)D(MI)EX(3)DW(IN)N(10)	153	KNN_BT(NE)D(MA)DW(SI)N(1)	227	KNN_BT(RA)D(EU)DW(SI)N(100)
6	DT_SC(towing)MS(100)	80	KNN_BT(SM)D(MI)EX(3)DW(IN)N(100)	154	KNN_BT(NE)D(MA)DW(SI)N(10)	228	KNN_BT(RA)D(MA)DW(EQ)N(1)
7	DT_SC(deviance)MS(4)	81	KNN_BT(SM)D(MI)EX(3)DW(SI)N(1)	155	KNN_BT(NE)D(MA)DW(SI)N(100)	229	KNN_BT(RA)D(MA)DW(EQ)N(10)
8	DT_SC(deviance)MS(20)	82	KNN_BT(SM)D(MI)EX(3)DW(SI)N(10)	156	KNN_BT(NE)D(MI)EX(3)DW(EQ)N(1)	230	KNN_BT(RA)D(MA)DW(EQ)N(100)
9	DT_SC(deviance)MS(100)	83	KNN_BT(SM)D(MI)EX(3)DW(SI)N(100)	157	KNN_BT(NE)D(MI)EX(3)DW(EQ)N(10)	231	KNN_BT(RA)D(MA)DW(IN)N(1)
10	DA_T(linear)	84	KNN_BT(SM)D(SE)DW(EQ)N(1)	158	KNN_BT(NE)D(MI)EX(3)DW(EQ)N(100)	232	KNN_BT(RA)D(MA)DW(IN)N(10)
11	DA_T(diagLinear)	85	KNN_BT(SM)D(SE)DW(EQ)N(10)	159	KNN_BT(NE)D(MI)EX(3)DW(IN)N(1)	233	KNN_BT(RA)D(MA)DW(IN)N(100)
12	DA_T(diagQuadratic)	86	KNN_BT(SM)D(SE)DW(EQ)N(100)	160	KNN_BT(NE)D(MI)EX(3)DW(IN)N(10)	234	KNN_BT(RA)D(MA)DW(SI)N(1)
13	DA_T(pseudoLinear)	87	KNN_BT(SM)D(SE)DW(IN)N(1)	161	KNN_BT(NE)D(MI)EX(3)DW(IN)N(100)	235	KNN_BT(RA)D(MA)DW(SI)N(10)
14	DA_T(pseudoQuadratic)	88	KNN_BT(SM)D(SE)DW(IN)N(10)	162	KNN_BT(NE)D(MI)EX(3)DW(SI)N(1)	236	KNN_BT(RA)D(MA)DW(SI)N(100)
15	SVM_KF(linear)C(OO) KS(auto)	89	KNN_BT(SM)D(SE)DW(IN)N(100)	163	KNN_BT(NE)D(MI)EX(3)DW(SI)N(10)	237	KNN_BT(RA)D(MI)EX(3)DW(EQ)N(1)
16	SVM_KF(P)C(OO)PO(2)KS(auto)	90	KNN_BT(SM)D(SE)DW(SI)N(1)	164	KNN_BT(NE)D(MI)EX(3)DW(SI)N(100)	238	KNN_BT(RA)D(MI)EX(3)DW(EQ)N(10)
17	SVM_KF(P)C(OO)PO(3)KS(auto)	91	KNN_BT(SM)D(SE)DW(SI)N(10)	165	KNN_BT(NE)D(SE)DW(EQ)N(1)	239	KNN_BT(RA)D(MI)EX(3)DW(EQ)N(100)
18	SVM_KF(GA)C(OO) KS(1.2)	92	KNN_BT(SM)D(SE)DW(SI)N(100)	166	KNN_BT(NE)D(SE)DW(EQ)N(10)	240	KNN_BT(RA)D(MI)EX(3)DW(IN)N(1)
19	SVM_KF(GA)C(OO) KS(4.9)	93	KNN_BT(SM)D(SP)DW(EQ)N(1)	167	KNN_BT(NE)D(SE)DW(EQ)N(100)	241	KNN_BT(RA)D(MI)EX(3)DW(IN)N(10)
20	SVM_KF(GA)C(OO) KS(20)	94	KNN_BT(SM)D(SP)DW(EQ)N(10)	168	KNN_BT(NE)D(SE)DW(IN)N(1)	242	KNN_BT(RA)D(MI)EX(3)DW(IN)N(100)
21	KNN_BT(SM)D(CB)DW(EQ)N(1)	95	KNN_BT(SM)D(SP)DW(EQ)N(100)	169	KNN_BT(NE)D(SE)DW(IN)N(10)	243	KNN_BT(RA)D(MI)EX(3)DW(SI)N(1)
22	KNN_BT(SM)D(CB)DW(EQ)N(10)	96	KNN_BT(SM)D(SP)DW(IN)N(1)	170	KNN_BT(NE)D(SE)DW(IN)N(100)	244	KNN_BT(RA)D(MI)EX(3)DW(SI)N(10)
23	KNN_BT(SM)D(CB)DW(EQ)N(100)	97	KNN_BT(SM)D(SP)DW(IN)N(10)	171	KNN_BT(NE)D(SE)DW(SI)N(1)	245	KNN_BT(RA)D(MI)EX(3)DW(SI)N(100)
24	KNN_BT(SM)D(CB)DW(IN)N(1)	98	KNN_BT(SM)D(SP)DW(IN)N(100)	172	KNN_BT(NE)D(SE)DW(SI)N(10)	246	KNN_BT(RA)D(SE)DW(EQ)N(1)
25	KNN_BT(SM)D(CB)DW(IN)N(10)	99	KNN_BT(SM)D(SP)DW(SI)N(1)	173	KNN_BT(NE)D(SE)DW(SI)N(100)	247	KNN_BT(RA)D(SE)DW(EQ)N(10)
26	KNN_BT(SM)D(CB)DW(IN)N(100)	100	KNN_BT(SM)D(SP)DW(SI)N(10)	174	KNN_BT(NE)D(SP)DW(EQ)N(1)	248	KNN_BT(RA)D(SE)DW(EQ)N(100)
27	KNN_BT(SM)D(CB)DW(SI)N(1)	101	KNN_BT(SM)D(SP)DW(SI)N(100)	175	KNN_BT(NE)D(SP)DW(EQ)N(10)	249	KNN_BT(RA)D(SE)DW(IN)N(1)
28	KNN_BT(SM)D(CB)DW(SI)N(10)	102	KNN_BT(NE)D(CB)DW(EQ)N(1)	176	KNN_BT(NE)D(SP)DW(EQ)N(100)	250	KNN_BT(RA)D(SE)DW(IN)N(10)
29	KNN_BT(SM)D(CB)DW(SI)N(100)	103	KNN_BT(NE)D(CB)DW(EQ)N(10)	177	KNN_BT(NE)D(SP)DW(IN)N(1)	251	KNN_BT(RA)D(SE)DW(IN)N(100)
30	KNN_BT(SM)D(CC)DW(EQ)N(1)	104	KNN_BT(NE)D(CB)DW(EQ)N(100)	178	KNN_BT(NE)D(SP)DW(IN)N(10)	252	KNN_BT(RA)D(SE)DW(SI)N(1)
31	KNN_BT(SM)D(CC)DW(EQ)N(10)	105	KNN_BT(NE)D(CB)DW(IN)N(1)	179	KNN_BT(NE)D(SP)DW(IN)N(100)	253	KNN_BT(RA)D(SE)DW(SI)N(10)
32	KNN_BT(SM)D(CC)DW(EQ)N(100)	106	KNN_BT(NE)D(CB)DW(IN)N(10)	180	KNN_BT(NE)D(SP)DW(SI)N(1)	254	KNN_BT(RA)D(SE)DW(SI)N(100)
33	KNN_BT(SM)D(CC)DW(IN)N(1)	107	KNN_BT(NE)D(CB)DW(IN)N(100)	181	KNN_BT(NE)D(SP)DW(SI)N(10)	255	KNN_BT(RA)D(SP)DW(EQ)N(1)
34	KNN_BT(SM)D(CC)DW(IN)N(10)	108	KNN_BT(NE)D(CB)DW(SI)N(1)	182	KNN_BT(NE)D(SP)DW(SI)N(100)	256	KNN_BT(RA)D(SP)DW(EQ)N(10)
35	KNN_BT(SM)D(CC)DW(IN)N(100)	109	KNN_BT(NE)D(CB)DW(SI)N(10)	183	KNN_BT(RA)D(CB)DW(EQ)N(1)	257	KNN_BT(RA)D(SP)DW(EQ)N(100)
36	KNN_BT(SM)D(CC)DW(SI)N(1)	110	KNN_BT(NE)D(CB)DW(SI)N(100)	184	KNN_BT(RA)D(CB)DW(EQ)N(10)	258	KNN_BT(RA)D(SP)DW(IN)N(1)
37	KNN_BT(SM)D(CC)DW(SI)N(10)	111	KNN_BT(NE)D(CC)DW(EQ)N(1)	185	KNN_BT(RA)D(CB)DW(EQ)N(100)	259	KNN_BT(RA)D(SP)DW(IN)N(10)
38	KNN_BT(SM)D(CC)DW(SI)N(100)	112	KNN_BT(NE)D(CC)DW(EQ)N(10)	186	KNN_BT(RA)D(CB)DW(IN)N(1)	260	KNN_BT(RA)D(SP)DW(IN)N(100)
39	KNN_BT(SM)D(CO)DW(EQ)N(1)	113	KNN_BT(NE)D(CC)DW(EQ)N(100)	187	KNN_BT(RA)D(CB)DW(IN)N(10)	261	KNN_BT(RA)D(SP)DW(SI)N(1)
40	KNN_BT(SM)D(CO)DW(EQ)N(10)	114	KNN_BT(NE)D(CC)DW(IN)N(1)	188	KNN_BT(RA)D(CB)DW(IN)N(100)	262	KNN_BT(RA)D(SP)DW(SI)N(10)
41	KNN_BT(SM)D(CO)DW(EQ)N(100)	115	KNN_BT(NE)D(CC)DW(IN)N(10)	189	KNN_BT(RA)D(CB)DW(SI)N(1)	263	KNN_BT(RA)D(SP)DW(SI)N(100)
42	KNN_BT(SM)D(CO)DW(IN)N(1)	116	KNN_BT(NE)D(CC)DW(IN)N(100)	190	KNN_BT(RA)D(CB)DW(SI)N(10)	264	EL(Discriminant)Method (Subspace)NL(10)
43	KNN_BT(SM)D(CO)DW(IN)N(10)	117	KNN_BT(NE)D(CC)DW(SI)N(1)	191	KNN_BT(RA)D(CB)DW(SI)N(100)	265	EL(Discriminant)Method (Subspace)NL(30)
44	KNN_BT(SM)D(CO)DW(IN)N(100)	118	KNN_BT(NE)D(CC)DW(SI)N(10)	192	KNN_BT(RA)D(CC)DW(EQ)N(1)	266	EL(Discriminant)Method (Subspace)NL(50)
45	KNN_BT(SM)D(CO)DW(SI)N(1)	119	KNN_BT(NE)D(CC)DW(SI)N(100)	193	KNN_BT(RA)D(CC)DW(EQ)N(10)	267	EL(KNN)Method (Subspace)NL(10)
46	KNN_BT(SM)D(CO)DW(SI)N(10)	120	KNN_BT(NE)D(CO)DW(EQ)N(1)	194	KNN_BT(RA)D(CC)DW(EQ)N(100)	268	EL(KNN)Method (Subspace)NL(30)
47	KNN_BT(SM)D(CO)DW(SI)N(100)	121	KNN_BT(NE)D(CO)DW(EQ)N(10)	195	KNN_BT(RA)D(CC)DW(IN)N(1)	269	EL(KNN)Method (Subspace)NL(50)
48	KNN_BT(SM)D(CS)DW(EQ)N(1)	122	KNN_BT(NE)D(CO)DW(EQ)N(100)	196	KNN_BT(RA)D(CC)DW(IN)N(10)	270	EL(Tree)Method(AdaBoostM2)NL(10)
49	KNN_BT(SM)D(CS)DW(EQ)N(10)	123	KNN_BT(NE)D(CO)DW(IN)N(1)	197	KNN_BT(RA)D(CC)DW(IN)N(100)	271	EL(Tree)Method(AdaBoostM2)NL(30)
50	KNN_BT(SM)D(CS)DW(EQ)N(100)	124	KNN_BT(NE)D(CO)DW(IN)N(10)	198	KNN_BT(RA)D(CC)DW(SI)N(1)	272	EL(Tree)Method(AdaBoostM2)NL(50)
51	KNN_BT(SM)D(CS)DW(IN)N(1)	125	KNN_BT(NE)D(CO)DW(IN)N(100)	199	KNN_BT(RA)D(CC)DW(SI)N(10)	273	EL(Tree)Method(RUSBoost)NL(10)
52	KNN_BT(SM)D(CS)DW(IN)N(10)	126	KNN_BT(NE)D(CO)DW(SI)N(1)	200	KNN_BT(RA)D(CC)DW(SI)N(100)	274	EL(Tree)Method(RUSBoost)NL(30)
53	KNN_BT(SM)D(CS)DW(IN)N(100)	127	KNN_BT(NE)D(CO)DW(SI)N(10)	201	KNN_BT(RA)D(CO)DW(EQ)N(1)	275	EL(Tree)Method(RUSBoost)NL(50)
54	KNN_BT(SM)D(CS)DW(SI)N(1)	128	KNN_BT(NE)D(CO)DW(SI)N(100)	202	KNN_BT(RA)D(CO)DW(EQ)N(10)	276	EL(Tree)Method(Bag)NL(10)
55	KNN_BT(SM)D(CS)DW(SI)N(10)	129	KNN_BT(NE)D(CS)DW(EQ)N(1)	203	KNN_BT(RA)D(CO)DW(EQ)N(100)	277	EL(Tree)Method(Bag)NL(30)
56	KNN_BT(SM)D(CS)DW(SI)N(100)	130	KNN_BT(NE)D(CS)DW(EQ)N(10)	204	KNN_BT(RA)D(CO)DW(IN)N(1)	278	EL(Tree)Method(Bag)NL(50)
57	KNN_BT(SM)D(EU)DW(EQ)N(1)	131	KNN_BT(NE)D(CS)DW(EQ)N(100)	205	KNN_BT(RA)D(CO)DW(IN)N(10)	279	NB_DI(kernel)Kernel(normal)
58	KNN_BT(SM)D(EU)DW(EQ)N(10)	132	KNN_BT(NE)D(CS)DW(IN)N(1)	206	KNN_BT(RA)D(CO)DW(IN)N(100)	280	NB_DI(kernel)Kernel(box)
59	KNN_BT(SM)D(EU)DW(EQ)N(100)	133	KNN_BT(NE)D(CS)DW(IN)N(10)	207	KNN_BT(RA)D(CO)DW(SI)N(1)	281	NB_DI(kernel)Kernel(epanechnikov)
60	KNN_BT(SM)D(EU)DW(IN)N(1)	134	KNN_BT(NE)D(CS)DW(IN)N(100)	208	KNN_BT(RA)D(CO)DW(SI)N(10)	282	NB_DI(kernel)Kernel(triangle)
61	KNN_BT(SM)D(EU)DW(IN)N(10)	135	KNN_BT(NE)D(CS)DW(SI)N(1)	209	KNN_BT(RA)D(CO)DW(SI)N(100)	283	NN_pattNet_TF(SCG)HU(10)
62	KNN_BT(SM)D(EU)DW(IN)N(100)	136	KNN_BT(NE)D(CS)DW(SI)N(10)	210	KNN_BT(RA)D(CS)DW(EQ)N(1)	284	NN_pattNet_TF(SCG)HU(20)
63	KNN_BT(SM)D(EU)DW(SI)N(1)	137	KNN_BT(NE)D(CS)DW(SI)N(100)	211	KNN_BT(RA)D(CS)DW(EQ)N(10)	285	NN_pattNet_TF(SCG)HU(40)
64	KNN_BT(SM)D(EU)DW(SI)N(10)	138	KNN_BT(NE)D(EU)DW(EQ)N(1)	212	KNN_BT(RA)D(CS)DW(EQ)N(100)	286	NN_pattNet_TF(RP)HU(10)
65	KNN_BT(SM)D(EU)DW(SI)N(100)	139	KNN_BT(NE)D(EU)DW(EQ)N(10)	213	KNN_BT(RA)D(CS)DW(IN)N(1)	287	NN_pattNet_TF(RP)HU(20)
66	KNN_BT(SM)D(MA)DW(EQ)N(1)	140	KNN_BT(NE)D(EU)DW(EQ)N(100)	214	KNN_BT(RA)D(CS)DW(IN)N(10)	288	NN_pattNet_TF(RP)HU(40)
67	KNN_BT(SM)D(MA)DW(EQ)N(10)	141	KNN_BT(NE)D(EU)DW(IN)N(1)	215	KNN_BT(RA)D(CS)DW(IN)N(100)	289	NN_pattNet_TF(LM)HU(10)
68	KNN_BT(SM)D(MA)DW(EQ)N(100)	142	KNN_BT(NE)D(EU)DW(IN)N(10)	216	KNN_BT(RA)D(CS)DW(SI)N(1)	290	NN_pattNet_TF(LM)HU(20)
69	KNN_BT(SM)D(MA)DW(IN)N(1)	143	KNN_BT(NE)D(EU)DW(IN)N(100)	217	KNN_BT(RA)D(CS)DW(SI)N(10)	291	NN_pattNet_TF(LM)HU(40)
70	KNN_BT(SM)D(MA)DW(IN)N(10)	144	KNN_BT(NE)D(EU)DW(SI)N(1)	218	KNN_BT(RA)D(CS)DW(SI)N(100)	292	NN_softmax_TF(SCG)
71	KNN_BT(SM)D(MA)DW(IN)N(100)	145	KNN_BT(NE)D(EU)DW(SI)N(10)	219	KNN_BT(RA)D(EU)DW(EQ)N(1)	293	NN_softmax_TF(LM)
72	KNN_BT(SM)D(MA)DW(SI)N(1)	146	KNN_BT(NE)D(EU)DW(SI)N(100)	220	KNN_BT(RA)D(EU)DW(EQ)N(10)		
73	KNN_BT(SM)D(MA)DW(SI)N(10)	147	KNN_BT(NE)D(MA)DW(EQ)N(1)	221	KNN_BT(RA)D(EU)DW(EQ)N(100)		
74	KNN_BT(SM)D(MA)DW(SI)N(100)	148	KNN_BT(NE)D(MA)DW(EQ)N(10)	222	KNN_BT(RA)D(EU)DW(IN)N(1)		

Figure 3.11: The list of the classifiers we explored in this chapter. The followings are the list of abbreviations: SC: Split Criterion, MS: Maximum number of Splits, T: Type, KF: Kernel Function, C: Coding, KS: Kernel Scale, P: Polynomial, GA: GAussian, OO: One-vs-One, PO: Polynomial Order, BT: Break Ties, D: Distance, DW: Distance Weight, EX: EXponent, N = number of Neighbors, SM: SMallest, NE: NEarest, RA: RAndom, CB: City Block, CC: ChebyChev, CO: COrrelation, CS: CoSine, EU: EUclidean, SE: Standardized Euclidean, MA: MAhalanobis, MI: MInkowski, SP: SPearman, EQ: EQual, IN: INverse, SI: SquaredInverse, EL: Ensemble Learner, NL = Number of Learners, DI: DIstribution, TF: Training Function, HU: number of Hidden Units, SCG: Scaled Conjugate Gradient, RP: Resilient backPropagation, LM: Levenberg-Marquardt backpropagation. The numbers indicate the classifiers IDs.

Chapter 4

Techniques to Improve the Classification Performance

Stream data from the wearable sensors can be evaluated in real time or can be transmitted to a central hub to be analyzed offline. The cloud Machine Learning (ML) services now enable us to build our models that work on any type of data with any size. Most wearable companies send preprocessed data to the cloud, where a more complex analysis can be performed. Regardless of the used approach, the main goal is to extract knowledge from the measurement information about the state of the user. The notion of state apparently depends on the particular application ranging from understanding what the user is performing to diagnosing anomalous events such as sleep apnea. As we described in the previous chapter, the first step in learning from existing training examples is to extract meaningful features and the second phase consists in reducing the dimensionality of the data by using methods such as PCA. Finally, we build a function of the measurements using statistical learning methods to describe the state of the person wearing the devices. In this chapter, we introduce a new feature extraction method and a novel multi-classification technique which improve two conflicting main objectives of classification problems i.e. classification accuracy and the worst-case sensitivity. The proposed techniques are investigated in two case studies, where different classes correspond to various daily activities and breathing disorders. We will also show that the time required by the trained model for classifying a new instance (test phase) can be reduced by constructing a hierarchical ensemble classification. Furthermore, we present a fast and innovative approach to speed up the conventional recognition methods by reducing the number of calls of feature extraction and classification functions.

4.1 Background and Motivation

In Chapter 3, different studies are explored to develop reasoning algorithms to infer activities from accelerometer sensors that can be unobtrusively attached to the body or can be part of clothing items to observe people's lifestyle and behavior changes. We showed that in the realistic scenarios with subject-independent evaluation, the accuracy of recognition is reduced since the trained model deals with a set of data, which might have new measurement characteristics. Therefore, there is a need for further studies investigating new relevant features and novel machine learning models to be sufficiently flexible in dealing with inter-person differences in the activities' performance. Enhancing a model performance can be done in various stages, starting from data collection to model building. Each stage majorly influences the outcome of the learning process. One of the most effective ways is to extract more information from existing data through defining new features. Furthermore, as seen before, some learning algorithms and parameter settings are better suited to a particular type of dataset. Hence, we should analyze the models in different ways and find an optimal ensemble of different classifications. Therefore, in this chapter, we introduce a new feature extraction method and a novel multi-classification technique, which improve two conflicting objectives that are classification accuracy and the worst-case sensitivity.

The medical research literature has broadly studied the beneficial effects of physical activity on health regardless of age. As we discussed in the previous chapter, the recent advances in wearable devices have led to an impressive growth for activity data. We can make use of available data to provide innovative ways to control the prevalence of overweight and obesity and enhance the quality of independent living of elderly or disabled people. In the first case study, we extend the human activity recognition problem discussed in Chapter 3 with a wider range of activities containing translational motions, jumps, and body part-specific activities (33 activities). We evaluate each sensor position and the specific fusion of two and three sensors to recognize fitness and ambulation activities.

As we thoroughly explored the HAR problem in Chapter 3, we will discuss another area of interest that is detecting the changes in the anterior–posterior diameter of the chest wall during breathing function using accelerometer sensors. The goal is to design a diagnosis system based on wearable sensors with the advantages of simple setup, high reliability, and accuracy as well as providing useful information for health-related applications. The respiratory disorder is a highly prevalent condition associated with many adverse health problems. An accurate identification of breathing disorders requires direct measurement of upper airway airflow and respiratory effort. Although the Polysomnography (PSG) is known as the de facto gold standard mean in respiratory disorders diagnosis, it is inconvenient, expensive, time-consuming and has to be conducted in the laboratory [200]. Furthermore, it is scarce for everyone since there are few hospitals that provide PSG test, especially in rural areas. Due to this fact, a vast majority of patients with breathing problems remain undiagnosed which may increase the possibility of developing cardiovascular diseases such as stroke and heart failure.

Another traditional technique for diagnosis of breathing problems resulted from lung diseases is stethoscope. It is a widely used tool for the identification of various lungs' disorders. However, the interpretation of lung sounds strongly depends on the experience of the physician [201].

The problem of diagnosis is modeled as a supervised classification problem, where a respiration disorder is assigned into a predefined class based on a number of observed attributes. Once the classifier is developed, it is used to anticipate the breathing problems that correspond to unseen samples [202]. Different machine learning techniques, such as linear and quadratic discriminant model [203], regression tree method [204], Bayesian hierarchical [205] and Support Vector Machine (SVM) [206] have been used for automatic recognition of Obstructive Sleep Apnea (OSA). The classifiers mostly used the features extracted from Heart Rate Variability (HRV) and ECG-derived respiration (EDR) signals. In [207], the authors applied the wavelet transform and an artificial Neural Network (NN) algorithm to the electroencephalogram (EEG) signal for identifying sleep apnea episodes. The EEG signals are classified into four frequency bands of basis waves: delta (δ), theta (θ), alpha (α) and beta (β). In case of apnea, the EEG signal shifts above the delta frequency band. Then, sleep EEG activity shifts from a delta wave to theta and alpha waves frequency bands in the range of 4~14Hz once an episode of apnea ends. The system's identification achieved a sensitivity of approximately 69.64% and a specificity of approximately 44.44%. In 2013, Koley *et al.* [208] presented a real-time portable apnea and hypopnea detection system based on SVM with Gaussian Radial Basis Function (GRBF) kernel and oronasal airflow signal. They achieved the detection accuracy of 93.4% and 91.8% for eight different subjects in the offline and online tests, respectively. Although useful, all these methods require signals, which are only available in hospitals or laboratories and could not provide automated wireless remote detection.

There exist approaches that aim to classify the abnormal breathing from normal respiratory conditions [208]-[211]. For instance, [208] used a multi-layer perceptron neural network classifier applied on spirometry data. The total accuracy, sensitivity, and specificity of 97.6%, 97.5%, and 98.8% are achieved, respectively. Mahesh *et al.* [210] discussed the problem of binary classification with 92% accuracy through pulmonary function test and neural network. A Radial Basis Function neural network is described in [211] with a flow-meter spirometer to differentiate between normal and obstructive abnormality. The validity of their result was tested with the accuracy of 90%.

In [212], the authors provided a combined two sequential binary neural network classifiers to detect normal, obstructive, and restrictive breathing models. The first classifier separates the normal and abnormal patterns followed by the second binary classification between obstructive and restrictive breathing patterns. They could obtain an average accuracy of 92.5%. An SVM classifier with linear and second-order polynomial kernels has been presented in [213] for automatic recognition of OSA. They evaluated their technique on Polysomnographic data for 50 OSA patients and 50 control subjects considering different types of features such as HRV, respiratory, oxygen saturation, and combined features. Among the three signals, oxygen saturation always provided the best specificity (up to 98%), while the respiratory efforts had the maximum sensitivity (up to 72%). There was an increase in the sensitivity from 25% (using the linear kernel) to 60% (using the polynomial kernel) in case of oxygen saturation. This lets the overall accuracy reach 80% in minute-by-minute classification and 95% in subject classification. Varady *et al.* showed that phase difference between the thoracic and abdominal respiratory signals has 80–90% accuracy in identifying selected 1-min segments from OSA and control subjects [214]. An example of contactless monitoring system was investigated in [215], which applied six load cells under the bed to monitor the movements, heart rate, and respiration. The Bayesian classifier is used with different features to distinguish among normal breathing, central and obstructive sleep apnea. The accuracy and minimum sensitivity of the classifier are reported as 76.89% and 65%, respectively.

The breath sound has been widely used in diagnosing of respiratory diseases, such as flu, pneumonia, and bronchitis. Palaniappan *et al.* [216], proposed a method that used MelFrequency Cepstral Coefficients (MFCC) as features extracted from respiratory sounds. They applied SVM classifier to distinguish normal, obstruction pathology airway, and parenchymal pathology. They achieved an average classification accuracy of 90.77%. Recently, a binary classification technique is presented based on the maximum likelihood approach by using Hidden Markov Models (HMMs) [217]. They include the impacts of both lung and heart sounds in their feature extraction phase. The classification rate of 81.3% is reported for differentiating between healthy people and patients when the classifier is trained only by the lung sound (Baseline) [218]. However, this rate increases to 83% with both lung and heart sound parameters. The lung sound classification is also used for Pulmonary Emphysema (PE) diagnosis in [219]. The accuracy of 83.9% between healthy subjects and patients is achieved. All these techniques are based on the classification of breath sounds either alone or combined with heart sound. Breath sound is often considered as a band-limited or broadband noise [220] and needs enhanced signal processing to be integrated into a reliable breath disorders diagnosis.

In [126], we introduced the use of accelerometer sensors for detecting nine different breathing patterns in the stationary positions. Novel approaches were discussed for extracting information-rich features from accelerometer-derived respiration signals. The selected features fed six different classifiers and the best models were obtained considering extensive sets of performance metrics. The experimental results conducted with ten subjects showed the best accuracy rates of 97.50% by SVM classifier and 97.37%

Table 4.1: List of previous works in breathing disorders classification

Ref#	Technique	Detection	Wireless	Device / Signal	Accuracy (%)	Sensitivity (%)
[126]	DTB	Normal/Abnormal (9 types)	Yes	Acceleration	97.5	95.12
[219]	HMM	Normal/Abnormal	No	Microphone	83.9	79.1
[218]	HMM	Normal/Abnormal	No	Microphone	81.3	67.9
[217]	HMM	Normal/Abnormal	No	Microphone (Lung + Hearth sounds)	83	73
[216]	SVM	Normal/Abnormal (2 types)	No	Microphone	90.77	88
[212]	NN	Normal/Obstructive + Restricted	No	Spirometer	92.5	95
[211]	RBF NN	Normal/Obstructive breathing	No	Spirometer	90	91.6
[210]	NN	Normal/Restricted breathing	No	Spirometer	92	92.3
[208]	NN	Normal/Obstructive +Restricted + Mix	No	Spirometer	97.56	97.5
[208]	SVM	Normal/Apnea/Hypoapnea	No	Airflow (oronasal airflow)	91.8	88.9
[206]	SVM	Normal/Apnea	No	ECG	92.85	92.3
[205]	Hierarchical Bayesian	Normal/Apnea	No	ECG	93.33	NA
[204]	Regression Tree	Normal/OSAS	No	ECG + EEG + EOG + Pulse Oximetry	91.16	92.4
[203]	Quadric Discrimination (QD)	Normal/Apnea(OSA or Mixed)	No	ECG(Single lead)	90	86.4
[213]	SVM	Normal/Apnea	No	PSG	95	91.8
[215]	Bayesian	Normal/Central/Obstructive Sleep Apnea	Yes	Load cells under the bed	76.89	65

with Decision Tree Bagging (DTB) with all features and after feature selection, correspondingly. Table 4.1 summarizes the results of related work. In this chapter, rather than constraining the model to a single type of classifier, a hierarchical ensemble of different classification algorithms are considered. This work seeks to pave the path to a new generation of accelerometer-based respiration monitoring approaches for their use in the real world.

Regardless of where the ML model is deployed, the number of the prediction functions' calls plays an important role in the computation cost. For each window of sensor data, different steps including features extraction, features selection, and machine learning model need to be run. Each step requires computational power and time in the processing of the data. Building the models in the Cloud also adds more costs per each call via a RESTful interface. For real-time and frequent predictions, it is important to ensure that infrastructure resources are not disproportionately used in an inefficient manner. In different sensor-based classification applications, such as HAR and breathing disorders diagnosis, in many time intervals, we deal with a periodic signal that repeats over almost identical subsequent periods. For instance, in HAR problem, it is likely that the data of two adjacent windows is defining the same activity, as most likely the person performs the same activity longer than just a few seconds and do not change all the time from one activity to another [221]. To name another example, when a subject breathes normally, it is not necessary to repeat the classification computations every couple of seconds if there is no major change in the chest motion pattern recorded by an accelerometer. Therefore, in this chapter, we also propose a novel approach to speed up the conventional recognition methods by reducing the number of calls of feature extraction and classification functions. It is a very fast algorithm to analyze the dynamical characteristics of sensor data at each sample to detect any significant changes in the signal.

4.2 Template-Based Feature Extraction

In this section, a new feature is presented to carry important information and is evaluated in different tasks of recognition. The classification models can take great advantage of an informative-rich feature to classify different patterns based on comparing a sensor signal in each window with a predefined template. We will demonstrate the feasibility of the proposed method to better classify the motion patterns in health and fitness applications. To generate a template, the candidate feature vectors should be first determined (Algorithm 4.1) and then Dynamic Time Warping (DTW) technique runs non-linear alignments between candidate time series. This process does not affect the online computations in real-time applications. The proposed algorithm is composed of three main steps that are extracting candidate feature vectors, generating templates and providing new features. Algorithm 4.1 provides the details of extracting the feature vectors (*candidateFeatures*) that are properly classified by the employed machine learning models. For each label, the Candidate Feature Vectors (CFV) are prioritized according to classification scores (*scoreThreshold*) in line 15 and the number of learning models (*numberOfLearners*) which could classify the label, properly in line 11. The classification scores (*scoreMat*) are returned by the classifiers indicating the likelihood that a label comes from a particular class. The normalization function (line 13) is exploited to bring all scores values in the range [0, 1]. The variables '*scoreThreshold*' and '*factor*' are used in lines 5 and 6 to decrease the sensitivity of the CFV selection process gradually.

After finding the candidate feature vectors, the template of each class is deployed as explained in Algorithm 4.2. The sensor data (*data*) associated with each CFV is derived according to the window size, overlap value and sampling rate in lines 5-6. In each iteration, DTW technique [222] is applied to return the warping path between *template* and *dataWindow.* We have two time sequences, *template* (X) and *dataWindow* (Y), with the same size N. We define the warping path as a sequence $P = (p_1, p_2, \dots, p_l)$ with $p_l = (n_l, m_l) \in [1\colon N] \times [1\colon N]$ for $l \in [1\colon L]$ which assigns x_{n_l} the element of X to $y_{n_l}$the element of Y. In an acceptable path, we have $p_1 = (1,1)$ and $p_l = (N, N)$ and the path proceeds similar to "chess king" moves as: $p_{l+1} - p_l \in \{(1,0), (0,1), (1,1)\}$ for $l \in [1\colon L - 1]$.

Where (1, 0), (0, 1) and (1, 1) denote horizontal, vertical and diagonal moves. If the *template* and *dataWindow* are very similar, the warping path runs close to the diagonal line. The distance or cost of different warping paths is defined as:

$$c_p(X, Y) \coloneqq \sum_{l=1}^{L} c\left(x_{n_l}, y_{m_l}\right) \tag{4-1}$$

Where $c(x_n, y_m)$ is the Euclidean distance between corresponding points x_n and y_m. We are required to find the optimal warping path P^* between two signals which has the

Algorithm 4.1: Extract_Candidates

```
Input: correctLabels, ObtainedLabels, numberOfLearners, scoresMat; output: candidateFeatures
numberOfLabels ← unique(correctLabels); % Number of unique labels/classes
candidates ← []; % Each column will be the selected features (windowed data) for each label
for label = 1:numberOfLabels {
    tempCandidates ← [];
    for scoreThreshold = 0.1:0.05:1 {
    % To prioritize the features based on their classification scores
        for factor = 1:-0.05:0.1 {
        % To prioritize the features based on number of models which correctly classify
            for i = 1:length (correctLabels) {
                selectThisFeatureVector ← true;
                if correctLabels(i) == label {
                    indices ← find (obtainedLabels(i, 1: numberOfLearners) == label);
                    % Find which models correctly classify
                    if length (indices) >= factor × numberOfLearners {
                        for j = 1:length (indices) {
                            normalizedScores ← normalization
                                    (scoresMat (i, :, indices (j));
                            normalizedScores (label) ← -inf;
                            if max (normalizedScores) > scoreThreshold {
                                selectThisFeatureVector ← false;
                                break; }}
                        if selectThisFeatureVector
                            tempCandidates ← [tempCandidates, i]; }}}
            if ~isempty (tempCandidates)
                break; }
        if ~isempty (tempCandidates)
            break; }
    candidateFeatures (1:length (tempCandidates), label) ← tempCandidates; }
return candidateFeatures;
```

Algorithm 4.2: Generate_Template

Input: *data*, *candidates*, *freq*, *windowSize*, *overlap*; **output:** *template*

1. *windowSize_samples* ← *windowSize* × *freq*; % Number of samples in each window
2. *overlapSize_sample* ← **floor** (*windowSize_samples* × *overlap*);
   % Number of samples overlap between adjacent windows
3. *template* ← [];
4. **for** *i* = *candidates* {
5. *startPoint* ← (*i* - 1) × (*windowSize_samples* - *overlapSize_sample*) + 1;
6. *endPoint* ← *i* × *windowSize_samples* - (*i* - 1) × *overlapSize_sample*;
7. **if** ~**isempty** (*template*) {
8. *template* ← **normalize**(*data* (*startPoint*:*endPoint*));
9. **else**
10. *dataWindow* ← **normalize** (*data* (*startPoint*:*endPoint*));
    % To be compared with the template
11. [~, *i1*, *i2*] ← **dtw** (*template*, *dataWindow*);
    % Apply Dynamic Time Warping algorithm
12. *template* ← **resampling**((*template* (*i1*) + *dataWindow* (*i2*) ./ 2)); }}
    % Update the template
13. **return** *template;*

minimum total cost among all possible warping paths. The minimum distance is also considered as an indicator of the similarity of two patterns [222]. Finding the optimal path can be converted to a Dynamic Programming problem that is solved in $O(N^2)$ time. It uses an accumulated cost matrix as defined below:

$$D(n,m) := \left\{ \begin{array}{ll} 0 & if\ n = m = 0 \\ \sum_{k=1}^{n} c(x_k, y_1) & if\ m = 1 \\ \sum_{k=1}^{m} c(x_1, y_k) & if\ n = 1 \\ min \left\{ \begin{array}{c} D(n-1, m-1), D(n-1, m), \\ D(n, m-1) \end{array} \right\} + c(x_n, y_m) & , Otherwise \end{array} \right\} \tag{4-2}$$

Algorithm 4.3: TBFeatures

Input: data, labels, template, freq, windowSize, overlap; **output:** TBFeatures

1. windowSize_samples ← windowSize × freq; % Number of samples in each window
2. overlapSize_sample ← **floor** (windowSize_samples × overlap);
   % Number of samples overlap between adjacent windows
3. i ← 0;
4. **while** ((i + 1) × windowSize_samples - (i) × overlapSize_sample) **<** **length** (data) {
5. i ← i + 1;
6. startPoint ← (i - 1) × (windowSize_samples - overlapSize_sample) + 1;
7. endPoint ← i × windowSize_samples - (i - 1) × overlapSize_sample;
8. **if length** (**unique** (labels (startPoint:endPoint))) == 1 {
9. dataWindow ← **normalize** (data (startPoint:endPoint));
   % To be compared with the template
10. [dist, ~, ~] ← **dtw** (template, dataWindow);
    % Apply Dynamic Time Warping algorithm
11. TBFeatures (i) ← dist;
12. **return** TBFeatures;

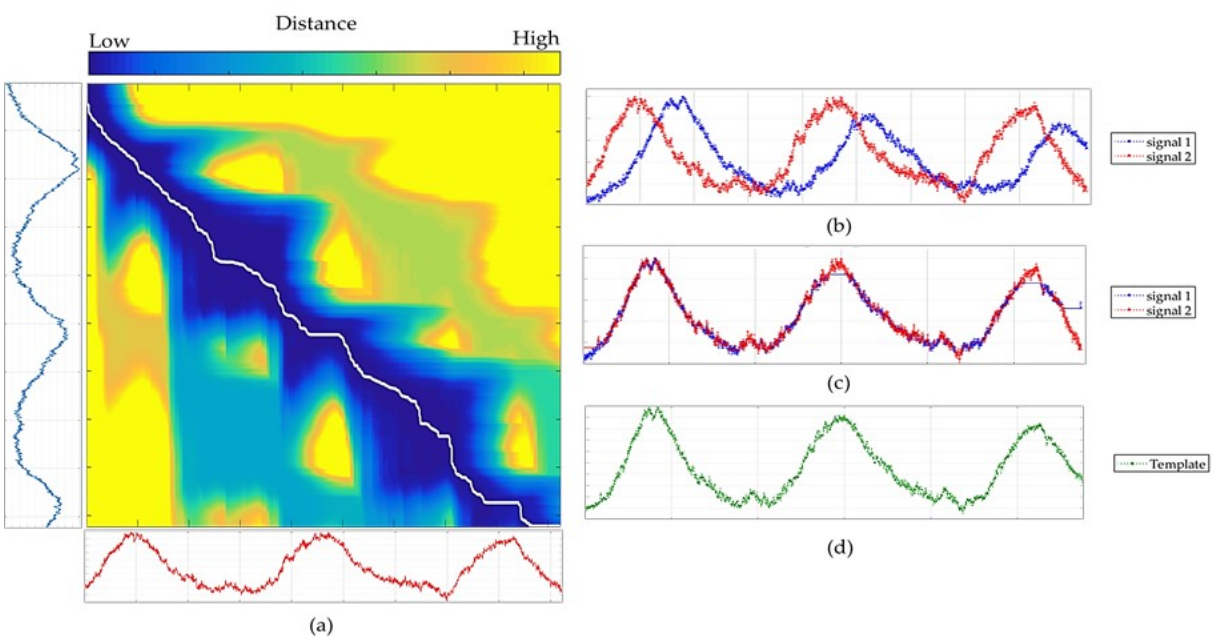

Figure 4.1: (a) Dynamic time warping technique and warping path for two sample signals, (b)Original signals, (c) warped signals, (d) the obtained template

The *D (N, N)* is the distance between two time sequences, *template* (*X*) and *dataWindow* (*Y*). For further details and thorough explanation of DTW, the reader is referred to [222]. It is important to preserve the template size same as *dataWindow* size. Otherwise, the template keeps getting larger in each iteration as warped signals probably have more samples than original ones. Therefore, in line 12 of Algorithm 4.2, after averaging and rational fraction estimation, we resample our template by an anti-aliasing low-pass FIR filter during the resampling process. Figure 4.1 depicts an example of generating a template. In the last step, the distance of each windowed data with all templates is calculated in line 10 of Algorithm 4.3 and added as new features into the feature vector. Algorithm 4.3 is run for each class template for preparing new features (*TBFeatures*) to be utilized in the training and testing phases of our classification. After extracting the new features, a filter-based feature selection called Correlation-based Feature Selection (CFS) is used to pick up three features that are highly correlated with the class, but uncorrelated with each other. The CFS algorithm attempts to maximize the following objective in its heuristic search strategy [223].

$$M_s = \frac{k\bar{r}_{cf}}{\sqrt{k + k(1-k)\bar{r}_{ff}}} \tag{4-3}$$

Where M_s is the heuristic merit of feature subset S with k features, $\bar{r}_{cf}$ is the average feature-class correlation and $\bar{r}_{ff}$ is the mean feature-feature inter-correlation. Here, CFS starts from an empty set of features and uses a forward best first search.

4.3 Multi-objective Hierarchical Classification

As discussed in the previous chapter, a recognition problem can be formulated as a supervised machine learning problem which uses the class labels when discretizing features. Thus, after data segmentation, the training set is labeled, determining the corresponding classes. In this section, we present a novel algorithm to adopt different classification algorithms for generating classification hierarchies with any structures. The classifiers are arranged in a tree formation in a top-down manner. The feature vector proceeds the branches according to the classification results returned by the hosted classifier at each internal node. In the following section, we explain how the ensemble system is configured to produce a final classification model.

4.3.1 Evolutionary Hierarchical Model

In this section, we present an evolutionary hierarchical classification to not only maximize the accuracy of the classification, but also improve the worst-case sensitivity that is not generally discussed in the recognition systems. In this problem, we make use of a Pareto-based multi-objective optimization methodology based on Genetic Evolutionary algorithm. One of the potential benefits of Pareto-based learning approach is that using multi-objective techniques may help the learning algorithm to less likely get trapped at local optima, which results in improving the accuracy of the model. The proposed top-down hierarchical structure is constructed based on a tree, where each inter nodes represents a classifier, and leaf nodes are the classes. The tree is built from top to bottom by starting with a classifier with k groups of classes $\{G_{d,1}^{n_1},\ G_{d,2}^{n_2},\ \ldots\ G_{d,k}^{n_k}\}$. A unique number (node number) is assigned to each node to save the order in which the nodes are created in the tree. d is the parent's node number and n_i is the number of labels in i^{th} group. Note that $\forall i \neq j,\ G_{d,i}^{n_i} \cap\ G_{d,j}^{n_j} = \emptyset, G_{d,i}^{n_i} \neq \emptyset$ and $i,\ j$ are integers within interval [1, k]. At the tree root, the number of classes in each group vary between 1 and number of classes l ($1 \leq k < l$) and $\bigcup_{i=1:k}\ G_{1,i}^{n_i} =\ G_{0,1}^{l}$.

In this structure, $G_{0,1}^{l}$ and G_{*}^{1} denote the root (with no parent) and a leaf, correspondingly. The number of classifiers in this architecture can vary from 1 (similar to stand-alone multi-class classifiers) to $l-1$ (similar to binary hierarchical classifiers). We develop a new way of combining classifiers to deliver high accuracy with low computational complexity. To the best of our knowledge, there is no method in literate to find optimal order for the classifiers and properly distribute the class labels within the tree hierarchy. In addition, a complete search is impossible due to millions/billions of feasible trees for a problem like breathing disorders diagnosis or human activity recognition. Consequently, there is a great interest in evolutionary algorithm to discover near-optimal solutions within a reasonable time while effectively sampling large search spaces. Thus, we use a genetic algorithm to construct a number of trees, where the classifiers hosted at each non-leaf nodes direct new instances through the branches.

We choose multi-objective Genetic Algorithm (GA) as an optimization technique. It is a variant of NSGA-II [224] using a controlled elitist genetic algorithm that takes into account both individuals with better fitness value and those can help increase the variety of the population even if they have a worse fitness value. As the first step, a chromosome is defined by two main layers as $C = (C_{class}, C_{model})$. The first layer, $C_{class} = (C_{class}[1], C_{class}[2], \dots, C_{class}[l])$, is the sub-chromosome representing the form of grouping the classes in the tree structure. Each $C_{class}[i]$ is a real number within the interval $(0,\ l]$. The second layer $C_{model} = (C_{model}[1], C_{model}[2], \dots, C_{model}[l-1])$ determines the type of classifier in each node. Figure 4.2 represents an example of a chromosome and the layers. As highlighted in the figure, the first m genes of C_{model} represent the learning models of a tree with m inner nodes ($C_{model}[1{:}\,m]$). If M is the list of different classifiers utilized in constructing the tree, each $C_{model}[i]$ is an integer within interval $[1, |M|]$.

Algorithm 4.4 presents the tree generation procedure and the conditions. The algorithm starts with the root element with node number 1 (*nodeNumber*) containing entire labels (*labels*). The nodes are constructed from top to bottom based on the labels

Classifiers	DT	NB	DA	KNN	SVM	NN	DTB
Code	1	2	3	4	5	6	7

Classes	Apneustic	Biot's	Bradypnea	Cheyn-stokes	Kussmaul	Normal	OSA	Sighing	Tachypnea
Code	P1	P2	P3	P4	P5	P6	P7	P8	P9

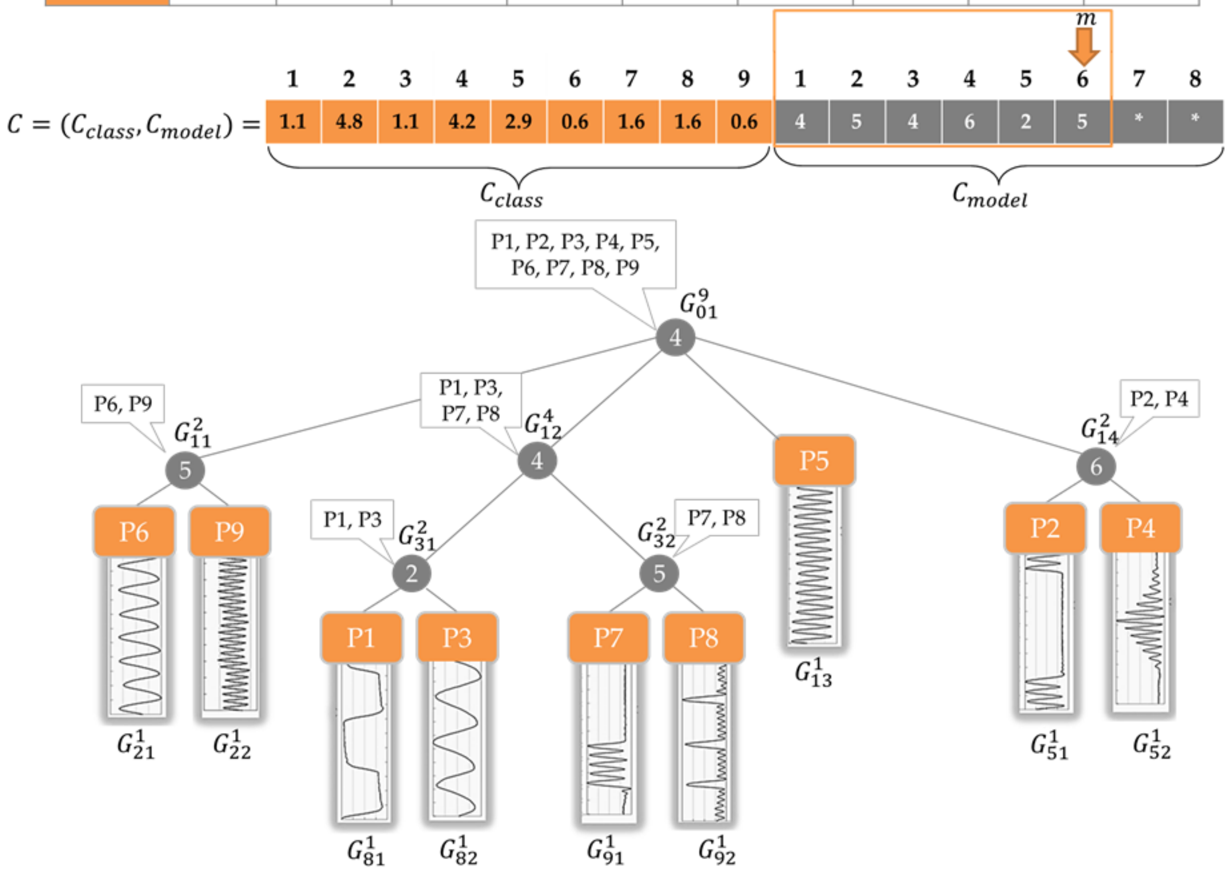

Figure 4.2: Example of the chromosome and corresponding hierarchical tree-structured classification

grouping technique (Algorithm 4.5) at each level. If the number of the assigned labels in a tree node is one (line 11), it is corresponding to a leaf. Otherwise, the node will be the root of a sub-tree as shown in lines 13-17 of Algorithm 4.4. To split the nodes in each level of the tree, the proposed technique uses a parameter named *span* that is set to 1 for the root.

The *span* value of each tree node (G_*^n) is updated by dividing the parent's *span* value by the number of labels involved in this node (n) in line 13. Therefore, any kind of tree

Algorithm 4.4: Build_Tree

```
Input: Cclass, span, labels; output: tree, treeNodes
1. tree.root ← labels; % Built a tree with a root and assign the labels
2. treeNodes ← [1]; nodeNumber ← 1; % At first, we have only the root (1)
3. endPoint ← 0; spans (nodeNumber) = span;
4. while (1) { % It repeats for each tree level
5.      if endPoint == treeNodes (end) {
6.           break;
7.      else
8.           endPoint ← treeNodes (end); }
9.      while (nodeNumber <= endPoint) {
10.          currentLabels ← tree.getLabels (nodeNumber); % Extract the labels of this node
11.          if length (currentLabels) > 1 {
             % if 'length(currentLabels) == 1', it means we reach a leaf
12.               if nodeNumber > 1 { % 'span' is already set for the root
13.                    span (nodeNumber) ← spans
                              (tree.getParent (nodeNumber)) / length (currentLabels); }
14.               [newBranches, numberOfBranches] ← labelsGrouping
                                        (Cclass, currentLabels, span (nodeNumber));
                % Grouping the labels based on the technique described in algorithm 2
15.               for i = 1:numberOfBranches {
16.                    [tree, nodeNumber] = tree.addNode
                                   (treeNodes (nodeNumber), newBranches (i).labels);
                       % Add a node (its parent is nodeNumber) and assign the labels
17.                    treeNodes = [treeNodes; nodeNumber]; }}
                       % Add the node number to the list
18.          nodeNumber ← nodeNumber + 1; }}
19. return tree, treeNodes;
```

can be constructed without any limitation such as having at most two children in the binary tree. This process recursively continues until there is no more sub-tree and all tree nodes only have one assigned label meaning they all are the leaves (G_*^1). The grouping technique summarized in Algorithm 4.5 is applied to join some labels to a group-class label. Note that this method does not allow overlapping between the class groups while splitting. It uses the updated *span* value of each node (lines 3-4) to distribute the class labels into the groups and determine new assigned labels. The procedure terminates

Algorithm 4.5: labelsGrouping

```
Input: Cclass, currentLabels, span; output: newBranches, numberOfBranches
1. i ← 0;
2. while (1) {
3.     startPoint ← ( i – 1) * span;
4.     endPoint ← i * span;
5.     indices ← find (Cclass (currentLabels) > startPoint &
                                             Cclass (currentLabels) <= endPoint);
   % Find which labels should be grouped together
6.     if ~isempty (indices) {
7.         j ← j + 1;
8.         newBranches (j).labels ← currentLabels (indices); }
           % Record the labels which grouped together in the new branch
9.     if length (newBranches (:).labels) == length (currentLabels);
10.        break; % All 'currentLabels' have been considered for grouping
11.    i ← i +1; }
12. if j == 1 {
13.     for j = 1: length (currentLabels)
14.         newBranches (j).labels ← currentLabels (j); }
15. numberOfBranches ← j;
16. return newBranches, numberOfBranches;
```

when there is no label left to be grouped in line 9. If there is only one group (line 12), it means we need to consider the *currentLabels* separately to be classified in lines 13-14.

After generating the tree based on the first layer of the chromosome, each node needs to be trained according to the selected classification model and the labels grouping results from Algorithm 4.5. The details are brought in Algorithm 4.6. For each branch node, we extract the grouped labels and provide the training feature vectors in lines 7-10. Then, the selected classifier $C_{class}[i]$, is trained with the new feature vectors (line 11) and the trained model is hosted in this node in line 12. The final ensemble model is a heterogeneous

Algorithm 4.6: Train_Tree

Input: *tree*, *trainingFeatures*, *trainingLabels*, C_{model} ; **output:** *tree* (*trained*)

1. **for** *i* = 1: *treeNodes* (*end*)
2. *tempTrainingFeatures* = []; *tempTrainingLabels* = [];
   % They are used for each node training
3. **if** ~**tree**.**isLeaf** (*i*) { % If it is a leaf, there is no need to find a classification model
4. *childrenNodes* ← **tree**.**getChildren** (*i*);
   % Number of children determines the number of classes for training the classification
   model of this node
5. **for** *j* = 1:**length** (*childsNodes*) {
6. *childLabels* ← **tree**.**getLabels** (*j*);
   % Find the labels associated with each child node
7. **for** *k* = 1:**length** (*childLabels*) {
   % Prepare the training data
8. *indices* ← (*trainingLabels* == *childLabels* (*k*));
9. *tempTrainingFeatures* ← [*tempTrainingFeatures*;
   trainingFeatures (*indices*, :)]
10. *tempTrainingLabels* ← [*tempTrainingLabels*;
    j * **ones** (1, **length** (*indices*))];}}
11. *trainedModels* ← **runClassifiers**
    (*tempTrainingFeatures*, *tempTrainingLabels*, C_{model} (*i*));
    % Run the selected classifiers based on new training data and extract their accuracies and models
12. **tree**.**setML** (*i*) ← *trainedModels* ; }}
    % Find the best classifier and assign it to the tree node i
13. **return** *tree*;

learner as it can use different classification algorithms at each node. Algorithm 4.7 describes the testing phase of the proposed classification model. In this phase, a feature vector is classified by following one branch in the hierarchy from the root to a leaf node, where it holds a class label (line 5). At each tree node, the trained model is extracted in line 8 and then run in line 9 with a test feature vector. The result of each classification decides how to direct new instances between nodes within the tree hierarchy (lines 10-11). It is worth mentioning that the training and testing feature vectors are determined

Algorithm 4.7: Test_Tree

```
Input: tree, testingFeatures, testingLabels; output: accuracy, sensitivity
1. for i = 1: length (testingFeatures) {
2.     nodeNumber ← 1; % Always start from root
3.     while (1) { % We start from tree root and stop when reach a leaf
4.         if tree.isLeaf (nodeNumber) { % If it is a leaf, we found the final label
5.             obtainedLabels (i) ← tree.getLabels (nodeNumber);
6              break;
7.         else
8.             model ← tree.setML (nodeNumber);
           % Extract the model was which trained before
9.             tempLabel ← runClassifier (model, testingFeatures(i, :));
               % Run the model with the testingFeatures and find out which branch is selected
               to continue
10.            childrenNodes ← tree.getChildren (nodeNumber); }}}
11.            nodeNumber ←  childrenNodes (tempLabel);
           % Find the next node to continue
12. confusionMatrix ← confusionmat (testingLabels, obtainedLabels);
    % Calculate the confusion matrix
13. accuracy ← sum (diag (confusionMatrix)) / sum (sum (confusionMatrix));
    % Calculate the classification accuracy
14.  sensitivity ← min (diag (bsxfun (@rdivide, confusionMatrix,
                         sum (confusionMatrix, 2)))); % Calculate the worst-case sensitivity
15. return [accuracy,  sensitivity] ;
```

based on the chosen cross-validation technique. Different performance measures are derived from the confusion matrix that contains information about actual and predicted classifications done by the final ensemble model (lines 12-14). We will evaluate the performance of the proposed technique in some state-of-the-art case studies conducted by human subjects in section 4.5.

4.3.2 Fitness Function

In this section, we define a fitness function to maximize the accuracy of the classification as well as obtain an acceptable level of accuracy for each class. The accuracy rate is used as the performance measure, which is defined as the proportion of correct classifications with respect to the total classified instances as Eq. (4-5). Each row in confusion matrix CM indicates the instances in a true class, while each column represents the instances in a predicted class. We also consider the minimum of the sensitivities of all classes, i.e. the lowest percentage of trials correctly predicted for each class with respect to the total number of trials in the corresponding class. These two objectives, after certain levels, are usually in conflict in the optimization process. Here, the sensitivity for multi-class classification is defined in Eq.(4-6):

$$CM = \begin{bmatrix} M_{11} & \cdots & M_{1l} \\ \vdots & \ddots & \vdots \\ M_{l1} & \cdots & M_{ll} \end{bmatrix} \tag{4-4}$$

$$Accuracy = A = \frac{\sum_{i=1}^{l} CM(i,i)}{\sum_{i=1}^{l}\sum_{j=1}^{l} CM(i,j)} \times 100 \tag{4-5}$$

$$Sensitivity\ (i) = \frac{CM(i,i)}{\sum_{j=1}^{l} CM(i,j)} \times 100 \tag{4-6}$$

$Sensitivity\ (i)$ is the number of patterns correctly predicted to be in class i with respect to the total number of patterns in class i (sensitivity for class i). From the above equation, we define the sensitivity of the classifier as the minimum value of the sensitivities for each class as follows:

$$S = \min_{i=1,\dots,l} Sensitivity\ (i) \tag{4-7}$$

Therefore, the main objective is summarized in Eq. (4-8):

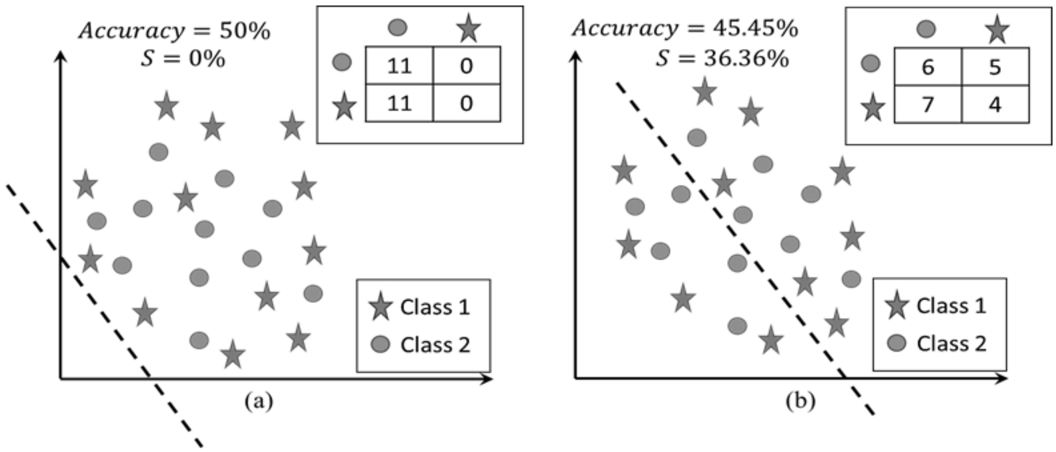

Figure 4.3: Accuracy and minimum sensitivity as conflicting objectives

$$Objective = Maximize(S, A) \tag{4-8}$$

The 2-D measure (S, A) associated with a given classifier is considered in this study. It is important to note that S and A are not cooperative in general. At the beginning of a learning process, accuracy and sensitivity could be cooperative, but after a certain level, these objectives become competitive while an increase in one objective tends to cause a decrease in the other one. This property has been also proved in [202] considering 17 classification benchmark problems. The example in Figure 4.3 shows that S and A are conflicting objectives in general. For that balanced two-class example, in the left graph, the linear classifier obtains $A = \frac{11}{22}$ and $S = 0$. If we want to improve the sensitivity, the decision boundary should be moved to separate the star class from the circle one resulted in reduction of the accuracy. We aim to find the hierarchical tree-structured model, which simultaneously optimizes two objectives: the global performance in the whole dataset and the performance in each class.

4.3.3 Genetic Operators

Genetic algorithm (GA) is a random search technique that applies the biological laws of evolution. This method is defined as $GA = \{C, E, P_0, M, \Phi, \Gamma, \psi, T\}$ [225]. Where C is the chromosome coding in GA, E is the individual fitness function, P_0 is the initial population, M is the size of the initial population, Φ is the selection operator, Γ is the crossover operator, ψ is the mutation operator, and T is the given termination condition. We used the *gamultiobj()* function in MATLAB, where $M = 30$ with 50 generations, Φ: tournament selection, Γ: two points crossover with their default settings and ψ is the adaptive feasible mutation.

4.4 ML Calls Optimization

In this section, we introduce an innovative technique that helps distinguish different patterns through analysis of dynamical characteristics of sensors data. It is an effective way to speed up the conventional recognition methods by reducing the number of calls of feature extraction and classification functions. It significantly reduces the usage of classification methods that require computationally expensive algorithms. The proposed algorithm is based on recurrence plot concept, which is the visualization of a square recurrence matrix of distance elements within a cut-off limit [226]. We use the higher-dimensional reconstruction by the method of time delays presented in [227]. From delayed coordinates of a signal *x(t)*, a pseudo-state space can be reconstructed as Eq. (4-9).

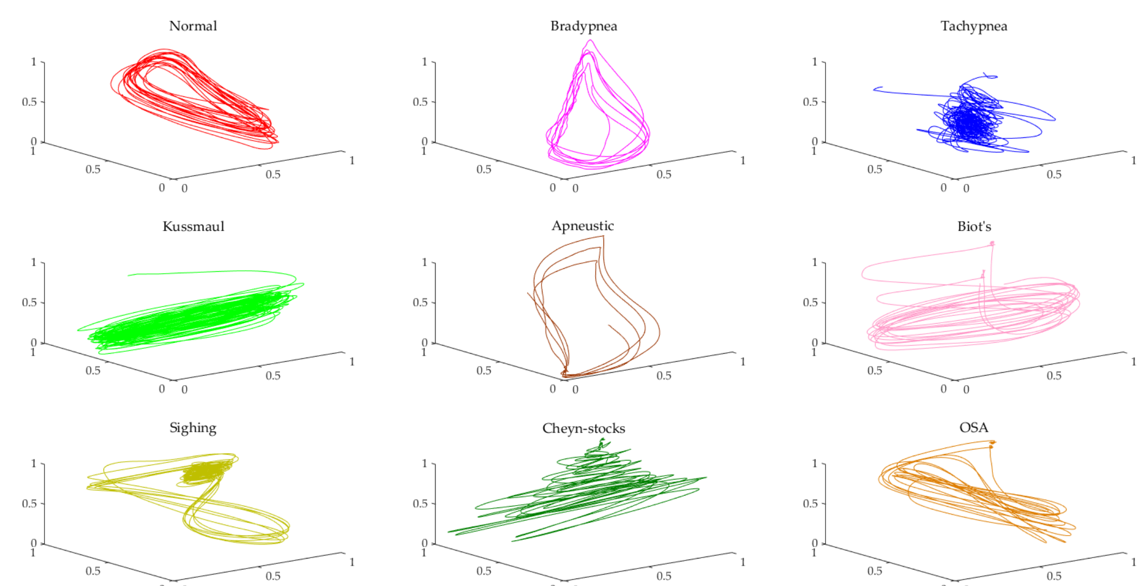

Figure 4.4: Delay representation of human breathing signals with embedding dimension 3 and tau 0.6 sec.

$$y(t_i) = [x(t_i), x(t_i + \tau), x(t_i + 2\tau), \dots, x(t_i + (D - 1)\tau)] \tag{4-9}$$

Where $y(t_i)$ is D-dimensional time-delayed vector of D points that are delayed or offset in time (τ). As shown in Figure 4.4, the lag-reconstructed the acceleration vector will provide space-time information for nine breathing patterns performed by a subject. The details of these patterns are brought in section 4.5.2. In this figure, each z-axis accelerometer signal is promoted into 3-dimensional space (D = 3) and therefore plotted against itself twice delayed (τ and 2 τ) on a three-axis plot (τ = 0.6 sec). As seen, the shape of the trajectory shows the periodic nature and dynamic of breathing patterns. The embedding dimension (D) and delay (τ) between sequential time points in the 1-dimensional signal has to be chosen with a preceding analysis of the data. In this study, the Mutual Information (MI) method [228] and the False Nearest Neighbors (FNN) [229] are employed to estimate the time delay and the embedding dimension, correspondingly. The most common method for choosing a proper time delay is based on finding the first local minimum of the Mutual Information (MI), defined as Eq. (4-10).

$$M(\tau) = \int_t p(t, t + \tau) log \frac{p(t, t + \tau)}{p(t)p(t + \tau)} dt \tag{4-10}$$

Where $p(t, \tau)$ is the joint density function, and $p(t)$ and $p(t + \tau)$ are marginal density functions of $x(t)$ and $x(t + \tau)$, respectively [229]. The first minimum of the MI denotes the time delay, where the signal $x(t + \tau)$ adds maximal information to the knowledge obtained from $x(t)$ [228]. The time delay should be selected in a way that the reconstructed vector serves as independent coordinates while keeping the connection with each other. After finding a proper time delay, the embedding dimension can be calculated. In our algorithm, we used the nearest-neighbor methodology to find the embedding dimension. It steadily increases the embedding dimension and checks whether the neighborhood of all points in the phase space change. The algorithm stops where the amount of false nearest neighbors becomes almost unchanging. In another word, the information of the system has been completely maximized and no new information can be gained by trying higher dimension [229].

4.4.1 The Proposed Method

Algorithm 4.8 describes how we used embedding dimension ($dims$) and time delay ($taus$) parameters to optimize machine learning calls during real-time classification problems. According to the employed methods explained above, the time delay and embedding dimension for each label are determined in line 2. When a new sensor sample is ready at time $t > (D-1)\tau$, a set of points, $\{points(t-(D-1)\tau), \ldots.points(t-2\tau), points(t-\tau), \ldots, points(t)\}$ are defined in line 12. We use binary code to represent positive and negative directions for each point from time *t-1* to *t*. For example, if the changes in three points values lie in the (−, +, +) directions, the binary coding for this will be (011) and the resulting decimal number is three (lines 11-17). The obtained decimal number denotes the state number and consequently there is a transition between states once a new sensor sample arrives. We expect to see very similar transitions over time while we are dealing with a periodic signal such as walking or normal breathing. To keep track of the previous recent changes, we use the idea of pheromone trail employed in ant colony optimization algorithm. For example, if the current state is three and the next changes lie in the (+, -, +) directions, binary coding for the new state will be (101) which is five. Therefore, for the transition $3 \rightarrow 5$, a specific amount of pheromone, Δ , will be deposited in line 28. In our experiments, initially there is no pheromone associated to each transition and the pheromone trails in each iteration (every $\frac{1}{f}$ sec) are updated by applying the evaporation technique as follows (line 29):

$$pt_{i,j} \leftarrow (1-\rho)pt_{i,j}, \forall(i,j) \tag{4-11}$$

Algorithm 4.8: withSmartCalls

```
Input: streamData, windowSize, overlap, freq, cModel, Δ, ρ, sensitivity, trainingData (labels, :),
maxTau, minDim, maxDim; output: improvement
1. newTransitions ← 0; smartCalls ← 0;  preState ← 1;  freshWindow ← false;
   numberOfSamples ← 0;
2. [taus, dims] ← Find_Taus_Dimensions (trainingData (labels, :),
                                                  maxTau, minDim, maxDim);
3. samplesToWait =  floor (windowSize × freq × (1 – overlap));
4.  while (~stop) { % It continues till sensor data is coming
5.       while (~ ready (streamData.newInstance));
         % Wait till there is a new sample of data (after resampling and filtering)
6.       numberOfSamples = numberOfSamples  + 1;
7.       if mod ( numberOfSamples,  samplesToWait) == 0
         % If we have enough data to run the classifier again
8.            endIndex =  numberOfSamples;
9.            freshWindow ← true;
10.           conventionalCalls ← conventionalCalls + 1;}
11.      for i = 1:dim {
12.           points (i) ← (end – (i –  1) × tau);
              % The points values are increased by 1. "end" is the index of the last sensor instance.
13.           if streamData (points (i)) <= (streamData (points (i) - 1)
14.                bin (i) ← 0;
15.           else
16.                bin (i) ← 1; }}
17.      nextState ← bin2Dec (bin); % Convert binary to decimal
18.      if transPheromones (nextState, preState) == 0 {
19.           newTransitions ← min (newTransitions + 1, 10);
20.      else
21.           newTransitions ← max (newTransitions – 1, 0); }
22.      if newTransitions > 10 – sensitivity ) &&  freshWindow  {
23.            freshWindow ← false;
24.           featuresVector ← featuresExtraction (streamData
                                    ( endIndex –  windowSize × freq  + 1: endIndex ));
25.           label ← runClassifier (cModel, featuresVector);
26.           tau ← taus (label); dim ← dims (label);
27.           smartCalls ← smartCalls + 1; }
28.      transPheromones (nextState, preState) ← Δ;
         %  Δ  is the amount of pheromone deposited for the most recent state transition
29.      transPheromones (:, :) ← max (( 1 – ρ ) × transPheromones (:, :), 0) ;
30.      preState  ← nextState; }
31. improvement ← ((conventionalCalls – smartCalls) / conventionalCalls) × 100
32. return improvement;
```

Algorithm 4.9: Find_Taus_Dimensions

Input: *training Data* (*labels*, :), *maxTau*, *minDim*, *maxDim*; **output:** *taus*, *dims*
for *i* = *labels* {
    MI ← **mutualInformation** (*trainingData* (*i*, :), *maxTau*);
    valleysLocations ← **valleysFinder** (*MI*);
    taus (*i*) ← *valleysLocations* (1) ; % First local minimum of the mutual information (MI)
    dims (*i*) ← **falseNearestNeighbors** (*trainingData* (*i*, :), *minDim*, *maxDim*); }
return *taus*, *dims*;

Where $pt_{i,j}$ is the existing pheromone trail between state i and j. ρ is the pheromone evaporation coefficient which satisfies $0 < \rho \leq 1$ and is set to $\frac{1}{pt_{i,j}}$ in our study.

The chosen value is high enough for a fair adaptation in the underlying problems. However, we believe that it should be experimentally determined under different scenarios. Thus, we read and write pheromones to track the signal behaviors, and more pheromones on each transition increase the probability of that transition being seen. Each new transition is counted, and accordingly, the number of unseen events (when there exists no pheromone associated with the new transition) is updated. However, we need to control the sensitivity of the system to avoid the transient noisy behavior. If the number of detected unseen events is more than the predetermined sensitivity, there exists a major change in the pattern, and the algorithm asks for running machine learning algorithms (*runClassifier*) in lines 22-27. The variable *freshWindow* (line 9 and line 23) is defined to control the number of calls as we have maximum one call for each new window of data according to the frequency and overlap value. If a new pattern keeps occurring, the algorithm will quickly adapt to new state transitions and stop calling the machine learning procedure until it detects a major change in the periodicity of the new pattern.

4.5 Case Studies and Results

In this section, two different case studies are evaluated based on the new proposed feature extraction and classification algorithms. First, we consider the problem of activity recognition, and then the respiratory disorders diagnosis with nine different patterns is investigated.

4.5.1 Case Study 1: Analysis of Motion Patterns for Recognition of Thirty-Three Human Activities

In the first case, we extend the human activity recognition problem discussed in Chapter 3 with more exercises. Recently, one of the most complete activity recognition datasets has been published and is now publicly available to the research community [71]. In this evaluation, we have used accelerometer sensor that is the most widely used sensor to recognize fitness and ambulation activities due to its compact size, low-power requirement, and capacity to provide data directly related to the kinematics of subject.

4.5.1.1 Test Setup

The dataset comprises the readings of nine Xsens MTx [231] motion sensors with sampling rate 50 Hz recorded from seven females and ten males, with ages ranging from 22 to 37 years old while performing thirty-three fitness activities. The dataset consists a wide variety of activities containing translational motions, jumps, and body part-specific activities focused on the trunk, upper and lower extremities as listed in Table 4.2 [71]. The sensors are mounted on different parts of the body including Right Upper Arm (RUA), Left Upper Arm (LUA), Right Lower Arm (RLA), Left Lower Arm (LLA), Right Upper Leg (RUL), Left Upper Leg (LUL), Right Lower Leg (RLL), Left Lower Leg (LLL) and Back (similar to Chest). Therefore, the sensory nodes can measure the motions experienced by each body limb and trunk, thus better capturing the body dynamics.

Table 4.2: List of activities in case study 1

Translational motions	L18: *Upper trunk and lower body opposite twist (20×)*
L1: *Walking (1 min)*	**Focused on upper extremities**
L2: *Jogging (1 min)*	L19: *Lateral elevation of arms (20×)*
L3: *Running (1 min)*	L20: *Frontal elevation of arms (20×)*
Jump	L21: *Frontal hand claps (20×)*
L4: *Jump up (20×)*	L22: *Frontal crossing of arms (20×)*
L5: *Jump front & back (20×)*	L23: *Shoulders high-amplitude rotation (20×)*
L6: *Jump sideways (20×)*	L24: *Shoulders low-amplitude rotation (20×)*
L7: *Jump leg/arms open/closed (20×)*	L25: *Arms inner rotation (20×)*
L8: *Jump rope (20×)*	
	Focused on lower extremities
Focused on the trunk	L26: *Knees (alternating) to the breast (20×)*
L9: *Trunk twist (arms outstretched) (20×)*	L27: *Heels (alternating) to the backside (20×)*
L10: *Trunk twist (elbows bent) (20×)*	L28: *Knees bending (crouching) (20×)*
L11: *Waist bends forward (20×)*	L29: *Knees (alternating) bending forward (20×)*
L12: *Waist rotation (20×)*	L30: *Rotation on the knees (20×)*
L13: *Waist bends (reach foot with opposite hand) (20×)*	
L14: *Reach heels backwards (20×)*	**General fitness exercises**
L15: *Lateral bend (10× to the left + 10× to the right)*	L31: *Rowing (1 min)*
L16: *Lateral bend with arm up (10× to the left + 10× to the right)*	L32: *Elliptical bike (1 min)*
L17: *Repetitive forward stretching (20×)*	L33: *Cycling (1 min)*

Figure 4.5 depicts two seconds of data of each activity in different sensors positions. This figure shows that each placement turns out to be more suitable for particular activities. A comprehensive study on this benchmark shows that K-Nearest Neighbors classifier among Decision Trees, Naive Bayes, and Nearest Centroid classifiers could provide the best recognition accuracy [149]. The time-domain features used in this paper are simple, easy to calculate and properly interpret the activity parameters while employing multiple body-worn sensors. These features include mean, standard deviation, maximum, minimum and zero crossing rate.

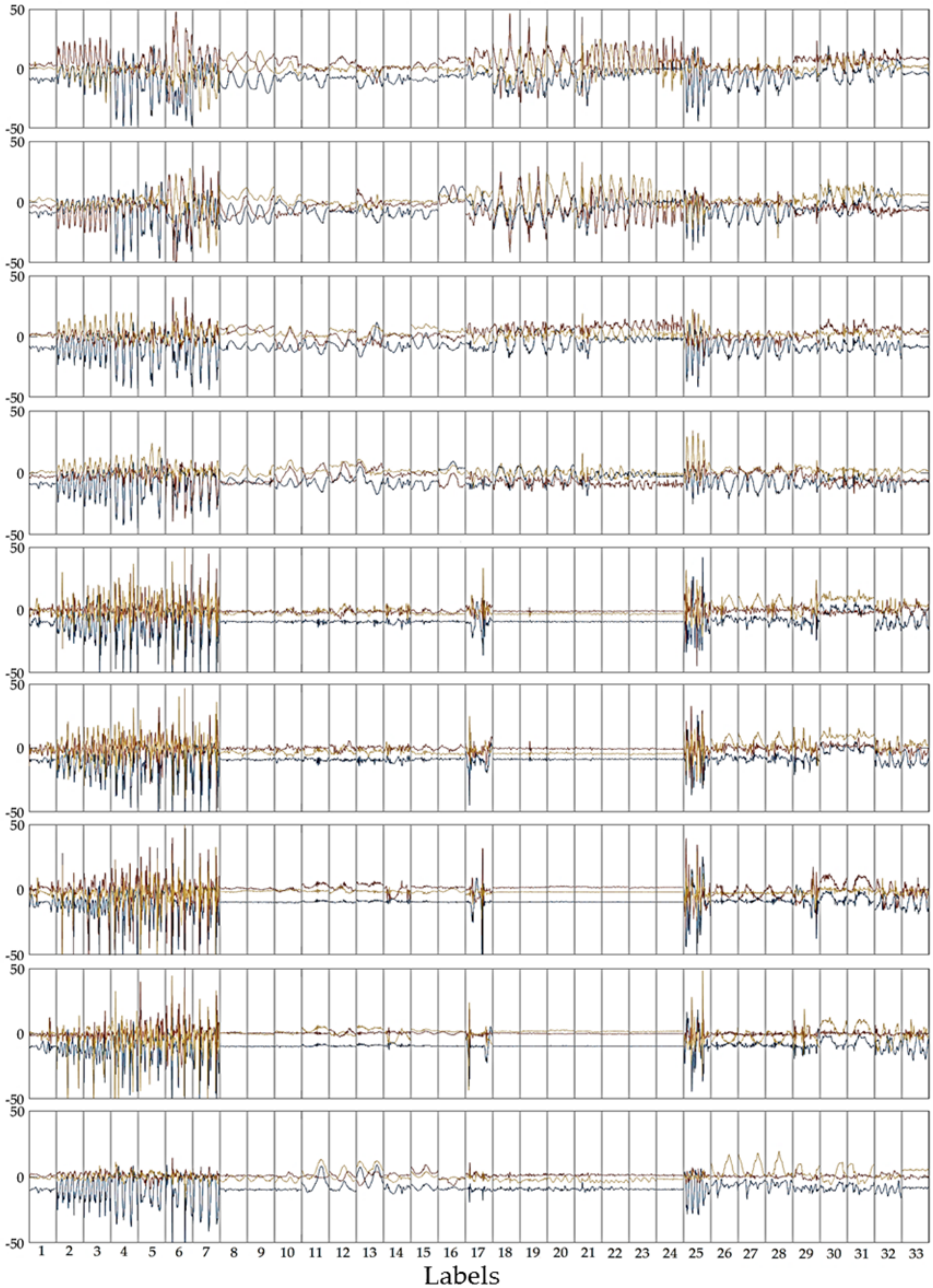

Figure 4.5: Two seconds (100 samples) of data in each - Right Lower Arm (RLA), Left Lower Arm (LLA), Right Upper Arm (RUA), Left Upper Arm (LUA), Right Upper Leg (RUL), Left Upper Leg (LUL), Right Lower Leg (RLL), Left Lower Leg (LLL), Back (from top to bottom)

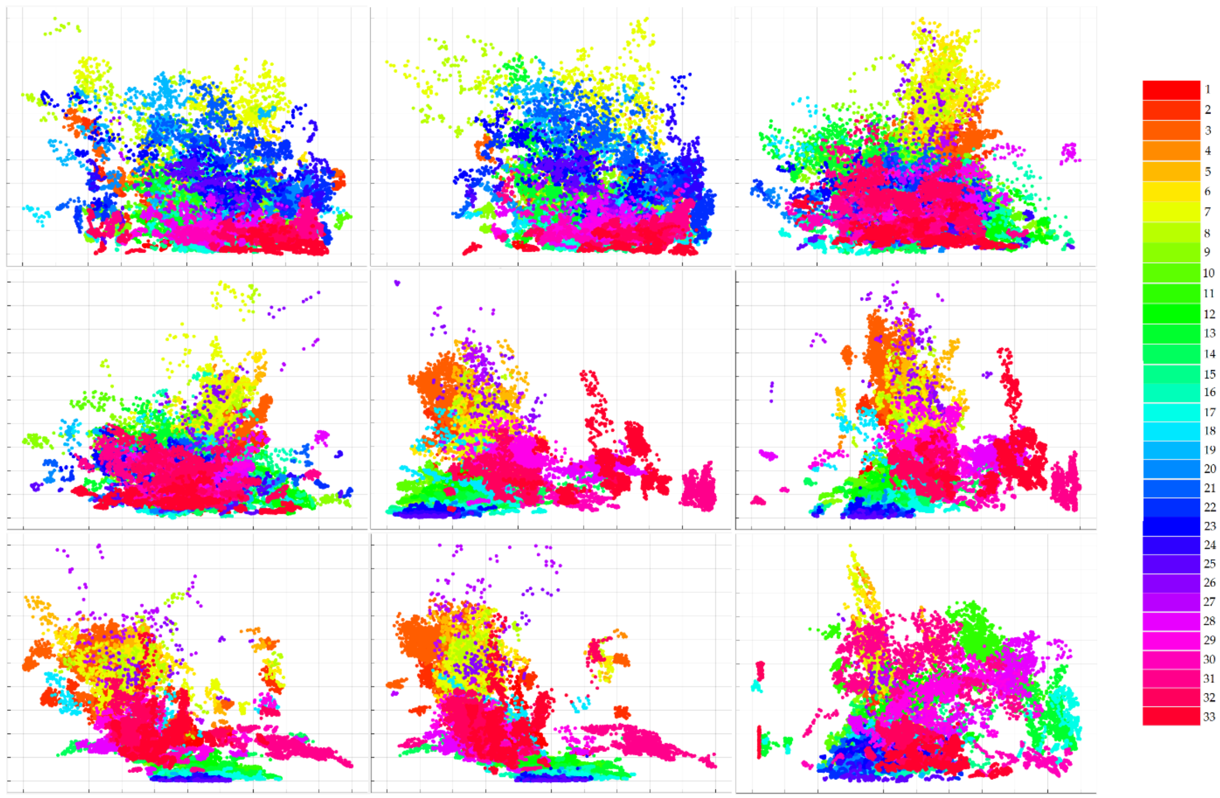

Figure 4.6: Two features i.e. mean and std with window size 6 and overlap 90% - from upper left to right - RLA, LLA, RUA, LUA, RUL, LUL, RLL, LLL and Back

The scatter plots of the mean and standard deviation of the accelerometer data with window size 6 sec are given in Figure 4.6.

4.5.1.2 Preliminary Results

In [163], we applied three classifiers i.e. Neural Network with 50 hidden neurons (M1), Support Vector Machine (M2) and bootstrap aggregation ensemble learning technique (M3) with the same lightweight time-domain features to distinguish among thirty three different fitness activities. To keep the experimental setup and classifiers performance comparable with [149], no feature selection has been applied in this investigation. We make use of SVM with Error-Correcting Output Codes (ECOC) with One-Versus-One (OVO) coding design in our multi-class classification. The number of learners for bagging schemes to combine the predictions has been selected to 50.

As we expected, the accuracy of recognition is very high using nine sensors worn on the body with 10-fold cross-validation evaluation. The results demonstrated that the best accuracy was improved by about 2% for identifying 33 activities compared to the best classification model (k-nearest neighbors) presented in [149]. However, the accuracies of all methods decreased in average by 9.45% while considering Leave-One-Subject-Out (LOSO) cross-validation. LOSO cross-validation is evaluated in which a single subject is iteratively left out from the training dataset and considered in the test set. The procedure is then repeated for all subjects whose data is complete.

As we discussed in the previous chapter, wearing a couple of IMUs can become burdensome and is invasive, expensive, and not suitable for continuous monitoring of daily activities. Therefore, we limited our modeling and analysis for single-accelerometer data to see how well a single sensor can recognize a wide range of everyday activities. The single sensor classification evaluation across all subjects and sensors showed an improvement of 7.19% with FNSW compared to [82], [149] while this number increases to approximately 20% using FOSW and 10-fold cross-validation. By randomly populating the folds from data, the performance of the classifiers is overestimated as examined in [163]. This issue becomes worse with the use of overlap between successive sliding windows, although it helps the classifiers to be trained with more feature vectors. Therefore, we use subject-independent LOSO cross-validation with overlap 90% to estimate realistic performance with each sensor. Table 4.3 presents the accuracy values of each sensor with window size 6 sec and overlap 90%. The first nine columns in Table 4.3 demonstrate the discrimination potential of each sensor. In overall, the highest classification accuracy was reported by M3. The second best technique was M2 followed by M1 and the KNN method. More precisely, the best accuracy results are RLA (70.06%), LLA (76.01%), RUA (73.86%), LUA (71.32%), RUL (73.12%), LUL (67.74%), RLL (60.48%), LLL (65.07%), and Back (67.55%).

Table 4.3: The accuracy rates and comparison between [149] and our three applied methods

Sensor Location / Methods	RLA	LLA	RUA	LUA	RUL	LUL	RLL	LLL	Back	LLA +RUL	LLA +Back	RUL +Back	LLA +RUL +Back
Banos *et al.*	67.66%	74.27%	68.67%	68.38%	60.32%	54.66%	46.94%	52.10%	59.67%	82.84%	79.65%	70.49%	84.80%
M1	65.71%	70.86%	72.26%	66.87%	70.23%	63.83%	56.18%	60.93%	62.97%	81.50%	77.10%	70.96%	83.19%
M2	68.22%	72.75%	72.80%	68.97%	**73.12%**	65.92%	59.30%	64.79%	66.95%	83.79%	79.70%	78.15%	85.87%
M3	**70.06%**	**76.01%**	**73.86%**	**71.32%**	70.80%	**67.74%**	**60.48%**	**65.07%**	**67.55%**	**88.77%**	**85.41%**	**80.85%**	**90.98%**
Improvements	3.55%	2.34%	7.56%	4.30%	21.22%	23.93%	28.85%	24.89%	13.21%	7.16%	7.23%	14.70%	7.29%

Apparently, a wide range of activities discussed in this section cannot be recognized very well with utilizing only one sensor. Therefore, we are going to fuse accelerometer data of LLA, RUL, and Back positions at the feature level to investigate the effect of combining data from accelerometers. The LLA and RUL positions are the best performing placements compared to the other sensors worn on the legs and arms for these activities. The Back position is also selected since it is a great place for many commercial wearables.

According to the results in Table 4.3 (columns 10-13), a fusion of LLA and RUL not only provides very promising results (88.77%), but also these placements are increasingly popular because most people are accustomed to carrying their smartphones in the front pants leg pocket and also wearing smartwatches. Moreover, these positions do not have the issues of wearability and usability. The big names in the industry such as Apple and Samsung joined the wearable revolution with introducing smartwatches over the past couple of years. The smartwatches can be easily paired with the smartphone, and both employ an embedded acceleration sensor. It is a great chance to fuse the sensors data of these two positions to report better performance while covering a wide range of activities containing translational motions, jumps, and various body part-specific activities. It is worthy to note that increasing the number of sensors from two to three had no substantial impact on the accuracy of the classifiers. Figure 4.7 displays the confusion matrices to give more details about the quality of the output of classifier M3 for each activity. The diagonal elements represent the number of feature vectors for which the predicted label is equal to the correct label, while off-diagonal elements are those that are mislabeled by the classifier. A high value for the diagonal elements indicated by the yellow color leads

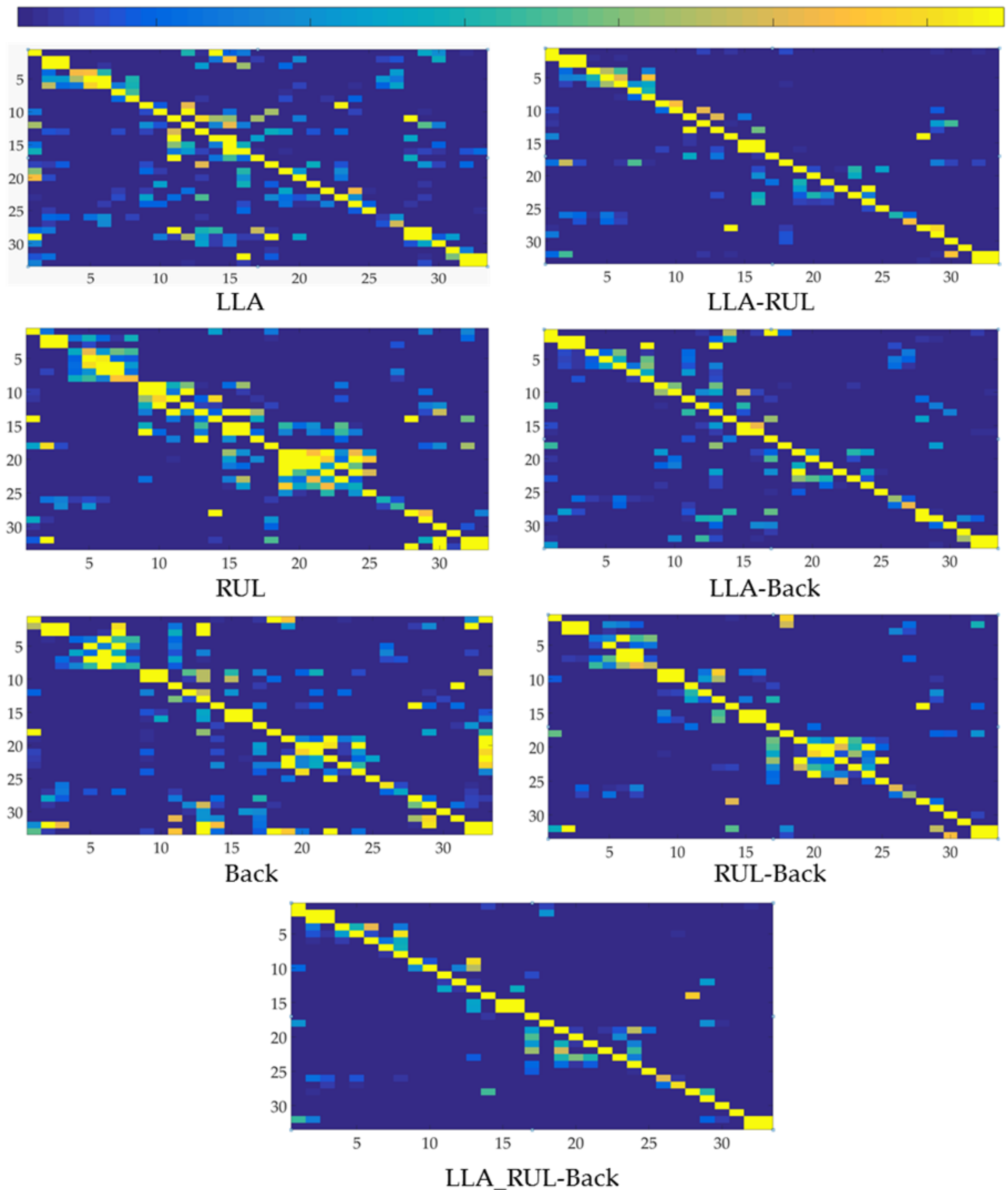

Figure 4.7: Confusion matrices derived from M3 for each sensors placements

to better classification performance. As can be observed, LLA sensor could not well discern activities focused on waist movements while RUL and Back performed worse in discriminating arm movements (L19-L25). The assessments showed an average improvement of 12.79% compared to the best results reported in [149].

To evaluate the performance of every class in the dataset, Figure 4.8 depicts the box plot of per-class sensitivity with different sensors data. The sensitivity is defined as the percentage of instances correctly predicted as belonging to each class with respect to the total number of instances in the corresponding class. As can be observed from the figure, the worst sensitivity is less than 40%, although we achieved a relatively high overall accuracy with the fusion of two and three sensors. In such a case, only accuracy could be misleading, and we need to develop a solution to obtain a satisfactory result for both metrics. In section 4.6, we will find the hierarchical tree-structured model, which uses the new proposed features in section 4.2, to optimize two conflicting objectives i.e. the global performance in the whole dataset and the performance in each class.

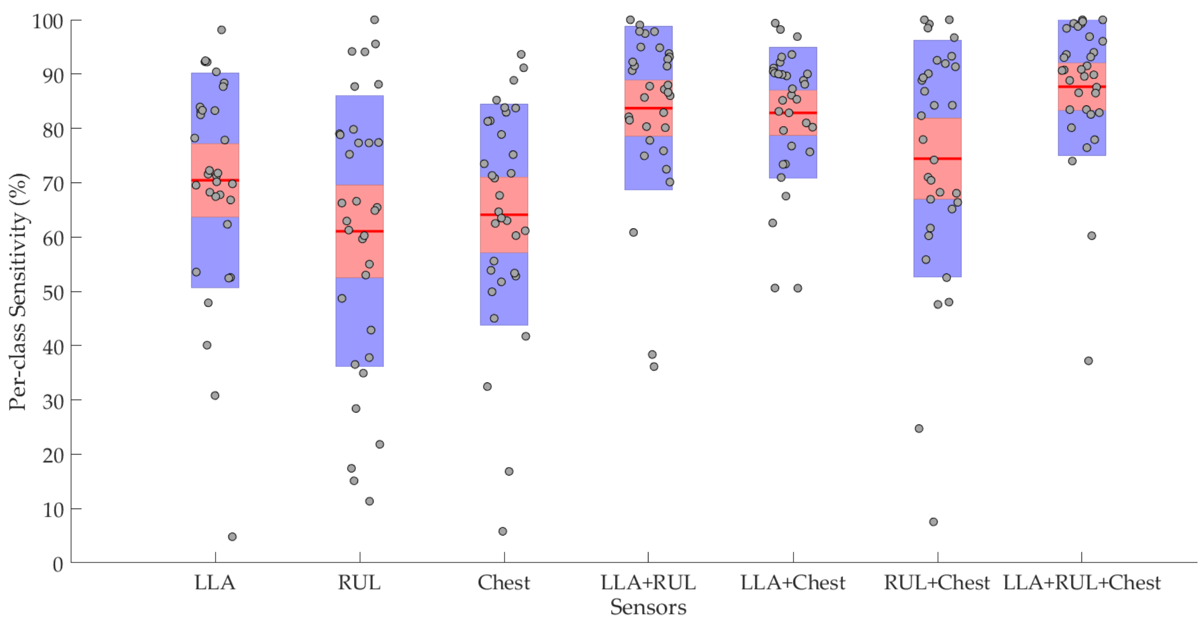

Figure 4.8: Box plot of per-class sensitivity with different sensors data

4.5.2 Case Study 2: Analysis of the Chest Wall Compartments Movements for Breathing Disorders Classification

In the second case study, we test our proposed techniques in respiration disorders classification. The recognition procedure starts with collecting data from two motion sensors (see Figure 4.9) for remote diagnosis of nine different breathing problems including Bradypnea [232], Tachypnea [233], Kussmaul [234], Cheyn–stokes [18], OSA [235], Biot's breathing [236], Sighing [237], and Apneustic [238].

Bradypnea is regular in rhythm but slower than normal in rate. It causes continuous disruption of breathing during sleep and is an age-dependent breathing disorder [239]. Tachypnea is the condition of rapid breathing, with respiration rate higher than 20 respirations per minute (rpm) at rest. Tachypnea may occur due to physiological or pathological problems [233]. Kussmaul is defined as a rapid, deep, and labored breathing that usually occurs in diabetic ketoacidosis. It is known as a type of hyperventilation, which reduces carbon dioxide in the blood due to the increased rate and depth of respiration [234]. Cheyn-stokes breathing pattern is determined by gradually increasing, then decreasing the lung volume with a period of apnea. Therefore, this type of breathing disorder is characterized by a high oscillatory tidal volume that is seen in people with heart failure, strokes, traumatic brain injuries, and brain tumors [18]. Biot's breathing is characterized by periods of rapid respirations followed by regular periods of apnea. Different reasons cause Biot's breathing, such as damage to the medulla oblongata by stroke or trauma, or pressure on the medulla because of uncal or tentorial herniation and prolonged opioid abuse [236]. OSA breathing pattern is similar to Biot's breathing pattern; however, it has a different phase shift between rib cage and abdomen compared to Biot's breathing. Sighing breathing, known as hyperventilation syndrome, is characterized by high irregular breathing punctuated by deep periodic inspirations.

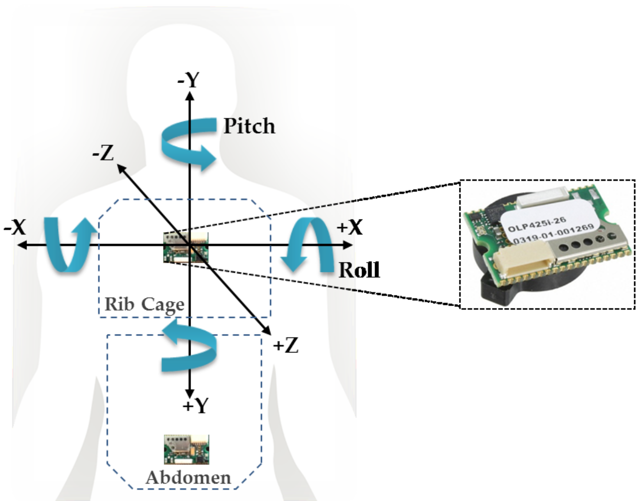

Figure 4.9: The accelerometer sensors' placements on the body

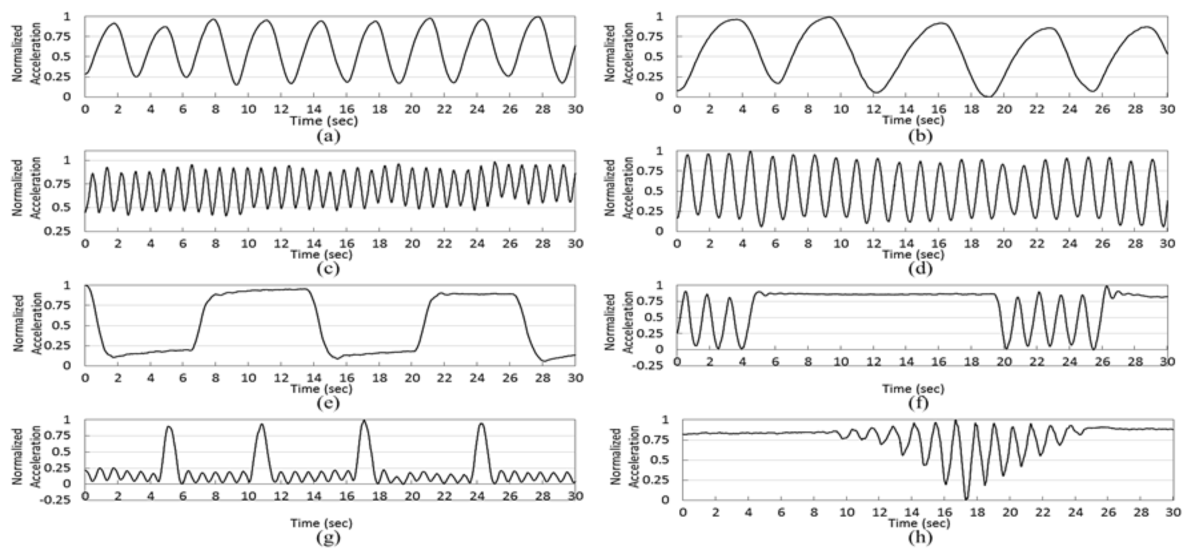

Figure 4.10: (a) Normal, (b) Bradypnea, (c) Tachypnea, (d) Kussmaul, (e) Apneustic, (f) Biot's, (g) Sighing and (h) Cheyn-stokes breathing patterns from accelerometer sensor mounted on the subject's rib cage

Sighing breathing is observed in people suffering from anxiety with no apparent organic disease [237]. Apneustic respiration is an abnormal pattern of breathing characterized by a prolonged inspiration phase with each breath, followed by an expanded expiratory phase. It is usually caused by damage to the upper part of the pons, which is the uppermost section of the brain stem and is known as one of the respiratory center parts of the brain [238]. Figure 4.10 shows 30-sec samples of eight respiration patterns derived

Table 4.4: Descriptions of some features for breathing disorder classification

Features	Description
Respiration Rate	$RR = \frac{P\times 60}{ws}$, where P is the number of local maxima and ws represents the window size in second
Pitch angle from accelerometer	$Pitch = \alpha = arctan(\frac{a_{x\prime}}{\sqrt{a_{y\prime}{}^2 + a_{z\prime}{}^2}})$
Roll angle from accelerometer	$Roll = \beta = arctan(\frac{a_{y\prime}}{\sqrt{a_{x\prime}{}^2 + a_{z\prime}{}^2}})$
Phase shift s: per breath normalized volume of the signal on the X-axis in the Lissajous figure m: the distance between the two intercepts of the loop with the ordinate at abscissa equal to 50% of the volume of the signal on the Y-axis in the Lissajous figure	If the slope of the main diagonal of the breathing loop is: Positive: $\theta = sin^{-1}\frac{m}{s}$ Negative: $\theta = 180 - \vartheta$, $sin\,\vartheta = m/s$
Accelerometer-based breath volume	$TV_i = p_i - \frac{(v_i + v_{i+1})}{2}, t = 3$
Tidal Volume variability	$TV_{var} = \frac{t\sum_{i=1}^{t} b_i TV_i - (\sum_{i=1}^{t} b_i)(\sum_{i=1}^{t} TV_i)}{t\sum_{i=1}^{t} b_i^2 - (\sum_{i=1}^{t} b_i)^2}$, $t = 3$

from the accelerometer sensor. To capture the dynamics of the signals, the data is partitioned into Fixed-size Overlapping Sliding Window (FOSW).

In [126], we have evaluated six different classifiers including SVM, NN, DA, NB, KNN, and DTB with new introduced informative features. Each feature has been individually evaluated on different groups of subjects [200], [240]. The proposed features were simple, easy to calculate and interpreted the respiration parameters, properly. These features include mean, Standard Deviation (SD), Respiration Rate (RR), average respiratory time parameters: inspiration time (T_i) and expiration time (T_e), average tilt angles (roll and pitch), mean tidal volume variability [240], average accelerometer-based breath volume [240], Symbolic Aggregate approximation (SAX) of the data and mean phase shift (θ) [200]. The descriptions of some features are summarized in Table 4.4. For

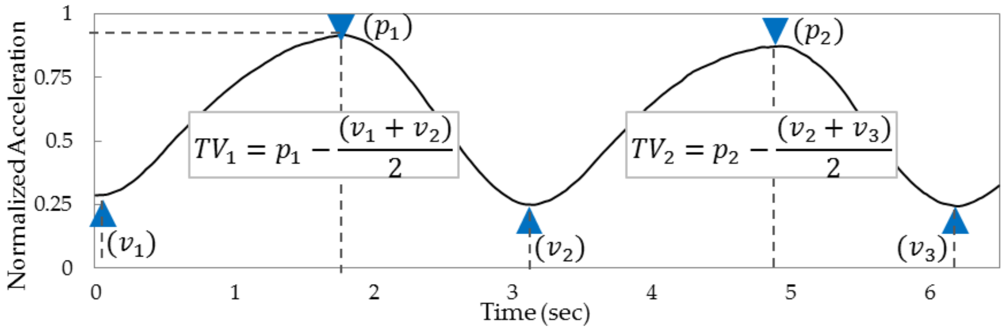

Figure 4.11: The tidal volume calculation after signal normalization

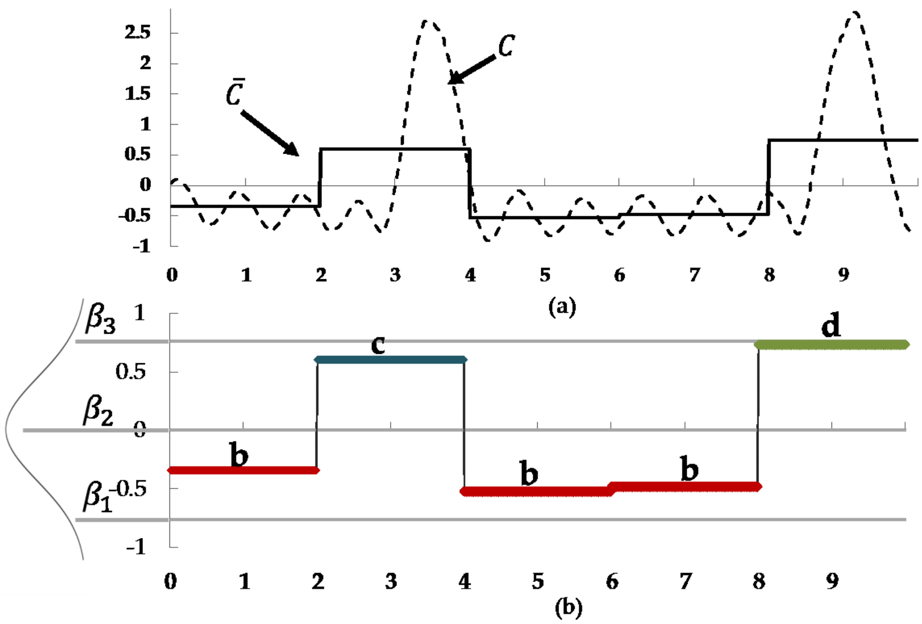

Figure 4.12: The main steps of SAX a) Piecewise Aggregate Approximation, b) Symbolic Discretization

calculating the accelerometer-based breath volume, first, the breathing signal is normalized and then the peak p_i and valley v_i values are extracted as plotted in Figure 4.11 to obtain TV_i in Table 4.4. The calculated volumes are linearly fitted with window size equal to 3 sec ($t = 3$) to obtain the trend of oscillations called TV_{var}.

We have discretized the breathing signal from the z-axis (main axis in respiration function) by Symbolic Aggregate approXimation technique. Lin *et al.* [241] introduced the

SAX that allows a time series C of length n to be represented in a w dimensional space by a vector $\overline{C} = \overline{c_1}, \dots, \overline{c_w}$. The $\overline{c_i}$ is calculated as follows [242]:

$$\overline{c_i} = \frac{w}{n} \sum_{j=\frac{n}{w}(i-1)+1}^{\frac{n}{w}i} c_j \tag{4-12}$$

The average value of the data within an episode is calculated, and a vector of these values over w intervals shows the dimensionality-reduced representation. Before this transformation, which shows the Piecewise Aggregate Approximation (PAA) of the time series, we have standardized the data to have a mean of zero and a standard deviation of one. If a time series is plotted in a Cartesian space, the PAA divides the x dimension into a set of intervals with an equal size [243]. Figure 4.12 (a) depicts an example of Sighing breathing and the PAA. A further transformation is applied to obtain a discrete representation known as Discretization. We need to have a technique that produces symbols with equiprobability [244], [245]. We have applied SAX on breathing signal and used the discretized signal as a feature in our classification.

The next extracted feature was phase shift (θ) between rib cage ($Acc1$) and abdomen ($Acc2$) which was calculated based on the degree of opening of Lissajous figure or Konno-Mead loop on accelerometer-derived respiration signals [246]. The phase angle (θ) is measured in degrees, changing from 0° to 180°. 0° and 180° represent the perfect synchronous pattern and paradoxical movement of the chest wall compartments, respectively. In Lissajous figure, the movements of one compartment are plotted versus the excursion of the second compartment in an X-Y graph during a single respiratory cycle [247], [248]. θ is defined in Table 4.4. Finally, we chose mean and standard deviation that carry discrimination potential and ease of interpretation in the acceleration domain. Besides, the standard deviation provides insights into the intensity and magnitude of the respiration function.

4.5.2.1 Test Setup

The evaluation was performed on data from 10 healthy volunteers, five males and five females aged 27 to 48 with (Mean ± SD) 34.80 ± 6.89. The tests lasted for about 35 minutes per subject. The subjects were asked to perform nine introduced breathing patterns, each for 1 minute in sitting position (torso at about 90° angle to the floor). For simulating apnea in Cheyn-stokes, Biot's and OSA breathing exercises, the subjects paused their breathing for at least 10 sec. We asked the participants to prolong their inspiration and expiration during Apneustic maneuver for at least 5 sec. Finally, for the Sighing pattern, they performed normal breathing, which is followed by deep periodic of inspiration every 3-7 sec. OSA breathing pattern is similar to Biot’s breathing pattern; however, considering two accelerometer sensors, it has a different phase shift between chest and abdomen compared to Biot’s breathing. The SPR-BTA spirometer [249] is also used in all tests to make sure that the subjects were not over emphasizing the breathing movements. Two LIS3DH 3-axis accelerometers with 12-bit resolution are used and secured by a soft and elastic strap which is easy to attach and comfortable to wear. The first sensor (Acc1) is mounted on the subject’s chest in the middle of sternum region and the second accelerometer (Acc2) sensor is attached to the subject’s umbilical region. In our tests, the sensors are sampling with 50Hz.

4.5.2.2 Preliminary Results

The evaluation of the breathing problems classification was performed through a 10-fold random-partitioning cross-validation process applied across all subjects and breathing patterns. This process was repeated ten times for each method to ensure the statistical robustness. The results are achieved for different window sizes with two segmentation techniques, i.e. FNSW and FOSW. We have swept the window size from 5 to 15 sec while five different overlap values including 10%, 25%, 50%, 75% and 90% are

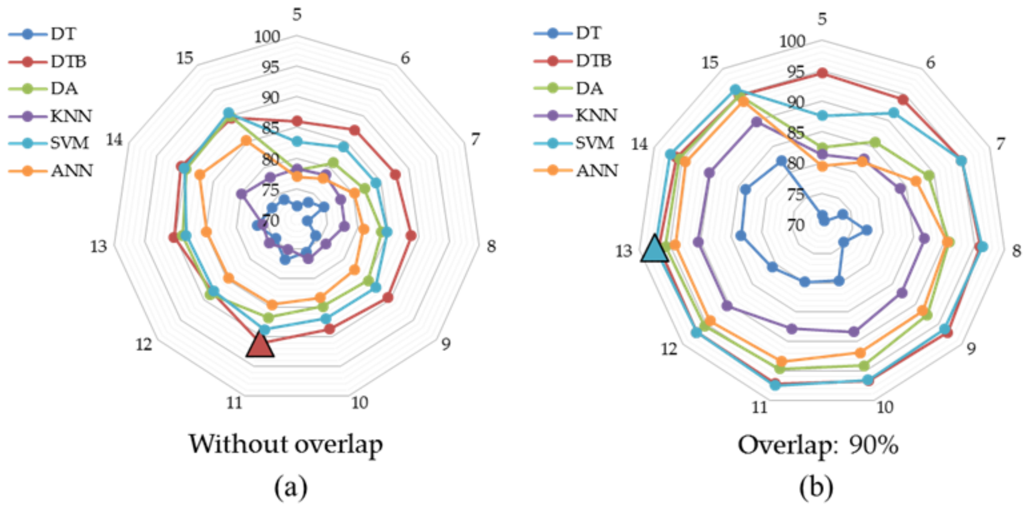

Figure 4.13: Accuracy rates with Acc1 and Acc2 sensors (a) without overlap and (b) with overlap 90% for window sizes from 5 to 15 sec

considered. The best accuracy (Acc1 + Acc2) reached 91% with DTB classifier and FNSW windowing method. SVM obtained the maximum accuracy of 97.50% with the window size 13 sec and overlap 90% (see Figure 4.13). The accuracy decreases to 90.98% considering Leave-One-Subject-Out evaluation.

DTB proved to be the most accurate model in case of using a single accelerometer. The best accuracies of 86.10% and 88.04% are achieved for sensors on chest (Acc1) and abdomen (Acc2) with all features and LOSO cross-validation, respectively. These assessments were computed based on FOSW segmentation with overlap value 90% and widow size 14 sec and 15 sec for Acc1 and Acc2. Therefore, decreasing the number of sensors represents a reduction of classification accuracy. It is also worth mentioning that using the accelerometer on the abdomen umbilical region overcomes the performance obtained from the sensor on the middle of sternum region. This improvement is due to the movement mechanism of the upper rib cage and lower rib cage/abdomen during respiration function [250]. Based on [250] the lower six ribs have a greater ability to move independently compared to the upper six ribs. Due to this fact, the breathing signals collected from Acc2 resulted in better classification accuracy compared to Acc1.

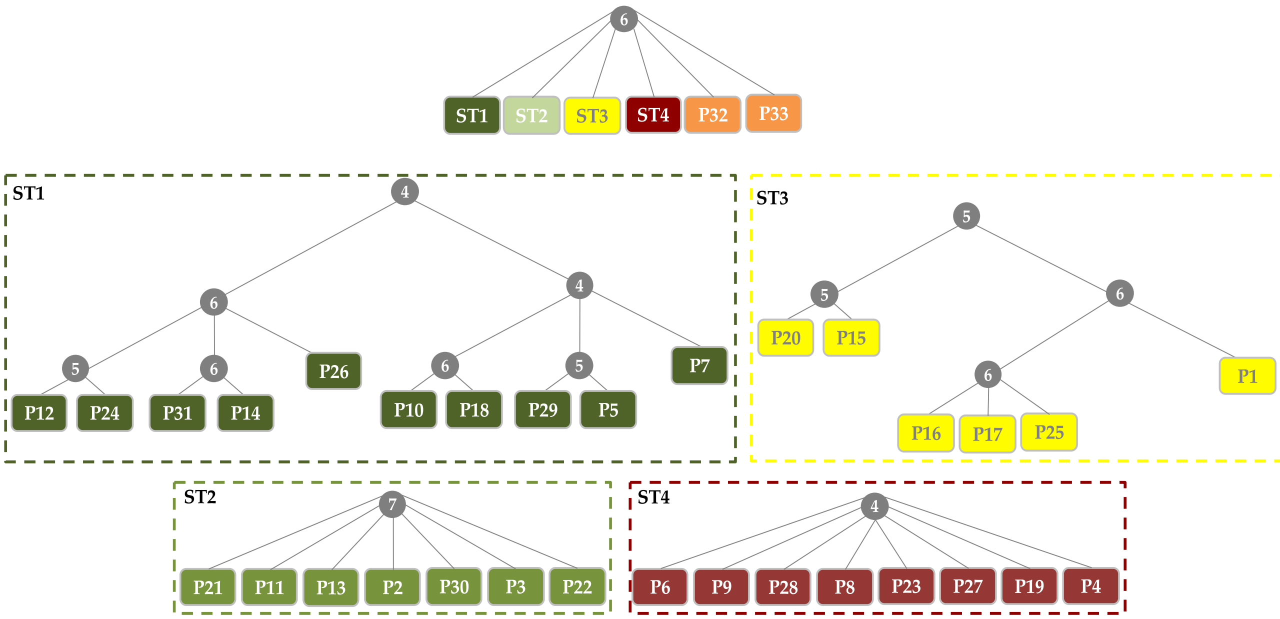

Figure 4.14: The obtained hierarchical tree-structure model for case study 1

4.6 Experimental Results

This section aims to analyze the capabilities of the proposed hierarchical models along with the new feature extraction technique in both case studies with LOSO cross-validation. Figure 4.14 shows the best model with accuracy (A) 92.16% and minimum sensitivity (S) 54.65% for case study 1. The recognition of each test pattern starts from the root of the tree. At each intermediate node of the tree, a decision is made about the assignment of the input pattern into one of the possible groups. Each of these groups may contain multiple classes. This is repeated recursively downward the tree until the sample reaches a leaf node that represents the class in which the pattern belongs. In this experiment, $M = \{KNN, NN, SVM, DTB\}$. In Figure 4.14, the numbers in gray circles denote the classifiers' IDs described in section 4.3.1. In this example, we had 33 different classes and new results assure that all activities are classified, individually by more than 54.65% with LOSO cross-validation. The results verified that, the combination of the results

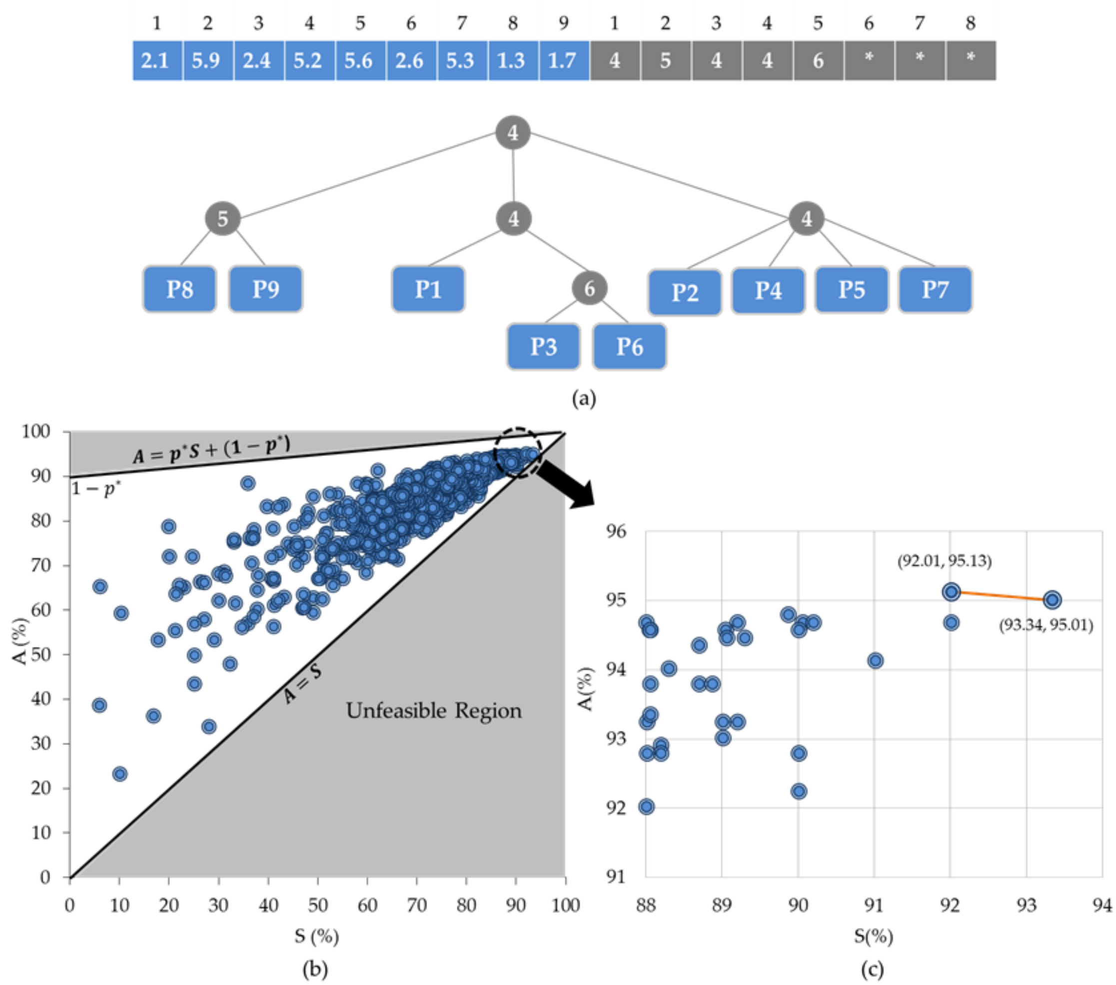

Figure 4.15: (a) The best classification model for case study 2 with Acc1 and Acc2, (b) Feasible and unfeasible regions in the 2-D (S, A) space and (c) Pareto front in testing with LOSO cross-validation

obtained by different hierarchical classifiers improves the outcomes that each provides, individually.

In Figure 4.15 (a), the best achieved model for case study 2 with $M = \{DT, NB, DA, KNN, NN, SVM\}$ is plotted. This figure shows the accuracy versus sensitivity for all population and generations when using both Acc1 and Acc2. The worst-case sensitivity (S) is represented in the horizontal axis and accuracy (A) on the vertical axis. A point (tree) in (S, A) space dominates another if it has higher accuracy and equal or greater S, or if it has greater S and equal or better accuracy. The accuracy and minimum sensitivity measures verify that:

$$S \leq A \leq 1 - (1 - S)p^{*} \tag{4-13}$$

Where p^{*} is the minimum of the estimated *prior* probabilities and in the balanced breathing classification problem with l classes is equal to $\frac{1}{l}$. Therefore, each tree is denoted as a point in the white region in Figure 4.15 (b) and the gray areas are marked as the unfeasible regions. Figure 4.15 (c) shows zoomed portions of the feasible solutions. In this scenario, we could obtain two points distributed on the Pareto front. The maximum accuracy of 95.13% is obtained with the worst-case sensitivity of 92.01% while the maximum S is achieved 93.34% with accuracy of 95.01%. In case of using accelerometer sensor on the abdomen region (Acc2), the best point (91.52, 93.98) is achieved for (S, A) which again dominates the results derived from Acc1 with (83.3, 91.23). Therefore, the results guarantee that each class is individually classified with more than 92% with all features. It is also worth mentioning that these results also surpass the accuracy and sensitivity outcomes from binary-tree models in which the (S, A) were (81.89, 89.96), (90.14, 92.92) and (91.37, 93.46) for Acc1, Acc2 and both sensors, respectively. These binary hierarchical models were trained only based on the features listed in Table 4.4.

Figure 4.16 and Figure 4.17 summarize the achieved classification and misclassification rates for each class in the proposed models for case study 1 and 2, respectively. According to confusion matrix defined in section 4.3.2, the misclassification rate is computed as follows:

$$MisclassificationRate(i) = \frac{\sum_{j=1, i \neq j}^{l} CM(i,j)}{\sum_{j=1}^{l} CM(i,j)} \times 100 \tag{4-14}$$

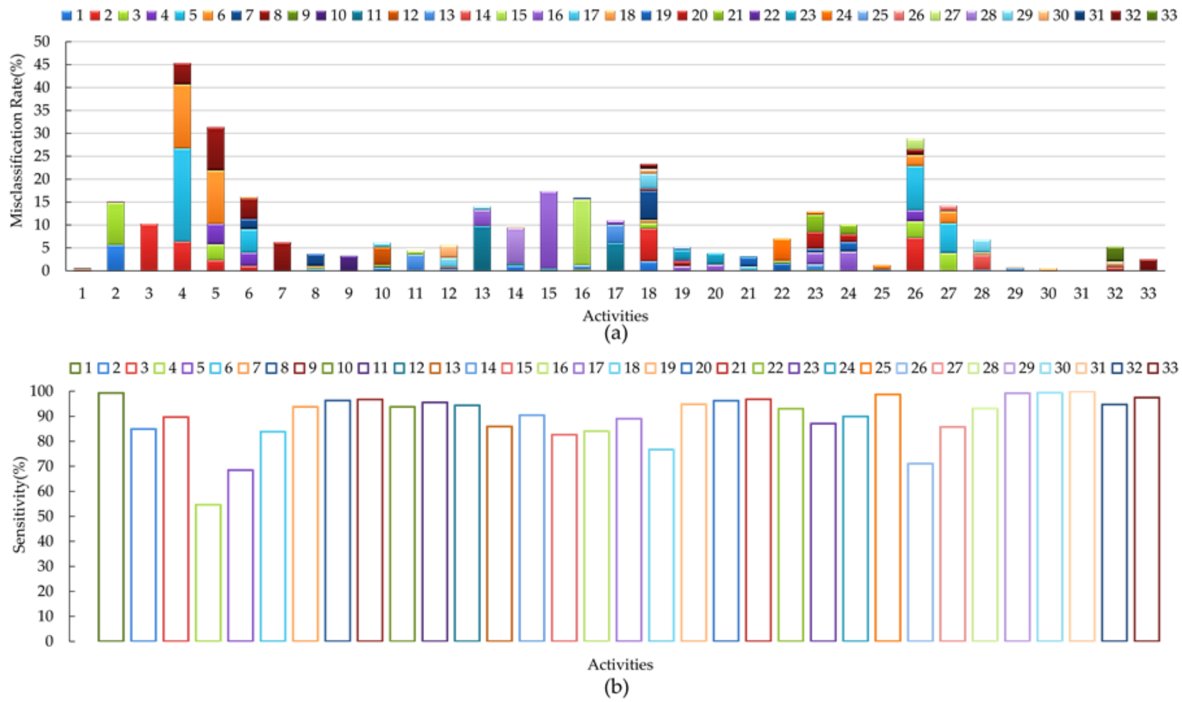

Figure 4.16: (a) Misclassification rates and (b) Sensitivities from the hierarchical classification based on LOSO cross-validation for case study 1 with two sensors LLA and RUL

Where $MisclassificationRate(i)$ indicates the false predicted portions of class i into other classes. Figure 4.16 shows which activities are confused with each other during classification procedure. For instance, jumping up (denoted by label '4') is misclassified by jogging (2), jumping front and back (5), jumping side way (6), and jumping rope (8) for 6.4%, 20.35%, 13.95% and 4.65%, respectively. Figure 4.17 (a), (b) also summarized the misclassification rates and sensitivities with all features for the second case study, where a single sensor is used on the subject's chest. For example, in Figure 4.17 (a), to determine whether a respiration disorder is the OSA breathing pattern, the classifier misclassifies it as Apneustic breathing for 2.1%, Biots for 1.9%, normal for 3.68%, and Sighing for 1% resulted in sensitivity of 91.32% shown in Figure 4.17 (b). Figure 4.17 (c) and (d) also depict the results for the sensor on the abdomen region. As expected, the sensitivities for all classes are higher compared to the sensor on the chest. Furthermore, based on the

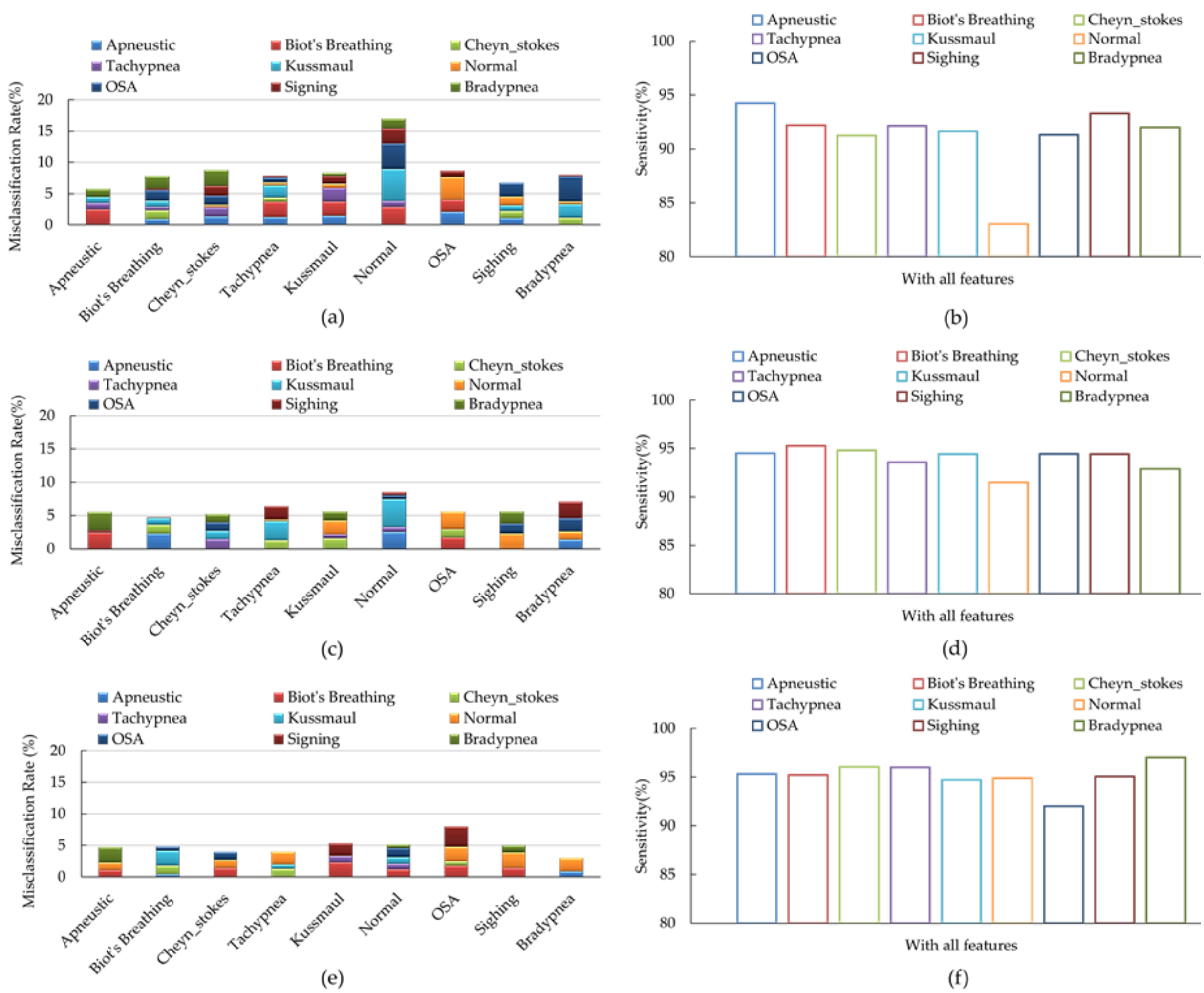

Figure 4.17: Misclassification rates and Sensitivities from the hierarchical classification based on LOSO cross-validation with (a), (b) Acc1, (c), (d) Acc2 and (e),(f) two sensors with all features

observation in Figure 4.17 (e) and (f), in case of using two accelerometer sensors, all misclassification rates are kept below 8% which indicates a high recognition rate (> 92%) for each class, individually. Table 4.5 compares the previous results explained in the first row of the table and the new results based on the proposed feature extraction and hierarchical tree-structured models. The achieved improvements demonstrate that, in all scenarios, the introduced models could surpass the previous single objective techniques in terms of both accuracy and sensitivity. In average, the accuracy improvements are 3.47% and 5.76% compared to the results reported in Chapter 3 and case study 2,

Table 4.5: Comparison between the preliminary and the new results with the highest accuracy, A and S denote the accuracy and minimum sensitivity, respectively

The best results from single objective techniques												
	Chapter 3								Case Study 1	Case Study 2		
Sensor Location	Waist	RLA	LLA	RUL	LUL	RLL	LLL	Chest	LLA+RUL	Chest (Acc1)	Abdomen (Acc2)	Both
A(%)	72.53	64.62	77.12	79.91	92.35	83.51	90.03	86.31	88.11	86.10	88.04	90.98
S(%)	33.70	20.21	20.53	41.90	67.5	59.03	68.32	59.95	36.14	77.39	83.51	88.36
The results with the best accuracy from multi-objective method												
	Chapter 3								Case Study 1	Case Study 2		
Sensor Location	Waist	RLA	LLA	RUL	LUL	RLL	LLL	Chest	LLA+RUL	Chest (Acc1)	Abdomen (Acc2)	Both
A(%)	73.84	70.12	79.60	84.17	93.61	84.40	92.02	89.95	92.16	91.23	93.98	95.14
S(%)	36.28	28.9	31.52	48.20	73.49	63.32	72.81	60.04	54.65	83.03	91.52	92.01
Achieved improvement												
	Chapter 3								Case Study 1	Case Study 2		
Sensor Location	Waist	RLA	LLA	RUL	LUL	RLL	LLL	Chest	LLA+RUL	Chest (Acc1)	Abdomen (Acc2)	Both
A(%)	1.81	8.51	3.22	5.33	1.36	1.07	2.21	4.22	4.6	5.96	6.75	4.65
S(%)	7.66	43.00	53.53	15.04	8.87	7.27	6.57	0.15	51.22	7.29	9.59	4.13

respectively. The classification results stated in Chapter 3 have been promoted while utilizing the top classifiers in Table 3.3 for each position. The improvements are even more in sensitivity values with average enhancements of 17.76% and 7%, correspondingly.

We have also compared the proposed methods with the preliminary results of case study 1. The improvements of 4.6% and more than 50% are obtained for accuracy and the worst-case sensitivity values that show the robustness of the new algorithms in various conditions. Another interesting observation is that the proposed methods could improve the runtime of the classification in case study 2. Although the computational complexity during training phase increases in the proposed architecture, the time required by the trained model for classifying a new instance (test phase) can be reduced by constructing the hierarchical ensemble classification model. We evaluated the computational complexity in the test phase of the best model depicted in Figure 4.15 (a), and the analysis of the results demonstrates that it is about three times faster than the best multi-class SVM classification model presented in [126]. This improvement is achieved based on the average times required for classifying unseen patterns in the test phase. It is worth noting that the classifiers hosted in the internal tree nodes have lower computational complexity compared to 9-class SVM with Error-Correcting Output Codes (ECOC) presented in [126]. Therefore, the proposed design helps a new feature vector to follow faster the branches in the hierarchy from the root to a leaf node. However, this conclusion is not consistent with the models such as KNN that the number of classes does not affect significantly on the prediction time. The depth of the tree has an adverse impact on the training and testing times. Therefore, the system designer has to consider the trade-off between accuracy/sensitivity and time in making a decision based on the requirements of any application.

4.6.1 Results on ML Calls Optimization

The proposed algorithm in 4.4 is validated on breathing disorder classification in which we deal with 1D motion signal (z-axis). Figure 4.18 plots a raw breathing signal for three different patterns. In this example, the time delay $\tau = 2$ sec is selected for the phase space reconstruction. Given the time delay, we take the embedding dimension as 4 for the windowed breathing signal. Therefore, we have $2^4 \times 2^4$ states. This figure also shows the amounts of pheromones ($\Delta = 12$) in each transition at nine different moments. The proposed technique can detect any major changes or motion artifacts in the signal.

In the previous section, we integrated the use of inertial sensors with new machine learning technique to model a wide range of human respiratory patterns for the goal of cloud-based recognition of respiratory problems. As the rib cage is the most popular position in industrial wearable patches for monitoring vital signs, we make use of accelerometer sensor data to analyze the changes in the anterior–posterior diameter of the chest wall during breathing function. Figure 4.19 shows the improvement in number

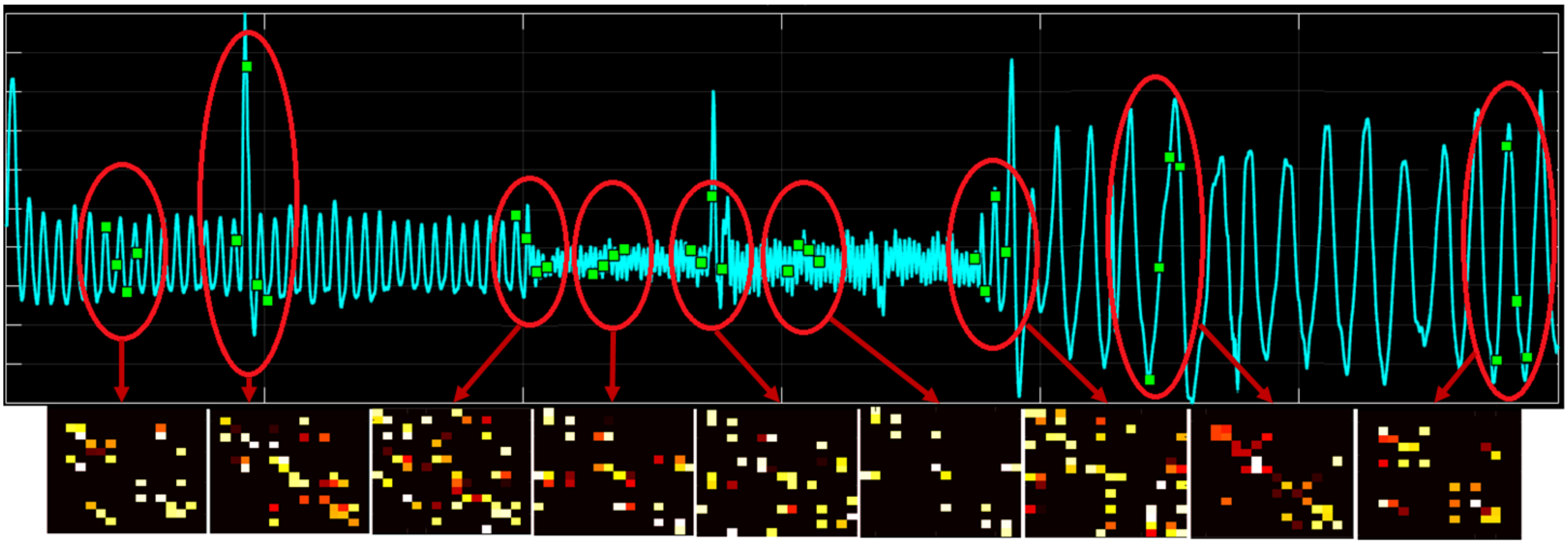

Figure 4.18: Raw breathing signal for three different patterns and the pheromone trail updates during the procedure. We show the *transPhermone* updates (see Algorithm 4.8) at nine different moments. As the embedding dimension is four in this test, the size of *transPhermone* is 16×16.

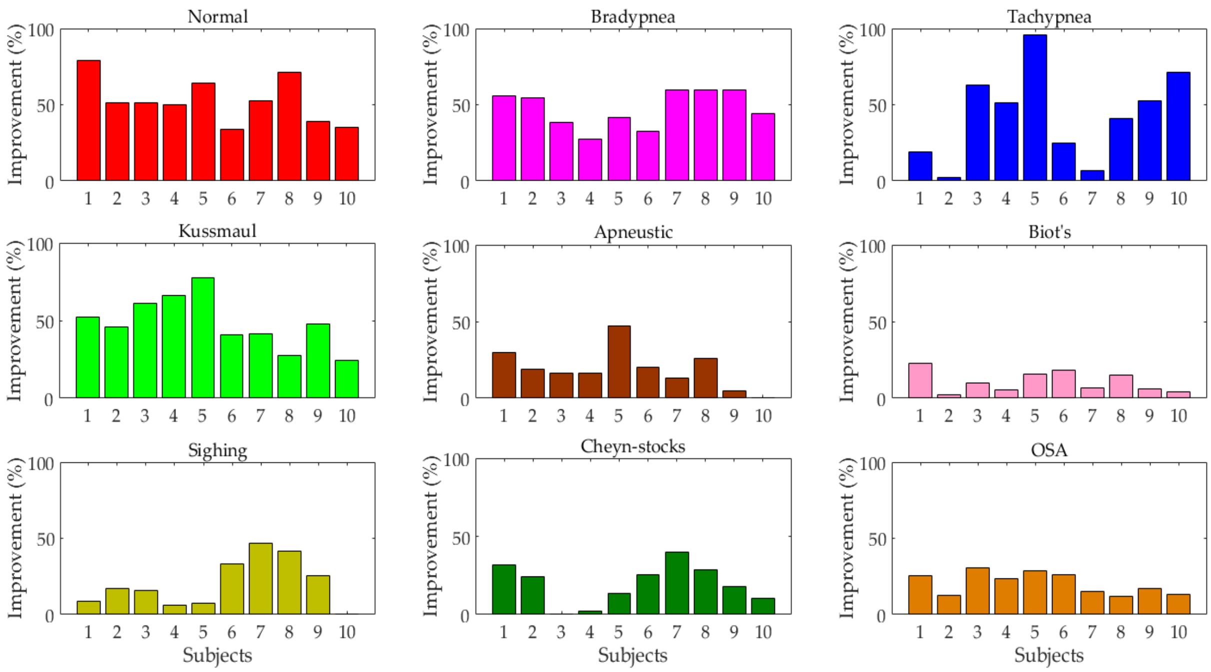

Figure 4.19: The improvement in number of machine learning functions calls in each breathing pattern performed by each subject

of machine learning functions calls in each breathing pattern performed by different subjects. In average, the number of function calls reduced by 52.75%, 47.37%, 42.71%, 48.35%, 19.28%, 10.69%, 20.21, 9.51%, 20.43% for Normal, Bradypnea, Tachypnea, Kussmaul, Apneustic, Biot's, Sighing, Cheyn-stocks and OSA breathing patterns, respectively. The results indicated an overall improvement of more than 31% on all different breathing maneuvers with no reduction in classification accuracy.

4.7 Conclusion

Being able to recognize the state of a person can provide us valuable information to have a better understanding of numerous medical conditions and treatments. In addition, a reliable long-term monitoring of respiratory parameters and diagnosis of breathing disorders at an early stage provides an improvement of medical act, life expectancy, and quality of life while decreasing the costs of treatment and medical services. With the integration of emerging sensor technology and analysis methods, the low-level sensor data can be translated into rich contextual information in a real-life application. In this chapter, we exploited recent advances in wearable sensing and machine learning principles to provide innovative decision-making capabilities for two state-of-the-art case studies i.e. recognition of a wide range of activities and diagnosing breathing disorders. Novel feature extraction and multi-classification techniques were developed to optimize the accuracy as well as the worst-case sensitivity in the multi-class classification problems. An evolutionary algorithm was applied which attempts to intelligently get closer and closer to the best hierarchical model in the tree-based model. The effectiveness of the proposed techniques has been compared with the previously published machine learning algorithms, which are stand-alone multi-class classifiers. The results demonstrated the possibility of acquiring a precise model with accelerometer sensors even with a subject-independent cross-validation. For the first case study, the accuracy of 92.16% was achieved for identifying 33 activities with the fusion of two sensors. We also could obtain a considerable increase of 51.22% in the worst-case sensitivity. We found that even when working with heterogeneous datasets presented in chapter 3, we could get promising results for all eight positions. Such a reliable recognition model could encourage people to do more outdoor activities and could be an assessment of activities of daily living for chronic treatment. The results of breathing patterns classification showed an overall classification accuracy of 91.23%, 83.98%, and 95.14% with Acc1, Acc2, and both sensors data, respectively. It is concluded that the proposed methods improved the worst-case sensitivity by about 7.29%, 9.59%, and 4.13% compared to the best classifier in a single objective problem. Finally, we proposed an innovative approach to speed up the conventional recognition methods by reducing the number of calls of feature extraction and classification functions. It is a very fast algorithm to analyze the dynamical characteristics of sensor data at each sample to detect any significant change in the signal. When working with breathing datasets, an average improvement of more than 30% was obtained. This finding enables the design of a highly effective real-time predictive model for wearable applications.

Chapter 5

Haptic Feedback and Sensory Substitution

The worth of haptic feedback in different notification systems has proven itself for delivering high-order tactile percepts to transfer complex meanings, and expressions. Instead of visual feedback or spoken commands played back over earplugs, the wearable haptic (touch) feedback could provide artificial tactile stimuli for improving walking stability, reducing joint loading, facilitating navigation for visually impaired individuals or the elderly. Furthermore, the tactile messages do not disturb nearby users, while also have less privacy-invasive compared to visual and auditory feedback. On the other hand, as we showed in the previous chapters, the sensing and computational devices have opened a new frontier for movement analysis. One or multiple accelerometer sensors worn across the body can be utilized to measure joint and segment kinematics. There is increasing potential for integration of wearable sensors and haptic systems to improve human motor learning in a wide range of applications including motor rehabilitation, dance, and sports training. It enthuses people with a feeling of feedback on quality and informs them of their progress in performing the prescribed exercises in real time. In the first part of this chapter, we show how real-time corrective vibratory feedback improves users' performance in breathing therapy using an accelerometer sensor to capture the interior/posterior motions of the subject's umbilical region. The goal is to evaluate the effect of a single-point vibration feedback system in improving the quality of prescribed breathing exercises. In the second part, we design a 2D customizable tactile display to transmit tactile stimuli onto the lower back of the users who can also personalize the vibration variables including spatial location, vibratory rhythm, burst duration, and intensity. This system not only could be beneficial for individuals with some level of sensory impairment such as a hearing or vision deficiency but also useful for learning motor skills.

5.1 Breathing Therapy with Haptic Feedback

Breathing is an unconscious, and unheeded function occurs about 20,000 times per day and 10 million times per year by a healthy individual [126]. Unlike other unconscious functions of the body, breathing can be controlled and regulated voluntarily. Breathing therapy was introduced to help people gradually refine their breathing patterns in terms of respiration rate and volume. It is very important for people to perform the exact instructions since otherwise it may cause lung problems. Therefore, the breath specialists and physicians try to provide instructions and feedback over multiple practice sessions.

To overcome these limitations, this section proposes and investigates artificial tactile stimuli for providing instructions and feedback on the performance of breathing exercises in real time. The proposed system comprises of a single wearable sensor that models the breathing functions from the interior/posterior motions of the subject's umbilical region integrated with a vibration motor to provide haptic feedback during breathing therapy. In this system, first, the correct ways of breathing maneuvers (reference patterns) are captured under the expert's supervision, and then the subjects try to practice the exercises on their own with the help of vibratory feedback. Their performance is tracked by an accelerometer sensor and compared with the reference patterns. The user performing the practices in a wrong way will receive vibrations proportional to the amount of error. The results are investigated based on five different yogic breathing patterns with ten healthy volunteers. The significant improvement in users' performance in breathing therapy when applying haptic feedback shows a potential to enrich the quality of wearable systems through the touch channel.

5.1.1 Motivation

Different studies indicate that the tactile stimuli could be beneficial and effective for learning motor skills such as snowboarding [251], rowing [252] and playing musical instruments [253]. In general, the participants could improve their movements while comparing to their performance without tactile cues. In [254], the effects of vibrotactile feedback on standing posture control in individuals with vestibulopathy have been studied. The findings of this work show that the subjects were able to use the vibrotactile information effectively to comply with the task of reducing trunk sway. Lieberman *et al.* [32] used a motion capture system to track and analyze of the participants' arm movements while mimicking an arm movement shown on a computer display. According to the deviations from the target movements, real-time tactile feedback at the arm has been presented to indicate the intended movement direction. They reported that the addition of tactile feedback to motor training improved performance and could support learning.

In the next section, we take this idea i.e. integration of a wearable sensor with real-time haptic feedback in breathing therapy application that to our knowledge has been introduced for the first time. This application is a form of conscious berating that educates people how to breathe fully, getting more oxygen to their brain and body. Human beings breathe, the way nature intended them to do; however, they have contracted wrong methods of standing, walking and sitting, which have robbed them of their birthright of natural and correct breathing [255]. Different studies [255], [256] show that the physical health depends very materially upon correct breathing. Breathing therapy has been proven itself to be an effective, drug-free remedy that aims to either correct dysfunctions of breathing or enhance its functions. Indeed, this reduces symptoms and improves the health of patients who have asthma [257], hypertension [258], diabetes, and ischemic heart disease [258], anxiety, speech disorders, chronic muscular skeletal dysfunction, and medically unexplained physical symptoms [259]. It is also found to be useful to improve hemodynamic and various cardiorespiratory risk factors in cardiac patients [250]. Yoga pranayama that refers to the “Control of breath in specific postures” directs the curative power of air energy to the certain parts of the human body [260]. Previous clinical research on pranayama as the art and science of yogic breathing techniques has indicated that pranayama might be of profit in the conditions such as insomnia [261], heart disease [262], epilepsy, obsessive-compulsive disorder, and depression [263]. While the pranayama breathing concentrates on the reduction of breathing frequency, the core Buteyko exercises consciously reduce either breathing rate or breathing volume [263].

Buteyko Breathing Technique (BBT) is a unique set of breathing exercises that uses breath-control and breath-holding to treat a wide range of health situations related to hyperventilation and low carbon dioxide. The BBT exercises try to augment the CO2 level while may also be useful in reducing hyperinflation [264]. In addition to the physical benefits derived from correct habits of breathing, an understanding of the "Science of Breath" may increase people’s mental power, happiness, self-control, and clear-sightedness [255]. Recently, one of the most important and challenging open areas of research is designing biofeedback-based advisory systems that help people to promote their daily practices in several e-health applications. Different studies exploited recent advances in wearable sensing, signal processing, and machine learning principles to provide innovative decision-making capabilities for subjects' breathing characteristics and to discern valuable information [30]. In section 5.1.2, we consider a new application called "Breathing Therapy" via motion sensor to evaluate our advisory system based on real-time haptic feedback. Despite other physiological functions, breathing can be controlled consciously, so that the proposed system enthuses people with a feeling of feedback on quality and informs them of their progress in performing the prescribed breathing models. We utilize an efficient algorithm to analyze the signals and provide vibratory feedback on performance accuracy in real time.

5.1.2 The Proposed System

In this section, we analyze the movements of humans' chest compartments via a motion sensor in different yogic breathing practices for designing our breathing therapy platform. In the proposed system, the participants are first asked to perform the breathing patterns under our supervision to record a reference pattern (*refPattern*) with the sensor worn on their abdomen. Then, the testing patterns are compared with the reference ones automatically, once the users are performing the prescribed exercises on their own. As we showed in chapter 4, using an accelerometer on the abdomen umbilical region overcomes the performance obtained from the sensor on the middle of sternum region. Therefore, we chose abdomen as a more functional position in our experiments. Through haptic feedback on performance accuracy of each breath, people are informed how well they are executing the patterns. The samples received from motion sensors carry noise and applying denoising algorithms is essential to facilitate an accurate assessment of human respiration signal. To this end, reference patterns are smoothed by a 15-point frame third order Savitzky-Golay (SG) smoothing filter since it does not delay the signal and is able to preserve features such as local minima and maxima. This filter is optimal as it minimizes the Least-Squares Error (LSE) in fitting a polynomial degree three to

Algorithm 5.1 Single-point Feedback

```
Input: refPattern, numberOfTrials; output: MAE
sensitivity = (max (refPattern) - min (refPattern)) / 10;
refSize ← length (refPattern);
while (stop);   % Wait till user is ready
 for  i = 1:1: numberOfTrials {
        for  j = 1:1: refSize
               while (!Ready (Accelerometer.newInstance));   % Wait for a new instance
                d ← Accelerometer.newInstance;
               zAxis (j) = d (3);
               absError (j) = |refPattern (j) – zAxis (j)|;
               if (1 × sensitivity ≤ absError (j) < 2 × sensitivity) writePWM (2);
                elseif (2 × sensitivity ≤ absError (j) < 3 × sensitivity) writePWM (2.4);
                elseif (3 × sensitivity ≤ absError (j) < 4 × sensitivity) writePWM (2.8);
                elseif (4 × sensitivity ≤ absError (j) < 5 × sensitivity) writePWM (3.2);
                elseif (5 × sensitivity ≤ absError (j) < 6 × sensitivity) writePWM (3.6);
                elseif (6 × sensitivity ≤ absError (j)) writePWM (max); }
        AE (i, :) = absError;
MAE= mean (AE);
return (MAE);
```

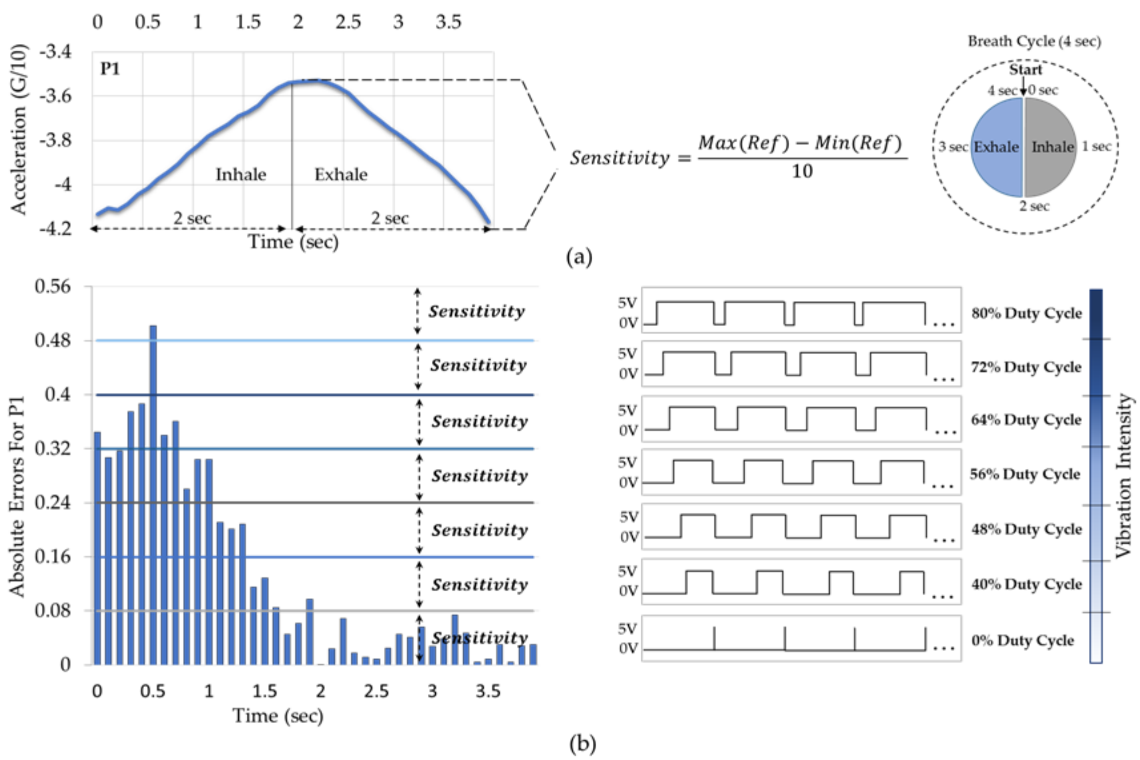

Figure 5.1 (a) Reference signal for Buteyko pattern of one subject and the breath cycle, (b) the absolute error of the test pattern versus reference pattern

frames of noisy data. To provide the vibratory feedback, the absolute difference between the reference and test patterns at each sample is calculated and compared with a sensitivity value obtained from (max (*refPattern*) – min (*refPattern*)) / 10. A Pulse Width Modulation (PWM) channel of the Arduino microcontroller drives the motor. The time that PWM signal is high and low can be varied, and therefore a DC voltage can be produced that is proportional to the duty cycle. As a result, the duty cycle of a PWM signal driving a motor will proportionally change the amplitude and frequency of the device's vibration.

In our system, the appropriate duty cycle is determined according to the sensitivity value. Algorithm 5.1 summarizes the proposed procedure. For calculating the errors, the algorithm checks whether a new instance (*d*) is ready in our data stream in line 7. The dissimilarity/distance of reference and test signals is calculated in line 9. Here, *refPattern* and *zAxis* are the reference and test signals, correspondingly. It is worth noting that, based on the body movement mechanism in sitting position; the z-axis is considered as the major axis. The vibration intensity is then selected in lines 10-15 based on the sensitivity value and absolute error. An example is shown in Figure 5.1. The top left figure represents the reference, and the circle on the right shows the breathing cycle of one subject during his Buteyko breathing maneuver. As can be found out in Figure 5.1(b), the test pattern has a significant distance from the reference pattern at the first few seconds of the practice (~2sec) due to timing and breathing volume mismatches.

5.1.3 Test Setup

The investigation is carried out with ten healthy volunteers (five males and five females) aged 18 to 46 with (Mean ± SD) 30.70 ± 8.87. The ethical approval was received from McGill University Ethics Committee. All participants were informed about the experimental procedures before starting the trial sessions.

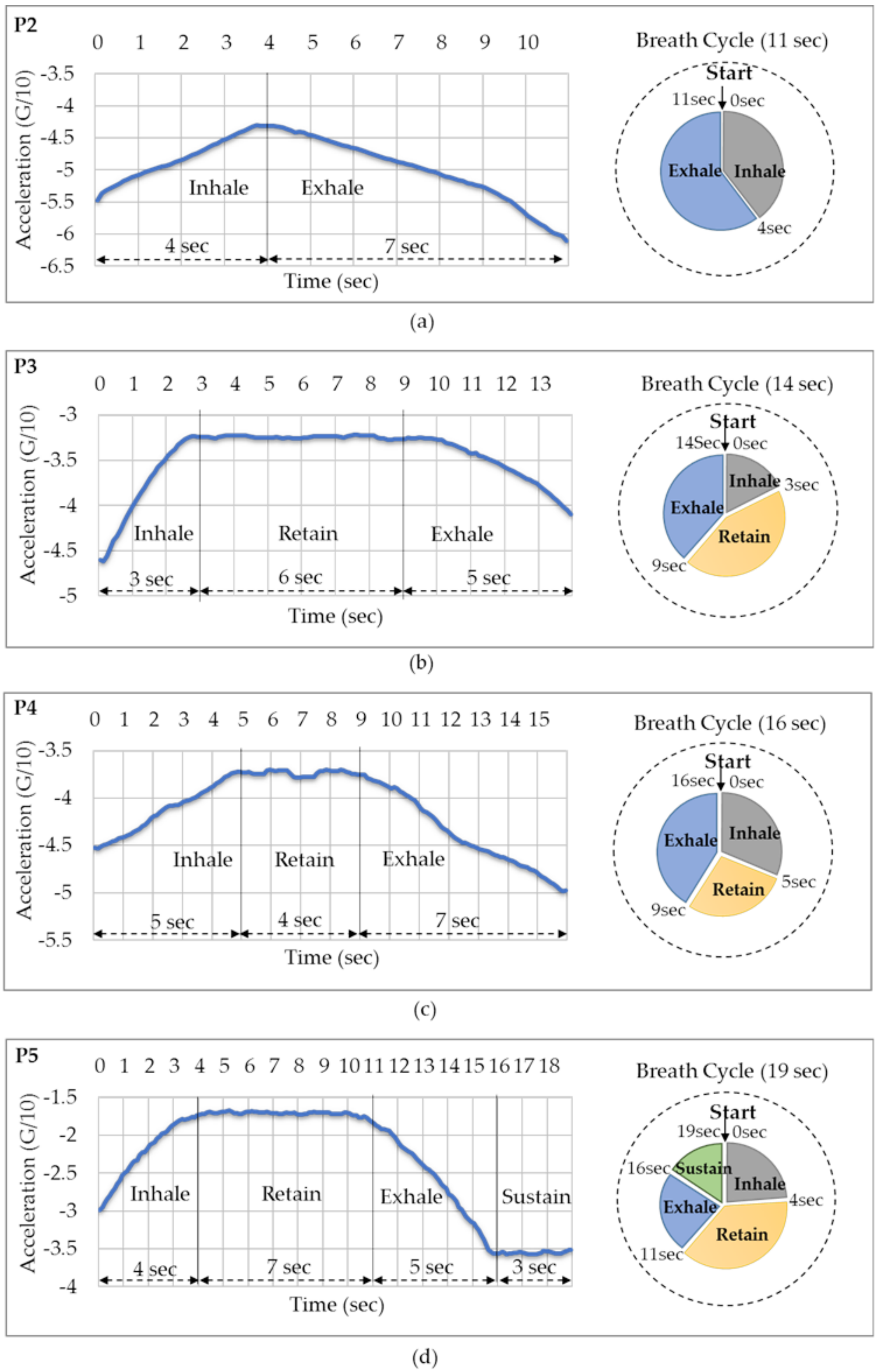

Figure 5.2 (a) Basic 1, (b) basic 2, (c) intermediate and (d) advanced pranayama breathing reference patterns of one subject obtained from an accelerometer sensor, respectively.

In our system, we used a 22.3×14.8 mm, cB-OLP425 BLE module [107], which is fully radio type approved for Europe, USA and Canada as well as compliant with EMC safety and medical standards. This module includes an ultra-low-power LIS3DH 3-axis accelerometer with 12-bit resolution. It was mounted on subjects' umbilical region, and the vibration motor was attached on their lower back by an adjustable back support belt. The used Precision Microdrives [265] 9mm encapsulated vibrator motor is based on a coreless motor design, with precious metal commutation circuitry and a toroidal neodymium magnet.

We asked the subjects to perform five different yogic breathing patterns in sitting position including the Buteyko (T_i: 2 sec, T_e: 2 sec) with 5-10% less breath volume than normal breathing (P1), basic 1 (P2) pranayama breathing pattern (T_i: 4 sec, T_e: 7 sec), basic 2 (P3) pranayama breathing (T_i: 3 sec, retain time: 6 sec and T_e: 5 sec), intermediate (P4) pranayama (T_i: 5 sec, retain time: 4 sec and T_e: 7 sec), and advanced (P5) pranayama (T_i: 4 sec, retain time: 7 sec, T_e: 5 sec and sustain time:3 sec). The reference patterns of one subject are depicted in Figure 5.2. For instant, the circle in Figure 5.2 (b) indicates that the subject should inhale for 3 sec, and then he should retain his breathing for 6 sec and finally exhale within 5 sec. Since our technique decides based on each subject's reference pattern individually rather than a fixed breath model, the potential influences of age, gender and body size are already implicated in the results.

In yoga, deep breathing is part of the practice of pranayama. Pranayama exercise slows down the rate of breathing and expands chest and lung capacity. In our tests, the subjects fulfill the yogic breathing requirements such as, keeping the upper body straight, the back, head, and neck are in alignment, and the body remains motionless during the practices. To test our system, the supervised reference patterns are first recorded, and then the test patterns are performed by each volunteer for all yogic breathing, each for three times with and without real-time feedback.

5.1.4 Experimental Results

In this section, we present the experimental results on evaluating the proposed breathing therapy platform. Different yoga-based breathing exercises are chosen from recent medical investigations to test the new developed biofeedback mechanism. The evaluations are based on five different breathing exercises. Figure 5.3 (a), (f), (k), (p), and (u) depict five testing breathing patterns, each for three times for subject #1 without haptic feedback. The errors are shown in Figure 5.3 (b), (g), (l), (q), and (v).

The Mean Absolute Error (MAE) of 0.33 is obtained with no feedback for this subject. The same experiments are repeated with applying real-time feedback shown in Figure 5.3 (c), (h), (m), (r), and (w). The errors in Figure 5.3 (d), (i), (n), (s), (x) and average errors for each breathing cycle in Figure 5.3 (e), (j), (o), (t), (y) show that the subject was able to perform the prescribed breathing exercises 54.78% better compared to without feedback. The MAEs of each subject for all breathing patterns with and without feedback are highlighted in Figure 5.4.

For example, Figure 5.4 (c) indicates that subject #3 was able to mimic the reference pattern 48.03% in average better with feedback than without it. However, the simultaneous feedback appears to confuse subject #2, where the haptic instructions did not significantly (3.59%) help him during his experimental sessions (see Figure 5.4 (b)). The average improvement of 40.63% is achieved considering all subjects and patterns when using haptic feedback. The paired sample t-test also supports this with statistically significant p-values listed in Table 5.1 for each breathing exercise. These results reveal that the subjects' performance was substantially better while perceiving errors through the touch channel. To evaluate the comfortability and usability of the proposed system, we asked our subjects to provide us a number between 0 and 10 on three questions summarized in Figure 5.5. No participants had experience with tactile instructions on yogic breathing patterns.

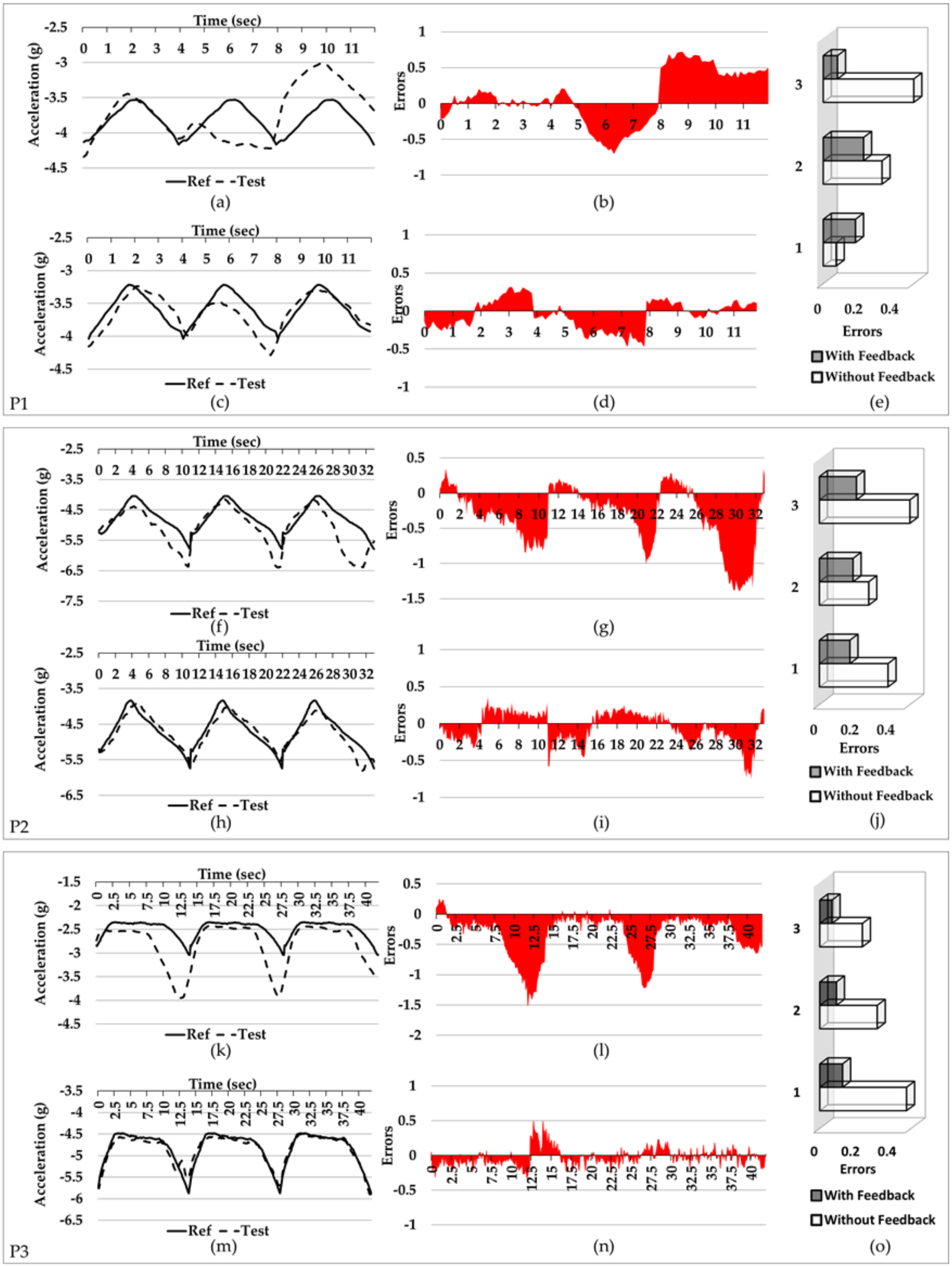
Time (sec)
Acceleration (g)
Errors
Ref
Test
With Feedback
Without Feedback
(a)
(b)
(c)
(d)
(e)
(f)
(g)
(h)
(i)
(j)
(k)
(l)
(m)
(n)
(o)
P1
P2
P3

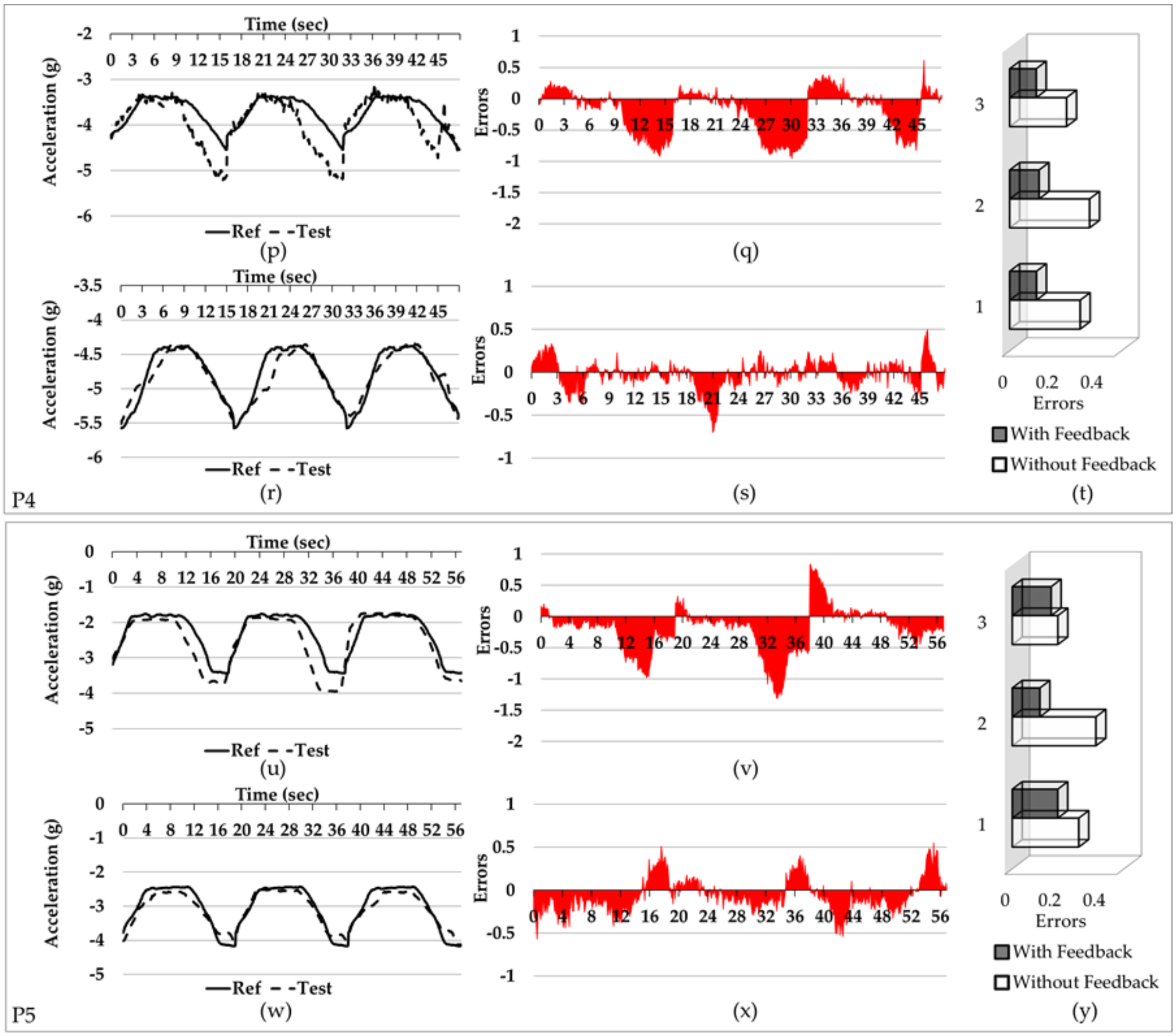

Figure 5.3 (a), (f), (k), (p), (u) five test yogic breathing patterns performed for three times by one subject without haptic feedback, (b), (g), (l), (q), (v) the errors of five test yogic breathing patterns versus the reference pattern without haptic feedback, (c), (h), (m), (r), (w) five test yogic breathing patterns performed for three times by one subject with haptic feedback, (d), (i), (n), (s), (x) the errors of five test yogic breathing patterns versus the reference pattern with haptic feedback, (e), (j), (o), (t), (y) average error of each breathing exercise for five different yogic breathing patterns.

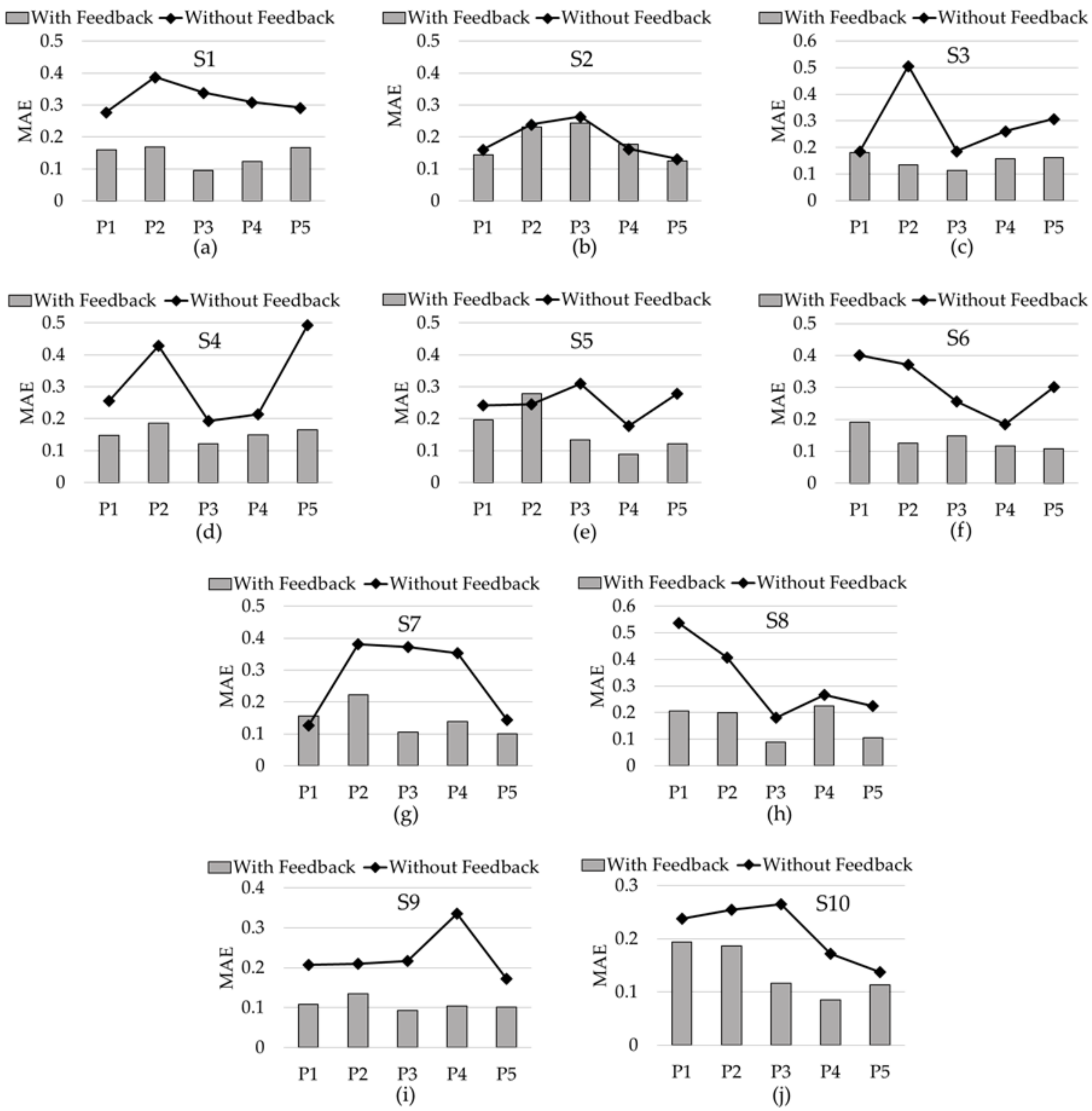

Figure 5.4 The MAE of all five breathing patterns with and without feedback for (a) subject 1, (b) subject 2, (c) subject 3, (d) subject 4, (e) subject 5, (f) subject 6, (g) subject 7, (h) subject 8, (i) subject 9, and (j) subject 10.

The average scores are obtained 8.05, 7.80, and 8.4, which demonstrate the comfort and helpfulness of the proposed system while giving more credits to the fusion of motion sensor and haptic as a simple and cost-effective solution for health applications. The presented wearable system showed that even a single-point vibration feedback could

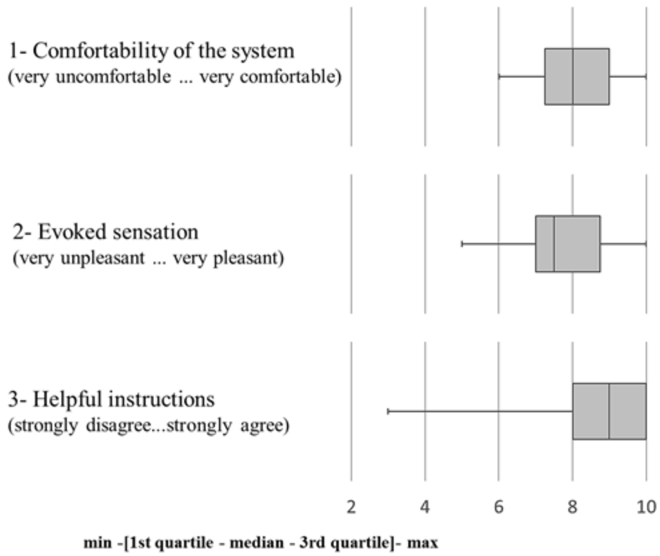

Figure 5.5 Likert scale ratings of the participants' opinions on three questions

Table 5.1 MAE and Paired Sample T-test

Breathing Exercise	Without Feedback (mean±SD)	With Feedback (mean±SD)	p-value
P1	0.27±0.12	0.17±0.03	4.99E-03
P2	0.34±0.09	0.19±0.05	1.66E-03
P3	0.26±0.07	0.13±0.05	2.31E-04
P4	0.24±0.07	0.14±0.04	9.72E-04
P5	0.25±0.11	0.13±0.03	1.44E-03

significantly improve the performance of the users while refining their movement patterns. The participants were able to improve the quality of prescribed breathing exercises compared to ones without tactile cues. However, the delivered information through one vibration motor is limited to be used in the sensory substitution and augmentation applications. In the next section, we design a platform that allows for the generation of 2D tactile patterns using a small number of vibrotactile actuators arranged in a rectangular grid, where stimuli are delivered by the harmonized use of multiple vibrating actuators to transform information into the form of tactile patterns.

5.2 Sensory Substitution with Personalized Tactile Patterns

The sense of touch provides a considerable haptic space for presenting tactile information. The vibrotactile display has been extensively studied in the context of sensory substitution. It could be used to represent visual or auditory cues to impaired users. Sensory substitution has been proven successful as the participants evidently showed the ability to identify contexts mapped to tactile stimulation. However, the subjects might need extensive pre-trainings leading to exhaustion and frustration over time. Low space resolution of the vibration stimulus arrays and bandwidth capability of human tactile sensitivity should be considered while designing the patterns. The goal of this section is to investigate the ability of the subjects to recognize alphanumeric letters on the 3×3 vibration array, where the subjects can fully personalize the motors variables including spatial location, vibratory rhythm, burst duration, and intensity. We present a vibrotactile device for delivering the spatiotemporal patterns of alphanumeric letters (similar to the handwriting styles) to the skin while maintaining the high level of expressiveness. We extended the applicability of this system to color and multi-character messages identification tasks. The results prove that this system is an effective solution with a low cognitive load for visually/auditory impaired people and for any context that would benefit from leaving the eyes/ears free for other tasks.

5.2.1 Motivation and Background

The skin has been thoroughly considered as a conduit for information. A vibrotactile display is constructed by arranging vibration actuators into an array form with the varied size of 2×2 to 64×64 [266]. It is mostly applied to the skin on the back, abdomen, forehead, thigh, or the fingers [267]. As discussed in [268], different spatial arrangements of tactors on a body position such as forearm can result in noticeably different levels of performance. A haptic back display was developed in [266] using a 3×3 tactor array to deliver attention and direction related information to its user. The discriminability of a set of directional lines drawn on the subjects' back using the sensory saltation phenomenon was also studied. They found that the directions of a set of horizontal, vertical, and diagonal directional lines could be effectively used with minimal user training. The haptic navigation guidance or situation awareness system can benefit from these directional lines. Oron-Gilad *et al.* examined the use of spatially stabilizing cues for feedback of subtle changes in position to guide an operator toward the desired position [269]. They showed that performance is enhanced with tactile simulation indicating the direction and magnitude of the positional error. The error is computed according to the amount of deviation from the point of origin.

A new bilateral haptic device called T-hive is proposed in [270] to deliver spatial directional information on the handle using vibrotactile display. The user could perceive the spatial locations of vibrotactile stimulus and associate them with directional information by activating a specific vibrating panel on the sphere-shape handle. They discussed the combination of stimulus and the way to achieve fine resolution with a small number of tactors. It proved to be effective in the practical application for teleoperation of the robot in a virtual environment. Pradeep *et al.* presented a low-power wearable system for the visually impaired in performing routine mobility tasks [271]. They used a head-mounted two-camera system and a tactile vest for providing a safe path for traversal through a cluttered environment. Another wearable navigation system named Tyflos consisting of two miniature cameras (attached to a pair of dark glasses), a microphone, an ear speaker, the 4×4 vibration array, and a portable computer was developed in [272]. The obtained 3D representations of processed captured images are projected on the 2D vibration array attached to the user's chest. It vibrates in various levels corresponding to the distances of the surrounding obstacles. Sung *et al.* proposed a Haptic Audio Visual System (HAVS) to improve the sensory qualities of media by providing users a touchable video and a tactile audio experience [273]. Each grid in the video screen has customizable tactile information that corresponds to the visual content, and meanwhile, the vibration responses are synchronized to specific sound effects or audio signatures. The presentation of image and sound in the form of haptic rendering can be applied in different applications such as home shopping, rehabilitation applications, gaming, and entertainment in virtual environments.

A sound-to-touch sensory substitution device was recently presented to deliver processed auditory information to the skin of the torso using vibratory motors [41]. This solution has been proven successful as the participants evidently showed the ability to identify spoken word audio mapped to tactile stimulation. However, the subjects need extensive pre-trainings leading to exhaustion and frustration over time. In [267], an image is captured by the camera and the 2D contour is extracted and transformed into vibrotactile stimuli (2D tactile images) using a dynamic tactile coding scheme. The resolution of the image needs to be reduced to fit the low resolution of the tactor array as their system consists 48 (6×8) vibrating motors. They also compared their method (M1) in tactilely displaying of the letter with two other typical continuous vibration modes [274], [275]. The first one is an improved handwriting pattern, and the actuation order is similar to handwriting. The vibrating duration time is overlapped between the adjacent motors (M2). In another approach which is called scanning mode (M3), the motors are triggered in the lines from top to bottom. As an initial study in pattern identification task, the capital letters were displayed to experienced and inexperienced subjects, using a 20×20 matrix of vibratory tactors placed against the back in [275]. They reported the results of four modes of stimulus presentation i.e. “full-field, stationary-letter (M4)”, "full-field, moving letter (M5)", "moving-slit, stationary-letter (M6)" and "stationary-slit, moving-letter (M7)". Each letter was presented 42 times under each mode. They found that the sequential tracing by a single moving point leads to the highest recognition accuracy. A tactile stimulator (M8) mounted on the back of a wheelchair is presented in [276], where the capital letters of the alphabet were converted into tactile letters using 17×17 Tactile Vision Substitution Systems (TVSS). The dark region of the visual display captured by a stationary camera activated the tactors in the corresponding areas of the tactile matrix. Each black line of a letter drawn on white cardboard square activated a line of two tactors wide in the tactile matrix. The experiments conducted by four blind subjects and the results demonstrate that at least three independent basic letter features i.e. enclosing shapes, vertical parallel lines, and angle of lines play important parts in tactile letter recognition.

The possibility of differentiating alphanumeric letters by using only a 3×3 array of vibrating motors on the back of a chair has been examined in [277]. They provided a sequential pattern for each letter with a "tracing mode." This work (M9) could obtain high recognition rate in reading tactile alphanumeric characters. Recently, a system of spatiotemporal vibration patterns called EdgeVib, for delivering both alphabet (M10) and digits (M11) on wrist-worn vibrotactile displays was presented in [278]. Each unistroke pattern that is longer than four vibrations is split into multiple 2/3-vibration patterns. The new patterns are consecutively displayed to assist the users recognizing the alphanumerical patterns. The user study results revealed that the recognition rate is significantly improved by modifying the unistroke patterns in both alphabet and digits. Various factors such as familiarity with the displayed character set, stimulus duration, inter-stimulus onset interval, type of vibration motors, number of trails, number of letters, and cognition load affect the quality of recognition. Therefore, different studies cannot be directly compared. The results along with some details are brought in Table 5.2. The

Table 5.2 Previous published results

Vibration modes	Average recognition rate	Cognition load (average repeated times)	Number of letters
M1	82.0% ± 23.3%	2.05	10
M2	76.8% ± 23.5%	2.1	10
M3	47.5% ± 27.5%	2.6	10
M4	34%	1-2$^{\alpha,\beta}$	26
M5	41%	1-2$^{\alpha,\beta}$	26
M6	47%	1-2$^{\alpha,\beta}$	26
M7	51%	1-2$^{\alpha,\beta}$	26
M8	67.53% ± 20%	1$^{\alpha,\gamma}$	26
M4	86% ± 9.7%	1$^{\alpha}$	34
M10	85.9% ± 6.3%	NA$^{\delta}$	26
M11	88.6% ± 10.4%	NA$^{\delta}$	10

α: The subjects had no time limits for letter perception and they were given as much time to respond as they needed.

β: If the first response was incorrect, they responded with the second guess, after which they were informed of the correct response.

γ: The subjects were trained until they had acquired an identification accuracy of over 80% in each subset of alphabet. The error correction was given when the subjects misidentified. The number of trials per subject was not the same.

δ: After training session, a brief test was performed to ensure that each participant could memorize the patterns correctly. The participants could ask to repeat the questions, as many times as necessary if they were not confident of their answers. After they gave their answer, the screen prompted the actual answer.

discrepancy between studies is due to the differences in equipment, procedure, and style of letters. As summarized in Table 5.2, the subjects had no time limits for letter perception, and they were given as much time to respond as they needed. Moreover, most of the previous studies only focused on a subset of alphanumeric and the participants were informed of the correct response that is not a real scenario in practice. To overcome these limitations, in this chapter, we develop a fully customizable vibrotactile system to deliver any patterns including all alphanumeric patterns under time constraints for letters perception (very low cognitive conditions).

We also extend its applicability in identifying colors and multi-character verbs (2-4 characters).

5.2.2 The Proposed System

The proposed tactile display is implemented on an adjustable belt that can be easily attached on the back to transfer reliable tactile information to a human. The system composed of nine cylindrical eccentric rotating mass (ERM) motors from Precision Microdrive (8.7mm in diameter and 25.1mm in length) that are used to generate tactile and shown in Figure 5.6 (a). The motors are glued to the elastic belt with a spacing of approximately 5 cm between the centers of each pair of adjacent tactors (see Figure 5.6 (c)). This gap between tactors is necessary for the users to perform vibration localization robustly. The belt is to ensure that the motors are pressed firmly against the participant's back. The motors have the benefits of being easy in controlling the intensity and have fine temporal haptic characteristics (8 ms from off to a perceivable intensity, 21 ms from fully on to off using active breaking with H-bridges).

The intensity of the tactors is controlled by Pulse Width Modulation (PWM) signals. The vibration intensity is set to 10 levels from very low to very high. To fully control each motor individually, we used Adafruit 16-Channel 12-bit PWM Driver Shield [278] that can drive up to 16 motors over I2C with only two pins (see Figure 5.6 (b)). The on-board PWM controller will simultaneously drive all 16 channels with no extra microcontroller processing overhead. Therefore, the system can incorporate the control of a vast number of different types of feedback devices into a single and unified interface.

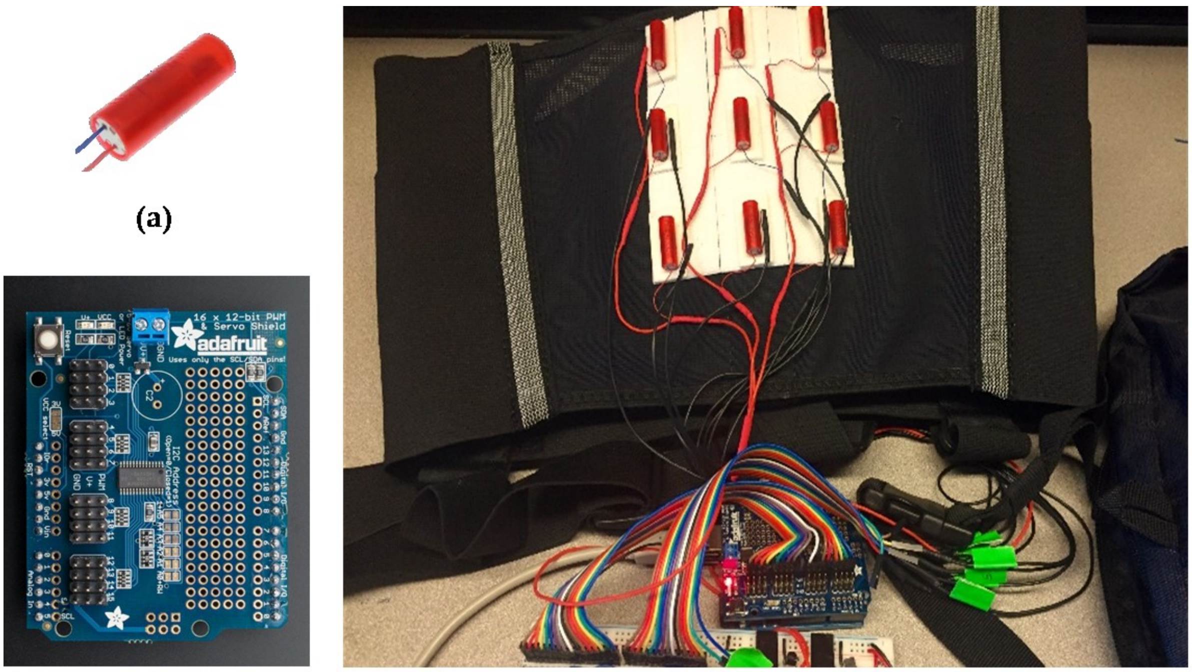

Figure 5.6 (a) 9mm vibration motor from Precision Microdrive, model: 307-103, (b) 16-Channel 12-bit PWM Driver Shield, (c) Back belt with 3×3 tactor array

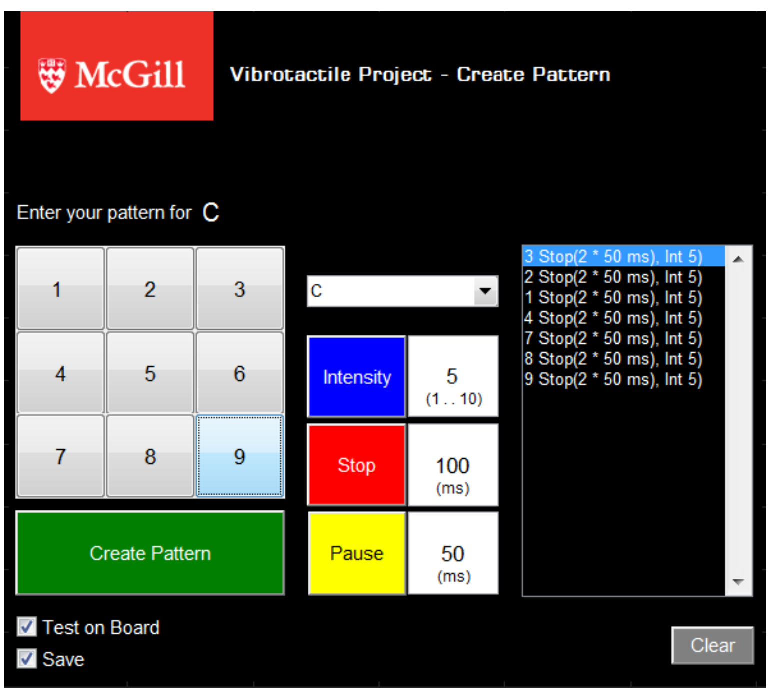

Figure 5.7 Developed GUI to customize the patterns

The shield plugs in directly into any shield-compatible Arduino. The 5V power from the Arduino is used to power the PWM chip and controls the PWM signal and I2C logic levels. A lithium ion battery made of three-balanced 2200mAh cells (total of 6600mA) capacity is used to power up the motors. In the proposed platform, the users have full control on the motors variables including spatial location, vibratory rhythm, burst duration, and intensity to generate vibratory patterns.

For this purpose, a Graphical User Interface (GUI) is developed in MATLAB to help the users effortlessly create or revise the patterns (Figure 5.7). Indeed, the GUI is designed to optimize the temporal-spatial tactile coding according to human tactile perception. All customized patterns are stored in each user's individual profile. Several experiments are conducted with the 3×3 tactors array to evaluate the effectiveness of the fully customizable tactile display in alphanumeric letters perception. First, we report the recognition rate about tactilely displayed alphanumeric letters with both default and personalized vibratory patterns. Then, we expand its applicability to colors and words identification tasks. Algorithm 5.2 describes the test cases, where each session is composed of a number of trials with randomly selected alphabetic or alphanumeric characters. Algorithm 5.3 extracts any changes in the motors (*events*) from the input pattern (line 2). The events are stored in a time-sorted array to control the motors' operations and their intensities. Ten levels of vibration intensity are defined from very low to very high value in line 9. It is worth mentioning that, for some participants, it was difficult to distinguish small intensity changes. The tactors are activated or deactivated based on the vibrating order, spatial and temporal properties in lines 10-12. The details of these experiments are brought in the next sections.

5.2.3 Test Setup

We first conduct an experiment consisted of two sessions of vibrotactile pattern identification task, one done before and the other after the development of each subject's

Algorithm 5.2: Test_Cases

```
Input: testCase, defaultPatterns, customizedPatterns; output: recognitionRate
alphaNumerics ← 'ABCDEFGHIJKLMNOPQRSTUVWXYZ0123456789';
numberOfRounds ← 3;
switch testCase {
    case: 'alphaNumericsRecognition_def' {
        targets ← randomPermutation (alphaNumerics(1:end));
        % Make a random order of alphanumeric
        hapticPatterns ← extractPatterns (targets, defaultPatterns); }
        % Extract the haptic patterns for the targets according to the default pattern
    case: 'alphaNumericsRecognition_per' {
        targets ← randomPermutation (alphaNumerics (1:end));
        hapticPatterns ← extractPatterns (targets, customizedPatterns); }
        % Extract the haptic patterns for the targets according to the personalized pattern
        through GUI
    case: 'colorsRecognition' {
        targets ← randomPermutation (alphaNumerics ([2, 3, 7, 13, 18, 21, 23, 25]));
        % White (W), Black (B), Red (R), Green (G), BlUe (U), Yellow (Y), Cyan (C), Magenta (M)
          are used.
        hapticPatterns ← extractPatterns (targets, customizedPatterns, 3); }
        % "3": For the colors except white and black, the motors vibrate in three levels
          corresponding to the color intensities i.e. light, regular and dark.

    case: 'wordsRecognition' {
        words ← ['BE:HAVE:DO:SAY:GET:MAKE:GO:
                 KNOW:TAKE:SEE:COME:THINK:LOOK:WANT:
                 GIVE:USE:FIND:TELL:ASK:WORK:'];
        targets ← randomPermutation (words (1:end));
        hapticPatterns ← extractPatterns (targets, customizedPatterns);
        numberOfRounds ← 1; }}
    for i = 1:1: numberOfRounds
        for j ← 1:1: length (hapticPatterns)
            runHaptic (hapticPatterns (j));
            % Generate each pattern on the vibration motors
    recognitionRate ←accuracy (confMat (targets, userResponses));
return recognitionRate;
```

Algorithm 5.3: runHaptic

```
Input: hapticPattern;
1. resetVibMotors (1:9); % Turn off all 9 motors
2. [events, intensities] = FetchEvents (hapticPattern);
   % Extract the events from the pattern (i.e. default pattern or customized pattern). Events is a
   time-sorted array.events(i): is 1 if a motor should be turned on at this time, events(i): is 0 if a
   motor should be turned off at this time. intensities(i): intensity of the vibration motor which is
   turned on at this time.
3. i = 0;
4. while (1) {
5.        i = i + 1;
6.        wait (ti); % Wait till it is time for next event.
7.        selectedMotor = events (i).motor;
8.        if (events (i)) { % If at this time a vibration motor should be turned on
9.              intensity = (((maxPW – minPW) × (intensities (i)) / 10) + minPW;
                % Depending on the vibration motors, the pulse width min(minPW) and max(maxPW)
                may vary. We define 10 levels of intensities while a user is making the patterns.
10.             setPWM (selectedMotor, intensity); }
                % Turn on a vibration motor with the determined intensity
11.       else { % If at this time a vibration motor should be turned off
12.             setPWM (selectedMotor, 0); } % Turn off a vibration motor
13.       if (i == length (events))
14.             break; }
```

personalized alphanumeric letters. The experiment is carried out with ten healthy volunteers (five males and five females) aged 18 to 46 with (Mean ± SD) 30.70 ± 8.87. The ethical approval was received from McGill University Ethics Committee. The participants were informed about the experimental procedures before starting the trial sessions, and none of them had experience of vibrotactile display devices.

The subjects were asked to wear the designed belt in upright sitting position. We asked the participants to match what they tactually felt with the alphabets or digits. They had a time limit of 2 sec for letter perception, and there was no another chance to repeat

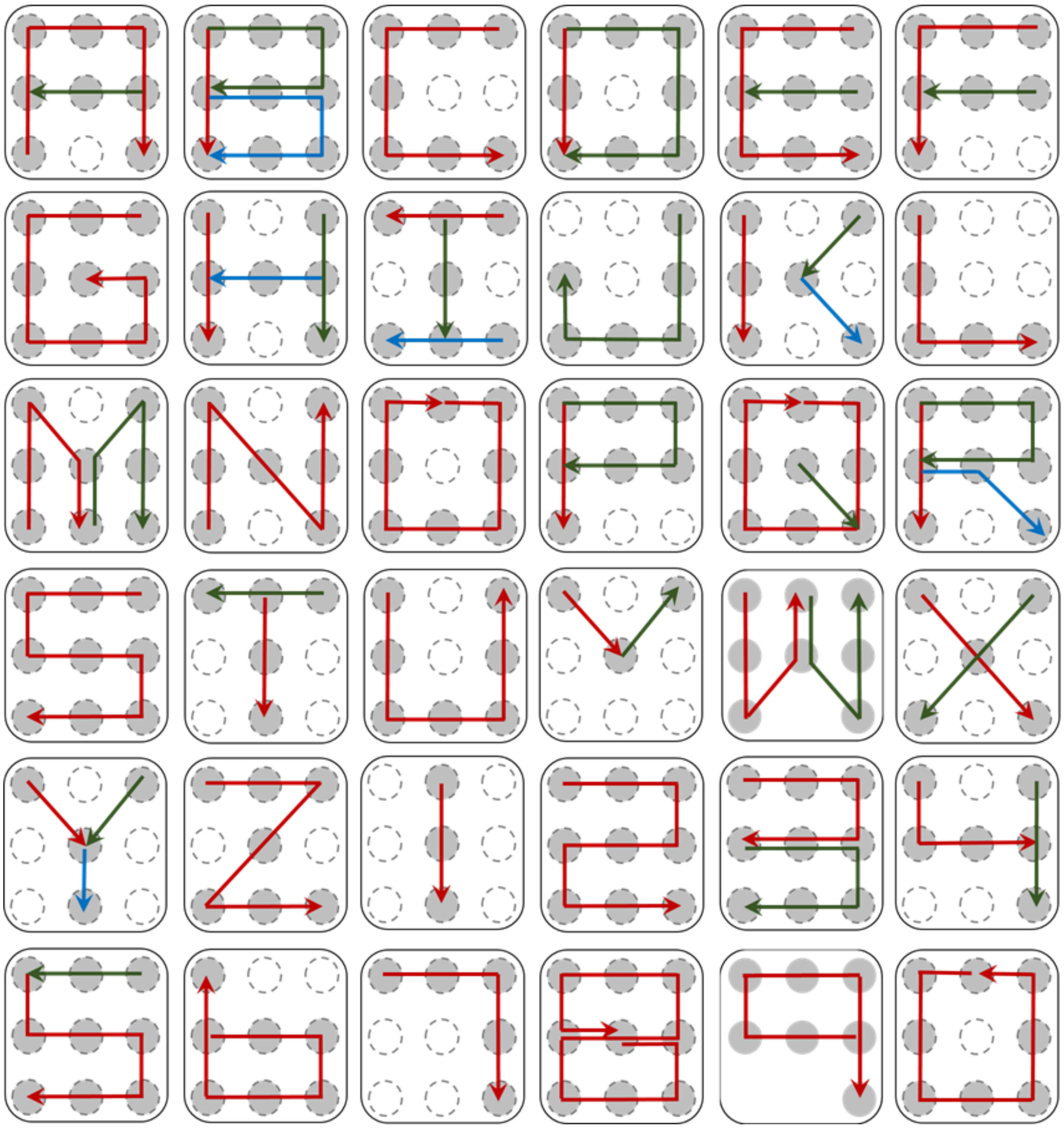

Figure 5.8 The sequence of tactors to be activated 36 different alphabets and digits in the default version - The arrows orders: red, green, and blue.

the presented tactile stimuli. To have a more realistic scenario, they were not allowed to use any headset to block out the sound caused by the vibrators and environment. We wanted to analyze the results with a minimum cognitive load that is calculated by the average repeated time for the subject to conduct the letter's identification [267]. In the training phase, the subjects know the characters they perceive through 3×3 tactile grid display. The training and testing phases are composed of 108 (3×36) trials with 3 sets of randomly selected alphanumeric characters i.e. ‘A’, ‘B’, ‘C’, ‘D’, ‘E’,’ F’, ‘G’, ‘H’, ‘I’, ‘J’, ‘K’, ‘L’, ‘M’, ‘N’, ‘O’, ‘P’, ‘Q’, ‘R’, ‘S’, ‘T’, ‘U’, ‘V’, ‘W’, ‘X’, ‘Y’, ‘Z’, ‘1’, ‘2’, ‘3’, ‘4’, ‘5’, ‘6’, ‘7’, ‘8’, ‘9’ and ‘0’. Figure 5.8 illustrates the sequence of tactors to be activated in the default patterns setting designed by a left-handed supervisor. There is no time interval between the onsets of stimuli, and the stimulus duration is set to 200 msec. These default settings help the participants to perceive the letter as a continuous stroke. In the second session, the subjects could revise the default patterns through the GUI. Indeed, each subject can turn the motors on and off in succession and therefore they could customize the tactors’ vibration patterns with any preferences such as following their own writing habit. Personalizing the spatiotemporal vibration patterns could deliver more information with easier interpretation and memorizing. Therefore, this property greatly facilitates the users to distinguish the letters.

5.2.4 Experimental Results

Figure 5.9 shows the participants’ confusions between stimuli with the default patterns. Each cell value of the matrix $C_{i,j}$ shows the total number of trails that the response ‘j’ occurred upon the presentation of stimulus ’i’. The results indicate that with a low cognitive load, the subjects were able to readily recognize the patterns and achieve a mean identification rate of 70.83% ± 24.65%. The subjects reflected that sometimes they had difficulty in distinguishing the patterns that are different from their own writing habit such as letter ‘E’. The patterns ‘E’ and ‘7’ presented to the participants tended to get highly confused with letters ‘G’ and ‘1’, respectively. Obviously, the more similarity between the two patterns, the more likely the confusion. The letter ‘O’ and number ‘0’ activated the same dot matrix patterns, but they can be discriminated by the direction of the activated tactors. Most participants reported that sometimes they judged a pattern according to their own writing habits. We expect they may be less likely to be confused by revising the spatial locations, stimulus duration, directions, etc.

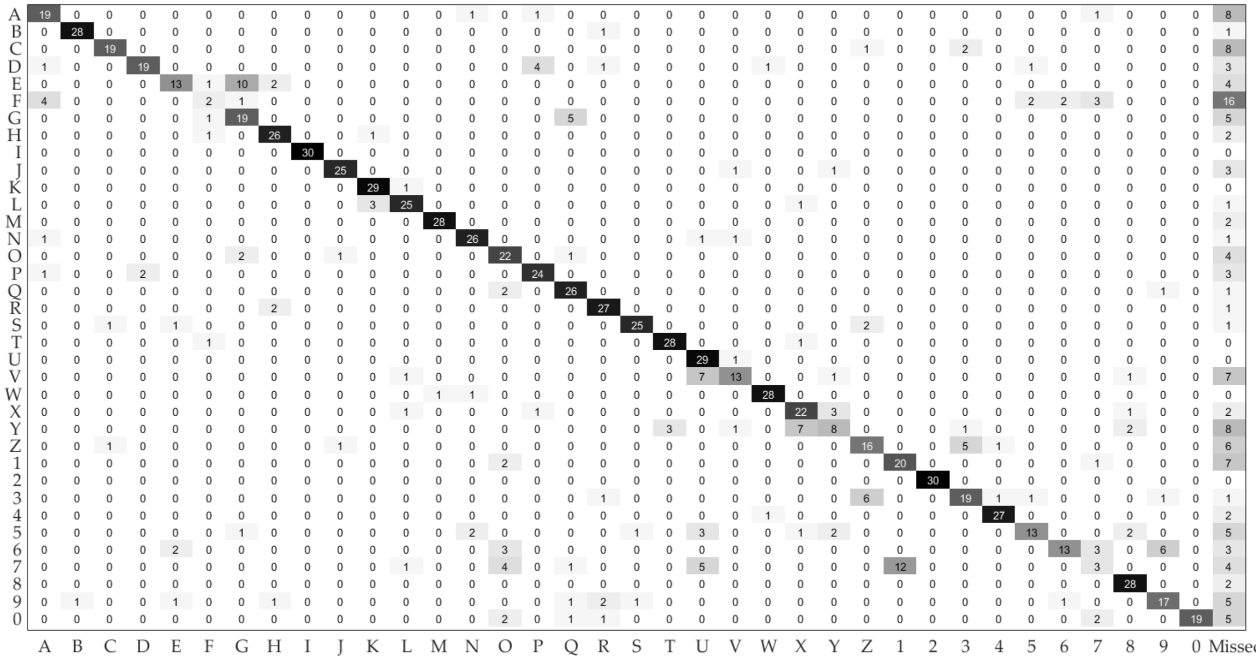

(a)

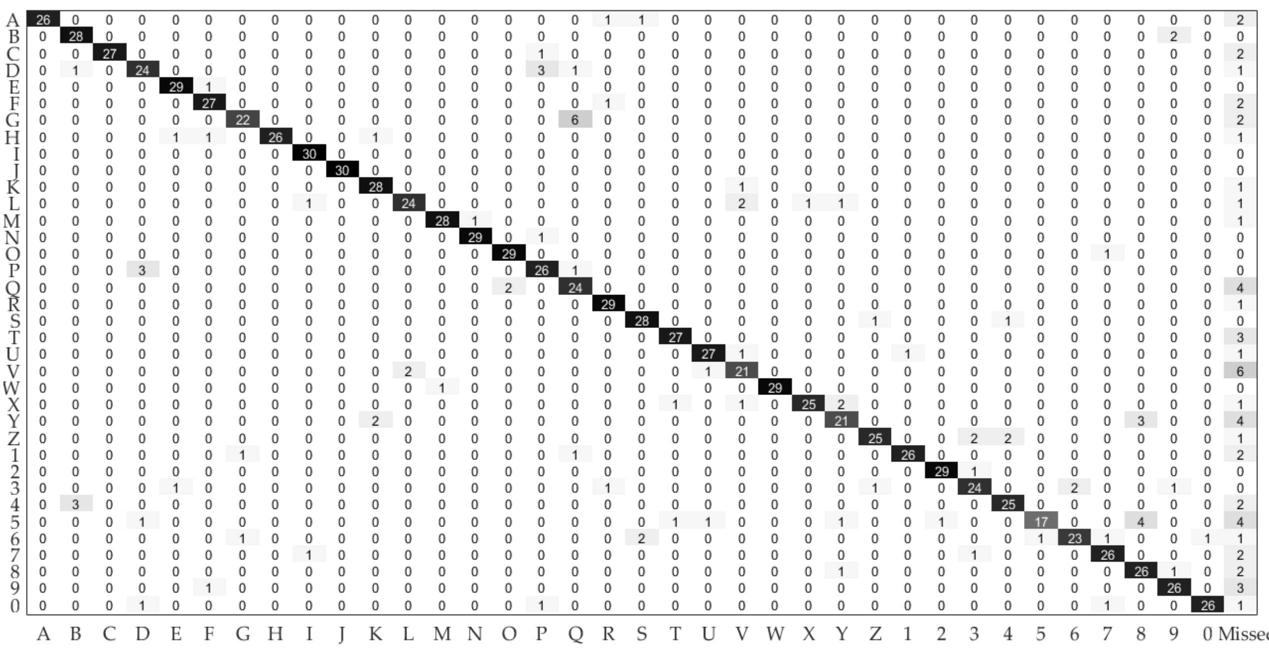

(b)

Figure 5.9 Confusion matrices for the recognition of (a) default patterns, (b) customized patterns

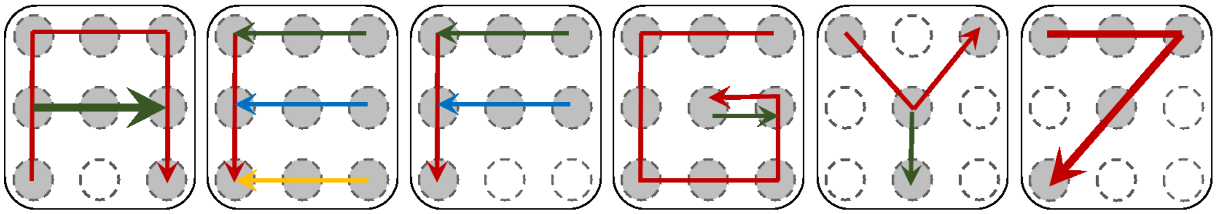

Figure 5.10 Examples of customized patterns by one of the participants

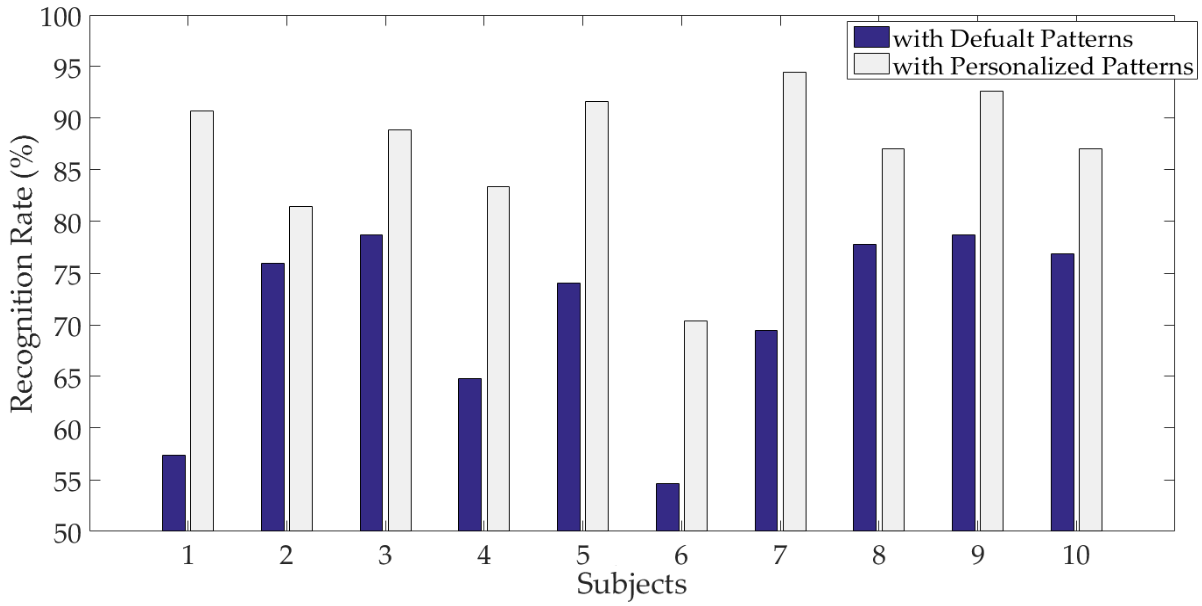

Figure 5.11 Recognition rates with default and personalized patterns for each subject

The subjects had a time limit of 2 sec for letter perception, and there was no other chance to repeat the presented tactile stimuli. If there was no answer after two seconds, the response was considered as 'Missed.' These constraints guarantee to record the first immediate guess and are beneficial for the multi-character words, where the characters are serially presented to the users. In the second session, where each subject was allowed to make modifications to the default patterns, we can see a more uniform confusion matrix. For instance, the letters 'X' and 'Y' have similar patterns directions, and therefore the subjects can apply an alternative writing sequence to create more differentiable patterns. Figure 5.10 demonstrates some more effective alternative patterns designed by a participant for letters 'A', 'E,' 'F,' 'G,' 'Y', and '7'. As depicted in Figure 5.10 the participant used higher level of intensities for letters 'A' and '7' (tick arrows). The results demonstrate that the pattern customization promoted the recognition of the letters. As seen in Figure 5.11, customizing the vibrotactile patterns improved the recognition accuracy by 22.49%. A student's t-test revealed that the customized patterns achieved significantly higher recognition rates than the default patterns (86.76% ± 9.44% vs. 70.83% ± 24.65%, p-value << 0.01). In overall, among the numeric letters, the number '2' yielded the best accuracy (96.67%), followed by '1', '7', '8', '9', '0', '3', '4', and '6', with '5' being the worst (56.67%). For alphabet letters, 'I' and 'J' yielded the best accuracy (100%) and the letters having the lowest recognition accuracies are: 'V' (70%), 'Y' (70%) and 'G' (73.33%). As seen in the confusion matrix, still some letters such as 'Q' and 'G' exhibited asymmetries meaning that the subjects mistakenly took 'Q' for 'G,' whereas they never confused 'G' with 'Q.'

Although in some cases, the updated patterns increase the total vibratory delivery time, they effectively resolve the confusion between letters and consequently reduce the misrecognition rates. According to the last column of confusion matrices (Missed), the most misidentifications are more likely due to time constraints for letters' perception. Contrary to other studies, the participants could not repeat the questions, if they were not confident of their answers and the error correction was not given when the subjects misidentified. These constraints guarantee that we only consider the first immediate guess and are beneficial for the multi-character words, where the characters are successively presented to the users. Another important observation worth highlighting is the reduction of 'Missed' answers (57.85%) after revising the letters. The subjects could judge the pattern in the first two seconds, and all participants agreed that their performance would be improved by tuning the vibratory variables again and practicing them for a couple of more trials.

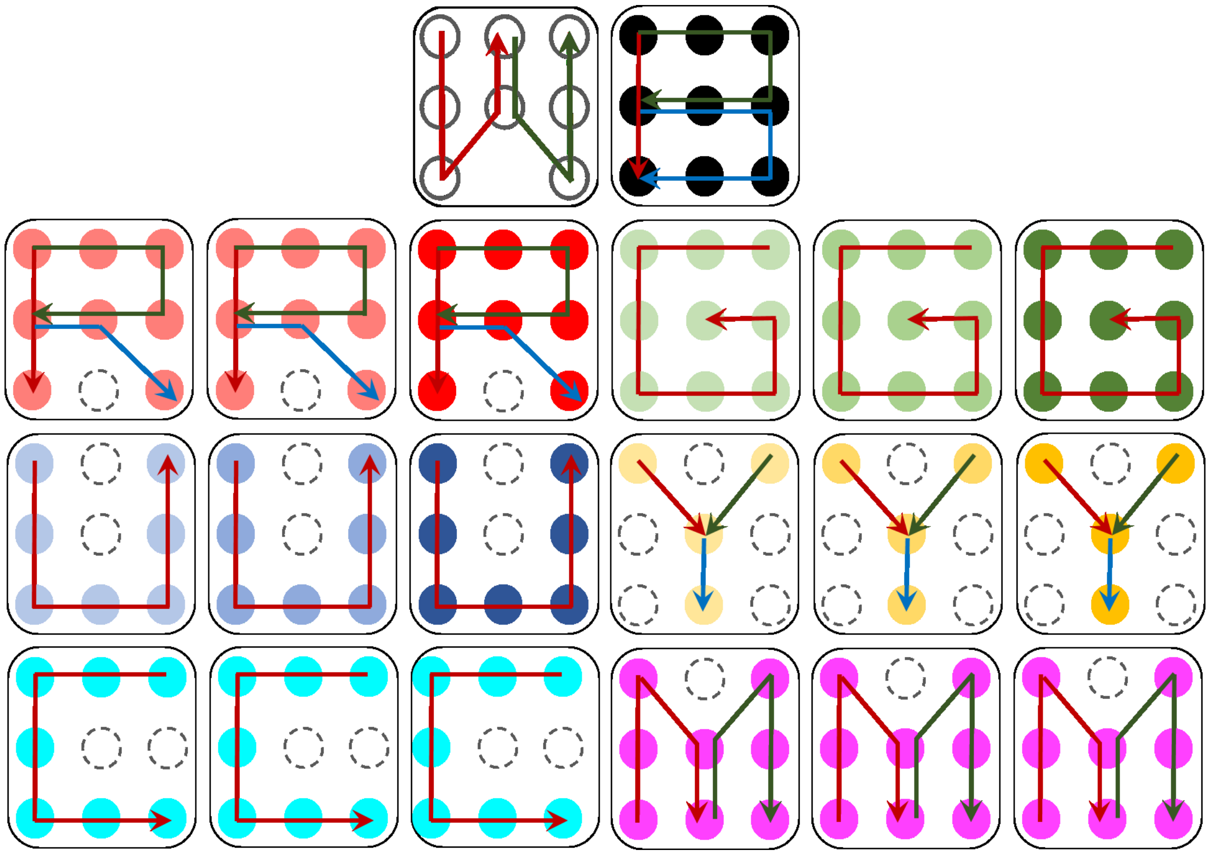

Figure 5.12 Presentation of the colors by means of alphabet patterns and three intensity levels

We also evaluate the feasibility and robustness of the proposed platform in two other applications. To the best of our knowledge, this is the first work that shows how to apply the personalized tactile patterns in recognizing verbs and colors. Color blind individuals need to learn about color through artificial means as the lack of color information rigorously impedes their spatial perception and social interactions. We have performed experiments on rendering color information using haptic feedback. As depicted in Figure 5.12, eight different colors **W**hite (W), **B**lack (B), **R**ed (R), **G**reen (G), bl**U**e (U), **Y**ellow (Y), **C**yan (C), **M**agenta (M) are going to be recognized by the subjects. For the colors except white and black, the motors vibrate in three levels corresponding to the color intensities i.e. light, regular, and dark. It helps people who are colorblind feel the colors around them. In this experiment, the participants were requested to perceive a predefined set of customized tactile patterns delivered by the tactors array. All patterns were vibrated three times in a random order. In total, data is composed of 600 trials ((2 colors + 6 colors × 3 intensity levels) × 3 rounds × 10 participants) for colors recognition task. The results of a 10-participant user study reveal the possibility of conveying color information by means of vibrations with an accuracy of 95.33%. The high recognition indicates the validity of our system to allow near real-time color perception. Twenty eight out of 600 trails have been misidentified, where the majority of recognition errors (22 out of 28) are due to the confusion between the levels of intensity.

The next point of interest is to extend the range of expressiveness by asking the participants to recognize the multi-character verbs (2-4 characters). We selected the most common verbs in English i.e. 'BE', 'HAVE', 'DO', 'SAY', 'GET', 'MAKE', 'GO', 'KNOW', 'TAKE', 'SEE', 'COME', 'THINK', 'LOOK', 'WANT', 'GIVE', 'USE', 'FIND', 'TELL', 'ASK' and 'WORK'. A delimiter discriminates the verbs. There was no training session, and therefore the participants did not know what words are going to be felt. On each trial, a random verb was chosen, and its customized characters were sequentially presented to participants as vibrotactile stimuli. The results indicated that the multi-character verbs could be delivered with recognition rate 90.50%. This evaluation provides the first steps toward achieving a realistic accuracy for the multi-character words identification task based on leveraging the spatial and temporal properties of skin. These short-term studies could provide initial insights into the use of tactile instructions in more complex scenarios.

To name other potential applications, as we mentioned earlier, the tactile stimuli could be also beneficial for learning motor skills and rehabilitation exercises. Another key advantage of this mode of information representation is that it can be present at the same time as visual/audio cues. For example, such a system can be generalized to deliver compound messages to allow the athletes to keep their eye on the activities. It helps to improve the quality of performance with the use of a haptic back display for providing instructions and feedback on exercises in real time. For instance, "LAU = Left Arm Up" message can be used to correct the left arm movement by lifting it up. The intensity of the vibration might be varied according to the magnitude of the error between the perfect (reference) and current movements. In addition, identification of the compound messages is of great interest to the phone users while receiving semantic information e.g. 'E12' could indicate 'You have 12 Emails'. Finally, using an identification task on the lower back, we found out the patterns customization can be considered as a promising method in relaying information through the skin. The applicability and usability of this light belt-like device can be extended to numerous health and fitness applications.

5.3 Conclusion

In the first part of this chapter, the idea of sensor-based breathing therapy was integrated with a single-point vibratory feedback to help people evaluate their breathing quality while practicing the prescribed respiration exercises. The spatial deviation from the desired movement felt tactually can provide training guidance sufficient to improve the quality of prescribed exercises. This system can enthuse people with a feeling of feedback on quality and inform them of their progress in performing the breathing models. Although a single-point vibration feedback could promote the performance of the users while refining their movement patterns, the delivered information through one vibration motor is limited in providing rich information. Therefore, in the second part of this chapter, we presented a tactile display as an information-transferring channel with the capability of customization. The designed user interface generates space-time vibration stimuli according to each subject's preferences. The experiments were conducted to investigate the effectiveness of the proposed customizable tactile display in alphanumeric letters perception. The results reveal that the fully customizable low-resolution vibrotactile display alleviates the perceptional and memory loadings of the users and they can easily learn and recognize new patterns with no extensive training sessions. We also validated the system with colors and words identification tasks and the promising results proved that this system is feasible to be used by people whose normal visual/auditory channels are saturated or obstructed. It was fascinating to observe that the minimally trained subjects were able to perceive the 20 colors and 20 verbs with an overall accuracy of 95.33% and 90.50%, respectively. Based on our findings, we conclude that applying personalized tactile instructions can be used as a major component of an assistive wearable device for people with hearing and visual impairments. In addition, the flexibility of the system helps people to acquire physical skills during training.

Chapter 6

Conclusion and Future Work

This chapter summarizes the work that was presented in this thesis, along with some suggested future work.

6.1 Conclusion

The smartphones or wearable devices with the embedded accelerometer sensor can be strapped to different body parts including wrist, arm, or ankle to determine frequency and intensity of movements. We can take the wearables ideas one step further with the artificial intelligence to provide analysis of different areas of body awareness. We applied machine learning techniques to the task of predicting physical activity type from a single body-mounted tri-axial accelerometer. An efficient HAR solution automatically provides people with vital retrospective behavioral information so that they can get a much better understanding of their health conditions. It also enables clinicians to improve or maintain well-being in populations who suffer from a chronic disease whose progression is linked to a decrease in movement and mobility.

In Chapter 3, different classification techniques were deeply explored when heterogeneity of devices and their usage scenarios are considered. In addition, each sensor position was analyzed based on the aggregated tri-axial accelerometer data from different datasets. We also presented a complete evaluation to determine the window and overlap size impacts within the activity recognition process. The averaged results showed 96.44% ± 1.62 % accuracy when using K-fold and 79.92% ± 9.68 % when using a subject-independent cross-validation.

In Chapter 4, novel feature extraction and multi-classification techniques were developed to optimize the accuracy as well as the worst-case sensitivity in the multi-class classification problems. An evolutionary algorithm was applied which attempts to intelligently get closer and closer to the best hierarchical model in the tree-based structure. The effectiveness of the proposed techniques was compared with the previously published machine learning algorithms, which are stand-alone multi-class classifiers. The proposed techniques were investigated in two case studies, where different classes correspond to various daily activities and breathing disorders. In the first case study, the best accuracy of 92.16% was achieved for identifying 33 activities with the fusion of two sensors. We also could obtain a great increase of 51.22% in the worst-case sensitivity. We demonstrated that different critical respiratory information with high accuracy could be derived from analyzing the interior/posterior movements of the chest wall during breathing function at rest. Accelerometer-derived respiration signal could be analyzed by following a set of signal processing and machine learning steps to develop the capabilities of diagnostic and treatment of respiratory disorders. The results of breathing patterns classification showed an overall classification accuracy of 91.23%, 83.98%, and 95.14% with Acc1, Acc2, and both sensors data, respectively. It is concluded that the proposed methods improved the worst-case sensitivity by about 7.29%, 9.59%, and 4.13% compared to the best classifier in a single objective problem. Furthermore, we found that even when working with heterogeneous datasets presented in Chapter 3, we could obtain the promising results for all eight positions. This chapter ended with the results of an innovative approach to speed up the recognition procedure. With the breathing datasets, an average improvement of more than 30% was obtained. This finding enables the design of a highly effective real-time predictive model for wearable applications.

Another powerful extension of wearable technology is to deliver interventions to encourage a positive behavior change. For instance, the breathing therapy that improves the health of patients suffering from asthma or other breathing disorders could be achieved by analyzing the chest movements with an ideal model. In the first part of Chapter 5, the idea of sensor-based breathing therapy was integrated with a single-point vibratory feedback to help people evaluate their breathing quality while practicing the prescribed respiration exercises. The device provided corresponding error information of breathing maneuvers through vibrations delivered to the lower back of the users. In the second part of this chapter, we presented a tactile display as an information-transferring channel with the capability of customization. The designed user interface generated space-time vibration stimuli according to each subject's preferences. The experiments were conducted to investigate the effectiveness of the proposed customizable tactile display in alphanumeric letters perception. The results reveal that the fully customizable low-resolution vibrotactile display alleviates the perceptional and memory loadings of the users and they can easily learn and recognize new patterns with no extensive training sessions. We also validated the system with colors and words identification tasks and the results proved that this system could be used by people whose normal visual/auditory channels are saturated or obstructed. It was interesting to observe that the minimally trained subjects were able to perceive the twenty colors and twenty verbs with an overall accuracy of 95.33% and 90.50%, respectively. This system can be beneficial and effective not only for delivering complex feedback, but also for people with hearing and visual impairments.

6.2 Future Work

The techniques and analyses investigated in this work are ready for pilot deployment in health and fitness applications. As seen in this thesis, much progress has been made in the area of the wearable sensor system, and there are good prospects for future applications.

- The real-time activity recognition system should be also validated to monitor daily activities for large-scale and long-term studies. Other wearable sensors capturing vital signs can be combined into the feature vectors. Heterogeneous sensors help to extend the applicability of the proposed techniques for a range of other health problems such as sleep apnea, cardiac arrhythmia, and chronic obstructive pulmonary disease. New algorithms need to be developed and verified by clinical trials before promotion to a wide population.
- As a promising research direction, this study can be extended in building deep learning schemes and automatic feature learning to improve the accuracy of classification and create an opportunity for a more in-depth understanding of wearable sensors.
- There are further research lines that require attention. Many possibilities exist in feature extraction and creating ensemble designs. The sensor position and orientation independence should be further investigated to generalize the solutions that provide promising levels of accuracy in the real-world environments.
- More research and development efforts are required to improve the reliability and comfort index of the system. This research direction is important as sensor-based monitoring system is meant to be unobtrusive and operate in daily life.

- For the breathing therapy project, the lack of long-term evaluation made it difficult to determine the existence of retained effect of feedback delivered to the users. Future studies should incorporate the prospective long-term effect of these devices on simple and more functional breathing assessments.
- The developed haptic solution facilitates new opportunities to monitor or measure wellness progress made by patients for other healthcare related applications, in particular, rehabilitation applications such as stroke rehabilitation. Virtual Reality technology as an emerging area can be integrated into the current system while providing increased standardization of assessment and training protocols.
- The design of vibrotactile display could be developed more wearable and more appropriate for outdoor uses. Future attempts can focus on testing the system in daily life and finding an estimate of the skin's achievable throughput. Potential studies involve expansion of the dataset by adding further participants to allow reasonable cross-study comparison and meta-analysis. The user's feedback is also necessary to optimize the functionality of the sensory substituting/augmentation systems for people with various degrees of impairments and age.
- Another point that deserves to be further assessed is the wearer's privacy. The use of inertial sensors less invade the wearer privacy compared to the use of cameras, but there exist specific requirements to realize privacy-preserving data aggregation and secure verifiable outsourcing computation in cloud-assisted wireless wearable communications.

References

[1] S. Kumar, W. Nilsen, M. Pavel, and M. Srivastava, "Mobile health: Revolutionizing healthcare through transdisciplinary research." IEEE Computer, vol. 46, no. 1, pp. 28-35, 2013.

[2] A. Merglen, A. Flatz, R.E Bélanger, P.A. Michaud,J.C. Suris, "Weekly sport practice and adolescent well-being", Arch. Dis. Child. vol. 99, pp. 208–210, 2014.

[3] W. Chodzko-Zajko, "Exercise and physical activity for older adults," Univ. Access Inf. Soc. vol. 3, pp. 101–106, 2014.

[4] I.M. Lee, E.J. Shiroma, F. Lobelo, P. Puska, S.N. Blair, P.T. Katzmarzyk, Lancet Physical Activity Series Working Group. "Effect of physical inactivity on major non-communicable diseases worldwide: An analysis of burden of disease and life expectancy," Lancet, vol. 380, pp. 219–229, 2012.

[5] World Health Organization: Obesity and overweight. [Online] Available: http://www.who.int/mediacentre/factsheets/fs311/en.

[6] National Diabetes Statistics Report, National Diabetes Education Program (NDEP), 2014.

[7] S.I. de Vries, F.G. Garre, L.H. Engbers, V.H. Hildebrandt, and S. van Buuren, "Evaluation of neural networks to identify types of activity using accelerometers," Medicine & Science in Sports & Exercise, 43(1):101, 2011.

[8] R. Khusainov, D. Azzi, I. Achumba, and S. Bersch, "Real-Time Human Ambulation, Activity, and Physiological Monitoring: Taxonomy of Issues, Techniques, Applications, Challenges and Limitations," Sensors, vol. 13, no. 10, pp. 12852–12902, Sep. 2013.

[9] UN (United Nations). World Population to reach 10 billion by 2100 if Fertility in all Countries Converges to Replacement Level; United Nations Press Release: New York, NY, USA, 3 May 2011.

[10] Ageing in the Twenty-First Century: A Celebration and A Challenge, Published by the United Nations Population Fund (UNFPA), 2012

[11] A. Wang, G. Chen, J. Yang, S. Zhao, C.H. Chang, "A Comparative Study on Human Activity Recognition Using Inertial Sensors in a Smartphone," IEEE Sens. J. vol. 16, pp. 4566–4578, 2016.

[12] A. Avci, S. Bosch, M. Marin-Perianu, R. Marin-Perianu, P. Havinga, "Activity recognition using inertial sensing for healthcare, wellbeing and sports applications: A survey," In Proceedings of the 2010 23rd International Conference on Architecture of Computing Systems (ARCS), Hannover, Germany, pp. 22–25 2010.

[13] M. Hassanalieragh, A. Page, T. Soyata, G. Sharma, M. Aktas, G. Mateos, B. Kantarci, S. Andreescu, "Health Monitoring and Management Using Internet-of-

Things (IoT) Sensing with Cloud-based Processing: Opportunities and Challenges," In Proceedings of the 2015 IEEE International Conference on Services Computing (SCC), New York, NY, USA, 2015.

[14] O.D. Lara, M.A. Labrador, "A survey on human activity recognition using wearable sensors," IEEE Commun. Surv. Tutor. vol. 15, pp. 1192–1209, 2013.

[15] L.K. Wang, "Recognition of Human Activities Using Continuous Autoencoders with Wearable Sensors," Sensors 2016, 16, 189.

[16] N. Ikizler, P. Duygulu, " Histogram of oriented rectangles: A new pose descriptor for human action recognition," Image Vis. Comput. vol. 27, pp. 1515–1526, 2009.

[17] S.Q. Wang, G. Zhou, "A review on radio based activity recognition," Dig. Commun. Netw. vol. 1, pp. 20–29, 2015.

[18] T. Brack, I. Thüer, C.F. Clarenbach, et al. "Daytime Cheyne–Stokes respiration in ambulatory patients with severe congestive heart failure is associated with increased mortality," Chest journal, 132(5):1463-71, 2007.

[19] Chronic obstructive pulmonary disease in Canadians, 2009 to 2011, Statistics Canada, [Online] Available: http://www.statcan.gc.ca/pub/82-625-x/2012001/article/11709-eng.htm.

[20] Fast Facts about Asthma: Data compiled from the 2011 Survey on Living with Chronic Diseases in Canada, Public Health Agency of Canada. [Online], Available: http://www.phac-aspc.gc.ca/cd-mc/crd-mrc/asthma_fs_asthme-eng.php.

[21] ASTHMA STATISTICS, American Academy of Allergy, Asthma & Immunology. [Online], Available: http://www.aaaai.org/about-aaaai/newsroom/asthma-statistics.

[22] BW Choi, K-H Yoo, J-W Jeong, *et al.* "Easy Diagnosis of Asthma: Computer-Assisted, Symptom-Based Diagnosis," Journal of Korean Medical Science.,22(5):832-838, 2007.

[23] Public Health Association of Canada The Canadian Community Health Survey: Rapid Response on sleep apnea. Statistics Canada, [Online], Available: www.statcan.gc.ca/daily-quotidien/091208/dq091208d-eng.htm.

[24] Z. Wang, Z. Yang, T. Dong, "A Review of Wearable Technologies for Elderly Care that Can Accurately Track Indoor Position, Recognize Physical Activities and Monitor Vital Signs in Real Time," Sensors 2017, 17, 341.

[25] M. Folke, L. Cernerud, M. Ekstrom, B. Hök, "Critical review of non-invasive respiratory monitoring in medical care," Med. Biol. Eng. Comput. vol. 41, pp. 377–383, 2003.

[26] L. Guo, L. Berglin, U. Wiklund, "Design of a garment-based sensing system for breathing monitoring," Text. Res. J. 2013, 83, 499–509.

[27] O. Atalay, W.R. Kennon, E. Demirok, "Weft-Knitted Strain Sensor for Monitoring Respiratory Rate and Its Electro-Mechanical Modeling," IEEE Sens. J. 2015, 15, 110–121.

[28] V.H. Larsen, P.H. Christensen, H. Oxhøj, T. Brask, “Impedance pneumography for long-term monitoring of respiration during sleep in adult males,” Clinical Physiology 4 (1984) 333–342.

[29] A. Bates, M.J. Ling, J. Mann, D. K. Arvind, "Respiratory Rate and Flow Waveform Estimation from Tri-axial Accelerometer Data," Body Sensor Networks (BSN), International Conference on, pp.144-150, 2010.

[30] A. Roshan Fekr, M. Janidarmian, K. Radecka, Z. Zilic, “A Medical Cloud-Based Platform for Respiration Rate Measurement and Hierarchical Classification of Breath Disorders,” Sensors 2014, 14, 11204-11224.

[31] K. Bark, J. Wheeler, P.B. Shull, J. Savall, M. Cutkosky, “Rotational skin stretch feedback: a wearable haptic display for motion,” IEEE Trans Haptics. 2010; 3:166–76.

[32] J. Lieberman, C. Breazeal, “TIKL: development of a wearable vibrotactile feedback suit for improved human motor learning,” IEEE Trans Robot. 2007; 23:919–26.

[33] P. Kapur, M. Jensen, L.J. Buxbaum, S.A. Jax, K.J. Kuchenbecker, “Spatially distributed tactile feedback for kinesthetic motion guidance,” In 2010 IEEE Haptics Symp. Proc. IEEE; 2010; 519–526.

[34] C. Wall, E. Kentala, “Effect of displacement, velocity, and combined vibrotactile tilt feedback on postural control of vestibulopathic subjects,” J Vestib Res Equilib Orientat. 2010; 20:61–9.

[35] K. Förster, M. Bächlin, G. Tröster, “Non-interrupting user Interfaces for Electronic Body-worn Swim Devices,” In: Proc 2nd Int Conf PErvsive Technol Relat to Assist Environ - PETRA ’09. New York, New York, USA: ACM Press; 2009. p. 1–4.

[36] PB Shull, K. Lurie, M.R. Cutkosky, T. Besier, “Training multi-parameter gaits to reduce the knee adduction moment with data-driven models and haptic feedback,” J Biomech. 2011; 44:1605–9.

[37] P. B. Shull, D. D. Damian, "Haptic wearables as sensory replacement sensory augmentation and trainer-a review", Journal of NeuroEngineering and Rehabilitation, vol. 12, no. 1, pp. 59, 2015.

[38] PB Shull, R. Shultz, A. Silder, J. L. Dragoo, T.F. Besier, M.R. Cutkosky, et al. “Toe-in gait reduces the first peak knee adduction moment in patients with medial compartment knee osteoarthritis,” J Biomech. 2013; 46:122–8.

[39] M. Dozza, C. Wall, R.J. Peterka, L. Chiari, F.B. Horak, “Effects of practicing tandem gait with and without vibrotactile biofeedback in subjects with unilateral vestibular loss,” J Vestib Res. 2007; 17:195–204.

[40] R. Sigrist, G. Rauter, R. Riener, P. Wolf, “Augmented visual, auditory, haptic, and multimodal feedback in motor learning: a review,” Psychon Bull Rev. 2013; 20:21–53.

[41] S. D. Novich, and D. M. Eagleman, “Using space and time to encode vibrotactile information: toward an estimate of the skin's achievable throughput”. Experimental Brain Research, issue 10, pp 2777-2788, 2015.

[42] T. Mcdaniel, S. Krishna, V. Balasubramanian, D. Colbry, S. Panchanathan, “Using a haptic belt to convey non-verbal communication cues during social interactions to individuals who are blind,” In HAVE Haptic Audio Vis Environ their Appl; 2008:1–6.

[43] (2016) Health care costs. [Online]. Available: http://www.chcf.org/~/media/MEDIA/LIBRARY/Files/PDF/HealthCareCosts16.pdf.

[44] A. Pantelopoulos, N. Bourbakis, “A Survey on Wearable Sensor-Based Systems for Health Monitoring and Prognosis,” IEEE Trans. Syst. Man Cybern. C 2010, 40, 1–12.

[45] (2015) Growth trends, consumer attitudes, and why smartwatches will dominate. [Online]. Available: http://www.businessinsider.com/the-wearable-computing-market-report-2014-10.

[46] J. Sun Lee, J. Young NAM, H. Joo Lee, K. Hyun Kim, “Haptic actuator integrated with sensor electrode and wearable device comprising the same”, US Patent, US 9529436 B2, 2015.

[47] N. Agoulmine, M. Deen, J. Lee, M. Meyyappan, “U-Health Smart Home,” IEEE Nanotechnol. Mag. 2011, 5, 6–11.

[48] A. Dementyev, S. Hodges, S. Taylor, J. Smith, “Power consumption analysis of Bluetooth Low Energy, ZigBee and ANT sensor nodes in a cyclic sleep scenario,” In Proceedings of the 2013 IEEE International Wireless Symposium (IWS), Beijing, China, 14–18 April 2013; pp. 1–4.

[49] V. Coskun, B. Ozdenizci, K. Ok, “A Survey on Near Field Communication (NFC) Technology,” Wirel. Pers. Commun. 2013, 71, 2259–2294.

[50] W. Xu, "System Problem Detection by Mining Console Logs," University of California, Berkeley, Berkeley, Technical Report No. UCB/EECS-2010-112, 2010.

[51] M. Tentori, G. R. Hayes, and M. Reddy, “Pervasive computing for hospital, chronic, and preventive care,” Found. Trends Hum.-Comput. Interact., 5(1):1–95, January 2012.

[52] S. Majumder, T. Mondal, M.J. Deen, “Wearable Sensors for Remote Health Monitoring,” Sensors 2017, 17, 130.

[53] K.C. Tseng, B.S. Lin, L.D. Liao, Y.T. Wang, Y.L. Wang, “Development of a Wearable Mobile Electrocardiogram Monitoring System by Using Novel Dry Foam Electrodes,” IEEE Syst. J. 2014, 8, 900–906.

[54] G. Andreoni, P. Perego, C. Standoli, “Wearable monitoring of elderly in an ecologic setting: The SMARTA project,” Available online: https://sciforum.net/conference/ecsa-2/paper/3192/download/pdf (accessed on 5

January 2017).
[55] T. Komensky, M. Jurcisin, K. Ruman, O. Kovac, D. Laqua, P. Husar, “Ultra-wearable capacitive coupled and common electrode-free ECG monitoring system,” In Proceedings of the 2012 Annual International Conference of the IEEE Engineering in Medicine and Biology Society, San Diego, CA, USA, 2012; pp. 1594–1597.
[56] R. Ciobotariu, F. Adochiei, C. Rotariu, H. Costin, “Wireless Breathing System for Long Term Telemonitoring of Respiratory Activity”, Advanced Topics in Electrical Engineering, Proc. of the 7th International Symposium, pp.635-638, May 2011.
[57] P.K. Dehkordi, M. Marzencki, K. Tavakolian, M. Kaminska, B. Kaminska, "Validation of respiratory signal derived from suprasternal notch acceleration for sleep apnea detection," Engineering in Medicine and Biology Society, EMBC, International Conference of the IEEE, pp. 3824-3827, 2011.
[58] C. L. Que, C. Kolmaga, L. G. Durand, S. M. Kelly, and P. T. Macklem, “Phonospirometry for noninvasive measurement of ventilation: methodology and preliminary results.” J Appl Physiol, vol. 93, no. 4, pp.1515– 1526, Oct 2002.
[59] P. Oguz, G. Ertas, “Wireless dual channel human body temperature measurement device,” In Proceedings of the 2013 International Conference on Electronics, Computer and Computation (ICECCO), Ankara, Turkey, 7–9 November 2013; pp. 52–55.
[60] H. Mansor, M.H.A Shukor, S.S. Meskam, N.Q.A.M. Rusli, N.S. Zamery, “Body temperature measurement for remote health monitoring system,” In Proceedings of the 2013 IEEE International Conference on Smart Instrumentation, Measurement and Applications (ICSIMA), Kuala Lumpur, Malaysia, 2013; pp. 1–5.
[61] S. Milici, S. Amendola, A. Bianco, G. Marrocco, “Epidermal RFID passive sensor for body temperature measurements,” In Proceedings of the 2014 IEEE RFID Technology and Applications Conference (RFID-TA), Tampere, Finland, 2014; pp. 140–144.
[62] M.Z. Poh, N.C. Swenson, R.W. Picard, “A Wearable Sensor for Unobtrusive, Long-Term Assessment of Electrodermal Activity,” IEEE Trans. Biomed. Eng. 2010, 57, 1243–1252.
[63] J. Kim, S. Kwon, S. Seo, K. Park, “Highly wearable galvanic skin response sensor using flexible and conductive polymer foam,” In Proceedings of the 2014 36th Annual International Conference of the IEEE Engineering in Medicine and Biology Society, Chicago, IL, USA, 2014; pp. 6631–6634.
[64] G. Crifaci, L. Billeci, G. Tartarisco, R. Balocchi, G. Pioggia, E. Brunori, S. Maestro, M.A. Morales, “ECG and GSR measure and analysis using wearable systems: Application in anorexia nervosa adolescents,” In Proceedings of the 2013 8th

International Symposium on Image and Signal Processing and Analysis (ISPA), Trieste, Italy, 2013; pp. 499–504.

[65] K. Li, S. Warren, "A Wireless Reflectance Pulse Oximeter with Digital Baseline Control for Unfiltered Photoplethysmograms," IEEE Trans. Biomed. Circuits Syst. 2012, 6, 269–278.

[66] Q. Cai, J. Sun, L. Xia, X. Zhao, "Implementation of a wireless pulse oximeter based on wrist band sensor," In Proceedings of the 2010 3rd International Conference on Biomedical Engineering and Informatics, Yantai, China, 2010; pp. 1897–1900.

[67] Y. Mendelson, R.J. Duckworth, G. Comtois, "A Wearable Reflectance Pulse Oximeter for Remote Physiological Monitoring," In Proceedings of the 2006 International Conference of the IEEE Engineering in Medicine and Biology Society, New York, NY, USA, 2006; pp. 912–915.

[68] R.G. Haahr, S.B. Duun, M.H. Toft, B. Belhage, J. Larsen, K. Birkelund, E.V. Thomsen, "An Electronic Patch for Wearable Health Monitoring by Reflectance Pulse Oximetry," IEEE Trans. Biomed. Circuits Syst. 2012, 6, 45–53.

[69] P. Casale, O. Pujol and P. Radeva, "Personalization and user verification in wearable systems using biometric walking patterns," Personal and Ubiquitous Computing, 16(5), 563-580, 2012.

[70] Mi Zhang and Alexander A. Sawchuk, "USC-HAD: A Daily Activity Dataset for Ubiquitous Activity Recognition Using Wearable Sensors", ACM International Conference on Ubiquitous Computing (UbiComp) Workshop on Situation, Activity and Goal Awareness (SAGAware), Pittsburgh, Pennsylvania, USA, September 2012.

[71] O. Banos, M. A. Toth, M. Damas, H. Pomares, I. Rojas, O. Amft, "A benchmark dataset to evaluate sensor displacement in activity recognition", Proceedings of the 14th International Conference on Ubiquitous Computing (Ubicomp 2012), Pittsburgh, USA, September 5-8, (2012).

[72] https://www.fitbit.com

[73] http://myzeo.com

[74] https://www.zephyranywhere.com

[75] http://www.soterawireless.com/

[76] http://www.irhythmtech.com/

[77] http://www.equivital.co.uk/

[78] N. B. Priyantha, A. Chakraborty, and H. Balakrishnan, "The cricket location-support system." In Proceedings of the Sixth Annual ACM International Conference on Mobile Computing and Networking, pages 32–43, 2000.

[79] J. K. Aggarwal and M. S. Ryoo, "Human activity analysis: A review." ACM Computing Surveys, 43:16:1–16:43, 2011.

[80] ANDREJAIC, M. Mems accelerometers. Seminar (March 2008).

[81] M. Kangas, A. Kontilla, I. Winblad, T. Jamsa, "Determination of Simple

Thresholds for Accelerometry-based Parameters for Fall Detection." In Proceedings of the 29th Annual International Conference of the IEEE Engineering in Medicine and Biology Society, Lyon, France, 2007.

[82] O. Banos, M.A. Toth M. Damas, H. Pomares, I. Rojas, I. "Dealing with the effects of sensor displacement in wearable activity recognition." Sensors vol. 14, no. 6, pp. 9995-10023 (2014).

[83] G. Z. Yang, Body Sensor Networks. London, U.K.: Springer-Verlag, 2006.

[84] J. Feng, G. Qu, M. Potkonjak, "Sensor calibration using nonparametric statistical characterization of error models," Sensors, 2004. Proceedings of IEEE, vol., no., pp. 1456- 1459 vol.3, 2004.

[85] J. Feng, S. Megerian, M. Potkonjak, "Model-based calibration for sensor networks," Sensors, 2003. Proceedings of IEEE, vol.2, no., pp. 737- 742 Vol.2, 22-24 Oct. 2003.

[86] D. Hall, "Mathematical Techniques in Multisensor Data Fusion." Boston, MA: Artech House, 1992.

[87] L. A. Klein, "Sensor and Data Fusion Concepts and Applications," SPIE Opt. Engineering Press, Tutorial Texts, vol. 14, 1993.

[88] Z. Zilic and K. Radecka, "Fault tolerant glucose sensor readout and recalibration," Proceedings of Wireless Health, WH 2011, 2011.

[89] L. Balzano, "Addressing fault and calibration in wireless sensor networks." Master's thesis, University of California, Los Angeles, California, 2007.

[90] E. Waltz, "Data fusion for C3I: A tutorial," in Command, Control, Communications Intelligence (C3I) Handbook. Palo Alto, CA: EW Communications, 1986, pp. 217–226.

[91] J. Llinas and E. Waltz, "Multisensor Data Fusion." Boston, MA: Artech House, 1990.

[92] F. Koushanfar, S. Slijepcevic, M. Potkonjak, A. Sangiovanni-Vincentelli, "Error-Tolerant Multi-Modal Sensor Fusion," IEEE CAS Workshop on Wireless Communication and Networking, 2002.

[93] T. Clouqueur, K. K. Saluja, P. Ramanathan, "Fault Tolerance in Collaborative Sensor Networks for Target Detection", IEEE Trans. On Computers, Vol. 53, No. 3, March 2004, pp. 320-333.

[94] W. Elmenreich, "An Introduction to Sensor Fusion", Research Report, Technical University of Munich, 2001.

[95] O. Sarbishei, M. Janidarmian, A. Roshan Fekr, B. Nahill, K. Radecka, Z. Zilic, "Multi-sensory System Integration Dependability", Chapter 18 in Book Technologies for Smart Sensors and Sensor Fusion, edited by K. Yallup and K. Iniewski, pp. 319-335, 2013.

[96] R. Jia, B. Liu, Human daily activity recognition by fusing accelerometer and multi-lead ECG data, in: Signal Processing, Communication and Computing, ICSPCC,

2013 IEEE International Conference on, IEEE, 2013, pp. 1–4.
[97] S.O.H. Madgwick, A.J.L. Harrison, R. Vaidyanathan, “Estimation of IMU and MARG orientation using a gradient descent algorithm,” Rehabilitation Robotics (ICORR), 2011 IEEE International Conference on , vol., no., pp.1,7, 2011.
[98] M. Janidarmian, K. Radecka, Z. Zilic, “Automated Diagnosis of Knee Pathology Using Sensory Data”, IEEE International Conference on Wireless Mobile Communication and Healthcare - "Transforming healthcare through innovations in mobile and wireless technologies", Nov. 3-5, 2014, Athens, Greece.
[99] M. Janidarmian, A. Roshan Fekr, K. Radecka, Z. Zilic, “Affordable eRehabilitation Monitoring Platform”, IEEE International Humanitarian Technology Conference (IHTC), June 1-4, 2014, Montreal, Canada.
[100] “SensorTag”, Available: www.ti.com/sensortag-wiki
[101] N. Matsuhisa, M. Kaltenbrunner, T. Yokota, H. Jinno, K. Kuribara, T. Sekitani, T. Someya, “Printable elastic conductors with a high conductivity for electronic textile applications,” Nat. Commun. 2015, 6, 7461.
[102] M. Ghamari, H. Arora, R. S. Sherratt and W. Harwin, "Comparison of low-power wireless communication technologies for wearable health-monitoring applications," 2015 International Conference on Computer, Communications, and Control Technology (I4CT), Kuching, 2015, pp. 1-6.
[103] F. Touati, R. Tabish, “U-Healthcare System: State-of-the-Art Review and Challenges,” J. Med. Syst. 2013, 37, 1–20.
[104] K. Malhi, S. Mukhopadhyay, J. Schnepper, M. Haefke, H. Ewald, “A Zigbee-Based Wearable Physiological Parameters Monitoring System,” IEEE Sens. J. 2012, 12, 423–430.
[105] T. Halonen, J. Romero, J. Melero, “GSM, GPRS and EDGE Performance: Evolution towards 3G/UMTS”, John Wiley & Sons: Hoboken, NJ, USA, 2002.
[106] E. Dahlman, S. Parkvall, J. Skold, P. Beming, “3G Evolution: HSPA and LTE for Mobile Broadband,” Academic Press: Cambridge, MA, USA, 2010.
[107] “OLP425”, Available: http://www.connectblue.com.
[108] Mathworks Inc., MATLAB, The Language of Technical Computing, Natick, Massachusetts, accessed April 2015. [Online]. Available: http://www.mathworks.com/products/matlab/
[109] R Core Team, R: A Language and Environment for Statistical Computing, R Foundation for Statistical Computing, Vienna, Austria, accessed April 2015. [Online]. Available: http://www.R-project.org/
[110] [Online]. Available: http://scikit-learn.org/stable/
[111] L. Griebel, H.U. Prokosch, F. Köpcke, D. Toddenroth, J. Christoph, I. Leb, I. Engel, M. Sedlmayr, “A scoping review of cloud computing in healthcare,” BMC Med Inform Decis Mak 2015;15(17).
[112] M. Li, S. Yu, Y. Zheng, K. Ren, and W. Lou, “Scalable and secure sharing of

personal health records in cloud computing using attributebased encryption," IEEE Trans. Parallel Distrib. Syst., vol. 24, no. 1, pp. 131–143, Jan. 2013.

[113] W. Barfield and T. Caudell, editors. "Fundamentals of Wearable Computers and Augmented Reality." CRC Press, 2001.

[114] S. Bersch, C. Chislett, D. Azzi, R. Khusainov, J. Briggs, "Activity Detection Using Frequency Analysis and Off-the-Shelf Devices: Fall Detection from Accelerometer Data." In Proceedings of the 5th International Conference on Pervasive Computing Technologies for Healthcare (Workshop on Cognitive Sensor Networks for Pervasive Health), Dublin, Ireland, 2011; pp. 362–365.

[115] K. Bouton, M. Koekkoek, R. Verduin, J. Kodde, "A triaxial accelerometer, and portable data processing unit for the assessment of daily physical activity." IEEE Transactions on Biomedical Engineering, 44(3):136–147, 1997.

[116] S. Chen, J. Lach, B. Lo, G.Z. Yang, "Toward Pervasive Gait Analysis with Wearable Sensors: A Systematic Review," IEEE J. Biomed. Health Inform. 2016, 20, 1521–1537.

[117] M. Engelhard, S. Dandu, J. Lach, M. Goldman, S. Patek, "Toward detection and monitoring of gait pathology using inertial sensors under rotation, scale, and offset invariant dynamic time warping," In Proceedings of the 10th EAI International Conference on Body Area Networks, Sydney, Australia, 2010; pp. 265–275.

[118] W. Wang, Y. Guo, B. Huang, G. Zhao, "Analysis of Filtering Methods for 3D Acceleration Signals in Body Sensor Network." In Proceedings of the 2011 International Symposium on Bioelectronics and Bioinformatics, Suzhou, 2011; pp. 263–266.

[119] O. Sarbishei, B. Nahill, A. Roshan Fekr, M. Janidarmian, K. Radecka, Z. Zilic and B. Karajica, "An efficient fault-tolerant sensor fusion algorithm for accelerometers," IEEE International Conference on Body Sensor Networks (BSN), pp.1-6, 2013.

[120] Tilt measurement using a low-g 3-axis accelerometer, Application note AN3182, STMicroelectronics, 2010.

[121] A. Roshan Fekr, M. Janidarmian, K. Radecka, Z. Zilic, "Multi-Sensor Blind Recalibration in mHealth Applications", IEEE International Humanitarian Technology Conference (IHTC), pp.1-4, Canada, 2014.

[122] Freescale Semiconductor FRDM-KL25Z User's Manual, Revision 1.0, Sept. 2012 [Online].

[123] STMicroelectronics User Manual UM1472. (2012, Jan.). STM32F4DISCOVERY, STM32F4 High Performance Discovery Board [Online].Available: http://www.st.com/internet/com/TECHNICAL_RESOURCES/TECHNICAL_LITERATURE/USER_MANUAL/DM00039084.pdf

[124] E. Keogh, P. Smyth, "A Probabilistic Approach to Fast Pattern Matching in Time Series Databases." In Proceedings of the of the 3rd International Conference on

Knowledge Discovery and Data Mining, Newport Beach, CA, USA, 1997, pp. 20–24.

[125] S. Pirttikangas, K. Fujinami, and T. Seppanen. "Feature selection and activity recognition from wearable sensors." In Third Interna-tional Symposium Ubiquitous Computing Systems, volume 4239 of LNCS, pages 516-527, 2006.

[126] A. Roshan Fekr, M. Janidarmian, K. Radecka, Z. Zilic, "Respiration Disorders Classification with Informative Features for m-Health Applications," IEEE J. Biomed. Health Inform. 2016, 20, 733–747.

[127] N. C. Krishnan, C. Juillard, D. Colbry, and S. Panchanathan, "Recognition of hand movements using wearable accelerometers," JAISE, vol. 1, no. 2, pp. 143–155, 2009.

[128] D. Figo, P.C. Diniz, D.R. Ferreira, J.M.P. Cardoso, "Preprocessing techniques for context recognition from accelerometer data. Pers." Ubiquitous Comput. 2010, 14, 645–662.

[129] M. Dash, H. Liu, "Feature Selection for Classification," Intelligent Data Analysis 1 (1997) 131–156.

[130] J.C. Schlimmer, "Efficiently inducing determinations: A complete and systematic search algorithm that uses optimal pruning." In: Proceedings of Tenth International Conference on Machine Learning, 284–290, (1993).

[131] I.T. Jolliffe, "Principal Component Analysis," 2nd ed., Springer, 2002.

[132] C. M. Bishop. "Pattern Recognition and Machine Learning." Springer, 2006.

[133] O. Chapelle, P. Haffner, and V. N. Vapnik, "Support vector machines for histogram-based classification," IEEE Trans. Neural Netw., vol. 10, no. 5, pp. 1055–1064, Sep. 1999.

[134] Kaushal Kumar & Abhishek, "Artificial Neural Networks for Diagnosis of Kidney stone Disease", I.J. Information technology and computer science, vol.7, pp. 20-25, July 2012.

[135] Rokash L (2005) Ensemble methods for classifiers. In: Maimon O, Rokash L (eds) The data mining and knowledge discovery handbook. Springer, New York, pp 957–980.

[136] Z. Zhou, "Ensemble Methods: Foundations and Algorithms", Chapman & Hall/CRC Machine Learning & Pattern Recognition, CRC Press, 2012.

[137] R. Tang, X.D. Yang, S. Bateman, J. Jorge, A. Tang, "Physio@Home: Exploring Visual Guidance and Feedback Techniques for Physiotherapy Exercises," In Proceedings of the 33rd Annual ACM Conference on Human Factors in Computing Systems (CHI '15), Seoul, Korea, 2015; pp. 4123–4132.

[138] A.U. Alahakone, S.M.N.A. Senanayake, "Vibrotactile feedback systems: Current trends in rehabilitation, sports and information display," In Proceedings of the 2009 IEEE/ASME International Conference on Advanced Intelligent Mechatronics, Singapore, 2009; pp. 1148–1153.

[139] CZ-H Ma, DW-C Wong, WK Lam, AH-P Wan, WC-C Lee, "Balance Improvement Effects of Biofeedback Systems with State-of-the-Art Wearable Sensors: A Systematic Review," Sensors. 2016; 16(4):434.

[140] P.B. Shull, W. Jirattigalachote, X. Zhu, "An Overview of Wearable Sensing and Wearable Feedback for Gait Retraining," In: Lee J., Lee M.C., Liu H., Ryu JH. (eds) Intelligent Robotics and Applications. ICIRA 2013. Lecture Notes in Computer Science, vol 8102. Springer, Berlin, Heidelberg.

[141] J.A. Barrios, K.M. Crossley, I.S. Davis, "Gait Retraining to Reduce the Knee Adduction Moment through Real-time Visual Feedback of Dynamic Knee Alignment," J. Biomech. 43, 2208–2213 (2010).

[142] M.A. Hunt, M. Simic, R.S. Hinman, K. L. Bennell, T.V. Wrigley, "Feasibility of a Gait Retraining Strategy for Reducing Knee Joint Loading: Increased Trunk Lean Guided by Real-time Biofeedback," J. Biomech. 44, 943--947 (2011).

[143] D. Spelmezan, A. Schanowski, J. Borchers, "Wearable automatic feedback devices for physical activities," In Proceedings of the Fourth International Conference on Body Area Networks, Los Angeles, CA, USA, 2009.

[144] Leanna Bumatay, Jinsil Hwaryoung Seo, "Mobile haptic system design to evoke relaxation through paced breathing" 5 Posters, August 09 – 13, 2015, Los Angeles, CA.

[145] L. Chen, J. Hoey, C.D. Nugent, D.J. Cook, Z. Yu, "Sensor-Based Activity Recognition," Systems, Man, and Cybernetics, Part C: Applications and Reviews, IEEE Transactions on, vol.42, no.6, pp.790-808, 2012.

[146] Z. He, L. Jin, "Activity recognition from acceleration data using AR model representation and SVM," Machine Learning and Cybernetics, 2008 International Conference on, vol.4, no., pp.2245-2250, 2008.

[147] D. Anguita, A. Ghio, L. Oneto, X. Parra and J. L. Reyes-Ortiz. "A Public Domain Dataset for Human Activity Recognition Using Smartphones", 21th European Symposium on Artificial Neural Networks, Computational Intelligence and Machine Learning, ESANN 2013. Bruges, Belgium 24-26 April 2013.

[148] W. Ugulino, D. Cardador, K. Vega, E. Velloso, R. Milidiu and H. Fuks, "Wearable Computing: Accelerometers' Data Classification of Body Postures and Movements", Proceedings of 21st Brazilian Symposium on Artificial Intelligence. Advances in Artificial Intelligence - SBIA 2012. In: Lecture Notes in Computer Science. , pp. 52-61. Curitiba, PR: Springer Berlin / Heidelberg, 2012.

[149] O. Banos, J.-M. Galvez, M. Damas, H. Pomares, and I. Rojas, "Window Size Impact in Human Activity Recognition," Sensors, vol. 14, no. 4, pp. 6474–6499, Apr. 2014.

[150] S.J. Preece, J.Y. Goulermas, L.P. Kenney, D. Howard, K. Meijer, R. Crompton, "Activity identification using body-mounted sensors—A review of classification techniques" Physiological Measurement, vol. 30, no. 4, 2009.

[151] A. Stisen, H. Blunck, S. Bhattacharya, T. Prentow, M. Kjrgaard, A. Dey, T. Sonne, and M. Jensen, “Smart devices are different: Assessing and mitigating mobile sensing heterogeneities for activity recognition,” in Proc ACM SenSys. ACM, 2015, pp. 127-140.

[152] H. Blunck, S. Bhattacharya, A. Stisen, T. S. Prentow, M. B. Kjærgaard, A. Dey, M. M. Jensen, T. Sonne, "ACTIVITY RECOGNITION ON SMART DEVICES: Dealing with diversity in the wild", GetMobile: Mobile Comp. and Comm., Vol. 20 Issue 1, pp. 34-38, January 2016.

[153] M. A. Labrador, O. D. Lara Yejas, “Human Activity Recognition: Using Wearable Sensors and Smartphones”, Chapman & Hall/CRC Computer and Information Science Series, CRC Press Book, 2013.

[154] E. Keogh, S. Chu, D. Hart, M. Pazzani, “An Online Algorithm for Segmenting Time Series,” In Proceedings of the International Conference on Data Mining, San Jose, CA, USA, 2001; pp. 289–296.

[155] L. Sun, D. Zhang, B. Li, B. Guo, S. Li, “Activity Recognition on an Accelerometer Embedded Mobile Phone with Varying Positions and Orientations”. In Ubiquitous Intelligence and Computing; Springer: Berlin/Heidelberg, Germany, 2010 Vol. 6406, Lecture Notes in Computer Science, pp. 548–562.

[156] Z. He and L. Jin, "Activity recognition from acceleration data based on discrete consine transform and SVM," Systems, Man and Cybernetics, 2009. SMC 2009. IEEE International Conference on, San Antonio, TX, 2009, pp. 5041-5044.

[157] T. Peterek, M. Penhaker, P. Gajdoš, P. Dohnálek, “Comparison of classification algorithms for physical activity recognition, in: Innovations in Bio-inspired Computing and Applications”, Springer, Ostrava, Czech Republic, 2014, pp. 123–131.

[158] Nishkam Ravi, Nikhil Dandekar, Preetham Mysore, and Michael L. Littman. Activity recognition from accelerometer data. In Proceedings of 17th Conference on Innovative Applications of Artificial Intelligence (IAAI), pages 1541– 1546, Pittsburgh, PA, USA, July 2005.

[159] O. Banos, C. Villalonga, R. Garcia, A. Saez, M. Damas, J. A. Holgado, S. Lee, H. Pomares, I. Rojas, “Design, implementation and validation of a novel open framework for agile development of mobile health applications”, BioMedical Engineering OnLine, vol. 14, no. S2:S6, pp. 1-20, 2015.

[160] M. Shoaib, J. Scholten, P.J.M. Havinga, “Towards physical activity recognition using smartphone sensors”, 10th IEEE International Conference on Ubiquitous Intelligence and Computing, pp. 80-87, Italy, 2013.

[161] J. R. Kwapisz, G. M. Weiss and S. A. Moore, “Activity Recognition using Cell Phone Accelerometers”, Proceedings of the Fourth International Workshop on Knowledge Discovery from Sensor Data, pp. 74-82, Washington, USA, 2010.

[162] M. Shoaib, S. Bosch, O.D. Incel, H. Scholten, P.J.M. Havinga, “Fusion of Smartphone Motion Sensors for Physical Activity Recognition”, Sensors, 14, 10146-10176, 2014.

[163] M. Janidarmian, K. Radecka and Z. Zilic, "Analysis of Motion Patterns for Recognition of Human Activities," Wireless Mobile Communication and Healthcare (Mobihealth), 2015 ACM 5th International Conference on, London, 2015, pp 68-72.

[164] K. Altun, B. Barshan, and O. Tunçel, “Comparative study on classifying human activities with miniature inertial and magnetic sensors”, Pattern Recognition, 43(10):3605-3620, October 2010.

[165] Shaopeng Liu, Robert X. Gao, Dinesh John, John Staudenmayer, and Patty S. Freedson. “SVM-based multi-sensor fusion for free-living physical activity assessment,” In Proceedings of 33rd Annual International IEEE EMBS Conference, pages 3188–3191, Boston, MA, USA, August-September 2011.

[166] X. Long, B. Yin and R. M. Aarts, "Single-accelerometer-based daily physical activity classification," 2009 Annual International Conference of the IEEE Engineering in Medicine and Biology Society, Minneapolis, MN, 2009, pp. 6107-6110.

[167] Norbert Győrbíró, Ákos Fábián, and Gergely Hományi. “An activity recognition system for mobile phones,” Mobile Networks and Applications, 14(1):82–91, February 2009.

[168] A. Vahdatpour, N. Amini, and M. Sarrafzadeh, “On-body device localization for health and medical monitoring applications,” in Pervasive Computing and Communications (PerCom), 2011 IEEE International Conference on. IEEE, 2011, pp. 37–44.

[169] R. Saeedi, J. Purath, K. Venkatasubramanian and H. Ghasemzadeh, "Toward seamless wearable sensing: Automatic on-body sensor localization for physical activity monitoring," 2014 36th Annual International Conference of the IEEE Engineering in Medicine and Biology Society, Chicago, IL, 2014, pp. 5385-5388.

[170] B. Bruno, F. Mastrogiovanni, A. Sgorbissa, T. Vernazza and R. Zaccaria, “Analysis of human behavior recognition algorithms based on acceleration data,” IEEE International Conference on Robotics and Automation (ICRA), pp. 1602-1607, Karlsruhe, 2013.

[171] A. Yang, R. Jafari, S. Sastry, and R. Bajcsy, “Distributed Recognition of Human Actions Using Wearable Motion Sensor Networks”, JAISE, 2009.

[172] K. Frank, M. Röckl, M. J. Vera Nadales, P. Robertson and T. Pfeifer, “Comparison of exact static and dynamic Bayesian context inference methods for activity recognition,” Pervasive Computing and Communications Workshops (PERCOM Workshops), 8th IEEE International Conference on, Mannheim, pp. 189-195, 2010.

[173] P. Balaprakash, A. Tiwari, S. Wild, S. A. Jarvis, S. A. Wright, S. D. Hammond, "Multi objective optimization of hpc kernels for performance power and energy" in High Performance Computing Systems. Performance Modeling Benchmarking and Simulation ser. Springer Lecture Notes in Computer Science, pp. 239-260, 2014.

[174] Lior Rokach, Oded Maimon, “Data Mining with Decision Trees: Theroy and Applications,” World Scientific Publishing Co., Inc., River Edge, NJ, 2008.

[175] M. Zambon , R. Lawrence , A. Bunn and S. Powell “Effect of alternative splitting rules on image processing using classification tree analysis,” Photogramm. Eng. Remote Sens., vol. 72, no. 1, pp. 25 -30 2006.

[176] S. Theodoridis, K. Koutroumbas “Pattern Recognition” (4th ed.) Elsevier/Academic Press (2008).

[177] Enhao Zheng, Baojun Chen, Xuegang Wang, Yan Huang and Qining Wang. “On the Design of a Wearable Multi-sensor System for Recognizing Motion Modes and Sit-to-stand Transition.” Int J Adv Robot Syst, 2014.

[178] T. Chen et al., “On the trade-off of accuracy and computational complexity for classifying normal and abnormal ECG in remote CVD monitoring systems,” in Proc. IEEE Workshop Signal Processing Systems (SIPS), Quebec, pp. 37–42, Oct. 2012.

[179] Supervised Learning, Statistics Toolbox, MATLAB R2105b documentation.

[180] F.F. Chamasemani, Y.P. Singh, “Multi-class Support Vector Machine (SVM) Classifiers -- An Application in Hypothyroid Detection and Classification,” Bio-Inspired Computing: Theories and Applications (BIC-TA), 2011 Sixth International Conference on, pp.351-356, 2011.

[181] J. Parera, C. Angulo, A. Rodriguez-Molinero, and J. Cabestany. “User daily activity classification from accelerometry using feature selection and svm.” In Bio-Inspired Systems: Computational and Ambient Intelligence, LNCS, pages 1137-1144, 2009.

[182] H. He and E. A. Garcia. “Learning from imbalanced data.” IEEE Transactions on Knowledge and Data Engineering, 21(9):1263-1284, 2009.

[183] T. G. Dietterich and G. Bakiri, “Solving multiclass learning problem via error-correcting output codes,” Journal of Artificial Intelligence Research, pp. 263–286, 1995.

[184] K. Foorster, S. Monteleone, A. Calatroni, D. Roggen, and G. Trooster. “Incremental knn classifier exploiting correct – error teacher for activity recognition.” In Proceedings of the 9th International Conference on Machine Learning and Applications, pages 445-450, 2010.

[185] B.S. Everitt, S. Landau, M. Leese, and D. Stahl, “Miscellaneous Clustering Methods, in Cluster Analysis,” 5th Edition, John Wiley & Sons, Ltd, Chichester, UK, 2011.

[186] P. Hall, B.U. Park, and R. J. Samworth, "Choice of neighbour order in nearest-neighbour classification." Ann. Statist., 36, 2135–2152, 2008.
[187] K.G. Anil, "On optimum choice of k in nearest neighbor classification", Computational Statistics and Data Analysis, 50, pp. 3113–3123, 2006.
[188] L. Breiman, "Bagging predictors,"Technical Report 421, Department of Statistics, University of California at Berkeley, 1994.
[189] Kristina Machova, Frantisek Barcak, Peter Bednar Acta Polytechnica Hungarica, "A bagging method using decision trees in the role of base classifiers," Acta Polytechnica HungaricaVol. 3, No. 2, 2006.
[190] R. Schapire, Y. Freund, Boosting the margin: "A new explanation for the effectiveness of voting methods." The annals of statistics, 26(5):1651-1686, 1998.
[191] Y. Freund, and R. E. Schapire. "A Decision-Theoretic Generalization of On-Line Learning and an Application to Boosting," J. of Computer and System Sciences, Vol. 55, pp. 119–139, 1997.
[192] C. Seiffert, T. Khoshgoftaar, J. Hulse, and A. Napolitano. "RUSBoost: Improving classification performance when training data is skewed," 19th International Conference on Pattern Recognition, pp. 1–4, 2008.
[193] T.K. Ho, "The random subspace method for constructing decision forests," IEEE Transactions on Pattern Analysis and Machine Intelligence, Vol. 20, No. 8, pp. 832–844, 1998.
[194] J. Lester, T. Choudhury, N. Kern, G. Borriello, and B. Hannaford. "A hybrid discriminative/generative approach for modeling human activities." In Proceedings of the 19th international joint conference on Artificial Intelligence, pages 1541-1546, 2005.
[195] M. Cortina-Puig, G. Istamboulie, T. Noguer and J. Marty, "Analysis of Pesticide Mixtures Using Intelligent Biosensors," Book Article, Intelligent and Biosensors, 2010.
[196] A. Sharma, Young-Dong Lee; Wan-Young Chung, "High Accuracy Human Activity Monitoring Using Neural Network," Convergence and Hybrid Information Technology, 2008. ICCIT '08. Third International Conference on , vol.1, no., pp.430,435, 11-13 Nov. 2008.
[197] M. Riedmiller, and H. Braun, "A direct adaptive method for faster backpropagation learning: The RPROP algorithm," Proceedings of the IEEE International Conference on Neural Networks, pp. 586–591, 1993.
[198] M. Molier, "A Scaled Conjugate Gradient Algorithm for Fast Supervised Learning", Neural Networks, pp. 525-533, 1993.
[199] M.T. Hagan, and M. Menhaj, "Training feed-forward networks with the Marquardt algorithm," IEEE Transactions on Neural Networks, Vol. 5, No. 6, 1999, pp. 989–993, 1994.

[200] A. Roshan Fekr, M. Janidarmian, K. Radecka, Z. Zilic, “Design of an e-Health Respiration and Body Posture Monitoring System and Its Application for Rib Cage and Abdomen Synchrony Analysis”, 2014 IEEE International Conference on Bioinformatics and Bioengineering (BIBE), pp.141-148, Florida, 2014.
[201] Noam Gavriely, “Breath Sounds Methodology,” CRC Press: Florida, 1995.
[202] J. C. Fernandez, F. J. Martinez, C. Hervas, P. A. Gutierrez, "Sensitivity Versus Accuracy in Multiclass Problems Using Memetic Pareto Evolutionary Neural Networks," Neural Networks, IEEE Transactions on, vol.21, no.5, pp.750-770, May 2010.
[203] P. De Chazal, C. Heneghan, E. Sheridan, R. Reilly, P. Nolan, and M. O’Malley, “Automated processing of the single lead electrocardiogram for the detection of obstructive sleep apnoea,” IEEE Trans. Biomed. Eng., vol.50, no.6, pp.686-696, Jun 2003.
[204] F. Roche, V. Pichot, E. Sforza, I. Court-Fortune, D. Duverney, F. Costes, M. Garet, and J.-C. Barth´el´emy, “Predicting sleep apnoea syndrome from heart period: A time–frequency wavelet analysis,” Eur. Respir. J., vol.22, pp.937-942, 2003.
[205] N. F. Garcia, P. Gomis, A. La Cruz, G. Passeriello, and F. Mora, “Bayesian hierarchical model with wavelet transform coefficients of the ECG in obstructive sleep apnea screening,” Comput. Cardiol. vol.27, pp.275-278, 2000.
[206] A. H. Khandoker, M. Palaniswami, C. K. Karmakar, “Support vector machines for automated recognition of obstructive sleep apnea syndrome from ECG recordings,” IEEE Trans Inf Tech Biomedicine, vol.13, pp.37-48, 2009.
[207] R. Lin, R. Lee, C. Tseng, H. Zhou, C. Chao, J. Jiang, “A New Approach for Identifying Sleep Apnea Syndrome Using Wavelet Transform and Neural Networks,” Biomed. Eng. Appl. Basis Commun. 2006, 18:138–143.
[208] B. Koley and D. Dey, “Adaptive classification system for real-time detection of apnea and hypopnea events,” in Proc. IEEE Point-of-Care Healthcare Technol., pp. 42-45, 2013.
[209] S. Jafari, H. Arabalibeik, K. Agin, "Classification of normal and abnormal respiration patterns using flow volume curve and neural network," Health Informatics and Bioinformatics (HIBIT), International Symposium on, pp.110-113, April 2010.
[210] V. Mahesh, S. Ramakrishnan, "Assessment and classification of normal and restrictive respiratory conditions through pulmonary function test and neural network," J. Med. Eng. Techno., vol.31, pp.300-304, 2007.
[211] V. Mahesh, S. Ramakrishnan, “Detection of obstructive respiratory abnormality using flow-volume,” J. Med. Syst., vol. 31 (6), pp. 461-465, 2007.
[212] M. J. Baemani, A. Monadjemi, and P. Moallem, "Detection of respiratory abnormalities using artificial neural networks," Journal of Computer Science, vol. 4(8), pp. 663-667, 2008.

[213] M. Al-Angari and V. Sahakian, "Automated Recognition of Obstructive Sleep Apnea Syndrome Using Support Vector Machine Classifier," in IEEE Transactions on Information Technology in Biomedicine, vol. 16, no. 3, pp. 463-468, May 2012.

[214] P. Varady, S. Bong´ar, and Z. Beny´o, "Detection of airway obstructions and sleep apnea by analyzing the phase relation of respiration movement signals," IEEE Trans. Instrum. Measure, vol. 52, no. 1, pp. 2–6, Feb. 2003.

[215] Beattie, Zachary T. et al. "Classification of Breathing Events Using Load Cells under the Bed." Conference Proceedings 2009 (2009): 3921–3924. PMC. Web. 26 July 2016.

[216] R. Palaniappan, K. Sundaraj, "Respiratory sound classification using cepstral features and support vector machine" in Proc. IEEE Recent Advances in Intelligent Computational Systems (RAICS), pp. 132–136, December 2013.

[217] M. Yamashita, M. Himeshima, S. Matsunaga, "Robust classification between normal and abnormal lung sounds using adventitious-sound and heart-sound models," Acoustics, Speech and Signal Processing (ICASSP), IEEE International Conference on, pp.4418-4422, May 2014.

[218] S. Matsunaga, K. Yamauchi, M. Yamashita, S. Miyahara, "Classification between normal and abnormal respiratory sounds based on maximum likelihood approach," Acoustics, Speech and Signal Processing, pp.19-24, April 2009.

[219] T. Okubo, N. Nakamura, M. Yamashita, S. Matsunaga, "Classification of healthy subjects and patients with pulmonary emphysema using continuous respiratory sounds," Engineering in Medicine and Biology Society (EMBC), 36th Annual International Conference of the IEEE, pp.70-73, Aug. 2014.

[220] N. Gavriely, M. Nissan, A. H. E. Rubin, and D. W. Cugell, "Spectral characteristics of chest wall breath sounds in normal subjects," Thorax vol.50, pp.1292–1300, 1995.

[221] P. Siirtola, H. Koskimäki and J. Röning, "Periodic quick test for classifying long-term activities," 2011 IEEE Symposium on Computational Intelligence and Data Mining (CIDM), Paris, 2011, pp. 135-140.

[222] M. Muller, "Information Retrieval for Music and Motion", book series Database Management & Information Retrieval, Springer publisher, XVI, 318 p, 2007.

[223] M. Hall, "Correlation-based feature selection for machine learning," PhD Thesis., Department of Computer Science, Waikato University, New Zealand, 1999.

[224] Deb, Kalyanmoy. Multi-Objective Optimization Using Evolutionary Algorithms. John Wiley & Sons, 2001.

[225] D.E. Goldberg, "Genetic algorithms in search, optimization, and machine learning," Addison-Wesley Pub. Co. 1989.

[226] CL. Webber, JP. Zbilut (2005) "Recurrence quantification analysis of nonlinear dynamical systems," Tutorials in Contemporary Nonlinear Methods for the

Behavioural Sciences, eds Riley MA, Van Orden GC (National Science Foundation, Arlington, VA), pp 26–95.

[227] F. Takens, “Detecting Strange Attractors in Turbulence,” In: Dynamical Systems and Turbulence, Lecture Notes in Mathematics, 898, Berlin, 1981, 366-381.

[228] A.M. Fraser, and H.L. “Swinney, Independent coordinates for strange attractors from mutual information,” Phys. Rev. A 33 (1986) 1134.

[229] M. B. Kennel, B. Brown, & H.D.I. Abarbanel, “Determining embedding dimension for phase-space reconstruction using a geometrical construction,” Physical Review A, 45, 3403-3411, 1992.

[230] H. Kantz, T. Schreiber, “Nonlinear Time Series Analysis,” Cambridge: Cambridge University Press; 1997.

[231] Xsens Technologies B.V. XM-B Technical Documentation, 2009. Available online: http://www.xsens.com (accessed on 12 May 2014).

[232] Y. R. Kou and Y. Shuei Lin, “Bradypnea” Encyclopedia of Molecular Mechanisms of Disease. New York, NY, USA: Springer, 2009, pp. 241–243.

[233] H. William, L. Myron, D. Robin, and A. Mark, “Current Diagnosis and Treatment in Pediatrics,” 21 ed. New York, NY, USA: McGraw-Hill Professional, 2002, p. 989.

[234] P. Kaufmann, K. H. Smolle, S. Fleck andA. Lueger, “Ketoacidotic diabetic metabolic dysregulation: Pathophysiology, clinical aspects, diagnosis and therapy,” Wien. Klin. Wochenschr, vol. 106, pp. 119–127, 1994.

[235] D. A. Hofsoy, J. F. Clauss, and B.Wolf, “Monitoring and therapy of sleep related breathing disorders,” in Proc. 6th Int.Workshop Wearable Micro and Nano Technol. Pers. Health, Jun. 2009, pp. 41–44.

[236] R. J. Farney, J.M.Walker, K.M. Boyle, T. V. Cloward, and K. C. Shilling, “Adaptive servoventilation (ASV) in patients with sleep disordered breathing associated with chronic opioid medications for non-malignant pain,” J. Clin. Sleep Med., vol. 4, pp. 311–319, 2008.

[237] G. Aljadeff, M. Molho, I. Katz, S. Benzaray, Z. Yemini, and R. J. Shiner, “Pattern of lung volumes in patients with sighing breathing,” Thorax J., vol. 48, pp. 809–811, 1993.

[238] Respiratory center, The American Heritage R _ Medical Dictionary, 2007.

[239] “Stedman's Medical Dictionary” (28th ed.). Philadelphia: Lippincott Williams & Wilkins. pp.250.

[240] A. Roshan Fekr, K. Radecka and Z. Zilic, "Tidal volume variability and respiration rate estimation using a wearable accelerometer sensor," 2014 4th International Conference on Wireless Mobile Communication and Healthcare - Transforming Healthcare Through Innovations in Mobile and Wireless Technologies, Athens, 2014, pp. 1-6.

[241] J. Lin, E. Keogh, S. Lonardi, and B. Chiu. “A Symbolic Representation of Time Series, with Implications for Streaming Algorithms,” In proceedings of the 8th

ACM SIGMOD Workshop on Research Issues in Data Mining and Knowledge Discovery, pp.2-11, June 2003.

[242] E. Keogh, J. Lin, A. Fu, “HOT SAX: efficiently finding the most unusual time series subsequence,” In: Proceedings of the Fifth IEEE International Conference on Data Mining, pp. 226–233, 2005.

[243] J. Gama, “Knowledge Discovery from Data Streams” CRC Press, Boca Raton (2010).

[244] A. Apostolico, M.E. Bock, and S. Lonardi, “Monotony of Surprise and Large-Scale Quest for Unusual Words” In proceedings of the 6th Int’l Conference on Research in Computational Molecular Biology, pp.22-31, April 18-21.

[245] Y. Huang, P. S. Yu, “Adaptive Query Processing for Time- Series Data” In proceedings of the 5th Int'l Conference on Knowledge Discovery and Data Mining, pp.282-286, Aug 15-18.

[246] V. Parreira , D. Vieira, M. Myrrha, I. Pessoa, S. Lage, R. Britto, “Optoelectronic plethysmography: a review of the literature”, Braz. J. Phys. Ther, vol.16, no.6, pp.439-453, Dec 2012.

[247] J. Allen, M. Wolfson, K. McDowell, T. Shaffer, “Thoracoabdominal asynchrony in infants with airflow obstruction,” Am Rev Respir Dis, 1990.

[248] N. Kiciman, B. Andreásson, G. Bernstein, F. Mannino, W. Rich, C. Henderson, “Thoracoabdominal motion in newborns during ventilation delivered by endotracheal tube or nasal prongs,” Pediatr Pulmonol. pp. 175-81, 1998.

[249] “Spirometer”, Available: http://www.vernier.com/products/sensors/spr-bta/

[250] D.O. Rosalba Courtney, “DYSFUNCTIONAL BREATHING: ITS PARAMETERS, MEASUREMENT AND RELEVANCE,” Ph.D. Thesis School of Health Sciences Science, Engineering and Technology Portfolio RMIT University, Feb 2011.

[251] D. Spelmezan “An Investigation into the Use of Tactile Instructions in Snowboarding,” Proceedings of the 14th international conference on Human-computer interaction with mobile devices and services, Sep 2012, United States. pp.417–426, 2012.

[252] J. B. F., Van Erp. I. Saturday, C. Jansen, “Application of tactile displays in sports: where to, how and when to move,” Proc. EuroHaptics 2006, pp. 90–95.

[253] K. Huang, K., T. Starner, E. Do, G. Weiberg, D. Kohlsdorf, C. Ahlrichs, R. Leibrandt, “Mobile Music Touch: Mobile Tactile Stimulation for Passive Learning,” Proc. CHI 2010, ACM Press, 791–800.

[254] C. Wall III, “Application of vibrotactile feedback of body motion to improve rehabilitation in individuals with imbalance,” J. Neurol. Phys. Ther. JNPT 34(2), pp. 98–104, 2010.

[255] Y. Ramacharaka, “Science of breath: the oriental breathing philosophy” Chicago: Yogi Publication Society; 1904.

[256] A. Roshan Fekr, K. Radecka, Z. Zilic, “Design and Evaluation of an Intelligent

Remote Tidal Volume Variability Monitoring System in e-Health Applications", IEEE Journal of Biomedical and Health Informatics (J-BHI), vol.19, no.5, pp.1532-1548, 2015.

[257] R. Nagarathna, H. R. Nagendra, "Yoga for bronchial asthma: A controlled study," Br Med J. 1985; 291:1077–9.

[258] H. Benson, B. A. Rosener, B. Marzetta, K.M. Klemechu, "Decreased blood pressure in pharmacologically treated. Hypertensive patients who regularly elicited the relaxation response," Lancet., 1:289-92, 1974.

[259] C. Patel, M.G. Marmot, D. J. Terry, M. Carruther, B. Hunt, S. Patel, "Trial of relaxation in reducing coronary risk: Four-year follow-up," Br Med J. 290:1103–6, 1985.

[260] M. Thomas, R. K. McKinley, E. Freeman, C. Foy, "Prevalence of dysfunctional breathing in patients treated for asthma in primary care: cross sectional survey," BMJ, 322:1098–100, 2001.

[261] S. Khalsa, "Treatment of insommnia with yoga: a preliminary study with sleep-wake diaries." Applied Psychophysiology and Biofeedback 29(4): 269-278, 2004.

[262] D. Shannahoff-Khalsa, M. D. Sramek Kennel, S. W. Jamieson "Hemodynamic observations on a yogic breathing technique claimed to help eliminate and prevent heart attacks: a pilot study." J Alternative and Complementary Medicine 10(5): 757-766, 2004.

[263] A. Vedamurthachar, et al., "Antidepressant efficacy and hormonal effects of Sudarshana Kriya Yoga (SKY) in alcohol dependent individuals." J Affect Disord 94(1-3): 249-253, 2006.

[264] D.O. Rosalba Courtney, "The functions of breathing and its dysfunctions and their relationship to breathing therapy," Int. J. Orofacial Myology 12, pp.78-85, 2009.

[265] http://www.precisionmicrodrives.com.

[266] Y. Visell, "Tactile sensory substitution: Models for enaction in HCI," Interacting with Computers, vol. 21, no. 1–2, pp. 38-53, Jan. 2009.

[267] Wu, J., Zhang, J., Yan, J., Liu, W., Song, G.: Design of a Vibrotactile Vest for Contour Perception. International Journal of Advanced Robotic Systems 9, 166 (2012).

[268] I. Oakley, Y. Kim, J. Lee, and J. Ryu, "Determining the feasibility of forearm mounted vibrotactile displays," in Proc. 14th Symp. Haptic Interfaces Virtual Environ. Teleoperator Syst., 2006, pp. 27–34.

[269] T. Oron-gilad, J. L. Downs, R. D. Gilson, and P. A.Hancock, "Vibrotactile Guidance Cues for Target Acquisition," IEEE Transactions on System, Man, and Cybernetics, vol. 37, no. 5, pp. 993-1004, 2007.

[270] D. Ryu, G. H. Yang, and S. Kang, "T-hive:Vibrotactile interface presenting spatial information on handle surface," in 2009 IEEE International Conference on Robotics

and Automation, pp. 683-688, May 2009.

[271] V. Pradeep, G. Medioni, and J. Weiland, “A wearable system for the visually impaired,” in 32nd Annual International Conference of the IEEE Engineering in Medicine and Biology Society, vol. 2010, pp. 6233-6, Jan. 2010.

[272] D. Dakopoulos, S. K. Boddhu, N. Bourbakis, “A 2D vibration array as an assistive device for visually impaired,” in Proceedings of the 7th IEEE International Conference on Bioinformatics and Bioengineering(BIBE 2007), pp. 930-937, Oct. 2007.

[273] M. Y. Sung, K. Jun, D. Ji, H. Lee, and K. Kim, “Touchable Video and Tactile Audio,” in 11th IEEE International Symposium on Multimedia, pp. 425-431, 2009.

[274] H. Kim, C. Seo, J. Lee, J. Ryu, S. Yu, and S. Lee, “Vibrotactile Display for Driving Safety Information,” in 2006 IEEE Intelligent Transportation Systems Conference, pp. 573-577, 2006.

[275] J. M. Loomis, “Tactile letter recognition under different modes of stimulus presentation,” Perception & Psychophysics, vol. 16, no. 2, pp. 401–408, 1974.

[276] T. Kikuchi, Y. Yamashita, K. Sagawa, and T. Wake, “An analysis of tactile letter confusions,” Perception & Psychophysics, 26(4), 1979, pp. 295–301.

[277] Y. Yanagida , M. Kakita , R. W. Lindeman , Y. Kume , N. Tetsutani, “Vibrotactile letter reading using a low-resolution tactor array,” Proceedings of the 12th international conference on Haptic interfaces for virtual environment and teleoperator systems, March 27-28, 2004, Chicago, Illinois, USA.

[278] Y. Liao, Yi. Chen, J. Lo, R. Liang, L. Chan, B. Chen, “EdgeVib: Effective Alphanumeric Character Output Using a Wrist-Worn Tactile Display,” Proceedings of the 29th Annual Symposium on User Interface Software and Technology, pp. 595-601, 2016.

[279] https://www.adafruit.com/product/1411